The Dissertation Committee for Alejandro Raul Avendaño Valderrama
certifies that this is the approved version of the following dissertation:

Pretensioned Box Beams:

Prestress Transfer and Shear Behavior

Committee:

Oguzhan Bayrak, Supervisor

James O. Jirsa

Sharon L. Wood

John E. Breen

Ofodike A. Ezekoye

Pretensioned Box Beams:

Prestress Transfer and Shear Behavior

by

Alejandro Raul Avendaño Valderrama, B.C.E.; M.S.E.

Dissertation

Presented to the Faculty of the Graduate School of

The University of Texas at Austin

in Partial Fulfillment

of the Requirements

for the Degree of

Doctor of Philosophy

The University of Texas at Austin

December 2011

To Analissa

Acknowledgments

First, I would like to express my gratitude to the Fulbright Scholarship Program, the Texas Department of Transportation and The Technological University of Panama for financing me.

Next, I must thank my advisor, Oguzhan Bayrak, for giving me the opportunity to work with him. Beyond his technical contribution to my professional formation, Dr. Bayrak was always available to me as a friend and mentor.

The guidance provided by my dissertation committee is much appreciated. Likewise, the input and recommendations of the engineers at the TxDOT Bridge Division was highly valuable to this dissertation.

The hard work, patience and commitment of the staff members at FSEL are greatly appreciated. Dennis, Blake, Andrew, Eric, Mike, Jessica and Barbara, I am truly grateful.

I could not have fabricated my specimens or kept my sanity without the help of fellow graduate students Andy Moore, David Dunkman, Catherine Hovell, Jeremiah Fasl, Kerry Kreitman, Zach Webb, Nancy Larson, Eulalio Fernandez, David Garber, Eisuke Nakamura, Brian Hanson, David Wald, David Langefeld, Kevin Moyer, Neil Satrom, Jose Garcia, Eric Giannini and many others. Other students were a big part of my early PhD years: Brian Schnittker, Chris Heckman, Jason Stith and others. Much thanks to all of you. I only hope I have been of equal help to all of you. Thank you all so much.

The unconditional support and believe of my family and friends reminded me of the real reasons to venture away from home.

To my wife, Analissa, thank you for bearing with me through my toughest times. Your courage inspired me and your sweetness gave me calm when I needed it.

Finally, thank you God for keeping me close to you and putting such great people in my path.

Pretensioned Box Beams:
Prestress Transfer and Shear Behavior

Alejandro R. Avendaño V., Ph.D.

The University of Texas at Austin, 2011

Supervisor: Oguzhan Bayrak

Pretensioned concrete box beams have been used in highway bridges for more than half a century. Due to their geometry, they have often been used as a viable alternative to the classic I-shaped girders. Box beams are highly effective in cases where speed of construction is a priority. However, the detailing and design of box beams are more complicated than that of I-shaped girders. The flow of forces at the beam's end blocks must be understood in order to detail reinforcement adequately.

The following were the objectives of this research study: (i) quantify the demands placed on box beam end blocks upon prestress transfer, (ii) characterize the demands placed on box beam end blocks upon the application of superimposed loads, (iii) evaluate the effects of alternative void geometries at skewed ends of box beams on curing temperatures, (iv) based on the knowledge gained in (i), (ii) and (iii), improve the box beam end blocks, (v) test the improved end block under worst case scenario demands at prestress transfer and under extreme loading conditions, and (vi) validate currently used shear strength design methodologies in their application to pretensioned box beams.

In order to achieve these objectives, an experimental program was conducted. The experimental program included the load testing of ten 4B28 and five 5B40 box beams, for a total of twenty nine load tests. The influence of several factors that distinguish box beam behavior from the better-understood I-shaped girder behavior was studied.

Additionally, the experimental program included the fabrication, instrumentation and early-age behavior study of five 5B40 box beams. The first three beams were used to

assess the behavior of box beams fabricated with the current TxDOT standard details (from December 2006). The fourth beam incorporated modifications to the standard reinforcement details based on the observations made through the study of the first three 5B40 box beams. The last specimen corresponded to a new box beam cross section (5XB40) optimized to be used in a spread-box beams configuration.

Table of Contents

List of Tables

List of Figures

xvii

xx

CHAPTER 1

Introduction

1.1 OVERVIEW

The pretensioned concrete bridge industry expanded greatly in the 1950s and 1960s with the introduction of high-strength strands. Since then, several different beam cross sections have been used, ranging not only in depth but also in their basic shape. Without a doubt, the most popular cross section used has been the classical I-shaped beam, referred to more commonly as an I-beam. The wide-spread use of the I-beam has made fabricators extremely proficient at expediting their production, improving the quality of the product and reducing their cost.

In some cases, such as bridge replacements and bridge expansions, speed of construction is a priority. In these cases, box beams offer significant advantages over their I-beam counterparts. By being placed side by side with no space between them, box beams eliminate the need for false work. Once all box beams have been erected into place, the superstructure is practically ready to be decked and topped with a wearing surface. This configuration of box beams also provides for a smaller superstructure depth as the main webs in the bridge superstructure are placed closer together.

Box beams have also been noted for their aesthetics. Specifically, box beams are sometimes favored because their use eliminates the unsightly appearance of the underside of an I-beam bridge.

In box beams, two vertical walls (i.e. webs) are separated by a polystyrene void former. At the beam end, a solid end block is used to close the section and transfer loads from the webs to a central support. In relatively long box beams, intermediate diaphragms are often used to stiffen the section and to allow for transverse post-tensioning of the group of beams constituting the entire bridge superstructure.

The reinforcement detail of the box beam end block is often complicated, congested and consequently drives up the cost of the beam. In short, the main goals of the

1

current research project were to improve the constructability of the reinforcement in the box beam end blocks and proportion such reinforcement to minimize crack widths occurring at prestress transfer.

In order to improve the constructability and potentially reduce the amount of reinforcement placed in the box beam end block, one must understand the demands placed on it. During prestress transfer, the end region of the beam, and thus the end block, is subject to transverse forces that have been found to be proportional to the prestressing force applied to the section. Additionally, under the application of gravity loads (self-weight, superimposed dead loads and live loads), further demands are placed on the end region. The end block must preserve its integrity in order to maximize the strength of the beam.

The demands exerted on the end block due to prestress transfer and external load application are complicated even further when the beams are aligned at a skew and the end block must accommodate this geometry. Skewed end blocks create a more complicated load path from the top of the beam to the supports. Similarly, the reinforcement detail of skewed end blocks becomes more complicated and difficult to construct. Hence, optimizing both square and skewed end blocks is another goal of this project.

Besides their strength, durability of any pretensioned concrete beam is an important design consideration. A significant volume of concrete is placed in the box beam end blocks. High ambient temperatures and the heat generated by the hydration of cementitious products in the concrete combine to create potential for durability problems.

When excessively high temperatures are endured during the curing process, a deleterious reaction known as Delayed Ettringite Formation (DEF) can occur (Day, 1992 and Lawrence, 1994). Ettringite is a normal hydration product. However, when ettringite forms in hardened concrete, an expansive process takes place, resulting in cracks that ease water ingress and worsen the DEF process. Eventually, wide cracks may lead to corrosion of the reinforcing steel and the prestressing strands, compromising the durability of a pretensioned concrete beam. While high temperatures are associated with

DEF, large temperature differentials within the beam are also cause for concern as they may lead to thermal cracking. Curing temperatures and differentials can be reduced in many ways, one of them being a reduction in the volume of the concrete placed in box beam end blocks. Presumably, a larger end block provides more strength while a smaller end block reduces the chance for durability problems. Balance must be achieved in proportioning an efficient end block. TxDOT is aware of the potential problems resulting from high curing temperatures and large temperature differentials. To mitigate these issues, the use of fly-ash is now mandatory for prestressed concrete applications. The replacement of Type-III cement with fly-ash has been known to reduce curing temperatures. The downside of fly-ash replacement is a slower strength gain often to the dislike of beam manufacturers. Once again, a balance between lower temperatures and faster strength gains is desired.

In determining the shear strength of a prestressed concrete beam, several methods are available to the designer. All of these methods have been developed and validated for prestressed concrete applications mainly with the classical I-beam in mind. It is pertinent to assess the efficacy of these methods in estimating the shear strength of box beams, considering the fact that they are far more complicated that I-beams.

Within the context described above, TxDOT research project 0-5831 was funded in an effort to simplify the end region of box beams and U-beams. The research pertaining to box beams in this project is presented in this dissertation.

1.2   PROJECT OBJECTIVES

The project objectives can be summarized as follows:
(1). Quantify the demands placed on square and skewed box-beam end blocks upon prestress transfer.
(2). Characterize the demands placed on square and skewed box-beam end blocks upon the application of superimposed loads.
(3). Evaluate the effects of alternative void geometries at skewed ends of box beams on curing temperatures.

(4). Based on the knowledge gained in (1), (2) and (3), improve the reinforcement details of the box-beam end region.

(5). Test the proposed end-block reinforcement details under worst case scenario demands at prestress transfer, and under extreme loading conditions.

(6). Validate currently used shear strength design methodologies in their application to pretensioned box beams.

In this dissertation, the work performed to fulfill these six objectives is presented in detail. Some of the underlying work was performed under the general umbrella of Project 0-5831 and is pertinent to both box beam and U-beam behavior. For the sake of clarity, background material will be presented as it is relevant to box beams only.

1.3 RESEARCH SIGNIFICANCE

The research conducted herein constitutes the largest experimental investigation regarding early-age and shear behavior of box beams to date.

The following factors differentiate box beams from single-webbed beams:

i. the geometry of the box beam cross sections. Specifically, the presence of two webs

ii. the distribution of prestressing strands across a larger width

iii. the fabrication process

iv. how box beams are typically supported, and

v. the presence of square and skewed end blocks with different internal void geometries

How these factors influence the behavior and structural performance of box beams cannot be inferred from previous research conducted on single-webbed girders. Furthermore, the knowledge and understanding acquired through this experimental program can be applied to other two-webbed pretensioned cross sections such as U-beams and trapezoidal girders.

Additionally, the influence that the type of coarse aggregates (round river gravel versus crushed limestone) and the type of concrete (conventional versus self-consolidating) have on the shear behavior of pretensioned concrete girders was studied through full-scale beam specimens.

1.4   ORGANIZATION

Background material and a literature review are presented in Chapter 2. More specifically, background material on the shear strength of typical prestressed girders is presented leading to the issues that make box beam design particularly different. Previous box beam research is presented and, finally, background material on transverse stresses introduced at the time of prestress transfer is presented.

The experimental program is described in Chapter 3. In the first part of Chapter 3, shear tests conducted on ten 4B28 box beams (a TxDOT standard section 28 in. deep and 4 ft. wide) are presented. Then, the the in-house fabrication, the study of the transverse stresses at prestress transfer, study of internal curing temperatures and shear testing of five 5B40 box beams (a TxDOT standard section 40 in. deep and 5 ft. wide) is presented.

Results from the experimental program are presented in Chapters 4, 5 and 6. Results from the shear tests conducted on the ten 4B28 box beams are presented and discussed in Chapter 4. Results regarding the transverse stresses at prestress transfer and curing temperatures gathered during the in-house fabrication of box beams are discussed in Chapter 5. Chapter 6 contains results obtained from 9 shear tests conducted on the in-house fabricated beams.

The results presented in the aforementioned chapters are summarized in Chapter 7, which also includes the conclusions and recommendations of this research study.

Appendices A and B include additional information such as material properties and shop drawings for all the beams tested in this study, respectively. Detailed outputs from the load tests described in Chapter 4 are presented in Appendix C. Detailed temperature measurements gathered from the different end block geometries are included in Appendix D.

CHAPTER 2
Background

2.1 INTRODUCTION

Through the years, a great amount of research has been conducted in an effort to better understand the shear behavior of prestressed concrete beams. Before the background on box beam shear research is introduced, shear research in general is explained followed by a description of the current state of knowledge regarding shear behavior of prestressed concrete beams.

In North America, Japan and Europe alone, more than 10 different shear strength calculation methods are used for prestressed concrete beams. Very recently, an experimental shear database (Nakamura, 2011) was compiled and the best shear strength calculation methods according to this database study are presented herein. The database and its contents are described briefly.

After the general context of shear behavior is established, the specific challenges introduced by the use of box beams are described and previous work regarding box beam shear behavior is presented.

Finally, background is presented in the study of early-age behavior of prestressed concrete beams. More specifically; background is presented in the study of the magnitude and location of transverse stresses in the end region of beams, resulting from the prestress transfer process.

2.2 SHEAR STRENGTH OF PRETENSIONED GIRDERS: BACKGROUND

Shear strength is highly dependent on the mechanical properties of concrete and therefore, a link exists between the variability in the assessment of shear capacity and the variability of mechanical properties of concrete. Basic mechanical properties of concrete are highly variable even within the same mixture. Compressive strength and tensile strength tests often vary as much as plus or minus 10-20% from an average value. The

high variability and uncertainty observed in the assessment of shear strength is what drives the research community to continue efforts to improve shear strength calculation methods.

The goal of shear research in general, is to account for all possible variables within the pretensioned concrete construction practice and assure safe shear strength calculations throughout. As new materials (e.g. high performance concrete, self-consolidating concrete, etc.) and practices (e.g. composite construction) emerge and gain acceptance, the research community follows and validates or modifies the use of current calculation methods to the new practice. Seldom is a new practice researched thoroughly before its implementation. Specific research is often triggered by deficiencies observed in the field.

Pretensioned concrete bridge beams have been used in the United States for more than 50 years. Since their introduction, research projects have been conducted in order to better understand shear behavior. In the early days of pretensioned concrete shear research (1950s-1960s), small specimens were tested and shear strength calculation methods specifically meant for pretensioned concrete were introduced and validated against a database of the shear tests on the aforementioned small specimens. The specimens used at that time were mostly 12 in. deep with very few of them as deep as 25.5 in.

In the 1970s, research suggested that smaller specimens had an apparent increased shear strength compared to larger beams. Since practically all pretensioned concrete bridge girders were deeper than 24 in. (as the deepest beams included in the early-days database), the need to validate shear strength calculation methods with full-scale beams became evident. Budget and equipment limitations make shear tests on full-scale beams difficult. It was not until the 1990s that full-scale tests became more common.

Nevertheless, while most of the current methods for shear strength calculations have been validated with shear tests with full-scale girders, a very limited amount of shear tests on full-scale box beams has been conducted prior to this investigation. The

few studies of shear strength of box beams found in the literature are reviewed in later sections of this chapter.

2.3   UTPCSDB

The University of Texas Prestressed Concrete Shear Database (UTPCSDB) is a living file of shear tests in the literature. Although the file had existed for many years prior, the database was not published until 2008 by Avendaño and Bayrak. The database published in 2008 contained results from 506 tests from 30 references published between 1954 and 2008. Most of the references were from the technical literature published in the United States.

Since then, the database has been updated constantly, with its most recently published version being in 2011 by Nakamura. Nakamura expanded the database to include references from Japan and Europe, as well as US research published after 2008. The following discussion is based on the 2011 version of the database or UTPCSDB-2011 for shorter reference.

2.3.1   Contents of the UTPCSDB-2011

UTPCSDB-2011 contains results from shear tests reported in 99 references dated from 1954 to 2010, including partial data from the present study (UTPCSDB-2011 was published before this study was concluded). In this background section, it is important to describe the content of the database prior to the addition of the results from this study. Excluding the partial results from this study did not affect the conclusions reached by Nakamura discussed in the subsequent sections.

Results from a total of 1696 tests are included in the UTPCSDB-2011. Of those 1696 tests, 8 tests (0.5%) correspond to shear tests on box beams tested prior to this program. However, not all 1696 tests can be used for the purposes of prestressed concrete shear research. Nakamura filtered the database according to specific criteria; resulting in a few different samples gathering a different number of tests depending on the filtering criteria as summarized in Table 2-1. It can be seen from Table 2-1 that there is a very

small number of box beam tests reported in the literature. More importantly, only 1 box beam test was used in the evaluation databases.

Samples identified as "Evaluation Database – Level I" and "Evaluation Database – Level II" were used by Nakamura to conduct evaluations of shear design equations as described in the next section of this document.

Table 2-1: Database test samples used by Nakamura (2011)

Database Sample	Description	Total Number of Tests	Box beams prior to this study
Complete	All tests included in 99 found references	1696	8 (0.5% of 1696)
"Filtered"	Exclusion Filters (Complying specimens are removed): • Tests resulting in failure modes other than traditional shear failure modes • Non-prestressed members • Members with initial defects • Members subject to moving loads • Tests with incomplete information	1146	4 (0.3% of 1146)
"Evaluation Database – Level I"	New exclusion filters: • Concrete strengths less than 4 ksi • Concrete type other than conventional concrete • Overall Member depth less than 12 in. • Shear span-to-depth ratio less than 2.0 (for concentrated loads) • Shear reinforcement not satisfying minimum code requirements from ACI 318 and AASHTO LRFD • Continuous Beams • Segmental Beams • Externally post-tensioned	223	1 (0.4% of 223)
"Evaluation Database – Level II"	New exclusion filters: • Shear failure with signs of horizontal shear distress • Shear failure with signs of anchorage zone distress	171	1 (0.6% of 171)

2.3.2 **Evaluation of Shear Design Equations by Nakamura (2011)**

Twelve different sets of shear design equations were evaluated by Nakamura, including shear design equations from the ACI 318-08, the AASHTO LRFD Bridge Design Specifications (2007 and 2010 versions) and design specifications from regions outside the United States such as Japan, Canada and all of Europe. The results from the

9

evaluation sample identified as "Evaluation Database – Level II" as presented by Nakamura are discussed in this section.

In the evaluation process, the experimental maximum shear registered in the database is divided by the shear capacity calculated by a given method to obtain a *shear strength ratio*. The variation of shear strength ratios across a sample of data from the database is then studied to obtain statistical parameters (average shear strength ratio, standard deviation, coefficient of variation, etc). The statistical parameters from the different sets of shear design equations are then compared.

Ideally, a good set of shear design equations will provide conservative shear strength calculations (shear strength ratios greater than 1.0) for the majority of cases above a certain acceptance criteria such as 95% of all cases. Additionally, a good set of equations is not overly conservative (shear strength ratios much greater than 1.0, e.g. 3.0) and has reasonably low scatter; measured through a low coefficient of variation. Statistics from shear design provisions yielding acceptable results are summarized in Table 2-2. The four methods included in Table 2-2 are described in section 2.4 of this document.

Table 2-2: Results from "Evaluation Database – Level II", from Nakamura (2011)

V_{test}/ V_{calc}	ACI 318 Detailed Method (2008)	AASHTO-LRFD General Procedure (2010)	AASHTO-LRFD Simplified Procedure (2010)	AASHTO-LRFD Segmental Bridges[1] (2010)
Average (N = 171)	1.39	1.43	1.43	1.73
COV	21%	18%	25%	21%
Minimum	0.82	0.94	0.81	0.86
Maximum	2.32	2.07	2.39	2.73
Cases < 1.0	11	1	15	2
%Cases < 1.0	6.4%	0.6%	8.8%	1.2%

[1] Shear design equations from the Segmental Bridge Specifications modified according to the recommendations by Avendaño and Bayrak (2008), i.e. the K factor is not limited to 1.0 based on the stress level at the extreme tension fiber.

Additionally, shear strength ratios are studied within specific variables (e.g. concrete strength) to determine if the equations are biased towards low or high values. A good set of shear design equations provides equally conservative shear strength ratios for a given variable across the whole range of values for which the equations are intended to

be used. Nakamura studied the influence of concrete compressive strength, effective depth of the specimen, shear span-to-depth ratio, amount of shear reinforcement and the effective prestress level on the conservativeness of the different shear design equations. In an evaluation process, as that conducted by Nakamura, Figure 2-1 through Figure 2-4 can be used to evaluate the influence of the overall member depth on the level of conservatism and accuracy associated with different shear strength calculation methods.
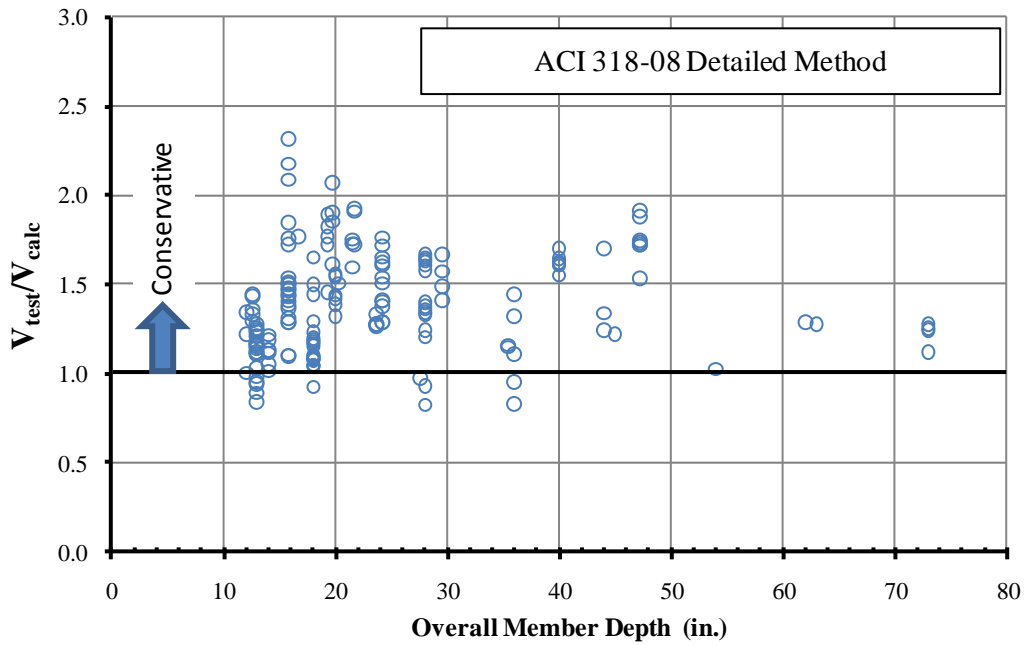
Figure 2-1: Shear Strength Ratio (using the ACI 318-08 Detailed Method) versus Overall Member Depth, from UTPCSDB-2011-EDB − Level II (N=171)
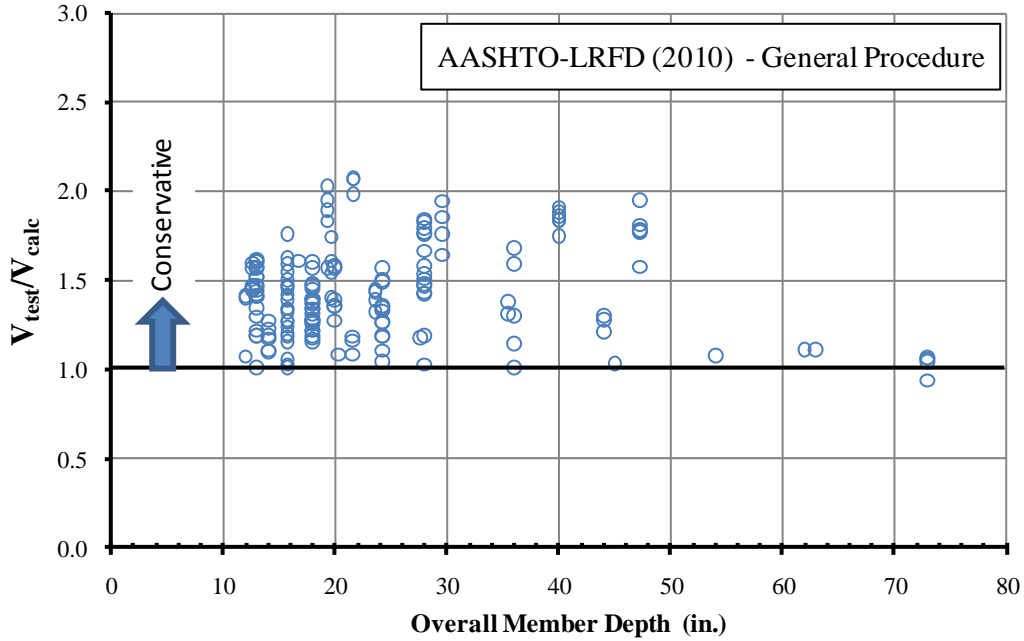
Figure 2-2: Shear Strength Ratio (using the AASHTO-LRFD (2010) General Procedure) versus Overall Member Depth, from UTPCSDB-2011-EDB – Level II (N=171)
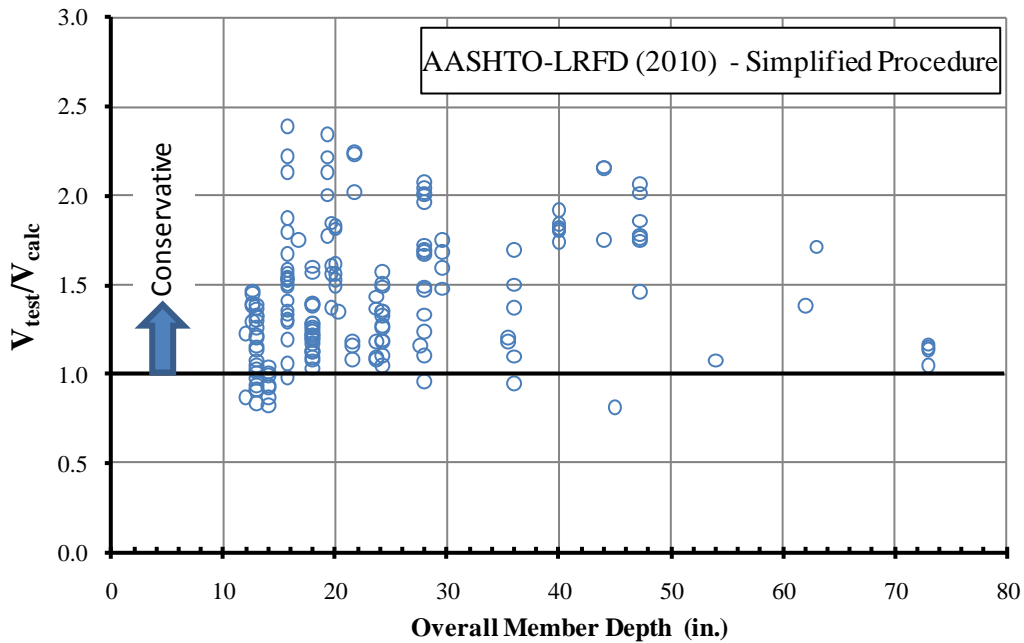
Figure 2-3: Shear Strength Ratio (using the AASHTO-LRFD (2010) Simplified Procedure) versus Overall Member Depth, from UTPCSDB-2011-EDB – Level II (N=171)
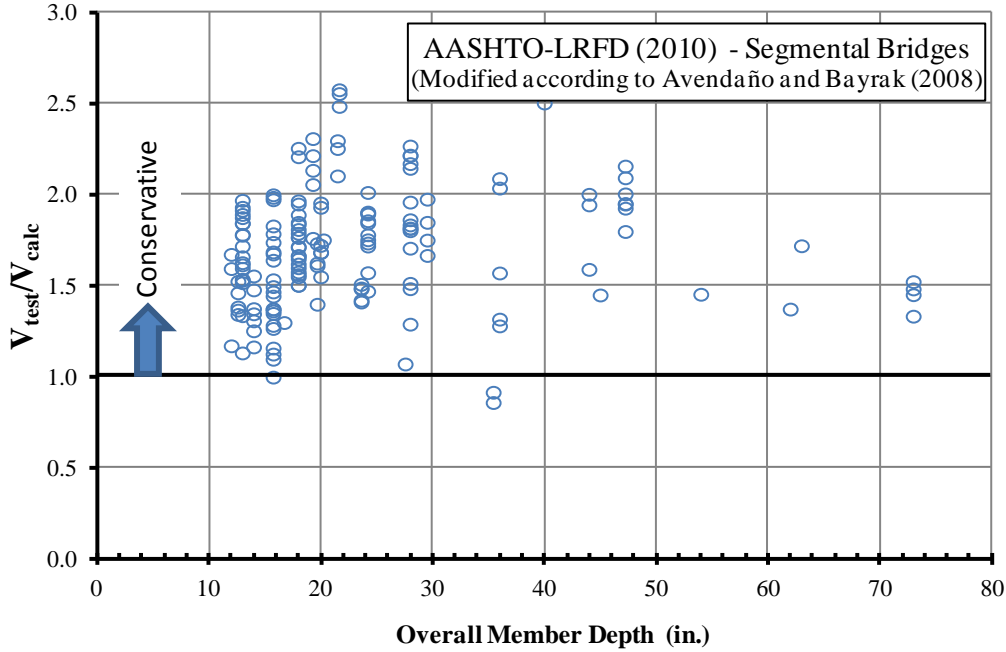
Figure 2-4: Shear Strength Ratio (using the AASHTO-LRFD (2010) Segmental Bridge Equations, modified according to Avendaño and Bayrak (2008)) versus Overall Member Depth, from UTPCSDB-2011-EDB – Level II (N=171)

After evaluating several shear strength calculation methods, Nakamura found the best method to be the General Procedure from AASHTO-LRFD (2010). The MCFT-based General Procedure presented an average shear strength ratio of 1.43 and the lowest scatter among the provisions evaluated (COV of 18%). Note that a shear strength ratio of 1.43 is greater than 1.0 without being too conservative. Although several other methods had similar statistics, the lack of bias within all of the studied variables is what makes the General Procedure the best method according to Nakamura (2011). Based on the analysis presented above, it can be said that on average, prestressed concrete beams exhibit over-strengths of 40% with respect to calculated shear capacities according to currently accepted design methods.

13

2.4 SHEAR STRENGTH CALCULATION METHODS

2.4.1 ACI 318 – 2008: Detailed Method

The Building Code Requirements for Structural Concrete from the American Concrete Institute (2008), referred from this point on as "ACI 318-08", contain two sets of equations recommended to calculate the shear strength of prestressed concrete members. One of these sets of equations is referred to as the "Detailed Method" and was found to be one of the best available methods for calculation of shear strength by Nakamura (2011).

Although the ACI 318-08 standard is meant for buildings, the equations from the detailed method were adopted by earlier versions of the AASHTO Bridge Design Specifications and hence have been used for many years in the design of highway bridges.

The nominal shear strength (V_n) is calculated as the sum of the concrete contribution to shear strength (V_c) and the steel reinforcement contribution to shear strength (V_s) as expressed follows:

$$V_n = V_c + V_s \qquad \textbf{Equation 2-1}$$

The concrete contribution to shear strength is taken as the lesser of V_{ci} and V_{cw} given by:

$$V_{ci} = 0.6\lambda\sqrt{f_c^{'}}b_w d_p + V_d + \frac{V_i M_{cre}}{M_{max}} \geq 1.7\lambda\sqrt{f_c^{'}}b_w d \qquad \textbf{Equation 2-2}$$

and
$$V_{cw} = (3.5\lambda\sqrt{f_c^{'}} + 0.3 f_{pc})b_w d_p + V_p \qquad \textbf{Equation 2-3}$$

where:

V_{ci} = nominal shear strength provided by concrete when diagonal cracking results from combined shear and moment (lb)

14

V_{cw} = nominal shear strength provided by concrete when diagonal cracking results from high principal tensile stress in the web (lb)

λ = 1.0 for normal weight concrete

f_c' = compressive strength of concrete (psi)

b_w = web width (in.)

d_p = distance from the extreme compression fiber to the centroid of the prestressing steel (in.)

V_d = shear force at section due to unfactored dead load (lb)

V_i = factored shear force at section due to externally applied loads occurring simultaneously with M_{max} (lb)

M_{cre} = moment causing flexural cracking at section due to externally applied loads (in.-lb)

$$M_{cre} = \left(\frac{I_{trans}}{y_t}\right) \cdot (6\lambda\sqrt{f_c'} + f_{pe} - f_d) \qquad \textbf{Equation 2-4}$$

M_{max} = maximum factored moment at section due to externally applied loads (in.-lb)

f_{pc} = compressive stress in concrete (after allowing for prestress losses) at centroid of cross section resisting externally applied loads or at junction of web and flange when the centroid lies within the flange (psi), and

V_p = vertical component of effective prestress force at section (lb)

I_{trans} = moment of inertia of the transformed section (in.^{4})

y_t = distance from the centroid of the transformed section to the extreme tension fiber (in.)

f_{pe} = compressive stress in concrete due to effective prestress forces only (after allowance for all prestress losses) at extreme fiber of section where tensile stress is caused by externally applied loads (psi)

f_d = stress due to unfactored dead load, at extreme fiber of section where tensile stress is caused by externally applied loads (psi)

The nominal shear strength provided by shear reinforcement, when all reinforcement is oriented perpendicular to the longitudinal axis of the member is given by:

$$V_s = \frac{A_v f_{yt} d}{s}$$
    Equation 2-5

where:

 A_v = area of shear reinforcement spacing s (in.^{2})

 f_{yt} = specified yield strength f_y of transverse reinforcement (psi)

 d = distance from extreme compression fiber to centroid of longitudinal tension reinforcement (in.)

 s = center-to-center spacing of transverse reinforcement (in.)

This expression for V_s is based on a 45 degree truss model in which cracks are oriented at a 45 degree angle with respect to the longitudinal axis of the beam. The ratio of d to s in Equation 2-5 can be interpreted as the number of stirrups, of area A_v, crossing the diagonal crack.

2.4.2 AASHTO LRFD Bridge Design Specifications

From the AASHTO LRFD Bridge Design Specifications (interim 2010), three methods for calculating the shear strength of prestressed concrete members are presented herein: The General Procedure, the Simplified Procedure, and the Segmental Bridge Procedure. In subsequent discussions, the AASHTO LRFD Bridge Design Specifications (interim 2010) are referred simply as AASHTO-LRFD (2010).

When using the general procedure or the simplified procedure described in this section, the nominal shear strength of a member is given by the lesser of:

$$V_n = V_c + V_s + V_p \qquad\qquad \textbf{Equation 2-6}$$

and

$$V_n = 0.25 f'_c b_v d_v + V_p \qquad\qquad \textbf{Equation 2-7}$$

where:

V_c = nominal shear resistance of concrete calculated using either the general procedure described in section 2.4.2.1 or the simplified procedure described in section 2.4.2.2 of this document (kip)

V_s = shear resistance provided by shear reinforcement (kip)

V_p = component of prestressing force in the direction of the shear force, positive if resisting the applied shear (kip)

f'_c = specified compressive strength of concrete for use in design (ksi)

b_v = effective web width taken as the minimum web width within d_v (in.)

d_v = effective shear depth taken as the distance, measured perpendicular to the neutral axis, between the resultants of the tensile and compressive forces due to flexure; it need not be taken to be less than the greater of *0.9d_e* or *0.72h*

d_e = effective depth from extreme compression fiber to the centroid of the tensile force in the tensile reinforcement

When using either the general procedure or the simplified procedure, the shear resistance provided by shear reinforcement (V_s) is given by:

$$V_s = \frac{A_v f_y d_v (\cot \theta + \cot \alpha) \sin \alpha}{s}$$

Equation 2-8

where:

A_v = area of shear reinforcement within a distance s (in.^{2})

f_y = specified minimum yield strength of shear reinforcing bars (ksi)

θ = angle of inclination of diagonal compressive stresses determined by:

$$\theta = 29 + 3500 \cdot \varepsilon_s \quad \text{(degrees)}$$

Equation 2-9

α = angle of inclination of transverse reinforcement to longitudinal axis (degrees)

s = spacing of transverse reinforcement measured in a direction parallel to the longitudinal reinforcement (in.)

ε_s = net longitudinal tensile strain in the section at the centroid of the tension reinforcement. ε_s may be determined by:

$$\varepsilon_s = \frac{\left(\dfrac{|M_u|}{d_v} + 0.5N_u + |V_u - V_p| - A_{ps} f_{po} \right)}{E_s A_s + E_p A_{ps}}$$

Equation 2-10

$|M_u|$ = factored moment, not to be taken less than $|V_u - V_p| \cdot d_v$ (kip·in.)

V_u = factored shear force (kip)

N_u = factored axial force, taken as positive if tensile (kip)

A_{ps} = area of prestressing steel on the flexural tension side of the member (in.^{2})

f_{po} = a parameter taken as modulus of elasticity of prestressing tendons multiplied by the locked-in difference in strain between the prestressing tendons and the surrounding concrete (ksi).

E_s = modulus of elasticity of reinforcing bars on the flexural tension side of member (ksi)

A_s = area of reinforcing bars on the flexural tension side of member (in.^{2})

E_p = modulus of elasticity of prestressing steel on the flexural tension side of member (ksi)

s_{xe} = crack spacing parameter given by:

$$s_{xe} = s_x \frac{1.38}{a_g + 0.63}$$ (in.)   **Equation 2-11**

s_x = the lesser of either d_v or the maximum distance between layers of longitudinal crack control reinforcement, where the area of the reinforcement in each layer is not less than $0.003b_v s_x$ (in.)

a_g = maximum aggregate size (in.)

As can be seen in Equation 2-8, the general procedure and the simplified procedure use a variable truss angle. This angle makes a big difference in prestressed concrete. The axial forces introduced by the prestressing reinforcement have a "flattening effect" on the principle stresses and crack angles. Typically, a prestressed concrete beam will have principal diagonal compressive stresses oriented at a 30 degree angle measured from the horizontal. Accounting for a 30 degree inclination makes the shear reinforcement contribution to shear strength around 70% greater than if a 45 degree truss model was assumed.

2.4.2.1 General Procedure – Concrete contribution to shear strength

The general procedure from AASHTO-LRFD is based on the modified compression field theory (MCFT). The capacity of diagonally-cracked concrete to carry shear is estimated based on an approximated strain of longitudinal reinforcement in the flexural tension side of the member.

The concrete contribution to shear strength (V_c) is given by:

$$V_c = 0.0316\beta\sqrt{f_c'}\,b_v d_v$$ **Equation 2-12**

where:

β = factor indicating the ability of diagonally cracked concrete to transmit tension and shear. For sections containing at least the minimum amount of transverse reinforcement specified in AASHTO-LRFD §5.8.2.5, β may be determined by:

$$\beta = \frac{4.8}{(1+750\varepsilon_s)} \qquad \textbf{Equation 2-13}$$

When sections do not contain at least the minimum amount of shear reinforcement, β may be determined by:

$$\beta = \frac{4.8}{(1+750\varepsilon_s)}\frac{51}{(39+s_{xe})} \qquad \textbf{Equation 2-14}$$

2.4.2.2   Simplified Procedure– Concrete contribution to shear strength

The simplified procedure from AASHTO-LRFD is very much like the detailed method from ACI 318 described previously in section 2.4.1. The equations from the simplified procedure underwent a calibration process by Hawkins et. al. (2005). The numerical factors in the equations were adjusted for a better fit across reinforced concrete and prestressed concrete shear tests included in a database compiled by Hawkins et. al. The AASHTO-LRFD specifications adopted the equations as recommended by Hawkins et. al.

When the simplified procedure is used, V_p in Equation 2-6 must be taken as zero (it is then accounted for in Equation 2-16). The concrete contribution to shear strength (V_c) is taken as the lesser of:

$$V_{ci} = 0.02\sqrt{f'_c}b_v d_v + V_d + \frac{V_i M_{cre}}{M_{max}} \geq 0.06\sqrt{f'_c}b_v d_v \qquad \textbf{Equation 2-15}$$

$$V_{cw} = (0.06\sqrt{f'_c}+0.30f_{pc})\cdot b_v d_v + V_p \qquad \textbf{Equation 2-16}$$

where:

f'_c = specified compressive strength of concrete for use in design (ksi)

b_v = effective web width taken as the minimum web width within d_v (in.)

d_v = effective shear depth (in.)

V_d = shear force at section due to unfactored dead load (kip)

V_i = factored shear force at section due to externally applied loads occurring simultaneously with M_{max} (kip)

M_{cre} = moment causing flexural cracking at section due to externally applied loads (kip·in.). M_{cre} shall be determined as:

$$M_{cre} = S_c \left(f_r + f_{cpe} - \frac{M_{dnc}}{S_{nc}} \right)$$ **Equation 2-17**

M_{max} = maximum factored moment at section due to externally applied loads (kip·in.)

f_{pc} = compressive stress in concrete after all prestress losses have occurred either at the centroid of the cross section resisting live load or at the junction of the web and flange when the centroid lies in the flange (ksi)

f_{cpe} = compressive stress in concrete due to effective prestress forces only (after allowance for all prestress losses) at extreme fiber of section where tensile stress is caused by externally applied loads (ksi)

f_r = modulus of rupture of concrete, taken as $0.2\sqrt{f_c'}$ (ksi)

M_{dnc} = total unfactored dead load moment acting on the monolithic or composite section (kip·in.)

S_c = section modulus for the extreme fiber of the composite section where tensile stress is caused by externally applied loads (in.^{3})

S_{nc} = section modulus for the extreme fiber of the monolithic or composite section where tensile stress is caused by externally applied loads (in.^{3})

When the simplified procedure is used, V_s shall be determined using Equation 2-8 with cot(θ) taken equal to 1.0 when V_{ci} is less than V_{cw} or, when V_{cw} is less than V_{ci}, cot(θ) given by:

$$cot(\theta) = 1.0 + 3\left(\frac{f_{pc}}{\sqrt{f_c'}}\right) \le 1.8 \qquad \textbf{Equation 2-18}$$

2.4.3 AASHTO LRFD Segmental Bridge Specifications

AASHTO-LRFD §5.8.6.5 allows the use of a much simpler set of equations to determine the nominal shear resistance of post-tensioned segmental concrete box girders in regions where it is reasonable to assume that plane sections remain plane after loading. Evaluations by Avendaño and Bayrak (2008), and Nakamura (2011) suggest that these same equations can be used with a reasonable level of conservatism in the design of non-segmental bridge girders. The simplicity of the equations is appealing to many designers.

The nominal shear resistance shall be determined as the lesser of:

$$V_n = V_c + V_s \qquad \textbf{Equation 2-19}$$

and $\qquad V_n = 0.379\sqrt{f_c'}b_v d_v \qquad \textbf{Equation 2-20}$

The concrete contribution to shear strength is given by:

$$V_c = 0.0632K\sqrt{f_c'}b_v d_v \qquad \textbf{Equation 2-21}$$

where:

d_v $= 0.8h$ or the distance from the extreme compression fiber to the centroid of the prestressing reinforcement, whichever is greater (in.)

K = stress variable given by Equation 2-21.

$$K = \sqrt{1 + \frac{f_{pc}}{0.0632\sqrt{f_c'}}} \le 2.0 \qquad \textbf{Equation 2-22}$$

The shear resistance provided by shear reinforcement is given by:

$$V_s = \frac{A_v f_y d_v}{s} \qquad \textbf{Equation 2-23}$$

The stress variable is specified in AASHTO-LRFD §5.8.6.3 not to be taken greater than 1.0 for any section where the stress in the extreme tension fiber, calculated on the

basis of gross section properties, due to factored load and effective prestress force after losses exceeds $0.19\sqrt{f_c^{'}}$ in tension. An evaluation of these provisions by Avendaño and Bayrak (2008) showed that accuracy is increased and scatter is reduced if this limit is omitted. The evaluations performed more recently by Nakamura (2011) showed the same result. Accordingly, these changes are incorporated in the results presented in Table 2-2 and Figure 2-4.

2.5   SHEAR IN BOX BEAMS

2.5.1   **Historical background**

As is true of many other precast prestressed members, the use of prestressed concrete box beams can be traced back to the late 1940s and early 1950s (Bender and Kriesel, 1969). With the introduction of high-strength prestressing strands, the precast prestressed concrete industry became highly competitive in the field of highway bridges. Box beams have always been a significant fraction of the total precast prestressed concrete girders used in bridges. Figure 2-5 illustrates the number of prestressed concrete box beam bridges built per 5 year period over the last 55 years. At their peak, 16% of all bridges built between the years 1990 and 1995 were prestressed concrete box beams. After 1995, the total number of bridges built per 5 year period has declined. Consequently, the number of box beam bridges built has declined as well. More recently, box beams represented 12% of the total number of bridges built between 2005 and 2010.
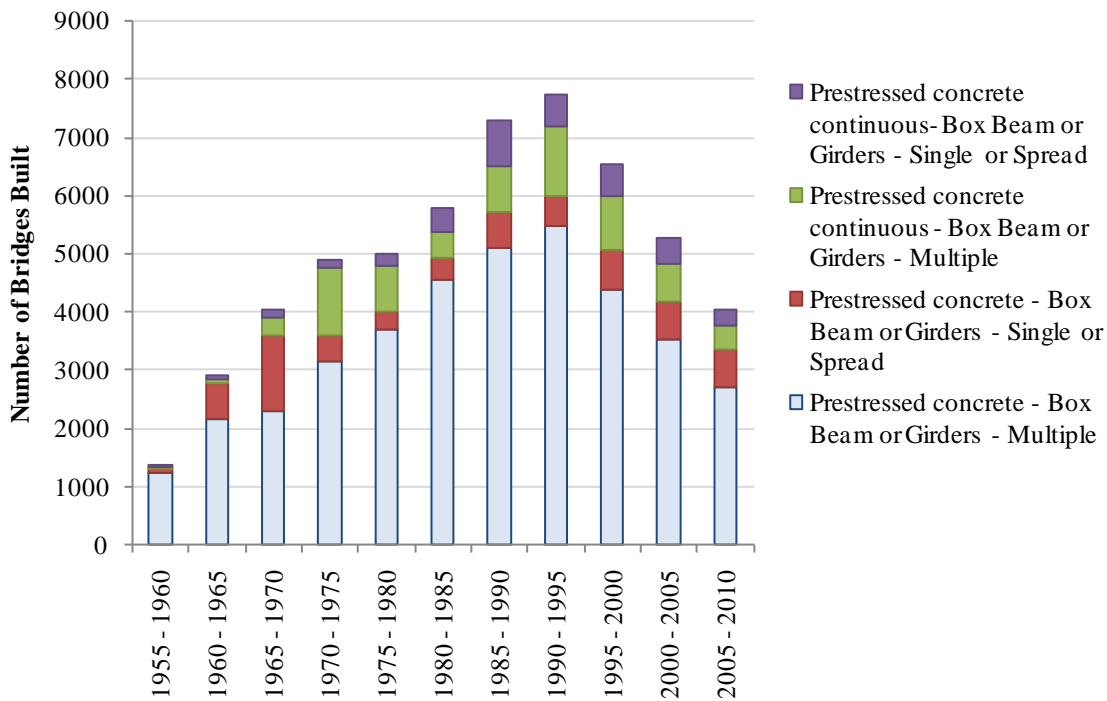
Figure 2-5: Prestressed Concrete Box Beam construction per year (National Bridge Inventory, 2010)

The use of box beams is an attractive option for bridge widening and bridge replacement given the relatively short period of time over which they can be built (Bender and Kriesel, 1969). Typically box beams are used in two configurations: adjacent box beams (see Figure 2-6) or spread box beams (see Figure 2-7). In adjacent box beam bridges, no space is left between adjacent beams, beams have transverse shear keys that are grouted in place after the beams have been erected, beams are connected transversely either through passive high-strength rods or through post-tensioned cables and usually a thin asphalt overlay constitutes the wearing surface. A cast-in-place concrete deck can be used as well. The adjacent precast box beam system is most popular for cases in which speed of construction is a priority. Since the beams are adjacent to one another, there is no need for false work between beams. Furthermore, since the beams have a prefabricated topping slab, when an asphalt overlay is used, the bridge construction can be finalized in less than one week (Bender and Kriesel, 1969).

Russell (2011) published a state-of-the-art report on the use of adjacent box beam bridges. His study included a survey of state highway agencies describing their practices regarding the use of box beams. Responses from a total of 58 agencies were evaluated. Results from the survey show that box beams are widely used across the United States and Canada. Among the highlights of the survey, the following interesting facts can be found:

- More than 70% of the responding agencies use box beams with spans greater than 80 ft
- More than 40% of the responding agencies limit the maximum skew to 30 degrees. The second most common maximum allowed skew is 45 degrees by around 15% of the responding agencies.
- 80% of the responding agencies have used box beams in simple spans with cast-in-place concrete wearing surfaces. Only 20% have used box beams in simple spans with a bituminous wearing surface.

In a spread box beam bridge, as illustrated in Figure 2-7, beams are spread apart similar to a typical I-girder bridge, no shear keys are used, no transverse post-tensioning is used and a composite cast-in-place (CIP) concrete deck is used over the beams.
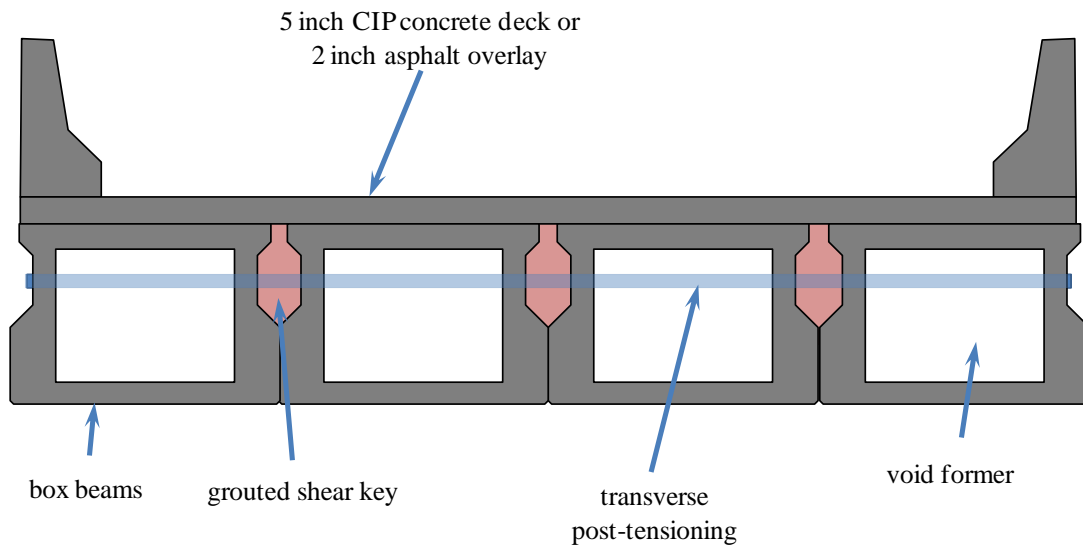
Figure 2-6: Typical adjacent box beam bridge configuration.
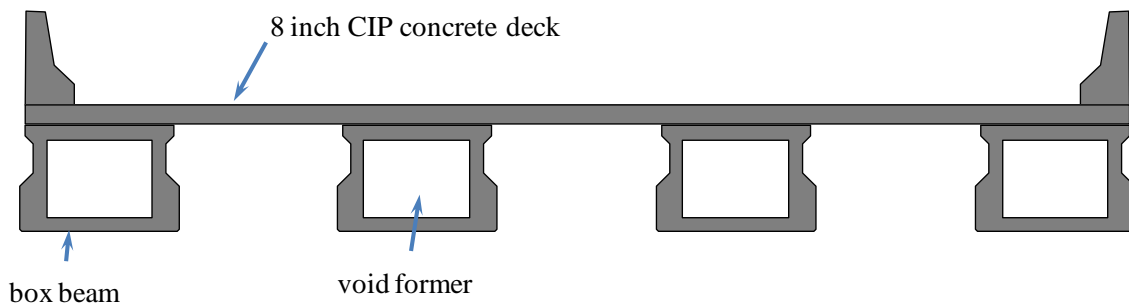
Figure 2-7: Spread box beam bridge configuration

2.5.2 **Challenges of box beam shear design**

While the use of box beams is not new to the prestressed concrete industry, the amount of research conducted towards understanding the shear behavior of box beams is modest at best. This section is intended to list the differences between typical single-webbed girders and box beams and how those differences may affect the applicability of shear design equations.

In box beams, shear must be carried by two webs connected by the top and bottom slabs. If no torsion is present, both webs (of equal thickness) can be assumed to be subject to equal shear forces. Thus, it has been common practice to use typical shear

27

design methods assuming that a box beam with two webs of thickness b_w can be designed as an equivalent I-girder with a single web of thickness $2b_w$ as illustrated in Figure 2-8.

Box beam cross section   Equivalent I-girder cross section
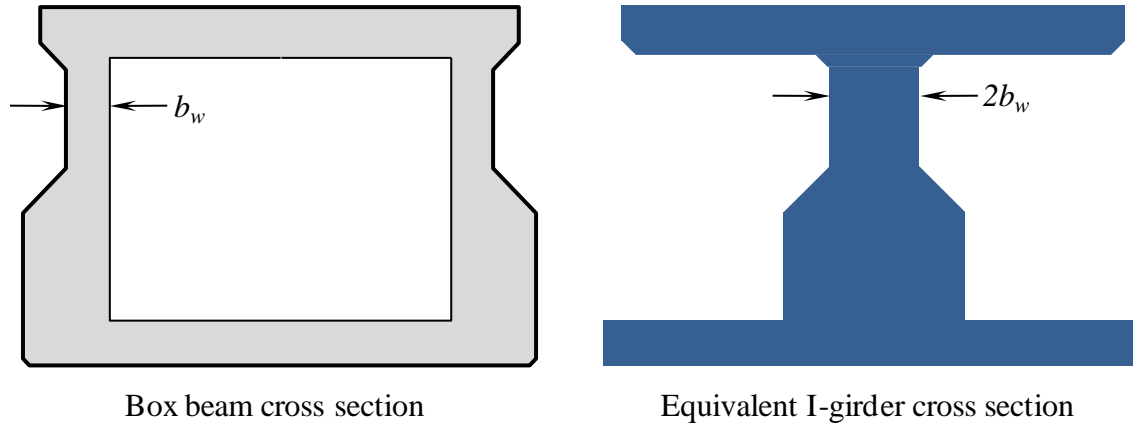
Figure 2-8: Equivalent I-girder cross section used in box beam shear design

Prestressing strands can be placed further away from the webs. With wider box beams, a larger percentage of the strands can be placed several thicknesses-of-the-web away from the web itself. If the bottom slab is too flexible, the transfer of forces transversely across the bottom slab might be ineffective. That is; the prestressing force introduced in the center of the bottom slab might not be transferred well into the webs, negating the beneficial effects of prestressing in the web.

Wide beams, such as box beams, are usually supported by three bearing pads; one centered on one end of the beam, and two spaced across the width of the beam at the opposite end. The three bearing pads are used to stabilize the beam, and minimize twisting of the section. When bridges are oriented at a skew as illustrated in Figure 2-9, a condition unique to wide beams is created. At the end supported by two bearing pads, illustrated on the top right of the figure, more of the load flows towards the support under the obtuse corner of the beam (marked with the letter A in Figure 2-9) compared to the support under the acute corner of the beam (marked with the letter B in Figure 2-9). One way to interpret this is to think of the two webs acting as two simply supported beams: one spanning from A to C and one spanning from B to C. The beam with the shorter span (A-C) is stiffer and therefore will attract a higher fraction of the load towards its support. With higher skew angles, the difference in the stiffness of the two simply supported

beams, and hence the difference in the load going to A as opposed to B, is more pronounced.
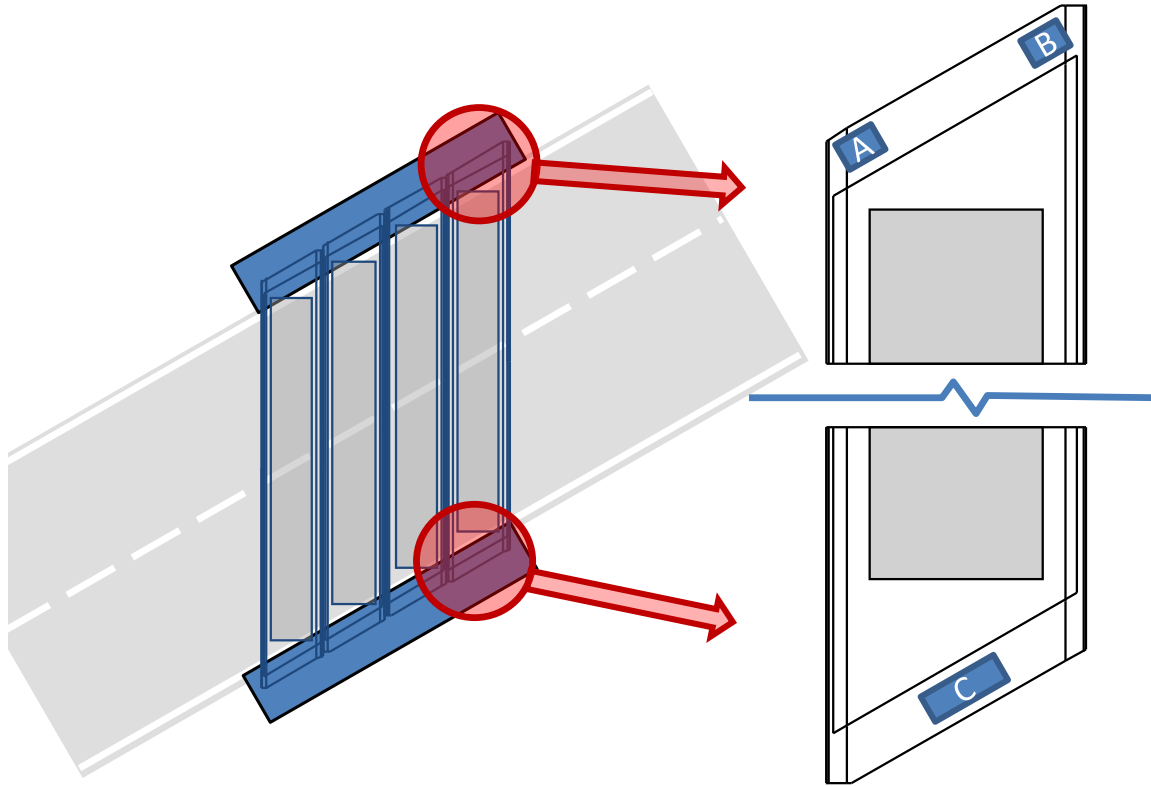
Figure 2-9: Skewed support condition on box beams.

2.6 PREVIOUS BOX BEAM RESEARCH

2.6.1 Hanson and Hulsbos (1971)

Hanson and Hulsbos recognized the discrepancy between the collection of specimens used to validate the shear strength equations available at the time and typical bridge beams. More specifically, the overall member depth of the tests conducted to that date was mostly of 12 in. with very few specimens as deep as 25.5 in. Conversely, prestressed concrete bridge girders of up 72 in. in depth were already being used in some states. While size effects among other issues were being raised by many researchers of

the time, full scale tests were outside the limits of contemporary research budgets and test facilities.

At the time Hanson and Hulsbos research program was conducted, very few others had tested specimens as deep as the ones included in their study (36 in.). Furthermore, other shear tests on box beams did not exist. Their test program included nine strength tests on two series of specimens: two 36 inch deep I-shaped beams and two 36 inch deep box beams. The box beams cross section tested, illustrated in Figure 2-10, share several characteristics with the box beams currently used in the state of Texas:

    i.   The web thickness is 5 in.

    ii.   The bottom slab thickness is 5 in.

    iii.   Shear reinforcement consisted of two bars spliced vertically in the web
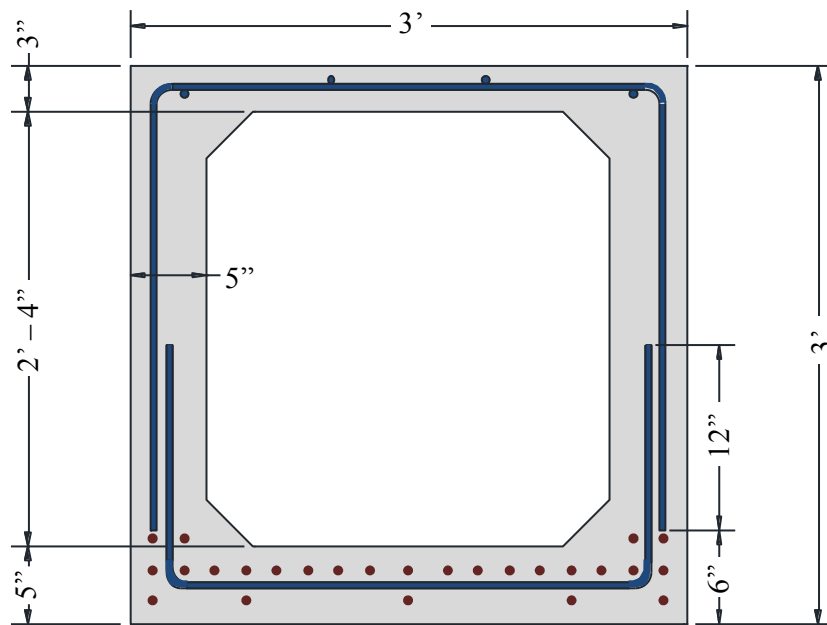
Figure 2-10: Box Beams tested by Hanson and Hulsbos (1971)

The box beams included in the current study were more heavily prestressed, with larger-diameter prestressing strands, than those tested by Hanson and Hulsbos. The differences are summarized in Table 2-3.

Table 2-3: Differences in prestressing strands used by Hanson and Hulsbos and those used in the box beams included in the current study.

	Hanson and Hulsbos (1971)	Box beams in current study
Prestressing Strand Type	Stress-relieved	Low-relaxation
Diameter (in.)	7/16	1/2
Ultimate Strength – f_{pu} (ksi)	212	270
Jacking Stress (ksi)	144	202.5

Despite these differences, the results from Hanson and Hulsbos test program raise several important issues. One of their tests consisted of a 27-ft span with a 9-ft region of constant moment centered on midspan and two symmetric shear regions towards the supports (9-ft shear spans). The amount of shear reinforcement in one end of the beam was twice the amount placed in the other end. However, a flexure-shear failure occurred in the region with more shear reinforcement after some torsional cracking was noted.

Flexure-shear failures have rarely been reported in the literature and understanding why the box beams tested by Hanson and Hulsbos failed in this failure mode is critical. In short, too little shear reinforcement was used in these beams. The shear strength contribution of the reinforcement (V_s) was approximately 18% of the contribution to shear strength by concrete (V_c) on the stronger side of the beam (in this context, V_c and V_s were calculated using the detailed method from ACI 318-08). This amount of shear reinforcement was barely enough to comply with the minimum shear reinforcement requirements of ACI 318 of 1963 (the controlling limit in 1963 would be the same today if ACI 318-08 were to be used).

Once a beam is cracked in flexure, in order for a beam to fail in flexure rather than in flexure-shear, the beam needs to have enough shear reinforcement to accommodate the additional shear associated with the increase from the cracking moment to the moment capacity of the beam. Nevertheless, providing this amount of steel does not preclude web-shear failures and hence, is not a real design objective. It is important to observe that beams with small amounts of shear reinforcement are more likely to fail in flexure-shear. In highly prestressed beams, like most of the pre-tensioned beams today, the cracking moment and the moment capacity are not too far apart and the amount of

shear reinforcement necessary to have flexural failure control is modest. Furthermore, maximum shear reinforcement spacing limits often govern over minimum reinforcement limits in deeper beams, making beams have shear reinforcement well in excess of the minimum area of shear reinforcement requirements.

Besides the importance of torsional effects and flexure shear, Hanson and Hulsbos study highlighted the weakness introduced by splices in the shear reinforcement as, in one of their tests, some of the stirrups pulled out of the concrete in the region where inclined cracks crossed the lapped splice. If the lapped splice in the shear reinforcement controls failure, the ultimate shear capacity of the beam may be adversely affected. Typical shear strength equations assume that shear reinforcement is sufficiently anchored to reach yield stress or strain. Once high strains are reached in the shear reinforcement, failure is bound to happen by stirrups rupturing or concrete crushing in the web. Statistically speaking, both of these failure modes are safely covered by today's shear strength provisions.

It is prudent to determine experimentally if the lapped splices used in box beams, as in the standard reinforcement details of Texas beams, can control failure and result in unconservative shear strength calculations when current shear design provisions are used. This was the case in one of the tests conducted by Hanson and Hulsbos (Test 1 on Beam G-1). The ratios of the experimental shear capacity to the calculated shear capacity and other test details are summarized in Table 2-4.

Table 2-4: Box beam shear test results summary (Hanson and Hulsbos, 1971)

Beam ID	Concrete Strength (psi)	Test	a/d	ρf_y (psi)	V_{test}/V_{calc}	Observations
G-1	7920	1	3.34	105	0.99	Torsion was observed, shear reinforcement anchorage failed
		2	3.34	59	1.15	Flexure-shear
G-3	7930	1	5.56	56	1.14	Flexure-shear
		2	2.78	70	0.96	Results influenced by damage sustained during Test 1

2.6.2 Tang (1974)

Tang's article on the shear design of large concrete box girders covers two topics that are very important to this study: *(i)* the influence of the overall member depth in the conservativeness of shear design equations and *(ii)* the influence of the flange width (i.e. slab width) to web thickness ratio on shear strength.

On the first topic, the author questioned the applicability of shear strength equations validated only with data from small test specimens. Although "small" is a rather loose term, it must be understood that the concern of the author was the difference in depth between the inventory of shear tests to that date (most of them not deeper than 24 in.) and the depth of prestressed concrete box girder bridges being built at the same time (the author cited segmental box beam bridges with beam depths of over 15 feet).

Tang explained how dowel action and aggregate interlock do not scale proportionally to overall member depth. In smaller specimens, one or two bars (or strands) of longitudinal reinforcement represent a significant fraction of the specimens area. Additionally, due to the limitation in the availability of bars of smaller diameters, the ratio of specimen dimensions to bar diameters is not nearly as big as in real bridges. This, as Tang explained in 1974, creates apparent increases in the shear strength of small specimens, not to be found in larger specimens.

A very similar situation is found with aggregate sizes. Coarse aggregates are only available in so many sizes. In smaller specimens, the contribution of aggregate interlock is rather important. In a full-scale girder, not only is the aggregate size smaller when compared to the dimensions of the girder, but the use of higher strength concrete also negates possible contribution of aggregate interlock as shear cracks mostly go through aggregates once concrete strength exceeds 8 ksi.

The inventory of shear tests that exists today does not include bridge girders as deep as those mentioned by Tang, but there has certainly been a substantial effort from the engineering community to test full scale specimens since the mid 1970's. More significantly, since the early 1990's, an increasing trend in the depth of specimens tested has been reported by Nakamura (2011) as can be seen in Figure 2-11.

33
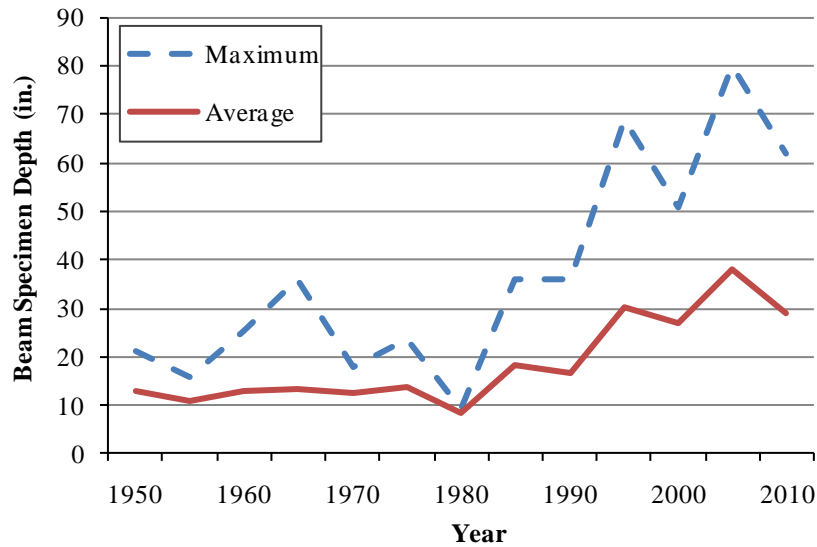
Figure 2-11: Historic progression of beam specimen depths in shear related research (UTPCSDB-2011)

The box beams tested as part of TxDOT Project 0-5831 are an important contribution to the inventory of full scale tests of beams. Although there is test data from deeper beams in the literature, none of them correspond to box beams.

The second topic of Tang's article, the influence of the flange width to web thickness ratio (b/b_w) on shear strength, is even more important within the context of the present study. The inventory of tests available at the time of Tang's article consisted mainly of rectangular tests ($b/b_w = 1$) and small I-shaped girders with small b/b_w ratios (~3). At the same time, box girder bridges with b/b_w ratios up to 18 were cited by Tang.

Tang explained, among other things, how longitudinal reinforcement in box beams is placed mostly in the bottom slab that is inherently flexible due to its slenderness. The flexibility of the bottom slab precludes it from transferring shear in the transverse direction; therefore any dowel action contribution by the longitudinal reinforcement placed in the bottom slab is negligible. Likewise, longitudinal reinforcement placed in the bottom slab can poorly contribute to restraining crack widths in the webs.

At the time Tang presented his work, the modified compression field theory (MCFT) had not been introduced. None of the shear strength equations that existed at that

34

time accounted for the state of distress to which the web was subjected, when estimating the concrete contribution to shear strength as MCFT does. The shear strength equations based on MCFT, as we know them today, account for the amount of longitudinal reinforcement in the beam as a measure of restraint to the axial strain in the web. Large axial strains in the web ultimately hinder the ability of cracked concrete to carry shear. The pertinent question now is: *how much of the longitudinal reinforcement placed in the bottom slab of box beams can be accounted to be effectively restraining the longitudinal strains in the webs?* The conservativeness of the MCFT-based equations available for shear strength calculations today are evaluated within this study. The aforementioned question will be addressed within the scope of the current research project in order to determine if the bottom flange-to-web thickness ratio of box beam girders studied herein is large enough to introduce any loss of strength or if the MCFT-based equations (and other available shear strength equations) can be used safely without any special considerations.

2.6.3 **Chamberlain (1997)**

In his experimental program, Chamberlain (1997) tested two box beams of the same cross section as the first series of box beams tested in TxDOT Project 0-5831 (4B28 box beams). The box beams tested by Chamberlain were part of a bridge constructed in 1976 and decommissioned in 1996 after TxDOT inspections revealed that longitudinal cracks on the bottom of the beam were propagating at a fast rate.

The decommissioned beams were transported to FSEL, where destructive load tests were conducted in order to determine the shear carrying capacity of the beams in their deteriorated state. The beams had a significant number of debonded strands, as illustrated in Figure 2-12, and had a 42 degree skew which makes them even more relevant to the present study. The shear reinforcement used is illustrated in Figure 2-12 as shown by Chamberlain in his report. Drawings in his report were marked as being not to scale. Hence, we will not pass a judgment on the short extension into the web of the reinforcement across the bottom of the beam. It is hard to believe that bars with such a

short splice would have not presented anchorage problems. However, since Chamberlain did not report any anchorage problems of the shear reinforcement, we will assume that the reinforcement was adequately anchored.

DEBONDING DISTANCES SHOWN BELOW

2'   6'   4'   6'   4'   6'   2'
   4'   2'   2'   2'   2'   4'
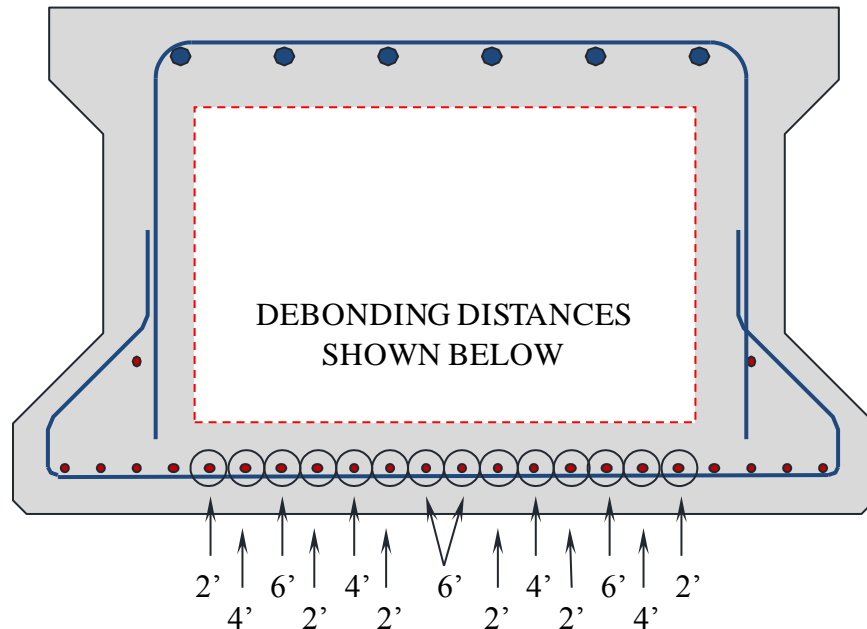
Figure 2-12: Box beam cross section and strand pattern (Chamberlain, 1997).

In Chamberlain's test setup, load was applied through a hydraulic ram, pushing down on a spreader beam system with 4 contact points forming a rectangle; 4 feet long, measured along the longitudinal axis of the beam, and as wide as the top of the beam (43.75 in.) in the transverse direction. The spreader beam system used by Chamberlain was similar to that used by Schnittker (2008), illustrated in Figure 2-13.

The spreader system was used to simulate a tandem axle. In these terms, the axle closest to the support was positioned at a distance of approximately 76 in. and 118 in. during the first and second test respectively. These distances correspond to shear span-to-depth ratios of 3.1 and 4.8 respectively, falling within the range of applicability of sectional behavior.

36
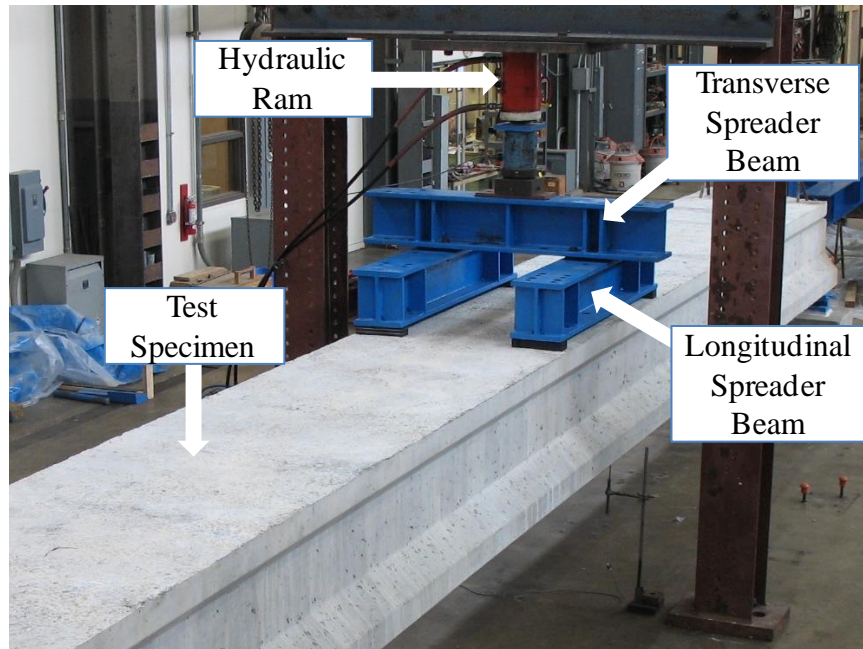
Figure 2-13: Spreader beam loading system used by Schnittker (2008)

During each test, new cracks formed on the underside of the beam and the existing cracks propagated further into the beam. Chamberlain reported that the beams also had spalling damage on the underside of the beam before the tests were conducted. From his illustrations, it can be estimated that the spalling damage was located close to the sides and covering the last 4 ft of the beam under the outermost 4 strands. Chamberlain reported that the spalling damage was a consequence of the beams being removed from the bridge site. Regardless of the cause of the damage, spalling under the strands in the end region would have hindered bond of the strands, decreased the effective prestress in the section, and ultimately reduced the beams shear carrying capacity.

To calculate the beams shear capacities, the AASHTO Standard Specifications for Highway Bridges of 1996 were used. The shear design provisions of this standard are equivalent to the equations found today in ACI 318-08 for web-shear (V_{cw}) and flexure-shear (V_{ci}) and an assumed 45 degree truss model for the stirrup contribution to shear strength. The calculated strengths and maximum applied shears are summarized in Table 2-5. The shear capacities of the beams were recalculated using the general procedure

from the AASHTO LRFD Bridge Design Specifications (interim 2010). Remarkably, the updated shear capacity calculations matched the results from 1997 within 0.7%.

Table 2-5: Test results summary from Chamberlain (1996)

	Nominal Shear Capacity, V_{calc} (kips)	Shear Force at Failure, V_{test} (kip)	V_{test}/V_{calc}
Test 1	154	131	0.85
Test 2	154	147	0.95

In both tests, failure was characterized by web-crushing on the side of the beam corresponding to the obtuse corner of the skew, as pointed out in Figure 2-14. Given the geometry of the skew in the box beams tested, the acute corner of the skew is more than three feet further away from the load point than the obtuse corner. It fair to say that: a higher fraction of the total load flowed towards the indicated side of the beam.
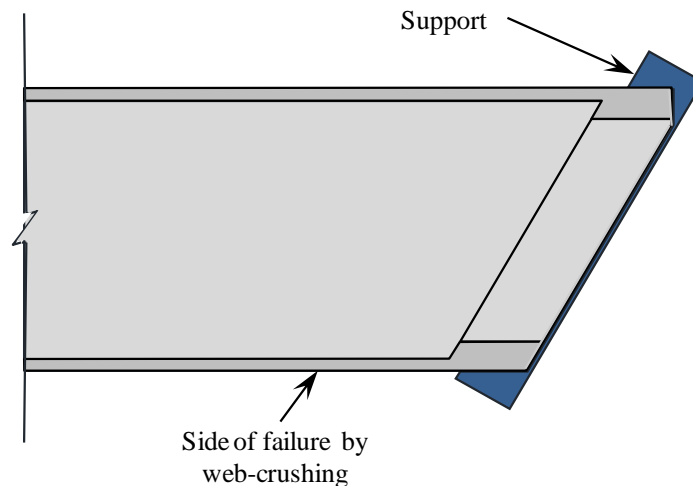
Figure 2-14: Plan view illustrating the end region of box beams tested (Chamberlain, 1997)

As indicated by Chamberlain, the ultimate shear strength might have been influenced by slip of the strands, correlated to the pre-existing damage observed on the underside of the beams. As for the cause of the initial deterioration, Chamberlain pointed to the number of debonded strands, the large concentration of debonded strands in the middle third of the beam and the lack of bonded longitudinal reinforcement in the same

region of the beams. The addition of mild longitudinal reinforcement (*hairpin*-shaped) in regions of heavy debonding was recommended.

All of the issues pointed out by Chamberlain and the results of his experimental program reinforce the questions originally posed within this research project. A study of the side-to-side distribution of reaction under skewed support conditions is needed. Comparative slip measurements of fully bonded strands, debonded strands, and strands placed in different locations across the width of box beams is pertinent.

2.6.4 **Saiidi and Bush (2006)**

Saiidi and Bush tested two box beams in shear. Beams tested were 34 ft long, 33 in. deep and they were topped with a 4 inch deep cast-in-place composite deck with a cross section illustrated in Figure 2-15. Their specimens originated from a 68 ft long beam, decommissioned from a bridge after 20 years of service. The decommissioning of the bridge was unrelated to the quality of the box beams tested in their study.

As in most box beams, shear reinforcement consisted of two bars spliced vertically in the web. Shear reinforcement was reported to be Grade 40 No. 3 bars spaced at 7 in. on center. Concrete core samples indicated an average compressive strength of 7890 psi. A total of 30-0.5 in. diameter, Grade 270, stress relieved strands were used. The existing prestress on the strands was determined through a previous testing program, to be ranging from 120 to 129 ksi.
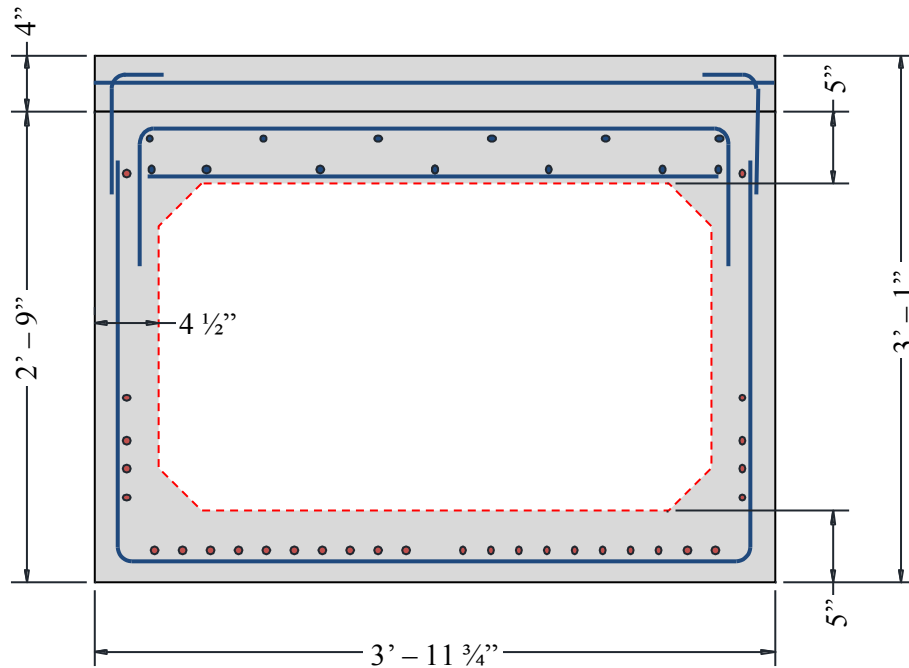
Figure 2-15: Box beams tested by Saiidi and Bush (2006)

The most relevant characteristic of Saiidi and Bush test program lies within their test procedure. One beam was loaded monotonically until it failed. The second beam went through 500,000 cycles of load large enough to cause a maximum stress in the bottom fiber of the concrete equal to $6\sqrt{f_c'}$ psi (where the compressive strength of concrete is used in *psi* units). During the cyclic loading, 9 overloads were carried out to a load large enough to cause a maximum stress in the bottom fiber of the concrete equal to $12\sqrt{f_c'}$ psi. Finally, the beam was loaded until its failure.

The beam subjected to cyclic loading failed at a shear 4% lower than the beam loaded only monotonically. Their results revealed that the cyclic loading and overloads did not reduce significantly the shear strength of the beam.

It is also important to say that the shear carrying capacity was calculated with conservative results with 5 different methodologies, including the web-shear and flexure-shear equations from ACI 318-08 and the MCFT based procedure from the 1998

AASHTO Bridge Design Specifications. Both of these methods will be used to assess the shear strength of the box beams in the present study.

2.6.5 Burgueño and Bendert (2007)

Burgueño and Bendert investigated the performance of box beams fabricated with conventional concrete compared to that of beams fabricated with self-consolidating concrete. A total of 4 shear tests were conducted in their experimental program. The box beams tested were 27 in. deep and 36 in. wide, and had 4.5 inch thick webs, a 4.5 inch deep bottom slab and a 5 inch deep top slab. The researchers indicated that the beams tested sustained shears 8-22% in excess of their calculated shear capacities according to the AASHTO-LRFD Simplified Procedure. However, all of the beams ultimately failed in flexure by crushing of the compression zone. Since the beams failed in a flexural mode, their results fall outside the scope of research of TxDOT Project 0-5831.

2.6.6 Schnittker and Bayrak (2008)

The first series of specimens tested in shear within the current experimental program were inherited from a previous research project. In that project, the 10 4B28 box beams were loaded at midspan until flexural cracks were developed. Results and observations from these load tests were presented by Schnittker and Bayrak and are summarized in this section.

The main purpose of Schnittker and Bayrak's research was to study the feasibility of allowing higher compressive stresses at the time of transfer of prestress. Current limits are set to keep the maximum compressive stress below $0.6f_{ci}^{'}$. Forty five I-shaped girders and ten box beams were fabricated and tested after they had been subjected to compressive stresses below and above the $0.6f_{ci}^{'}$ limit at the time of transfer of prestress. By doing this, the influence of the maximum compressive stress at the time of transfer on prestress losses was studied.

It was found that, once the compressive stress in the tensile zone at the time of transfer of prestress exceeded $0.65f_{ci}^{'}$, the flexural-cracking moments were overestimated

by all calculation methods by as much as 15%. This result was a consequence of the flexural-tension zone being strained into the non-linear range, causing micro-cracking to occur, hindering its tensile strength. Schnittker and Bayrak (2008) recommended to relax the limit on maximum compressive stresses up to $0.65 f_{ci}^{'}$ at prestress transfer for all beams except for those fabricated with self-consolidating concrete (SCC).

The exception for beams fabricated with SCC was a direct result of the observations made on the behavior of the box beams fabricated with SCC, compared to those fabricated with conventional concrete.

According to Schnittker and Bayrak, the box beams fabricated with SCC exhibited:

> *"increased amounts of top flange cracking at release, substantially lower modulus of elasticity (along with increased deflections under live loading), slightly higher cambers near 28 days, and lower than expected cracking loads."*

As shear capacity is influenced by the tensile strength of concrete, it is important to keep in mind Schnittker and Bayrak's observations while examining the shear behavior of the box beams fabricated with self-consolidating concrete inherited to the current research project.

2.7   TRANSVERSE STRESSES IN END REGIONS OF PRETENSIONED BEAMS

At prestress transfer, the end region of pretensioned members is subject to transverse forces. Transverse end region stresses are generally divided in two categories: bursting stresses and spalling stresses. Bursting stresses are tensile stresses that occur through a certain distance into the beam from the beam end, concentrated close to the line of action of the prestressing force and acting generally perpendicular to the applied prestressing force. Spalling stresses are also tensile stresses but they are more localized closer to the end face of the beam, they do not have a significant effect far into the beam, and they are concentrated away from the line of action of the prestressing force. The distribution of bursting and spalling stresses and the deformed shape of the beam end is illustrated in Figure 2-16. It is worth noting that only *vertical* bursting and spalling stresses are illustrated in Figure 2-16. Horizontal transverse stresses follow the same principles. The terms *bursting* and *spalling* stresses as described herein will be used throughout this document.

In pretensioned members, prestress transfer takes place over a certain length called the transfer length. The transfer length is a function of the diameter (d_b) of the prestressing strands used. For typical prestressing practices, the resulting transfer length is approximately $60d_b$. Results from O'Callaghan and Bayrak (2007) indicate that bursting stresses are significant through the transfer length, while spalling stresses are concentrated in a much shorter distance from the end of the beam and are smaller in magnitude compared to bursting stresses.

The purpose of this section is to familiarize the reader with the concepts of end region stresses, the design practices associated with such stresses and the particularities of end region stresses in box beams.
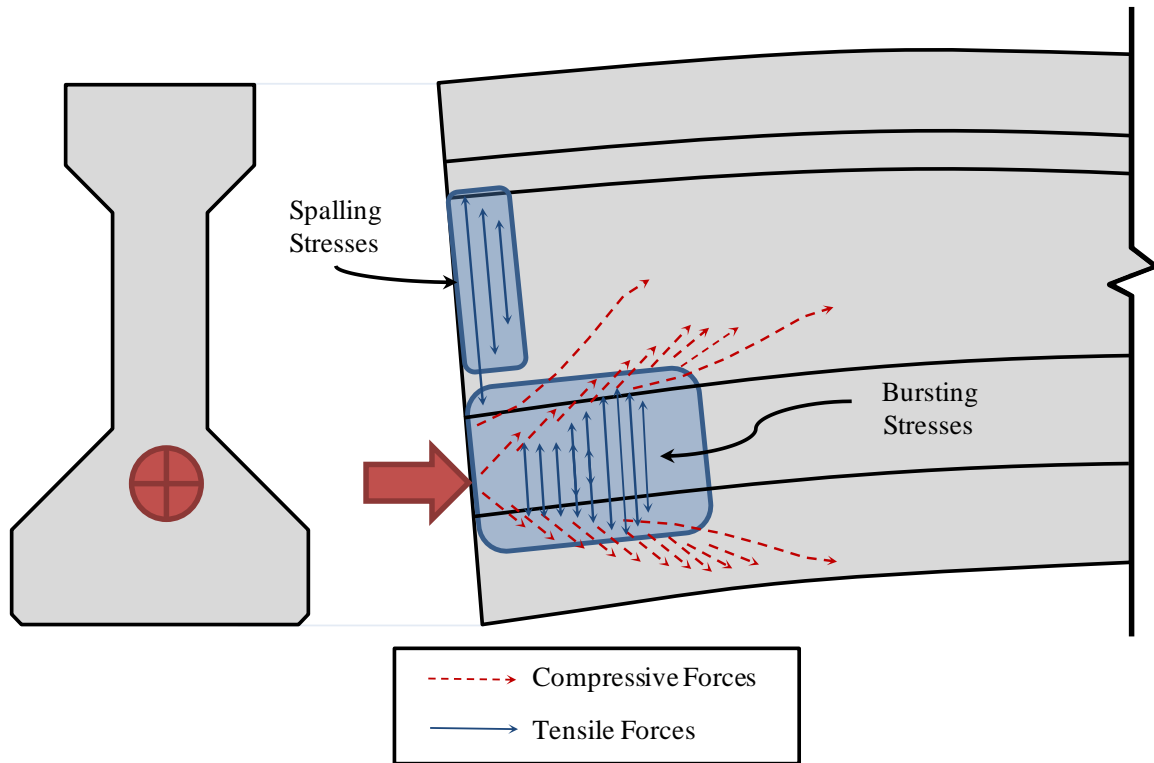
Figure 2-16: Distribution of Bursting and Spalling Forces

2.7.1 **Historical Background**

Thorough reviews of the historical background and past work on the study of transverse end region stresses have been presented recently by O'Callaghan and Bayrak (2007) and Dunkman (2009). These two publications cover in depth the development of the current code specifications regarding transverse stresses in end regions of prestressed beams and how they have evolved through the years. The experimental work that has served as background for such code provisions was also summarized by Dunkman (2009). In this section, a brief summary of previous experimental work is presented. Detail beyond what is presented in this section can be found easily within the work of O'Callaghan and Bayrak (2007), and Dunkman (2009).

Chronologically, the study of transverse stresses was not far behind the time when the use of prestressed concrete beams became popular. This time period followed the introduction of high strength prestressing strands. Early studies were conducted through

the late 1950s and early 1960s (Base, 1958; Marshall and Mattock, 1962; Gergely, Sozen and Siess, 1963). These early studies relied on surface strain measurements through target points adhered to the concrete through epoxy and laid out in a closely spaced grid. Strain gages were also placed on the transverse reinforcement with better success in terms of evaluating the total transverse force induced by prestressing. Strain measurements on the concrete surface, while useful to study the transverse strain/stress phenomena qualitatively, proved to be difficult to use to assess total forces as stress-strain relationships of concrete were much more complicated than that of steel reinforcement.

The work of Marshall and Mattock, and Gergely, Sozen and Siess, led to the introduction of transverse stress provisions in the design codes of the 1960s. The early design provisions have not changed much since.

Later, finite element studies were conducted (Yettram and Robbins, 1969; Uijl, 1983). More recently, experimental studies on large scale beams were conducted by Tuan et al. (2004), Crispino (2007), O'Callaghan and Bayrak (2008) and Dunkman (2009). The last two studies, conducted in the Ferguson Structural Laboratory at the University of Texas at Austin as the present study, included heavily instrumented beams through their end regions. Extensive instrumentation was possible due to the availability of the first large-scale prestressing bed facility inside a laboratory setting. The prestressing bed facility, shown in Figure 2-17, allows for the fabrication of beams of 30 ft in length, and the application of up to 3200 kip of prestressing force. The prestressing bed is capable of stressing all strands simultaneously ("gang stressing"); a practice commonly used in modern precast plants. Having this facility allowed the researchers the time to install extensive instrumentation.

All of the aforementioned work is what has led to the current understanding of transverse stresses in the end region of pretensioned beams.

Figure 2-17: Prestressing Bed facility in FSEL

2.7.2 **Magnitude of Transverse Stresses**

The magnitude of the transverse stresses is as important as the general distribution of bursting and spalling stresses within the beam. Currently, code provisions specify that the total transverse force (named differently in different codes) can be taken conservatively to be 4% of the net prestressing force. Dunkman gathered results from 53 test specimens from 5 references plus the work performed in his own experimental program. Later work presented by Hovell (2011) completed the data for a series of 4 U-beams studied within TxDOT Project 0-5831. Results from the first two of the 4 U-beams studied within TxDOT Project 0-5831 had been previously reported by Dunkman (2009).

In total, 53 results from previous references, plus the results from the U-beam program presented by Dunkman (2009) and Hovell (2011), confirm that 4% of the initial

(P_i) prestressing force can be used as a safe upper bound for the magnitude of the transverse forces experienced upon prestress transfer in the end region. These transverse forces are located in the region bound between the end of the beam and a section located a distance $h/4$ from the end of the beam. Results from the aforementioned references are illustrated in Figure 2-18.
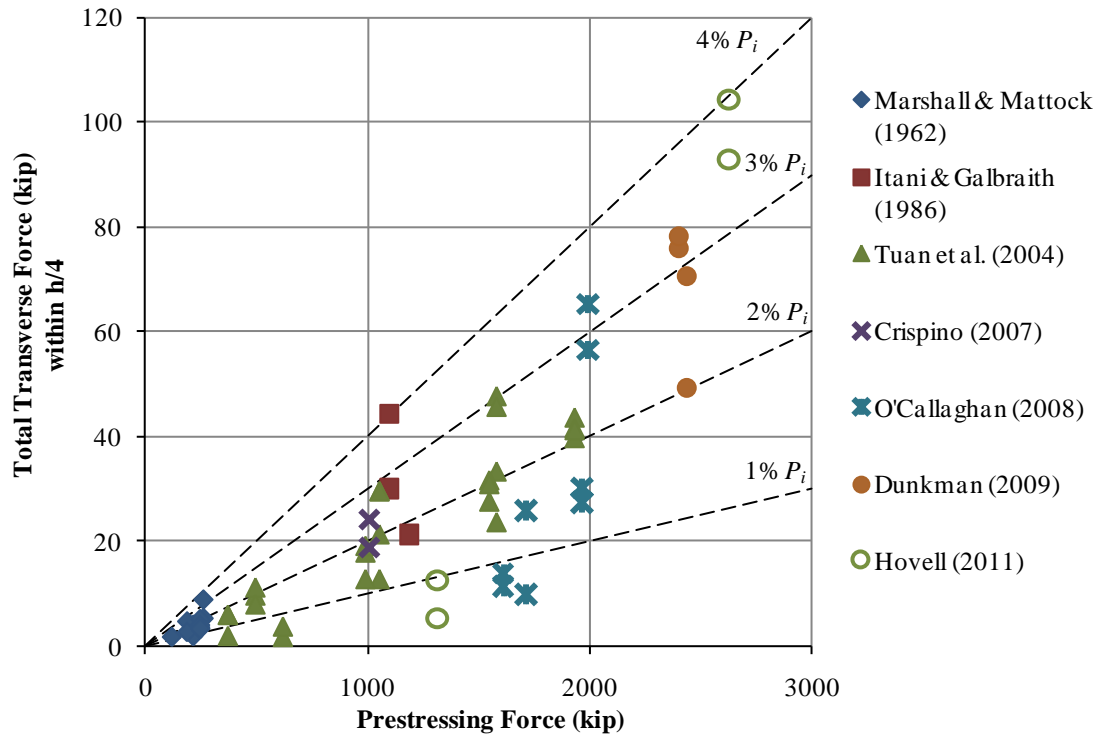
Figure 2-18: Results from experimental studies on Transverse Forces

In Figure 2-18, a large variability in the magnitude of the transverse force can be observed. This variability can be attributed to several factors including different beam shapes, different strand patterns, different methods of prestress transfer (flame-cutting strands versus gradual release by retracting hydraulic rams) and the accuracy of strains obtained from strain gages on the transverse reinforcement. When strain is measured on the transverse reinforcement, the magnitude of the measured stress is susceptible to how close to a crack the strain gauge is placed. In an ideal setting, the maximum strain in the reinforcement is measured when the gauge is placed exactly at the crack location.

Otherwise, the reinforcement as well as the concrete are subject to tensile stresses and the strain measured is not a maximum for the reinforcement.

2.7.3 **Location of Transverse Stresses**

The results reported by O'Callaghan and Bayrak (2008) are of special importance to this discussion. In their study, O'Callaghan and Bayrak (2008) fabricated beam specimens of three different depths: two 28-in. deep specimens, one 46-in. deep specimen and one 70-in. deep specimen. In all of the specimens, 0.6-in. diameter prestressing strands were used and the amount of strands was maximized in order to study a worst case scenario in terms of the transverse forces in the end region of the beam specimens.

All test specimens were instrumented with strain gages installed on the transverse reinforcement within the end region. The strain gages were monitored during and immediately after the prestress transfer process. Reinforcing bar stresses were calculated by using the strain readings gathered from the instrumentation.

O'Callaghan and Bayrak (2008) found that significant transverse forces developed between the end of the beam specimens and the point where the prestressing strands had transferred stress into the cross section (i.e. the transfer length of the strands). The location along the height of the girders suggested that the aforementioned forces correspond to bursting stresses. Spalling stresses were found to be concentrated in the region bound between the end of the beam specimen and a point located a distance into the beam's length equal to a quarter of the height of the beam (*h/4*).

At the time of O'Callaghan and Bayrak's (2008) study, the AASHTO-LRFD Bridge Design Specifications (2007) included provisions for the transverse forces concentrated in the region bound between the end of the beam and the distance h/4 from the end of the beam. In those specifications, the provisions were titled: "Factored *Bursting* Resistance". O'Callaghan and Bayrak (2008) indicated that the provisions were incorrectly titled and they suggested that that they should be renamed: "Factored *Spalling* Resistance". Most recently, the 2010 edition of the AASHTO-LRFD Bridge Design Specifications identified the same requirements as "*Splitting* Resistance". A more

48

detailed discussion on the current code and design specifications on this matter is presented in the subsequent section.

More importantly, O'Callaghan and Bayrak (2008) recommended the implementation of additional requirements for the region bound between a point located a distance *h/4* away from the beams end and the transfer length of the strands. Such region, according to O'Callaghan and Bayrak (2008) should be provided with supplemental reinforcement sufficient to resist a transverse force equal to 4% of the prestressing force at transfer without exceeding a stress in the reinforcement of 20 ksi.

2.7.4 Codes and Design Specifications

Codes and Design specifications predominantly used in the United States are developed and published by three organizations: the American Association of State and Highway Transportation Officials (AASHTO), the American Concrete Institute (ACI), and the Precast/Prestressed Concrete Institute (PCI). The design requirements of the latest edition of design standards published by these three organizations are reviewed herein.

2.7.4.1 AASHTO LRFD Bridge Design Specifications (2010)

AASHTO-LRFD §5.10.10.1 – *Splitting Resistance* addresses what is described herein as spalling stresses as it refers to reinforcement located close to the end region (within the first *h/4*-length of the beam). Versions of AASHTO-LRFD prior to the 2008 interim revisions referred to these stresses as bursting stresses. According to §5.10.10.1, the splitting resistance is given by:

$$P_r = f_s A_s$$
Equation 2-24

Where:

f_s = stress in the steel not to exceed 20 ksi

A_s = total area of reinforcement located within the distance $h/4$ from the end of the beam (in.^{2})

h = overall dimension of precast member in the direction in which splitting resistance is being evaluated (in.)

AASHTO-LRFD §5.10.10.1 requires that the splitting resistance shall not be less than four percent of the total prestressing force at transfer. As can be seen from Equation 2-24, requirements are very simple.

2.7.4.2 ACI 318 – 2008

Design of the end regions of pretensioned members is not specifically covered in ACI 318-08. Instead, general provisions for the design of anchorage zones in post-tensioned members through the use of strut-and-tie models are included.

2.7.4.3 PCI Design Handbook

Design requirements in the PCI handbook are similar to those from AASHTO-LRFD. A area of required reinforcement at the member end, uniformly distributed over a length $h/5$ from the beam end is given by:

$$A_r = 0.021\frac{P_o}{f_s}\frac{h}{l_t}$$

        Equation 2-25

Where:

P_o = prestressing force at transfer (after elastic losses)

f_s = maximum allowable stress in reinforcement

h = member depth (in.)

l_t = strand transfer length (in.)

In contrast with AASHTO-LRFD, the PCI handbook allows the stresses in the transverse reinforcement (f_s) to be as much as 30 ksi.

2.7.5   **Crack Control**

As mentioned in the previous section, stress limits are established (20 ksi by AASHTO and 30 ksi by PCI) for the reinforcement used to resist transverse stresses in the end regions of pretensioned beams. There are two reasons for the existence of such limits:

1. To limit the initial demand imposed on reinforcement that will be used to resist other demands. For example, vertical reinforcement in the end regions of pretensioned beams must also endure demands induced by shear due to superimposed loads.

2. To limit the width of cracks in the end regions. By doing so, the potential for water ingress and corrosion is reduced. Besides durability, aesthetics are paramount in the discussion of crack control.

Although an uncracked structure would be ideal, the occurrence of some cracks is practically inevitable in reinforced concrete structures. Restraining the growth of cracks and limiting their width can be achieved through efficient reinforcement detailing. However, defining and "acceptable" crack width as a design goal is not a simple task. AASHTO and PCI address crack control through limiting the stress in the reinforcement. On the other hand, several technical bodies have published recommendation in the matter of specific or ranges of acceptable crack widths.

The CEB-FIP (1990 provisions) provides a guide for reasonable crack widths under different exposure conditions. For concrete exposed to humidity, moist air and soil; a nominal limit value of 0.012 in. is recommended for crack widths. The Eurocode (EC2 1997) limits the maximum design crack with to the same value (0.012 in.) for sustained load under normal environmental conditions. In both documents mentioned above, it is noted that *a portion* of the cracks in the structure may exceed the recommended limits and engineering judgment shall always be exercised.

Halvorsen (1987) presented an extensive review of the development of crack control provisions over time. From the point of view of aesthetics and from the

information gathered by Halvorsen (1987) crack widths ranging from 0.006 in. to 0.012 in. could be considered unacceptable because they are visible to the naked eye.

The width of flexural cracks is subject to variation due to the transient nature of live load. Conversely, cracks present after prestress transfer are not likely to close upon the application of superimposed loads and thus can be considered more permanent than flexural cracks.

According to TxDOT, for prestressed concrete applications, all cracks resulting from prestress transfer exceeding 0.007-in. in width are subject to review and might require repairs through epoxy injection.

With all the aforementioned information in mind, an assessment on the acceptability of the width of the cracks encountered in the end regions of box beams can be made.

2.7.6 End Region Stresses in Box Beams

Two factors affecting end region stresses are particular to box beam behavior. The first one is the presence of an end block and its reinforcement. The second factor is strand distribution through the cross section.

The presence of an end-block facilitates the placement of transverse reinforcement within the end region of the beam. This is very important in the case of box beams given the larger width compared to I-girders of equal height.

Regarding strand distribution, most strands are placed in two regions: in the bottom slab under the void and through the depth of the webs. The amount of strands placed in each of these two regions must be accounted for in placement and proportion of the transverse reinforcement intended to manage the end region stresses.

Design provisions such as those included in AASHTO-LRFD and the PCI handbook assume that all transverse reinforcement within the end region is equally stressed. In I-girders, strands are clustered in the bottom flange and transverse vertical reinforcement can only be placed through the single web. In box beams, the horizontal distribution of strands across the section might not be uniform. More strands might be

placed in the bottom slab under the void or through the depth of the webs. This can create local concentrations of bursting stresses in either of these two regions. The designer must account for *uneven distributions* of strands across the section and proportion reinforcement accordingly.

Also related to strand distribution is the importance of horizontal bursting stresses. When the majority of strands are placed in the webs of box beams, horizontal bursting stresses can concentrate near the two groups of strands clustered under each web. In I-girders, this is not an issue as the majority of strands are located in a single cluster in the bottom flange of the beam. Furthermore, in box beams, horizontal transverse stresses induce vertically oriented cracks in the end face of the beam and longitudinal cracks along the bottom of the beam near the end region. Both of these cracks are managed in I-girders by confinement reinforcement which is not easily detailed for box beams given their geometry and the way they are fabricated.

2.8   SUMMARY

A lack of box beam research was observed in the shear database and in all technical literature, providing a sound justification for the experimental program conducted within this research project. While UTPCSDB (2011) contains results from 1676 tests before the addition of any result from this research program, only 8 (4 from Hanson and Hulsbos, and 4 from Burgueño and Bendert) correspond to shear tests conducted on box beams. Furthermore, only 1 from those 8 tests makes it through the filtering process used by Nakamura in selecting an adequate sample of data ("Evaluation Database – Level II") to evaluate the performance of shear strength equations.

While 4 additional tests (2 from Chamberlain and 2 from Saiidi and Bush) were found in the literature and described in this chapter, the total number of shear tests on box beams is rather small compared to that conducted on I-shaped girders. More importantly, and assuming that all of the 4 additional tests could be used to evaluate the performance of shear design equations applied to box beams, the total number of shear tests on box beams found in the literature (12) is too small to conduct a significant evaluation based

on these data alone. Hence, it is important to increase the number of box beams shear tests available in the literature, compare the test results to those conducted on other sections such as I-shaped girders and evaluate the performance of the currently used shear design equations. The current research is especially important after considering that box beams represent a significant fraction of the inventory of highway bridges as discussed previously. As the previous work on box beams presented herein suggests, attention must be paid to signs of torsional distress and the potential of shear reinforcement pulling out of the concrete due to the lap splices commonly used in box beam construction.

In terms of the early-age behavior of box beams and the transverse stresses in the end regions of beams induced by the transfer of prestress, a parallel to shear testing was observed. Transverse stresses in box beams have not been studied and the design practices used in box beams are derived from studies conducted on rectangular and I-shaped girders.

The following chapter describes the experimental program conducted as a part of TxDOT Project 0-5831. The experimental program is aimed at filling the knowledge gaps observed in shear design and, bursting and spalling stresses as discussed throughout this chapter.

CHAPTER 3

Experimental Program

3.1 INTRODUCTION

After an extensive literature review, a very limited amount of research was found pertaining to the shear performance of box beams. Furthermore, no previous research was found regarding the end region of box beams and the stresses found within this region at the time of prestress transfer.

Seeing the absence of box beam related research, a comprehensive experimental program was devised in order to satisfy all of the research objectives listed in Chapter 1. Two groups of specimens were investigated. The first group contained ten box beams inherited from a previous research project. These box beams were all four feet wide and twenty eight in. deep, with the corresponding TxDOT denomination: "4B28". The second group of specimens included five larger box beams; all being five feet wide and forty in. deep, with corresponding TxDOT denomination: "5B40". All the beams from the second group were fabricated in FSEL. Within each group, different aspects varied from beam to beam in order to create a comprehensive test matrix with several variables under investigation.

For clarity, the corresponding aspects of these two groups of test specimens are presented separately in this chapter. The same logic is later applied to the results presented in this document: results from the first group of specimens are presented in Chapter 4 (4B28 box beams), results from the second group of specimens are presented in Chapters 5 and 6.

3.2 4B28 BOX BEAMS

TxDOT Project 0-5197 investigated the feasibility of increasing the allowable compressive stress limit at prestress transfer for I-beams and box beams. As part of Project 0-5197, ten 4B28 box beams were procured and loaded at midspan until flexural

cracks developed. By doing so, it was possible to evaluate the accuracy of prestress loss equations under the high strains induced by high compressive stresses at prestress transfer.

After the flexural testing of the box beams was completed and seeing that the end regions of such beams were not damaged during the flexural tests, the ten box beams were tested in shear for the purposes of the current research project. It must be appreciated that when the box beams were designed and fabricated, the end regions were detailed in such a manner that they would provide a comprehensive study of the shear performance of box beams. The results from the first group of test specimens played a significant part in formulating the test program for the second group of box beams.

3.2.1   Specimen Description

The 4B28 box beams were 40 feet long with prestressing steel consisting of 30 half-inch diameter strands. Eight strands were debonded: four of them through 4 ft measured from the beams' end and four more debonded through 10 ft as illustrated in Figure 3-1. Shear reinforcement spacing was maximized to assure that shear failures would occur before flexural failure. Stirrups consisted of spliced #4 bars spaced at 20 in. This amount of reinforcement complies with the maximum stirrup spacing and minimum shear reinforcement requirements of current design provisions (ACI 318-08 and AASHTO-LRFD 2010). Moreover, reducing the contribution of shear reinforcement to the total shear strength facilitated the comparison between concrete contributions to shear strength for the different concrete mixtures utilized. Further discussion of concrete mixtures and the details of the end regions are included in the upcoming sections.
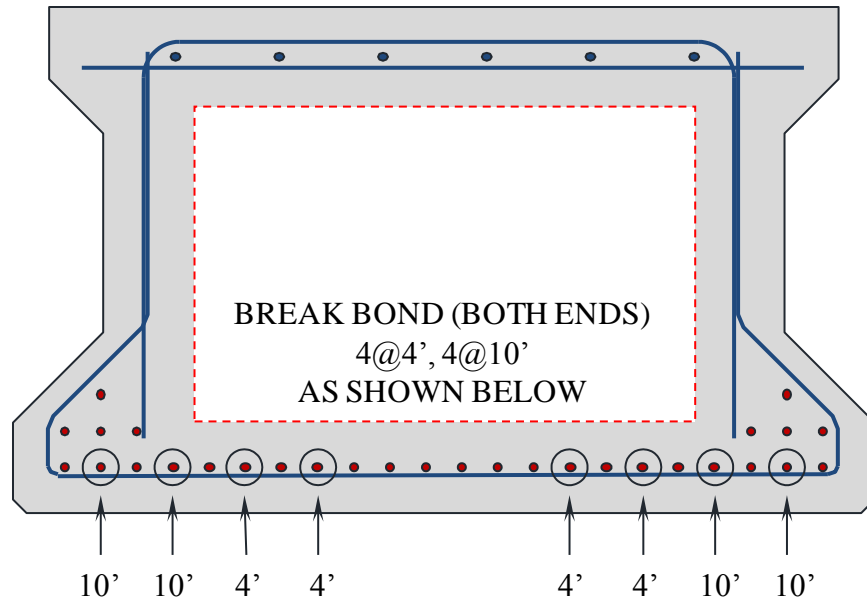
Figure 3-1: 4B28 cross section and debonding pattern.

3.2.1.1 Prestressing strands

The prestressing strands used were Grade 270, low relaxation and ½-in. diameter. In order to control stresses in the concrete at the time of release of the strands, some strands were debonded in the end region. A summary of the number of bonded and debonded strands is presented in Table 3-1. Strands were spaced at two in. on center both horizontally and vertically.

Table 3-1: Strand pattern for 4B28 box beams

| Row | Distance from the bottom (in.) | Number of Strands | | | |
		Fully Bonded	Debonded through 4 ft.	Debonded through 10 ft.	Total
1	2.5	14	4	4	22
2	4.5	6			6
3	6.5	2			2
	TOTAL	22			30

3.2.1.2 Shear reinforcement

Shear reinforcement constituted of two bars spliced within the webs of the beam specimens. The two bars, namely, Bar C in the bottom and Bar A on top, are illustrated

separately in Figure 3-2. In the beam, Bar C and Bar A must be at the same location in order to be properly spliced. The shear reinforcement bars, as shown in Figure 3-2, are different from the typical TxDOT standard detail (see Figure 3-14) but they are commonly used in prestressing plants. Each set of spliced bars was spaced at 20 in. to minimize shear strength, maximize the possible shear spans for which shear failures were possible and exacerbate the effects (if any) that any of the different concrete mixtures could have.
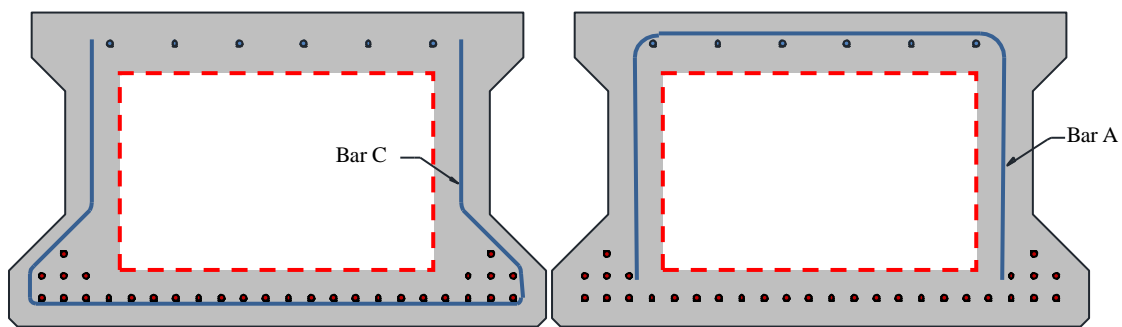
Figure 3-2: Shear reinforcement bars in 4B28 box beams.

3.2.2 **Primary Experimental Variables**

Several variables were studied though this experimental program. For clarity, each variable is discussed in the following sections.

3.2.2.1 Concrete mixture type

In total, four different concrete mixtures were used. During the course of TxDOT Project 0-5197, TxDOT expressed an interest in evaluating the performance of bridge beams fabricated with self-consolidating concrete (SCC). For this reason, five of the ten box beams were fabricated with SCC and five were fabricated with conventional concrete (CC) mixtures. Although there are several ways of achieving SCC, the SCC mixtures of this project were attained mainly by changing the coarse aggregate fraction. A concrete compressive strength of 4100 psi was specified to the fabricators in order to meet stress

limitations at the time of release of the strands. Ultimately, all beams had 28 day concrete strengths close to 10000 psi. Detailed mix proportions are presented in Appendix A.

As mentioned before, reducing the shear reinforcement contribution to the total shear strength was ideal to compare concrete contribution to shear strength. The calculated concrete contribution to shear strength represents close to 70% of the total strength of the 4B28 box beams discussed herein.

3.2.2.2 Coarse aggregate

In addition to varying the coarse aggregate fraction, the coarse aggregate type was varied. Crushed limestone and river gravel were used in separate concrete mixes. The corresponding combinations of concrete mix type and coarse aggregate type are detailed in Table 3-2.

Table 3-2: Outline of primary research variables per each specimen

Specimen	Concrete Mixture	Coarse Aggregate Type	Skewed End Void Geometry
BB-01	Conventional	Limestone	30° Skew
BB-02	Conventional	Limestone	Square
BB-03	Conventional	River Gravel	30° Skew
BB-04	Conventional	River Gravel	Square
BB-05	Conventional	River Gravel	Hybrid
BB-06	Self-Consolidating	Limestone	30° Skew
BB-07	Self-Consolidating	Limestone	Square
BB-08	Self-Consolidating	River Gravel	30° Skew
BB-09	Self-Consolidating	River Gravel	Square
BB-10	Self-Consolidating	River Gravel	Hybrid

3.2.2.3 Beam end geometry and skewed end internal void geometry

Each box beam was fabricated with one end square and one end skewed at 30 degrees. Three different void geometries were used for the skewed ends of the beam (Table 3-2). Four beams were fabricated with square voids at the skewed ends as illustrated in Figure 3-3. Square voids are the standard practice; however, the large

amount of concrete placed in the end block can lead to high temperatures during curing, which may lead to DEF as discussed in Chapter 2.

Figure 3-3: Square void at 30° skewed end of 4B28 Box Beam.

Four beams were fabricated with skewed voids as illustrated in Figure 3-4. In these cases, the end face of the polystyrene void form was kept parallel to the end face of the beam. This geometry reduced the amount of concrete placed in the end block, reducing curing temperatures and minimizing the potential of long-term durability problems. In return, there is a concern about how such geometry affects the flow of forces from the webs to the support when one central bearing pad is used. Furthermore, there is concern on how this geometry could potentially affect the shear performance of the end region.

Figure 3-4: Skewed void at 30° skewed end of 4B28 Box Beam.

The remaining two beams were fabricated with a hybrid void geometry as illustrated in Figure 3-5. The hybrid void's geometry is in between the square and the skewed geometry. This reduces the amount of concrete that needs to be placed in the end block while at the same time allowing a more direct flow of forces from the web of the beam to a central bearing pad at the support.

Figure 3-5: Hybrid void at 30° skewed end of 4B28 Box Beam.

The first three investigated variables mentioned are considered primary variables for their importance and due to the fact that they were established prior to fabrication of the 4B28 test specimens. These variables for each specimen are summarized in Table 3-2.

3.2.3   Secondary Experimental Variables

3.2.3.1 Shear span to depth ratio

Shear span selection is critical to assure that tests result in a particular mode of failure. In this case, shear failures were desired. If shear failure is to be obtained for a particular shear span, the beam must be able to withstand load beyond that causing nominal shear failure without failing in flexure or other failure modes. Furthermore, if sectional behavior is to be studied, a minimum shear span to depth ratio of roughly 2.5 is generally accepted. To determine how much load beyond the nominal shear capacity was likely to be resisted by the beam, the University of Texas Prestressed Concrete Shear Database (UTPCSDB) was used. Initial evaluations revealed that the 4B28 box beams were likely to resist transverse loads approximately 45% in excess of the nominal capacity calculated with the Detailed Method from ACI 318. Further calculations revealed that at a shear span to depth ratio of approximately 3.75 (shear span of 7.75 ft), the load causing flexural failure resulted in a shear force equal to the expected shear capacity ($1.45V_n$, calculated with the Detailed Method from ACI 318). For shear spans shorter than 7.75 ft, the load causing the expected shear capacity is reached before flexural failure occurs as illustrated in Figure 3-6. For these reasons, shear spans of 6 ft (a/d = 2.9) and 7 ft (a/d = 3.4) were used in this study.
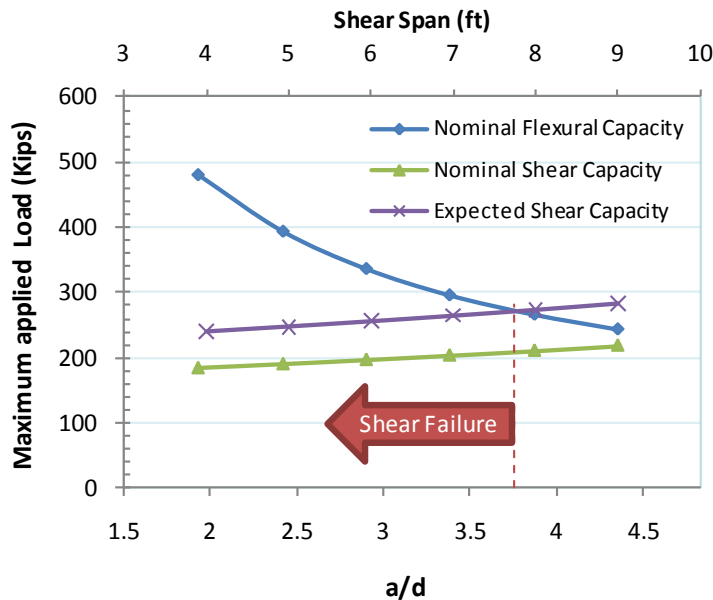
Figure 3-6: Feasible shear spans study for 4B28 beams.

3.2.3.2 Bearing pad configuration

The interaction of different bearing pad configurations with the different internal void geometries was investigated as well. In all cases, beams were supported on three bearing pads as per TxDOT specifications. Standard bearing pad sizes of 6" long by 7" wide (for two spaced bearing pads) and 6" long by 14" wide (for a single central bearing) were used. Figure 3-7 shows the two bearing pad configuration alternatives tested. This is of special concern for the case where the internal void geometry is skewed as shown in the figure. It is thought that when one central bearing pad is used, force must flow around the sharp corner of the internal void in order to reach the support. Conversely, force carried through the opposite web has a more direct load path from the web to the support. This disparity could cause local stress concentrations that could potentially hinder shear strength of the end region of box beams.
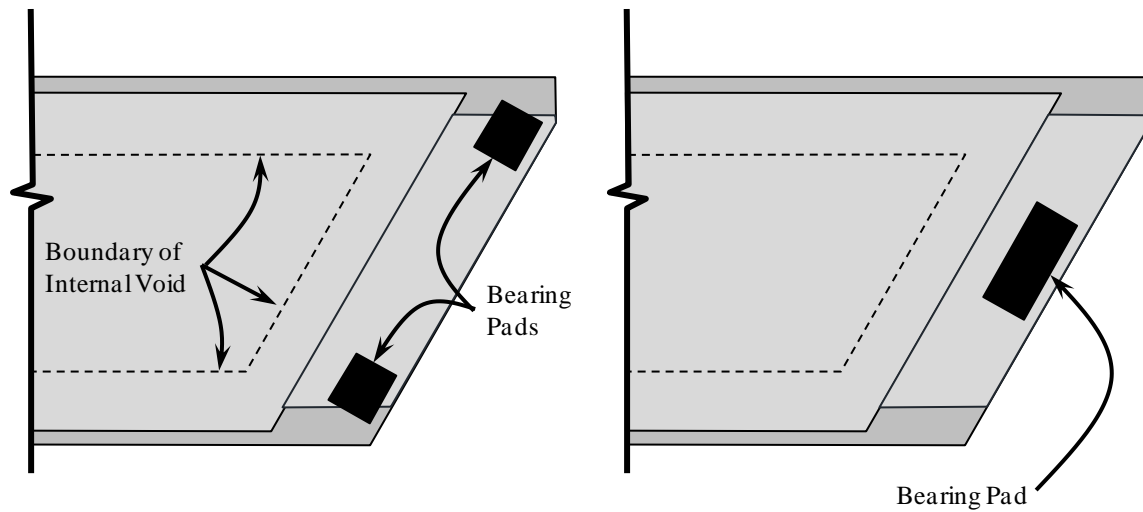
Figure 3-7: Different bearing pad configurations for skewed end.

3.2.4 Test Setup

Given that all specimens were tested twice (one test per end region), two typical test configurations can be described. In the *first test* configuration, shown in Figure 3-8, the beam is simply supported at the ends (span = 38.375') with a shear span of either 6' (a/d = 2.9) or 7' (a/d = 3.4). For the *second test* conducted on each beam (second test configuration as shown in Figure 3-9), the damaged part of the beam (8 ft) cantilevered out from one of the supports while the second end region was tested at a shear span of 6' or 7'. For a second test, the simply supported span was 30.375'.

6' or 7'

38.375'
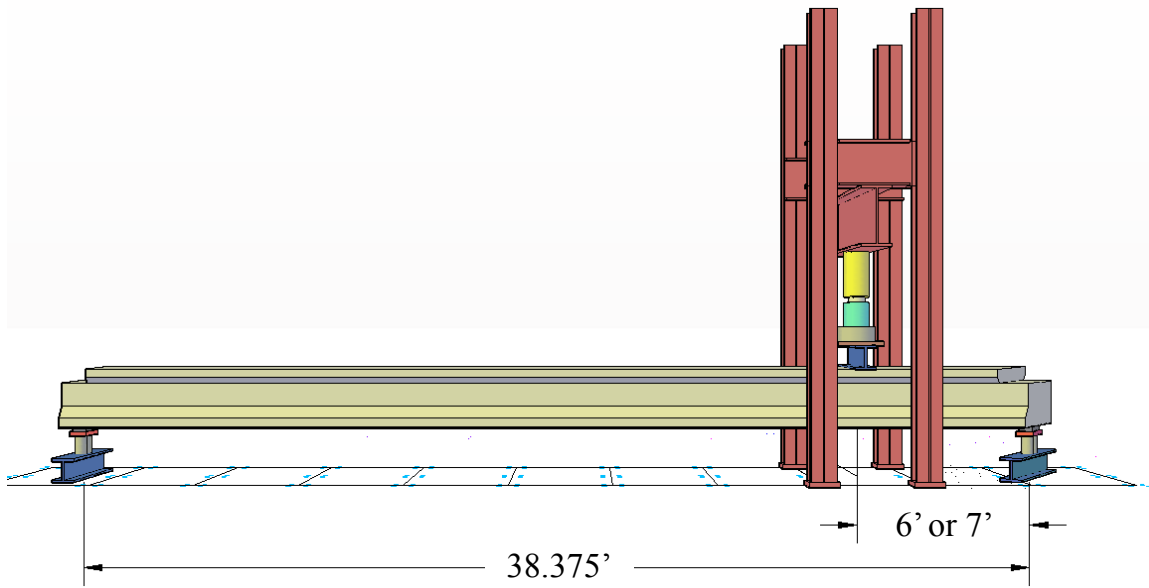
Figure 3-8: Typical first test setup.

DAMAGED IN
FIRST TEST

6' or 7'

30.375'
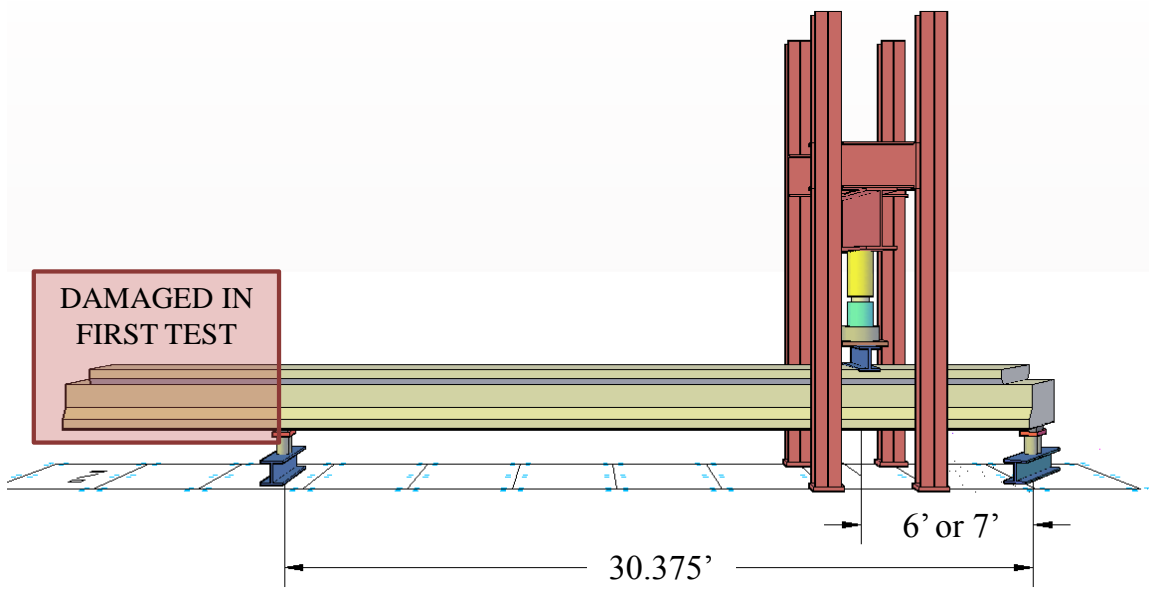
Figure 3-9: Typical second test setup.

3.2.5 Instrumentation

Load cells were used on top of the beam to measure the applied load (Figure 3-10a) and under the supports to measure reaction forces (Figure 3-10b). When testing was done with two separated bearing pads, each bearing pad was supported on an individual load cell. This allowed the research team to have an approximate idea of how much shear was carried by each web at any given time. However, for all calculations and evaluations of performance, shear was assumed to be resisted by a single equivalent web. The thickness of this single equivalent web was assumed to be equal to the sum of the thickness of the two webs (5 in. + 5 in. = 10 in.)
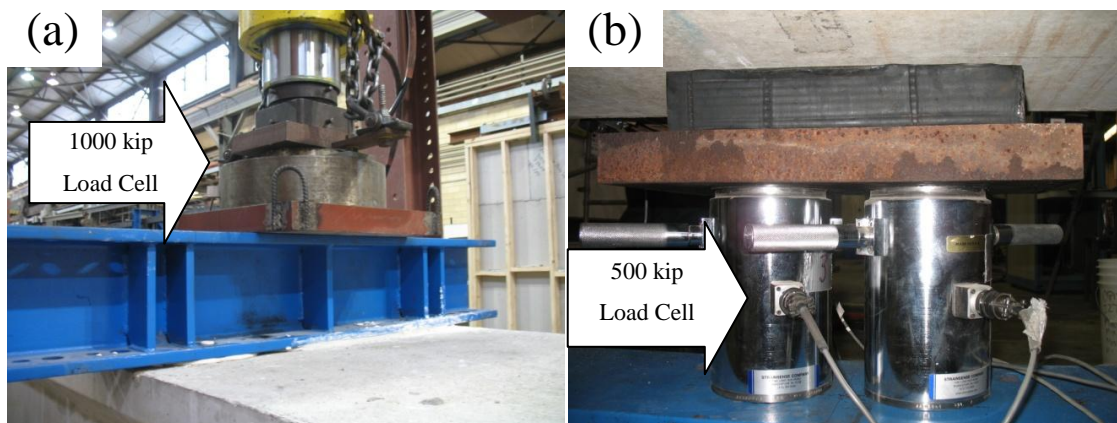
Figure 3-10: (a) Load cell used to measure applied load, (b) Load cells under support used to measure reaction.

To obtain load-deflection curves, linear potentiometers were placed under the beam to measure deflection under each support (due to compression of the bearing pads) and at midspan. Note that load is not applied at midspan yet deflection is measured at midspan. Given the explosive nature of shear failures, it was decided not to place linear potentiometers directly under the load point in order to avoid damaging valuable instruments. Nevertheless, deflections measured at midspan produce equally useful information in terms of the beam bending beyond the elastic range or the beam approaching failure by increasing deflections not accompanied by increasing load. In all cases, deflection was measured at both sides of the beam (under each web).

66

External instrumentation was used to measure shear deformation as illustrated in Figure 3-11. Rods were embedded into the sides of the beam and linear potentiometers were used to measure the deformation between the rods. Dividing the deformation between rods by the initial distance (or gage length) between rods can be considered an average strain along the axis of measurement. Also, by placing rods in three points forming a triangle, it was possible to calculate shear distortion of the test region. The distortion angle is defined herein as the change in the angle formed between the horizontal and vertical sides of the instrumentation triangle. This angle was initially equal to 90 degrees in all tests.

Figure 3-11: Shear deformation measurement instrumentation.

External instrumentation was also used to measure strand slip. Four strands were monitored in each test. Current debonding practice calls for debonding strands in the outer portion of the slab first and strands in the middle of the slab last. The researchers believe that strands under the web (those debonded first per current practice) have a more important role in shear performance than those towards the middle of the slab and hence, outer strands should be debonded last for box beams. Comparisons were made between slip measured in strands located under the web and those located in the middle of the bottom slab. Additionally, comparisons could be made between slip measured in strands under the two different webs.

Figure 3-12: Strand slip instrumentation.

3.3   5B40 BOX BEAMS

The upcoming sections contain the relevant information for the second group of box beams included in this study.

Having concluded the shear testing of ten 4B28 box beams, several key observations were made. These observations, along with data gathered from shear tests, provided information on box beams that was otherwise nonexistent in current technical literature. The 5B40 box beams were fabricated within FSEL, allowing for the study of the early stages of the beam to take place with relative ease. Besides shear tests, performed similarly to those conducted on 4B28 box beams, curing temperatures and release stresses were thoroughly monitored. The study of the later two aspects is rather difficult when beams are fabricated in prestressing yards.

As part of the current research project, the study of 5B40 box beams was divided in two phases. Phase I included a performance assessment of the end regions of the 5B40 box beams as detailed currently by TxDOT standards. Phase II was to incorporate results obtained during Phase I and improve on the current standard. Lastly, a new box beam prototype designed by TxDOT (5XB40) was fabricated and tested. Three beams (5B40-1,-2 and -3) were fabricated within Phase I of the 5B40 study and two more beams were fabricated as part of Phase II (5B40-4 and 5XB40).

3.3.1 **Specimen Description**

As other beams fabricated within FSEL, in-house fabricated box beams were 30 feet long. In the beams fabricated during Phase I and in the first beam of Phase II (5B40-4), one end was fabricated with a 30° skew while the other end is square (0° skew). In the skewed end, two different internal void geometries were used: *(i)* A square internal void; resulting in the largest possible end block, and *(ii)* A skewed internal void; resulting in the smallest possible end block.

No composite deck was cast over the specimens after considering the following:

    i.   In some cases, Texas box-beam bridges are fabricated with box beams topped with an asphalt overlay. This is the worst case scenario for the box beams compared to cases where a composite deck is used. Given the limited number of tests that can be conducted at full-scale, the worst case scenario of beams without composite decks is of interest; and

    ii.   Calculations suggested that the beams without a composite deck on top had sufficient flexural capacity to be tested at shear span to depth ratios up to 3.9 (shear span of 10.3 ft).

For the last beam of the study, the 5XB40, an 8 inch thick composite deck was added on top of the girder. The composite deck was 53.75 in. wide. Since the 5XB40 box beams are meant to be spaced apart from each other, there was no technical reason to investigate its shear behavior without a composite deck.

3.3.1.1 Cross section

The 5B40 box beam is very similar to the 4B28 box beam mentioned before. To fabricate a 5B40 box beam, the side forms used to fabricate a 4B28 are separated one foot further apart and set on top of 1 foot form boosters to make the section a foot deeper. The dimensions of the internal void are such that a minimum web thickness of 5 in. is attained and the bottom and top slabs are 5 in. and 5.5 in. deep respectively.

For comparison purposes, all the box beams tested in this study are illustrated in Figure 3-13. The 4B28 box beams described earlier in this chapter are illustrated in part

(a) of Figure 3-13. The standard 5B40 box beam is illustrated in part (b). Lastly, in part (c) of Figure 3-13, the 5XB40 box beam is illustrated. The 5XB40 box beam is intended to be used with space between adjacent beams and a typical 8 inch thick composite deck on top. This last beam has thicker webs (6.5 in. as opposed to the 5 in. in the 4B28 and 5B40 series) and a thicker bottom slab (2 in. thicker than the other beams tested in this study) to accommodate a full second row of prestressing strands in the bottom slab of the beam.
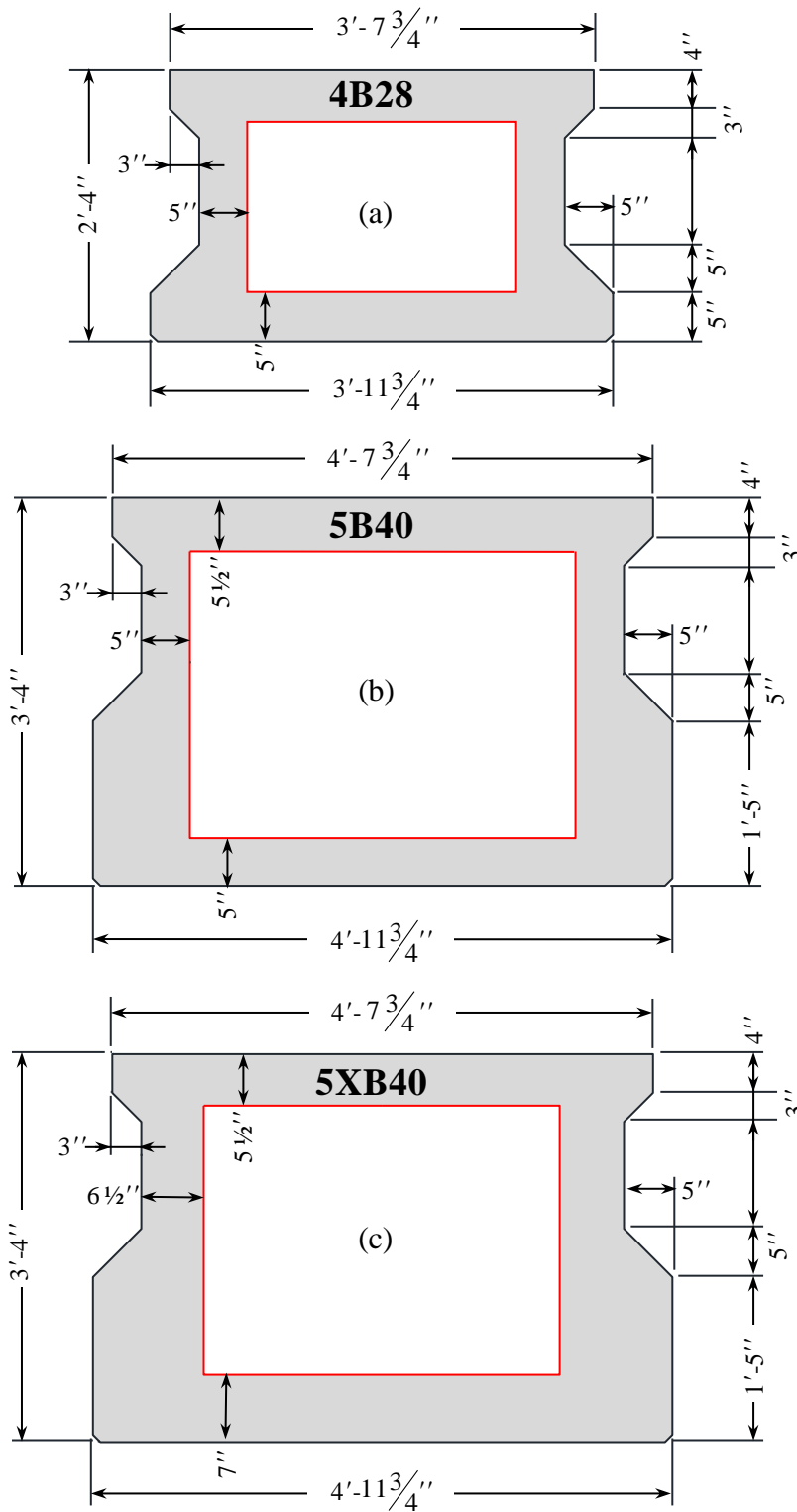
Figure 3-13: Cross sections for all box beams in this study. (a) 4B28, (b) 5B40, and (c) 5XB40

3.3.1.2 Prestressing strands

The prestressing strands used were Grade 270, Low relaxation and ½- in. diameter as in the 4B28 testing program. In order to maximize bursting stresses in the end region, the maximum number of prestressing strands was utilized. For the 5B40 box beam, the large number of prestressing strands required concrete compressive strengths of at least 6400 psi, at release, in order to comply with maximum allowable compressive and tensile stress limits. For the 5XB40, the strands were relatively placed at a higher eccentricity, creating larger moments induced by the prestressing strands and making the beam design controlled by tensile stresses in the top slab at prestress transfer. A target release strength of 7100 psi was set for the 5XB40 beam.

Strands were spaced at 2 in. on center horizontally and vertically. Ten rows of strands were placed in total, as summarized in Table 3-3.

Table 3-3: Strand pattern for 5B40 and 5XB40 box beams

Row	Distance from the bottom (in.)	5B40 (All fully bonded)	5XB40 Fully bonded	5XB40 Fully debonded
1	2.5	28	26	2
2	4.5	6	22	6
3	6.5	6	6	
4	8.5	6	6	
5	10.5	6	6	
6	12.5	6		
7	14.5	6		
8	16.5	6		
9	18.5	4		
10	20.5	2		
	TOTAL	76	66	8

3.3.1.3 Shear reinforcement

Standard TxDOT shear reinforcement details were used for the fabrication of the 5B40 specimens tested in Phase I. For the standard 5B40 box beams, shear reinforcement was spaced at 6 in. throughout the length of the member. The closely spaced shear reinforcement made the in-house fabricated beams significantly different than the 4B28

beams inherited from Project 0-5197. In 4B28 box beams, shear reinforcement (Spliced #4 A-bars and #4 C-bars, shown in Figure 3-2) was spaced at 20 in. on center to minimize shear strength, maximize the possible shear spans for which shear failures were feasible and maximize the effects (if any) that any of the different concrete mixtures could have on the shear strength.

Shear reinforcement in the 5B40 box beams has two bars spliced vertically within the webs. From the bottom, Bar C extends 36 in. up through the web. From the top, Bar A extends 22 in. down. The resulting lap splice is approximately 21 in. Bars are shown separately in Figure 3-14 although in the beam they must be in the same location so they can be adequately spliced. Other bars are not shown in Figure 3-14 for clarity. A complete set of drawings of all the beams can be found in Appendix B.
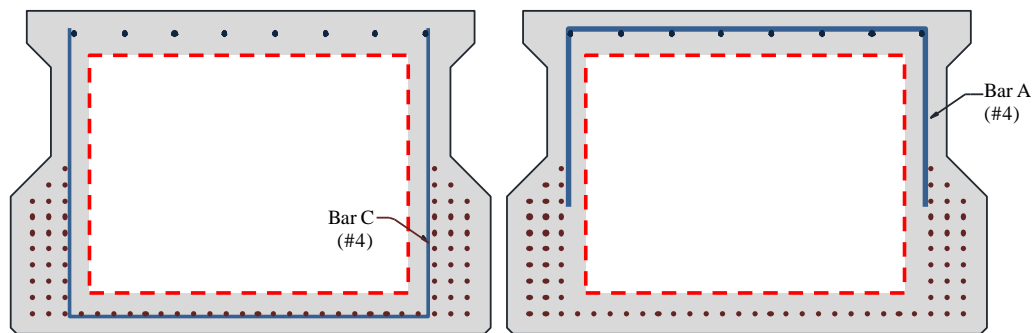
Figure 3-14: Shear reinforcement bars and strand pattern for 5B40 box beams.

For the 5XB40 box beam, shear reinforcement resembles more closely to that of a typical I shaped girder as can be seen in Figure 3-15. Bar R (#4) extends up through the web and is finished with a 180 degree hook extending back down into the web. Bars R are spliced within the bottom slab of the beam. This splice location is bound to have a much lesser influence in shear behavior compared to the detail used in the 5B40 box beams.
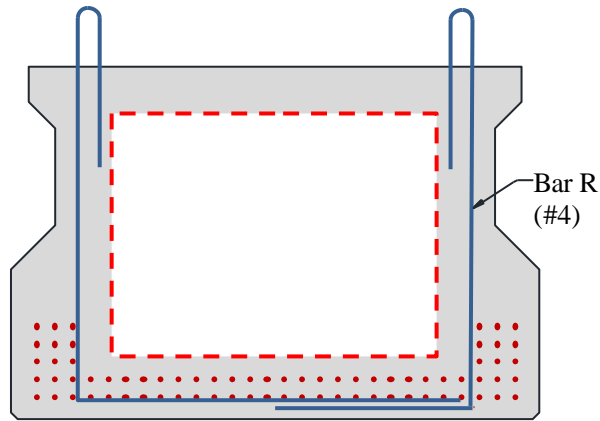
Figure 3-15: Shear reinforcement bars and strand pattern for 5XB40 box beams.

3.3.1.4 End-region reinforcement

The reinforcement placed in the end region followed standard reinforcement details currently used by TxDOT. In addition to the standard reinforcement, the end regions of Phase-I beams were reinforced with Bars E. Bars E were added per request of the TxDOT standards engineer to address problems observed at the fabrication stages in heavily prestressed beams. These Bars, illustrated in Figure 3-16, go across the end block and have a 90-degree hook outside the strands. Complete drawings of the beams can be found in Appendix B.
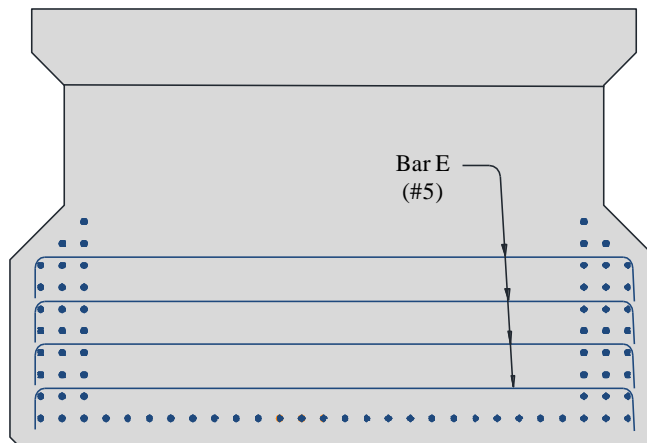
Figure 3-16: Bars E added to the standard reinforcement details

3.3.1.5 Concrete mixture and type of coarse aggregate

The concrete mixture used for the fabrication of the 5B40 beams was chosen to represent typical industry practice. Detailed mixture proportions for all beams are included in Appendix A. Crushed limestone was used as coarse aggregate in all beams.

3.3.2 Fabrication Process

The fabrication process of box beams is complicated. Fortunately, the research team had the opportunity to be present during the fabrication of the 4B28 box beams at local prestressing yards. This experience proved to be highly valuable for the fabrication of box beams within FSEL. The collaboration of the local precast industry was paramount in this task.

The difficulty of box beam fabrication lies within the many steps that need to be taken while concrete is still fresh. Because there are void formers to be inserted, the reinforcement cage is not completely in place at the beginning of concrete placement. Fabrication steps can be summarized as follows:

(1). Concrete is placed in the bottom slab of the beam to the specified depth (5 in. for standard box beams). Care must be taken not to place excess concrete in order to avoid complications in the next step. (Figure 3-17, Step 1)

(2). Polystyrene void formers are placed. Although the void formers are not heavy, it takes multiple workers to place them accurately. (Figure 3-17, Step 2)

(3). Diagonal dowels are embedded through adjacent void formers to prevent lateral movements. Plastic spacers are placed between the sides of the void formers and the side forms at web height to keep the void former from moving side-to-side. (Figure 3-17, Step 3)

(4). The joint between adjacent void formers is sealed to avoid having concrete fall between them. (Figure 3-17, Step 4)

(5). Bearing plates are placed over the polystyrene voids. The top ties are equipped with threaded rods to hold down the void and keep it from

floating. Bearing plates are necessary in order to keep the rods from punching through the foam. In typical industry practice, isolated concrete bearing plates are often used under each rod. The first two beams fabricated in this study were fabricated using isolated concrete bearing plates (known colloquially as *brownies* and *tacos* in local prestressing yards). A continuous steel plate was used for all box beams fabricated after that. The decision to change was made after having multiple issues with the isolated bearing plates, including splitting failures of the concrete bearing plates, insufficient bearing area and interference with the top reinforcement cage. (Figure 3-17, Step 5)

(6).   The top of the reinforcement cage is placed with the help of a gantry crane. Care must be taken to align the top shear reinforcement (Bar A) with the bottom shear reinforcement (Bar C) as these bars are meant to be spliced. Ideally, the top and bottom cages should be tied together at every splice location. (Figure 3-17, Step 6)

(7).   Top cross ties are installed to keep the width of the beam at the specified dimension. Metal cross pins are placed in the bottom leg of the cross ties in order to keep them from moving up. (Figure 3-17, Step 7)

(8).   Coil rods are ran down to keep the void formers from floating. Prior to screwing down the coil rods, metal pins must be inserted through the dowels of the top cross ties passing through the side forms. (Figure 3-17, Step 8)

(9).   Concrete is placed in the remainder of the beam. Steps (1) through (8) must be done in less than 1 hour and ideally, within 30 minutes. More importantly, concrete in the bottom slab needs to still be plastic in order to bond with the new concrete. (Figure 3-17, Step 9)

(10). The top of the beam is finished. (Figure 3-17, Step 10)

(11). The coil rods from step (8) can now be run up as the weight of the concrete should hold down the void in place. Concrete around the hole left by the rods needs to be vibrated once more. Although this is done in typical

practice, for the beams fabricated in this study, the rods were left in place until concrete had set and the polystyrene void could no longer move. (Figure 3-17, Step 11)

This fabrication process is referred to as *two-stage monolithic* concrete placement. To successfully fabricate box beams within FSEL, a good amount of preparation was needed. The fabrication procedure was explained to graduate researchers from multiple projects who volunteered to help on beam fabrication days. Approximately 15 graduate research assistants, and laboratory technicians participated in the fabrication of each beam. Beams fabricated in FSEL benefited from TxDOT inspectors as well.

Figure 3-17: Step-by-step Box Beam fabrication process

Figure 3-17: Step-by-step Box Beam fabrication process (continued)

3.3.3 Experimental Variables

In the 5B40 box beams, the width of the bottom slab is greater than in the 4B28 series. This difference in slab width makes the 5B40 bottom slab more flexible and

increases the web-to-bottom flange width ratio, which previous research has pointed out to create different shear behavior. Box beams of three different web-to-flange width ratios were tested through this experimental program as described in Table 3-4.

Table 3-4: Bottom flange-to-web width ratios for box beams in tested within this study

Beam	Bottom flange-to-web width ratio
4B28 Series	4.8
5B40	6.0
5XB40	4.6

Within the 5B40 series of box beams, the influence on shear performance of the beam end geometry and the internal void geometry at the skewed end was studied. Two different internal void geometries at the skewed ends were used; a square internal void and a skewed internal void. The later results in a lesser amount of concrete placed in the end block, potentially reducing curing temperatures within the end block.

Similar to the 4B28 box beams, the standard 5B40 box beams were fabricated with one end square and one end skewed at 30 degrees. The internal void geometry was varied at the skewed ends in order to study the temperature variations within the end block and to identify their possible influence on the shear performance.

In the case of the 5XB40 box beam, both ends were fabricated with a 0 degree skew (a square end). In all cases, the length of the end blocks was kept at 16 in. For skewed ends, the 16-inch measurement is taken from the obtuse corner of the beam, along the length of the beam, to the corner of the internal void former. This effectively results in an end block 21.75 in. long, measured along the length of the beam. The thickness of the end block, measured perpendicular to the skewed face of the beam, is 18.75 in. For clarity, these dimensions are illustrated in Figure 3-18.

A summary of the beams fabricated in FSEL and relevant information is presented in Table 3-5.
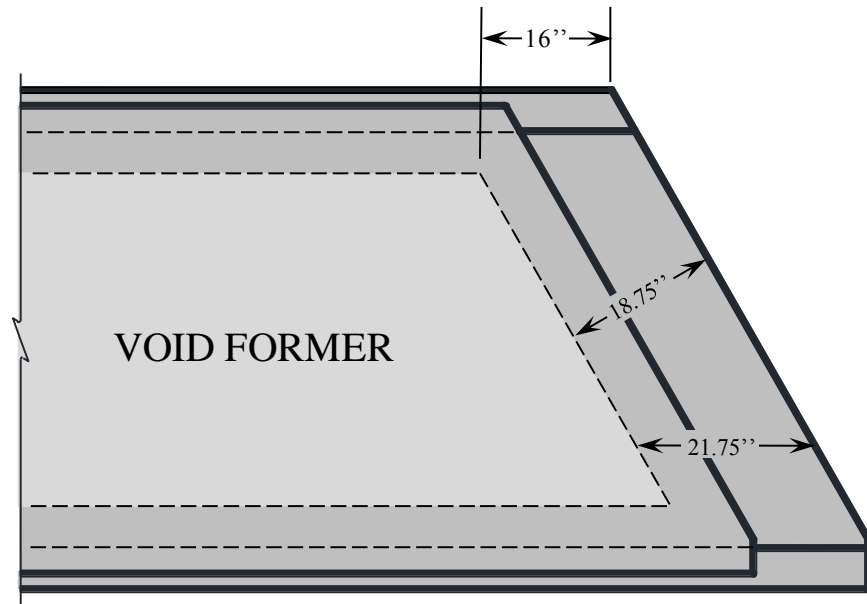
Figure 3-18: Plan View of Skewed End of 5B40 box beams with skewed internal void.

Table 3-5: 5B40 Box beams descriptions

	Beam ID	Skewed end internal void geometry	Bonded Strands	Target concrete strength at release	General Description
Phase I	5B40-1	Square void	76	6400 psi, limited by the maximum compressive stress in the section	Beam built according to standard TxDOT reinforcement detail[1]
	5B40-2	Skewed void	76	6400 psi, limited by the maximum compressive stress in the section	Beam built according to standard TxDOT reinforcement detail[1]
	5B40-3	Skewed void	76	6400 psi, limited by the maximum compressive stress in the section	Beam built according to standard TxDOT reinforcement detail[1]
Phase II	5B40-4	Skewed void	76	6400 psi, limited by the maximum compressive stress in the section	Beam built with a modified end-region reinforcement detail, incorporating results from beams 5B40-1,-2 and -3.
	5XB40	N/A (both ends of the beam were square)	66	7100 psi, limited by the maximum tensile stress in the section	Modified 5B40 cross section. Thicker webs, deeper bottom slab and different strand placement pattern. End-region reinforcement detail incorporates results from all previous beams.

[1] Bars E, illustrated in Figure 3-16, were added per TxDOT's request (not part of TxDOT standard reinforcement detail).

3.3.4 Test Setup

A load frame capable of applying 4 million pounds of force was assembled in FSEL for this research project. For the load tests on 5B40 box beams, two hydraulic rams were placed over the webs. Reactions at the supports were measured through load cells. Applied load was measured through pressure transducers connected to the hydraulic load system. The measured pressure was multiplied by the area of the rams to obtain a resulting load. A side elevation view of the test setup and a front elevation view are illustrated in Figure 3-19 and Figure 3-20 respectively.
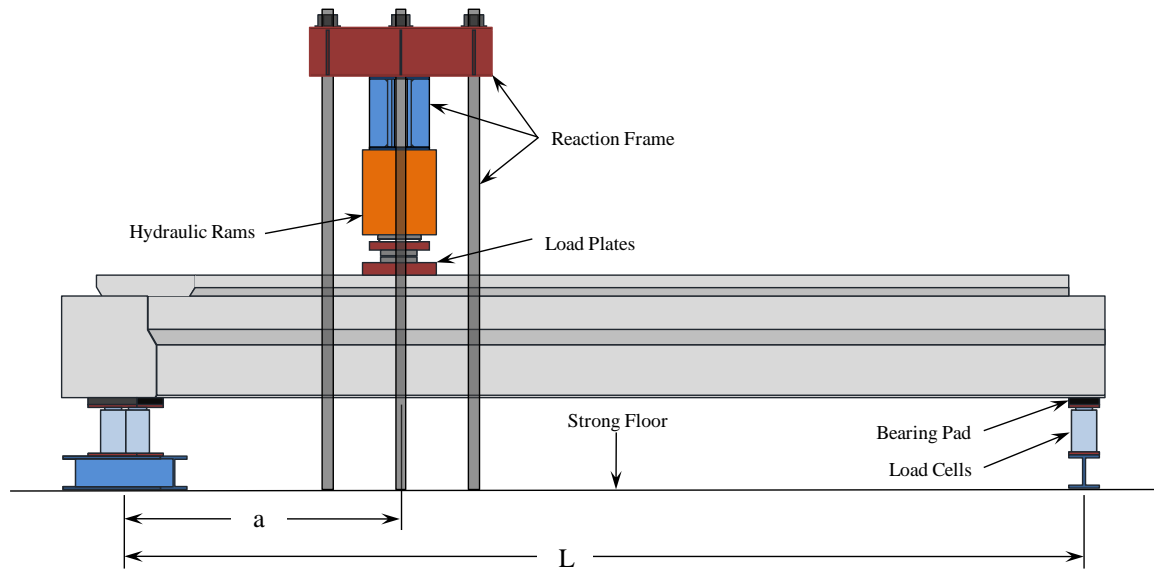
Figure 3-19: Side Elevation View of test setup for in-house fabricated beams.
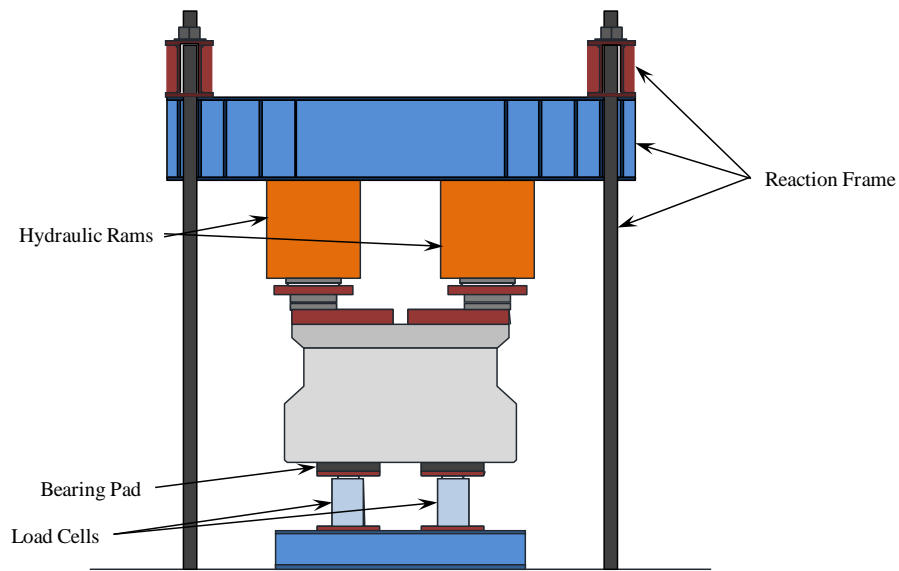
Figure 3-20: Front Elevation View of test setup for in-house fabricated beams.

3.3.5 **Instrumentation**

One substantial advantage offered by in-house fabrication of specimens is the availability (and affordability) of time to heavily instrument reinforcement and strands to

maximize the investigative value of each specimen. The first beam fabricated within FSEL had close to 150 internal instruments to measure strain and temperature along different points within the beam. Some of these instruments were monitored during the transfer of prestressing force to the beam and others during shear testing. Very few were monitored at both stages.

As with the 4B28 shear testing program, external instrumentation was used to measure shear deformation, strand slip, deflections, load applied and reactions during shear tests.

3.3.5.1 Strain Gages

Strain gages were placed with two main purposes: *(i)* to monitor reinforcing bar strains induced by the transfer of prestress into the beam, and *(ii)* to monitor reinforcing bar strains within the areas of interest during shear tests.

Strain gauge locations to be monitored during prestress transfer were initially selected based on the observation of bursting cracks found in 4B28 box beams. Mainly, gages were placed in the transverse (vertical) reinforcement half an inch above the height of the top of the bottom slab and just under the thinnest part of the web, where the web starts to flange out, as illustrated in Figure 3-21. In Figure 3-21, the distance in feet from the end of the beam is indicated above the beam, and the strain gages illustrated are placed either in Bars C or Bars U.
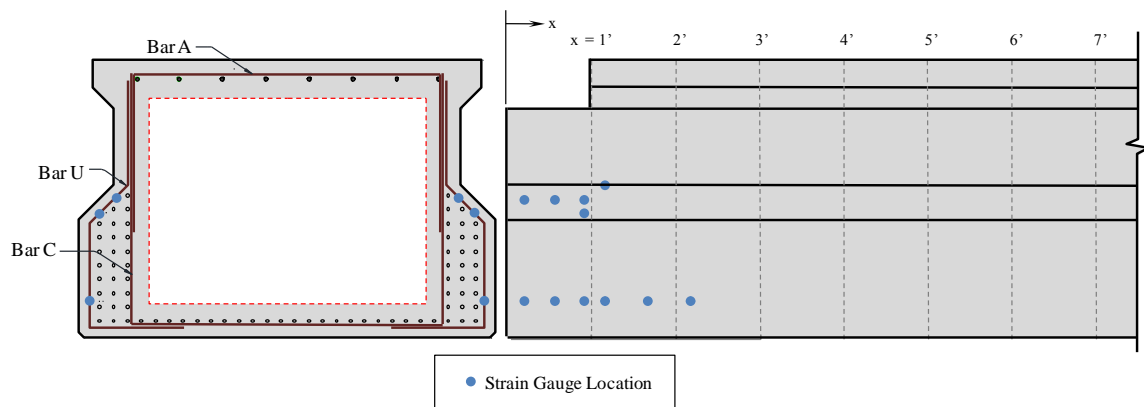
Figure 3-21: Strain gauge locations within the region of interest monitored during prestress transfer.

83

During the course of the research program, it was evident that bursting stresses were as important in the transverse horizontal direction as in the traditional transverse vertical direction. Therefore, starting from the second beam fabricated in FSEL (5B40-2), strain gages were also placed on the reinforcing bars going across the end block.

For shear tests, strain gauge locations were selected along a compression zone spanning from the load point to the support as illustrated in Figure 3-22. This was done in order to investigate the level of stress present in the shear reinforcement through the loading process.
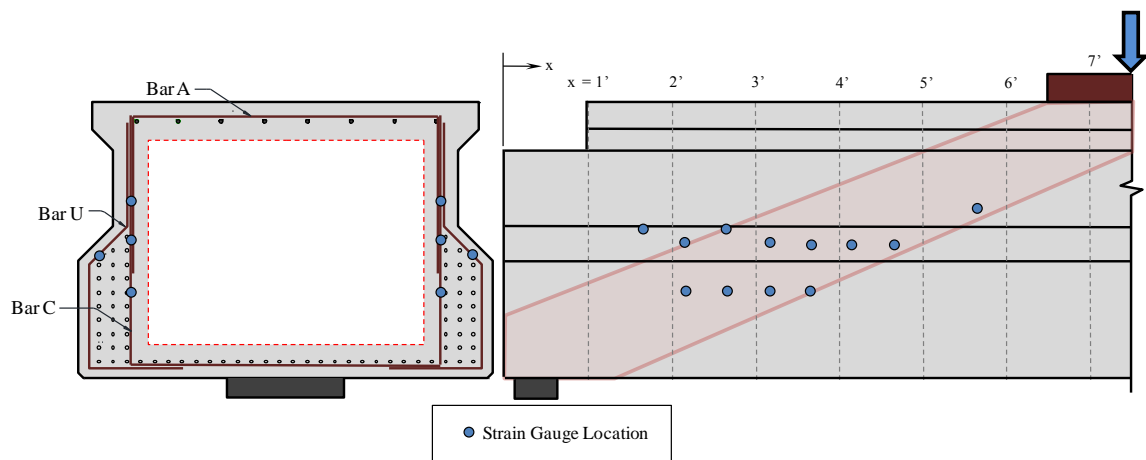
Figure 3-22: Strain gauge locations within the region of interest monitored during shear tests.

The selection of strain gauge locations was a very dynamic process through the experimental program. As new information became available from one test, gauge locations were modified accordingly in order to obtain the most relevant information possible from the subsequent tests. Although this process was not flawless, it was necessary in a program where so little background information was available.

Some strain gages were placed on the prestressing strands in order to monitor strains during jacking and release. Monitoring strains in the strands during shear tests was done depending on the availability of channels in the data acquisition system. It was decided to give priority to instrumentation geared to study web shear behavior.

3.3.5.2 Thermocouples

A total of 18 thermocouples were used in each beam specimen. Six thermocouples were placed in one end of the beam, connected to a wireless temperature match curing system used to determine when concrete had reached its design release strength. Twelve other thermocouples were placed at the opposite end (the skewed end for beams 5B40-1 through 5B40-4) to study temperature gradients across the section and how they varied depending on the geometry of the internal void former.

3.3.5.3 Test Instrumentation

As in the 4B28 box beam program, shear deformation measurement instrumentation was installed, as illustrated in Figure 3-11, in beams 5B40-1 and 5B40-2. After the shear tests were conducted on these two beams, it was clear that first diagonal cracks were located closer to the end regions, outside the area monitored by the shear deformation measurement instrumentation. Therefore, it was decided to discontinue the monitoring of these instruments in subsequent tests, allowing more of the internal instruments to be monitored.

Other instrumentation used was also akin to that used in the 4B28 shear test program. Load cells capable of measuring up to 1000 kip were used to measure reactions at each support as illustrated in Figure 3-23, deflections were measured on both sides of the beam at each support and under the load point and pressure transducers were used to measure the applied load.
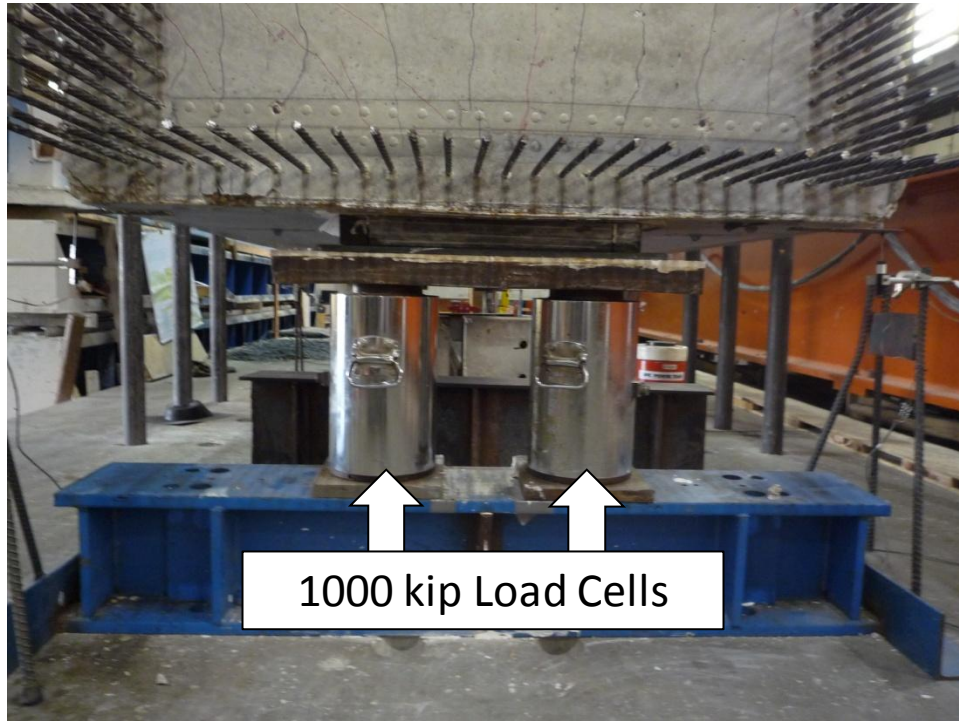
Figure 3-23: Load Cells measuring reactions in 5B40 shear test program.

3.3.6 **Feasible Shear Spans**

As previously explained, the selection of shear span is critical to ensure shear failure. The geometric properties of the in-house fabricated box beams allow for a wide range of feasible shear spans. As a safety measure, the maximum feasible shear span was limited to that for which shear failure is highly likely to occur before flexural failure. For the maximum feasible shear span, when the flexural capacity is reached; the associated shear is equal to expected shear capacity, equal to 1.75 times the calculated shear capacity. The selection of the value of 1.75 was based on the results of the shear tests on the box beams inherited from Project 0-5197 discussed in previous sections. Given these conditions, the maximum feasible shear span was determined to be approximately 10.3 ft (a/d = 3.9) as illustrated in Figure 3-24.

Ultimately, a shear span of 7.5 ft (a/d = 2.83) was selected considering:

    i.   Flexural failure is extremely unlikely with a/d = 2.83 (Figure 3-24).

ii. The second end region of the beam is likely to remain without diagonal cracks throughout the test of the first end region.

iii. Even if significant damage was sustained by the first end region tested, a second test with the same shear span can be performed on the second end region and still result in shear failure. This assertion accounts for a reduced total clear span in the second test as a result of overhanging the damaged part of the beam outside of the supports as was done previously and shown in Figure 3-9, and

iv. A shear span to depth ratio (*a/d*) greater than 2.5 generally considered an acceptable ratio for sectional behavior analysis.
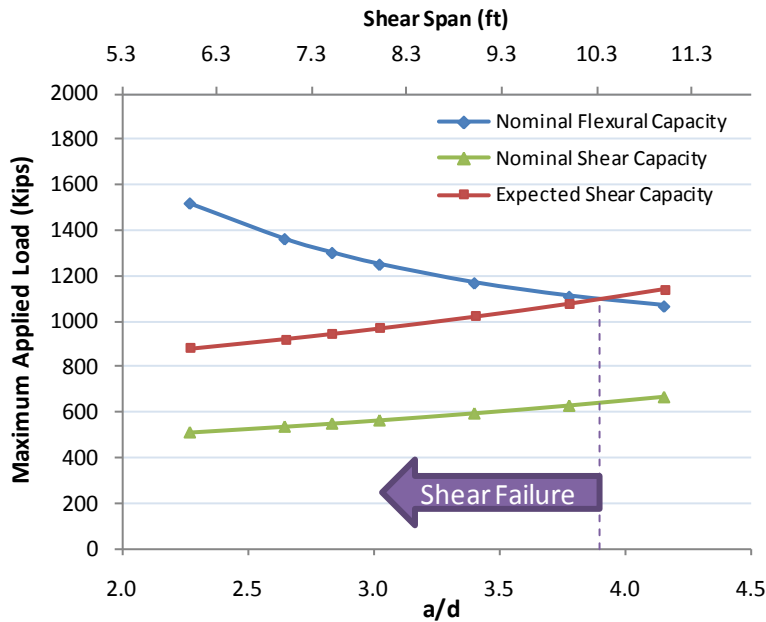
Figure 3-24: Feasible shear spans study for 5B40 box beams.

In the case of the 5XB40 box beam, given the addition of the composite deck, the total depth of the specimen was increased to 48 in. Statistically, for larger beams, shear strength equations do not underestimate strength as much as with smaller beams. Therefore, it was decided to use a 1.4 factor to determine the probable shear failure load. After evaluating possible test scenarios and feasible shear spans as illustrated in Figure

87

3-25, it was decided to conduct the shear tests at a shear span of 10 ft (a/d = 2.78). At this shear span, the load causing flexural failure causes a shear force that is 60% greater than the calculated shear capacity of the section. Given the total length of the beam (30 ft), there was still a possibility to conduct a second test in which the damaged portion of the beam overhangs outside the load region. In order to obtain similar overall behavior, the decision was made not to vary the shear span-to-depth ratio (a/d) between the tests conducted on 5B40 beams and the 5XB40 beam. The a/d ratios of 2.83 and 2.78, used for the tests on the 5B40 beams and the 5XB40 beam respectively, can be considered to be practically equal to one another.
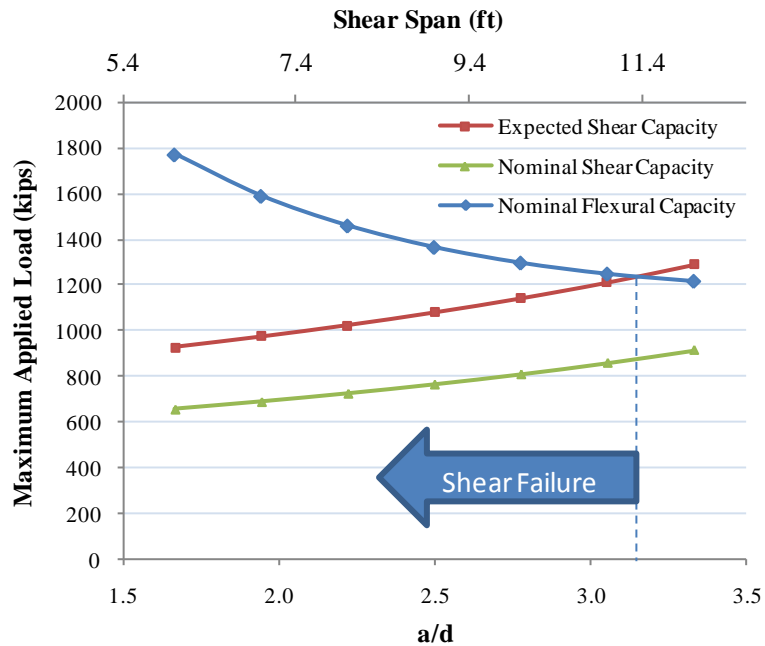
Figure 3-25: Feasible shear spans study for 5XB40 box beam.

3.4 SUMMARY

The experimental program of this study included a total of 29 tests of which 20 shear tests were conducted on 4B28 Box beam inherited from a previous research project. The effects that different concrete mixtures, aggregates, beam end geometries and internal void former geometry at skewed ends have on shear performance were investigated. Results from this part of the experimental program are presented in Chapter 4.

After the tests on the 4B28 box beams were completed, in-house fabrication and subsequent shear tests on a total of 5 beams was conducted. Four of these beams share the same cross section identified as 5B40. The last beam was box beam prototype identified as 5XB40. The 5XB40 box beam was essentially a modified 5B40; with thicker webs and bottom slab and a different strand placement pattern. Seven tests were conducted on 5B40 beams and two more were conducted on the 5XB40 beam for a total of 9 tests conducted on in-house fabricated beams.

As the beams in the second part of this experimental program were fabricated within FSEL, extensive internal instrumentation was used to monitor the stresses induced during prestress transfer and evaluate the current reinforcement details of the end regions of standard box beams in their ability to manage bursting stresses. Results from this part of the experimental program are presented in Chapter 5.

Finally, all of the beams fabricated within FSEL were tested in shear. Internal instrumentation was monitored during the shear tests to improve knowledge of box beam behavior. Results from the shear tests conducted on the in-house fabricated beams are presented in Chapter 6.

CHAPTER 4

Results and Analysis: Shear Performance of 4B28 Box Beams

4.1 INTRODUCTION

A large number of load tests on full-scale specimens were conducted in the current research program. Rather than presenting the results test-by-test, results are presented for all tests grouped by topic of interest so the reader can compare results of the different test specimens. To assist the reader in identifying plots and pictures, specimen names are arranged to serve as an identification key. The logic with which specimens and tests were named is explained in Figure 4-1.

$$BB07\text{-}SCC\text{-}LS\text{-}Q\text{-}1\text{-}2.9$$

Beam ID

CC =   Conventional Concrete

SCC = Self-consolidating
         Concrete

LS = Limestone aggregate

RG = River gravel aggregate

a/d ratio

# of Bearing Pads at
the end tested

Q = Square End

KK = Skewed End, Skewed Void

KQ = Skewed End, Square Void

KH = Skewed End, Hybrid Void
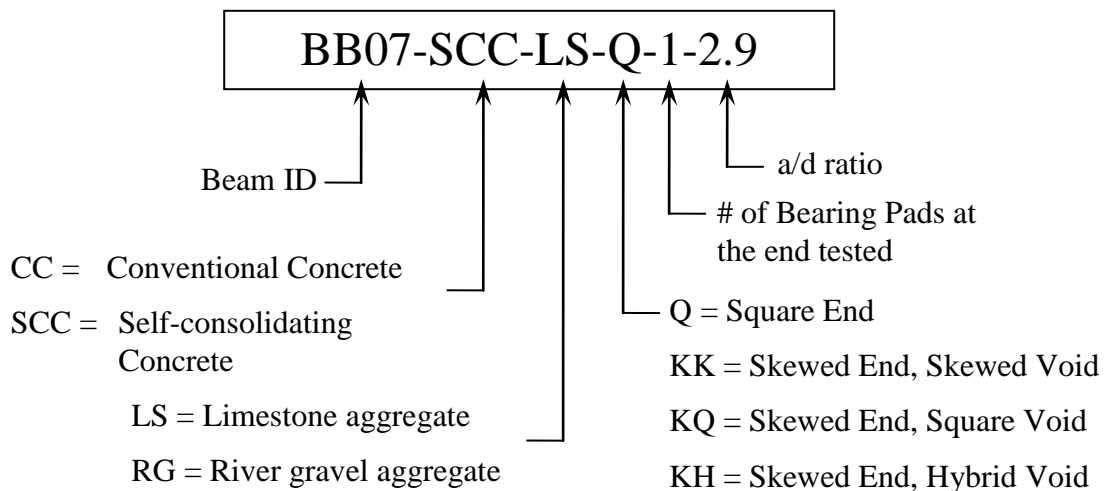
Figure 4-1: Specimen naming system/ Test identification key.

Some simplifying assumptions were made in the calculations presented in this chapter. The first the assumption is that box beams, despite having two webs separated by an internal void, can be designed as an equivalent I-shaped girder with a single web as thick as the sum of the thickness of the webs of the box beam.

Given the first assumption, the second assumption relates to the calculation of the shear span of an equivalent I-shaped girder. Where two bearing pads were used at skewed ends, as illustrated in Figure 4-2, the equivalent support point was assumed to be centered

between the two bearing pads both transversely and longitudinally. The longitudinal distance between the two bearing pads at a 30 degree skew was 18.88 in. Hence, the bearing pads are 9.44 in. closer to the load point on the short side of the beam and 9.44 in. further away from the load point on the long side of the beam. This distance is rather small when compared to the total span. If the span constitutes of the full length of the beam (30 ft), 9.44 in. is effectively 2.6% of the total span length.

Where a central bearing pad was used for testing, the equivalent support point is in fact the center of the single bearing pad. The distance from the equivalent support point to the end face of the beam was considered as an overhang with a length of 15.75 in.
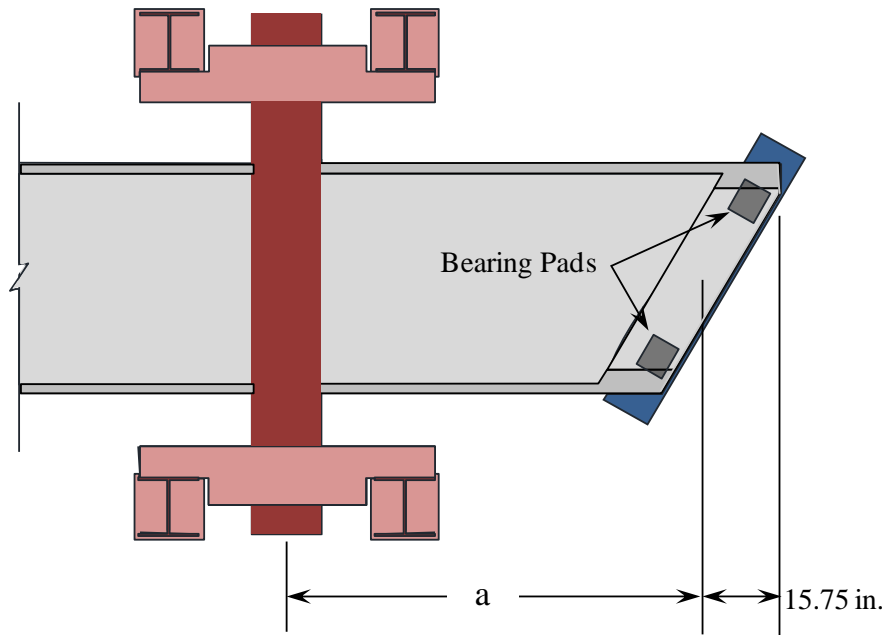
Figure 4-2: Shear Span definition for skewed supports when two bearing pads were used.

As explained in Chapter 3, each beam specimen was tested twice. A typical first test on a beam is illustrated in section (a) of Figure 4-3. A typical second test on a beam is illustrated in section (b) of Figure 4-3. A critical-shear section, located at the mid-length of the shear span, as illustrated in Figure 4-4, was used to evaluate the shear causing diagonal cracks in the web (see Section 4.2) and the shear strength calculation methods (see Section 4.7).
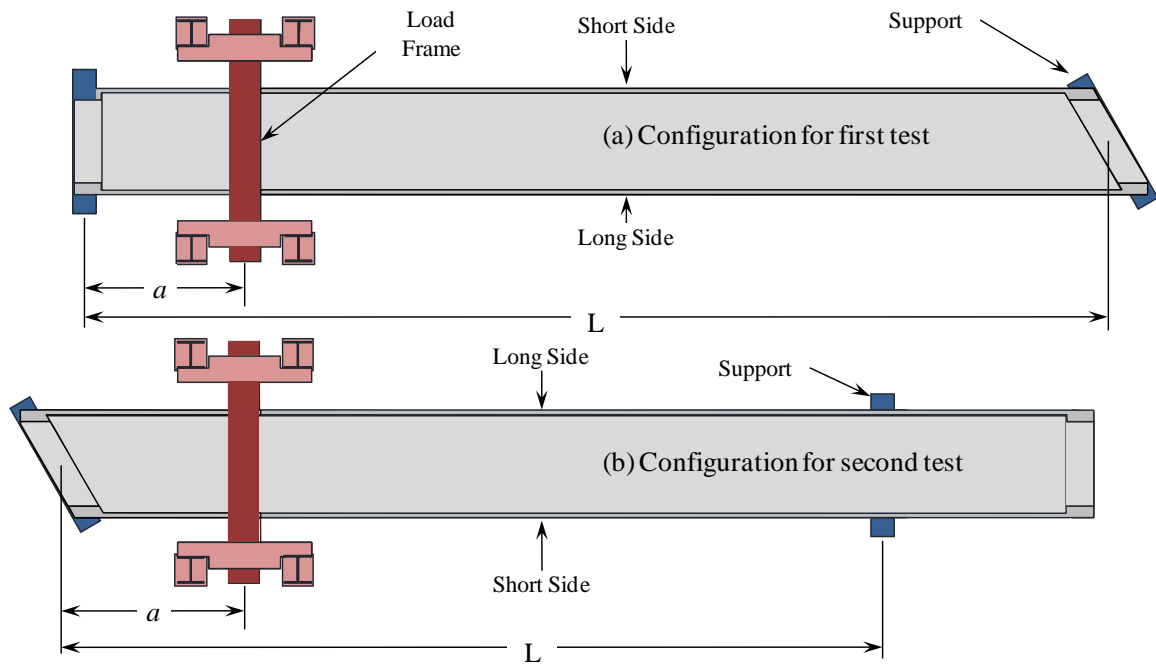
Figure 4-3: Plan view of shear test static configurations: (a) Configuration for first test, (b) Configuration for second test.
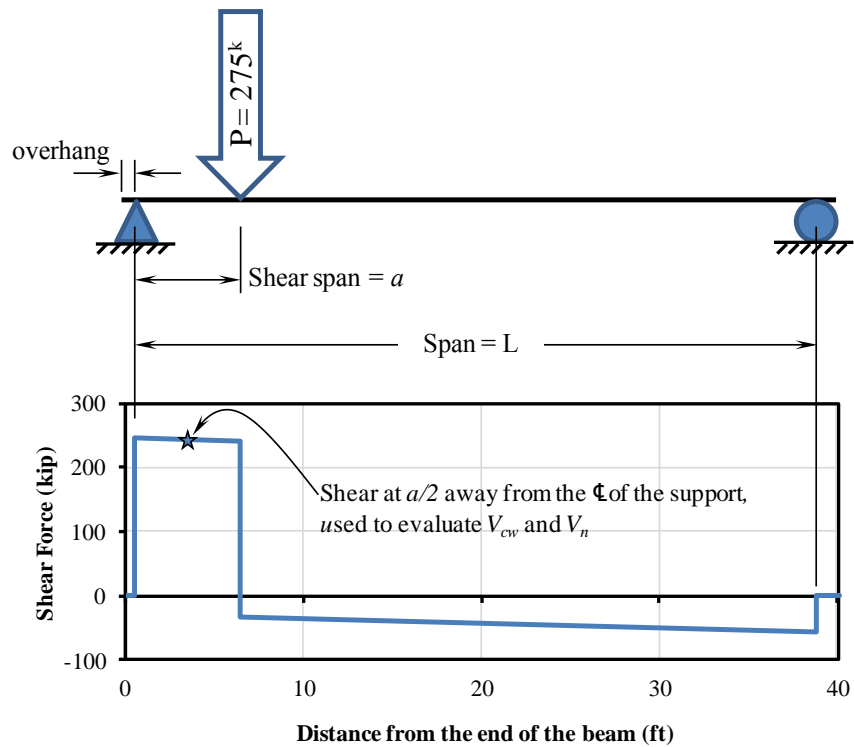
Figure 4-4: Shear force diagram for typical first test setup.

The shear spans and spans for all tests are summarized in Table 4-1. When the square end of a beam specimen was tested, the overhang at the test end was 5.25 in. This overhang was measured from the end of the beam at the square end to the center of the bearing pads. When the skewed end of a beam specimen was tested, the overhang at the test end was 15.75 in. This overhang was measured from the end of the beam on the "*long side*" of the skewed end to the center of the support as illustrated in Figure 4-2.

Table 4-1: Spans and Shear Spans for all tests

Test ID	Span (ft)	Shear Span (ft)
BB-01-CC-LS-Q-1-2.9	38.375	6
BB-01-CC-LS-KK-2-3.4	30.375	7
BB-02-CC-LS-Q-1-2.9	38.375	6
BB-02-CC-LS-KQ-1-3.4	30.375	7
BB-03-CC-RG-Q-2-2.9	38.375	6
BB-03-CC-RG-KK-2-3.4	30.375	7
BB-04-CC-RG-Q-2-2.9	38.375	6
BB-04-CC-RG-KQ-1-3.4	30.375	7
BB-05-CC-RG-Q-2-2.9	38.375	6
BB-05-CC-RG-KH-2-3.4	30.375	7
BB-06-SCC-LS-Q-2-2.9	38.375	6
BB-06-SCC-LS-KK-1-3.4	30.375	7
BB-07-SCC-LS-Q-1-2.9	38.375	6
BB-07-SCC-LS-KQ-1-3.4	30.375	7
BB-08-SCC-RG-Q-1-2.9	38.375	6
BB-08-SCC-RG-KK-1-3.4	30.375	7
BB-09-SCC-RG-Q-2-2.9	38.375	6
BB-09-SCC-RG-KQ-2-3.4	30.375	7
BB-10-SCC-RG-KH-1-3.4	38.375	7
BB-10-SCC-RG-Q-1-3.4	30.375	7

4.2   WEB-SHEAR CRACKING

4.2.1   Measured versus Calculated Load

The experimental load associated with diagonal cracking was determined by visual observation of diagonal cracks in the test zone. In most cases, diagonal cracking was accompanied by a loud *popping* sound. When this sound was heard, loading was interrupted to inspect the beams for diagonal cracks.

The two webs of the beam were denoted by the length of the side of the beam to which they correspond as illustrated in Figure 4-3. Since one end of the beams was fabricated square and the other end was fabricated at a 30 degree skew, one side is effectively "*longer*" than the other.

Two methods were used to calculate the load causing web-shear cracks (V_{cw}). Specifically, the Detailed Method presented in ACI 318-08 and the Simplified Procedure from AASHTO-LRFD (2010). These two methods, presented in Chapter 2, are very similar with the latter being a modification of the former; incorporating the results from a recent experimental database evaluation process (Hawkins et. al., 2005).

After the shear causing web-shear cracks was calculated by both methods, the load that would cause such shear at a location *a/2* away from the load point was calculated. This calculated load was then compared with the measured load at the time web-shear cracks were first observed. The ratios of the experimental web-shear cracking load to the calculated one for each web are presented in Table 4-2.

In most cases, upon the formation of diagonal cracks, the external instrumentation measured a sudden increase in the average diagonal strain. One example of this is shown in Figure 4-5 where the average diagonal strain (measured along the dashed red line in the inset photograph) increased abruptly at 156 kips of applied shear for the web on the short side of the beam.

In Figure 4-5, it can also be observed how the diagonal crack intersects the instrumentation measuring the diagonal strain. The external instrumentation was used as a secondary means of measurement to determine when diagonal cracks first appeared. A detailed explanation of this process is provided in the following section.

Table 4-2: Diagonal Cracking Shear Results Summary

Test ID	Measured Shear (kips)		Calculated Shear (kips)		Web Shear Cracking Load (Measured/Calculated)			
					ACI Detailed Method		AASHTO Simplified Procedure	
	Long Side	Short Side	ACI Detailed Method	AASHTO Simplified Procedure	Long Side	Short Side	Long Side	Short Side
BB-01-CC-LS-Q-1-2.9	120	120	154	102	0.78	0.78	1.18	1.18
BB-01-CC-LS-KK-2-3.4	174	127	154	102	1.13	0.83	1.70	1.24
BB-02-CC-LS-Q-1-2.9	107	129	154	102	0.70	0.84	1.05	1.26
BB-02-CC-LS-KQ-1-3.4	138	102	154	102	0.90	0.66	1.35	1.00
BB-03-CC-RG-Q-2-2.9	181	86	153	102	1.18	0.56	1.77	0.84
BB-03-CC-RG-KK-2-3.4	164	156	153	102	1.07	1.02	1.61	1.53
BB-04-CC-RG-Q-2-2.9	155	173	151	101	1.03	1.14	1.54	1.71
BB-04-CC-RG-KQ-1-3.4	165	165	151	101	1.09	1.09	1.64	1.64
BB-05-CC-RG-Q-2-2.9	155	147	152	101	1.02	0.96	1.53	1.44
BB-05-CC-RG-KH-2-3.4	172	140	152	101	1.13	0.92	1.69	1.38
BB-06-SCC-LS-Q-2-2.9	155	129	146	99	1.06	0.88	1.50	1.25
BB-06-SCC-LS-KK-1-3.4	129	77	146	99	0.88	0.53	1.09	0.65
BB-07-SCC-LS-Q-1-2.9	129	129	146	99	0.88	0.88	1.25	1.25
BB-07-SCC-LS-KQ-1-3.4	113	138	147	99	0.77	0.94	0.95	1.16
BB-08-SCC-RG-Q-1-2.9	164	113	143	97	1.15	0.79	1.62	1.12
BB-08-SCC-RG-KK-1-3.4	141	156	143	97	0.99	1.09	1.21	1.34
BB-09-SCC-RG-Q-2-2.9	113	121	144	97	0.79	0.84	1.11	1.19
BB-09-SCC-RG-KQ-2-3.4	173	77	144	97	1.20	0.53	1.48	0.66
BB-10-SCC-RG-KH-1-3.4	82	82	147	99	0.56	0.56	0.76	0.76
BB-10-SCC-RG-Q-1-3.4	137	137	147	99	0.93	0.93	1.15	1.15
Average					0.96	0.84	1.36	1.19
Min					0.56	0.53	0.76	0.65
Max					1.20	1.14	1.77	1.71
St. Dev.					0.18	0.19	0.29	0.30
COV					18%	23%	21%	25%
Cases < 1.0					10/20	16/20	2/20	5/20
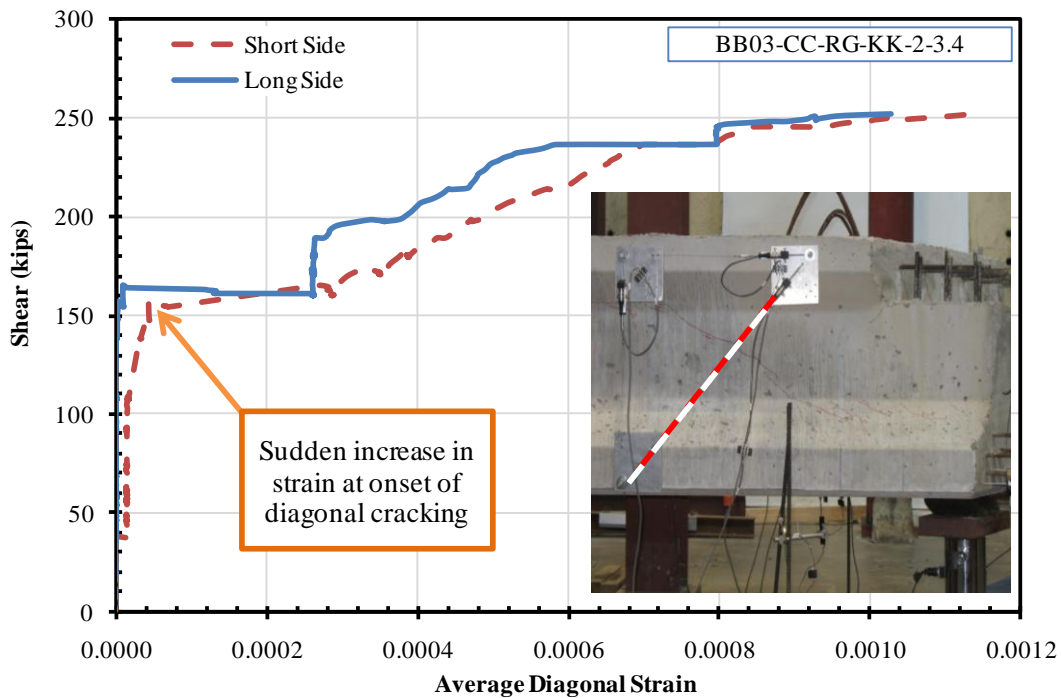
Figure 4-5: Determination of diagonal shear cracking load with external instrumentation. (From test on skewed end of BB-03)

In some cases, the first diagonal crack occurred outside the region monitored by the shear deformation instrumentation. More specifically, a very narrow diagonal crack opened within the web, centered approximately 26 to 28 in. from the end of the beam. An example of this occurrence is shown in Figure 4-6 where a diagonal crack opened at an applied shear of 107 kips. For the test shown (BB-02-CC-LS-Q-1-2.9, long side web), the calculated shear causing diagonal cracks on the web (V_{cw}, using the detailed method from ACI 318-08) is equal to 154 kips beyond the transfer length (30 in.). If V_{cw} is calculated at a location 26 in. from the end of the beam, a value of 146 kips, which is closer to the experimental shear, is obtained. This adjustment was deemed inconsequential as the improvement in the accuracy of the V_{cw} calculation was very small. Furthermore, the width (0.002 ~ 0.007 in.) of the diagonal cracks located this close to the end of the beam did not increase as more load was applied. Usually, more important diagonal cracks, located closer to mid-length of the shear span (*a/2*), formed and grew longer and wider as more load was applied.

96
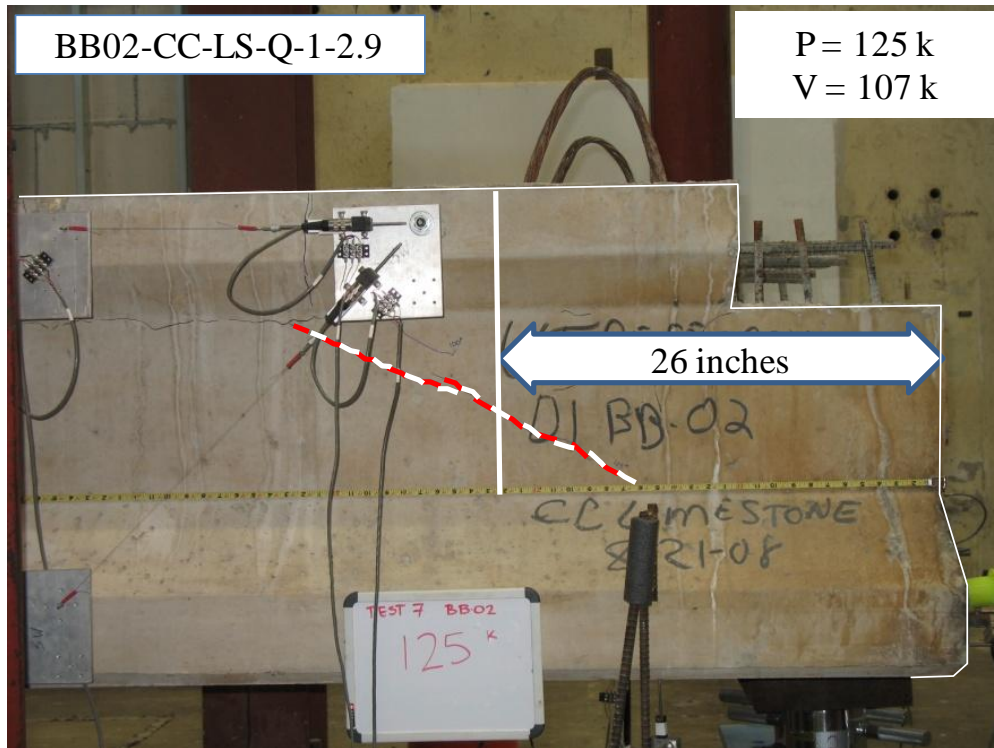
Figure 4-6: Diagonal crack centered 26 in. from the end of the beam. Test on the square end of BB-02 is shown (long side web).

By analyzing the results presented in Table 4-2, it can be seen that there was a large scatter in the accuracy and conservativeness of the web-shear cracking load calculations. Using the Simplified Procedure from AASHTO-LRFD (2010) the load causing web-shear cracking was, on average, underestimated by a larger margin than when using the Detailed Procedure from ACI 318-08. Nevertheless, the variability of the results with either method was high; with web-shear cracks occurring at loads above or below the calculated load by more than 30% on several occasions. The coefficient of variation for the ratios of the experimental to calculated web-shear cracking load, using the detailed method from ACI 318-08 and the simplified procedure from AASHTO-LRFD (2010), were 21% and 24% respectively, indicating their high variability. More important than the variability of the estimations, is the frequency with which the calculated web-shear cracking load was lower than the experimental load. This unconservative estimation of the cracking load happened in 65% of all cases (26 out of

97

40 webs) when the detailed method from ACI 318-08 was used and in 18% of all cases (7 out of 40 webs) when the simplified procedure from AASHTO-LRFD (2010) was used.

No discernible pattern was found in the conservativeness of the calculated web-shear cracking loads. That is, it cannot be said that one specific support condition or material was correlated with over or underestimations of the web-shear cracking load. One must admit that trying to keep box beam bridges without diagonal cracks seems to be a difficult task for bridge designers when there is no reliable method available to calculate the demands associated with web-shear cracks. It seems wiser to concentrate on controlling the width of the cracks through adequate reinforcement and limit environmental exposure through various protection methods. From results discussed in this section, it appears that the crack width measurements (Section 4.2.3) might be more useful to a bridge designer than the shear at web cracking.

4.2.2 Shear Distortions

The linear potentiometers installed on the side of the beams served as a secondary means of establishing the experimental diagonal cracking shear. Three threaded rods were embedded into the sides of a beam specimen, forming a triangle. By combining the deformation measurements of the horizontal, vertical and diagonal side of the triangle, it was possible to calculate an angle of shear distortion in the web. The distortion angle ($d\theta$) is defined herein as the change in the angle (θ) formed between the horizontal and vertical sides of the instrumentation triangle, as illustrated in Figure 4-7.

For each test, by using instrumentation triangles, the distortion angle ($d\theta$) was calculated for the two webs. The distortion angle was given by:

$$d\theta = \cos^{-1}\left(\frac{(H+dH)^2 + (V+dV)^2 - (D+dD)^2}{2 \cdot (H+dH) \cdot (V+dV)}\right) - 90° \qquad \textbf{Equation 4-1}$$

where:

H　　 = The horizontal distance between the two embedded rods in the top flange (in.). This distance was 24 in. and the line formed between the

corresponding two rods was horizontal before any superimposed load was applied

V   = The vertical distance between the embedded rod in the top flange, nearest to the load point and the embedded rod in the bottom flange (in.). This distance was 24 in and the line formed between the corresponding two rods was vertical before any superimposed load was applied.

D   = The diagonal distance between the embedded rod in the top flange, farthest from the load point and the embedded rod in the bottom flange (in.). This distance was 33.94 in and the line formed between the corresponding two rods was oriented at a 45° angle before any superimposed load was applied.

dH   = Change in the distance H (in.).

dV   = Change in the distance V (in.).

dD   = Change in the distance D (in.)
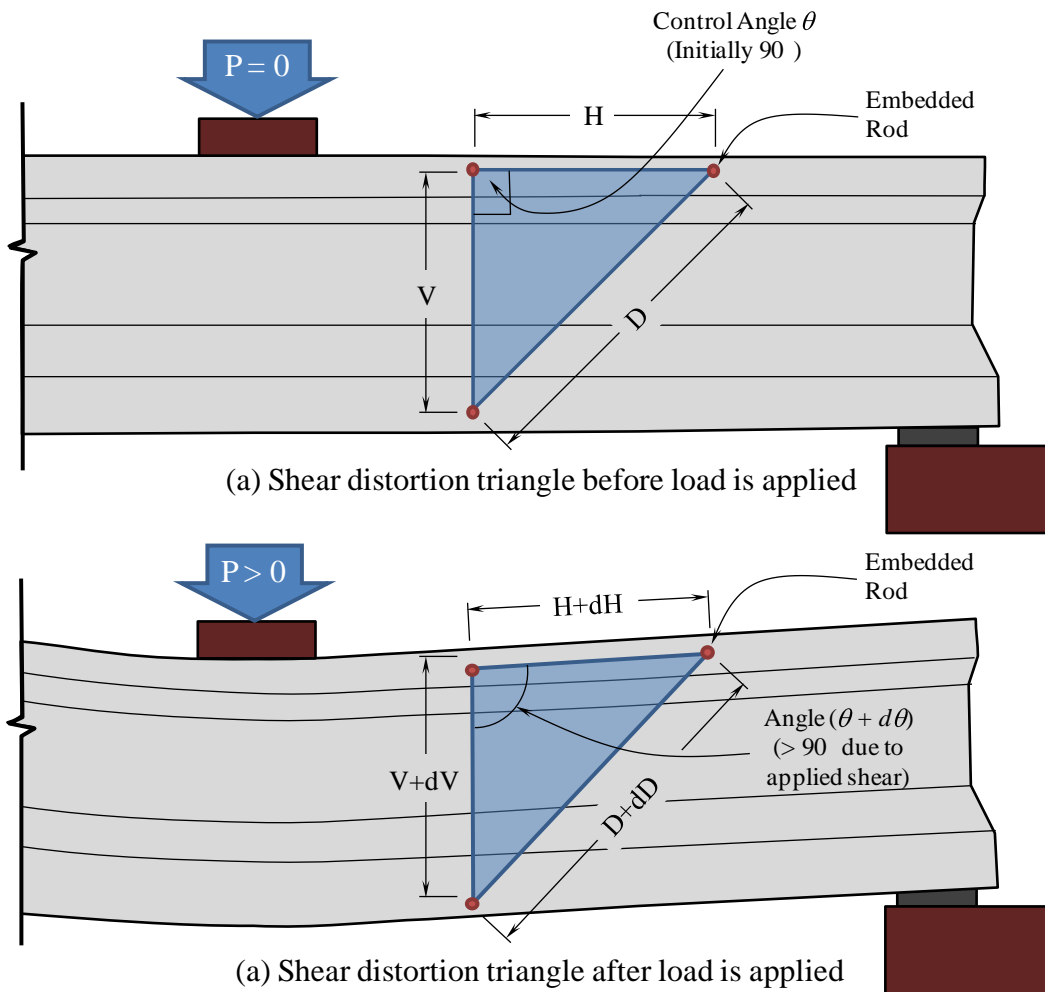
Figure 4-7: Shear Distortion triangle before and after load is applied

Whereas the aforementioned angle was initially 90 degrees in all cases, as load was applied, this angle increased slightly. The change in the angle was as much as ½ a degree in some cases but, in general, changes in the order of tenths of a degree were observed.

A sample shear-distortion plot is presented in Figure 4-8. In the sample plot, it can be seen that a sudden increase in the distortion angle corresponded with the first observation of a diagonal crack in the corresponding side of the beam. This agreement between the shear-distortion curves and observations of diagonal cracks was consistent through all tests. Shear-distortion plots for all tests can be found in Appendix C.

In general, the distortion in the two sides of the beam was approximately the same before diagonal cracks appeared, regardless of the geometry of the beam end being tested (square or skewed end). After diagonal cracks were present in the webs, the two shear-distortion plots drifted from one another as can be seen in Figure 4-8. It was seen that the magnitude of the distortion angle, measured after diagonal cracks had appeared, was related to the relative location of the diagonal crack(s) with respect to the location of the instrumentation triangle. Since diagonal cracks were rarely matched in both webs (the same location and corresponding applied shear), one can expect the distortion angle to be different for both webs under the same applied shear. No correlation was observed between a larger distortion angle in a particular web and the likelihood of that web to fail before the opposite web. The shear-distortion curves from test BB03-CC-RG-Q-2-2.9, illustrated in the sample plot, suggest that the "*short side*" web was likely to fail before the *"long side"* web. However, in that test, crushing occurred in both webs at the same time.
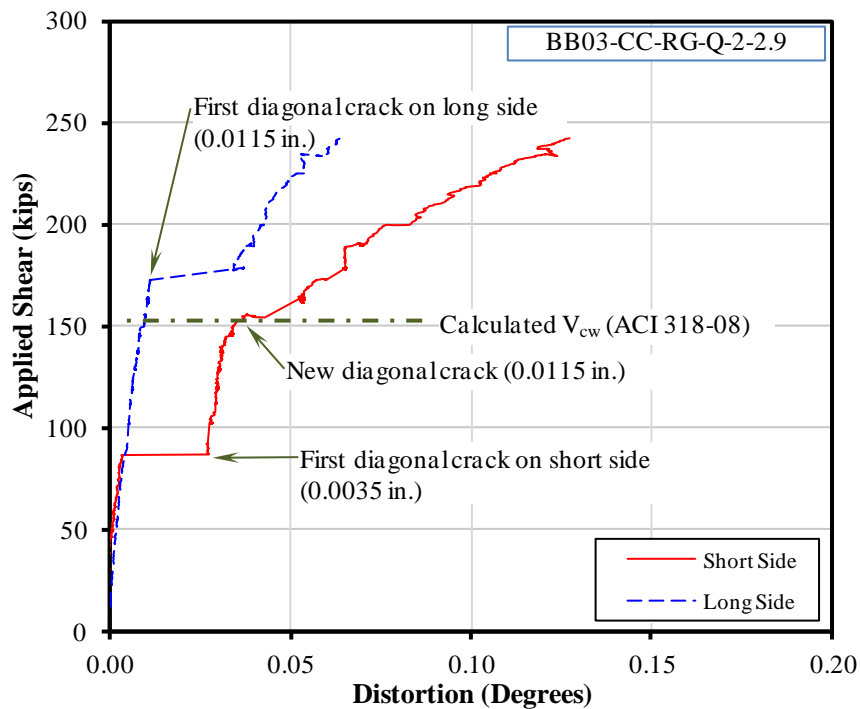
Figure 4-8: Shear-Distortion plots for

101

4.2.3 Web-Shear Crack Width Measurements

Once cracks were visible, crack width measurements were taken. In most of the earlier tests conducted at FSEL, all crack widths were taken with plastic crack width comparators. However, observation showed that initial cracks in beams fabricated with SCC were narrower than those in beams fabricated with conventional concrete. This was confirmed later when a graduated 100X Crack Microscope (minimum reticule division = 0.0005") was utilized to measure crack widths at the initial stages where the sensitivity of the plastic comparator was inadequate. Crack width measurements gathered by the two methods illustrated in Figure 4-9 had similar variability as can be seen in Figure 4-10. Initial crack widths for SCC beams ranged from 0.0025" to 0.0050" whereas for conventional concrete beams the range was between 0.0050" and 0.0150".

In every test, the measured crack width increased as applied load increased. However, it was not uncommon to see the crack width decrease in one location after a new crack developed in close proximity to the earlier crack. As can be expected, crack widths were larger away from the location of the stirrups (stirrups were spaced at 20 in. on center).

In all cases, the maximum crack width at each load step was documented. Plotting the documented crack widths for all tests versus the ratio of the corresponding load to the failure load, as can be seen in Figure 4-10, allows for some general inference to be made. For example, by using the lower bound of the scatter of the crack widths it can be said that; when crack widths exceeded 0.02 in., the beam was loaded beyond 60% of its capacity. Similar observations are gathered in Table 4-3. Care should be taken when using this guide as they are very specific to the beams in this study. If shear reinforcement spacing is different than 20 in., one can expect to see a different crack width distribution. Also, crack widths were always documented under sustained load and with a clean surface free of dust and debris. In a bridge inspection setting, only dead loads are sustained while live load is highly variable even within seconds. Furthermore, the exposed side of a beam is susceptible to the environment and accumulated dust can make the crack widths appear narrower.

102
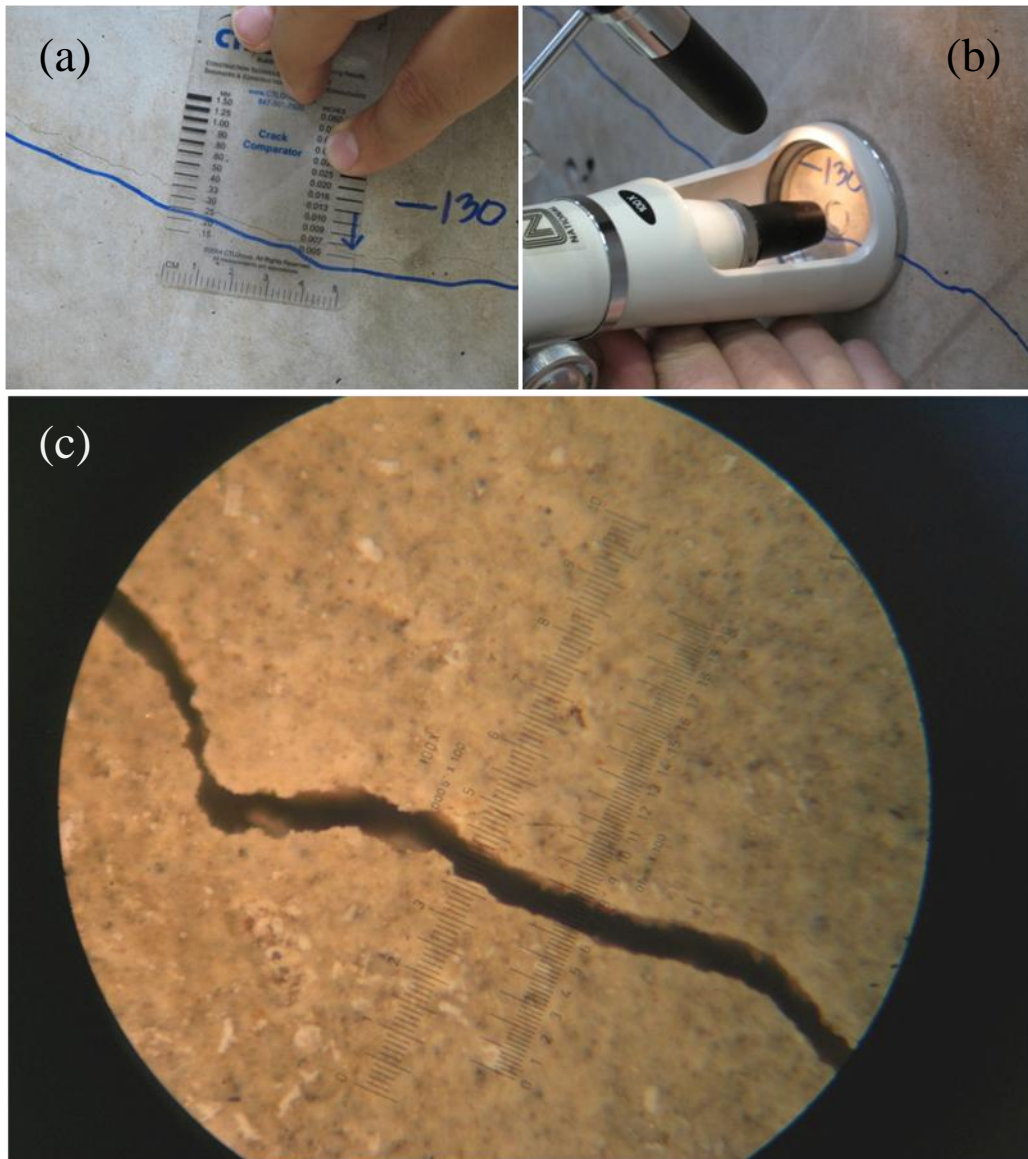
Figure 4-9: Crack width measurement techniques. (a) Plastic crack width comparator, (b) 100X Microscope, and (c) Crack width measurement through microscope (0.0025").
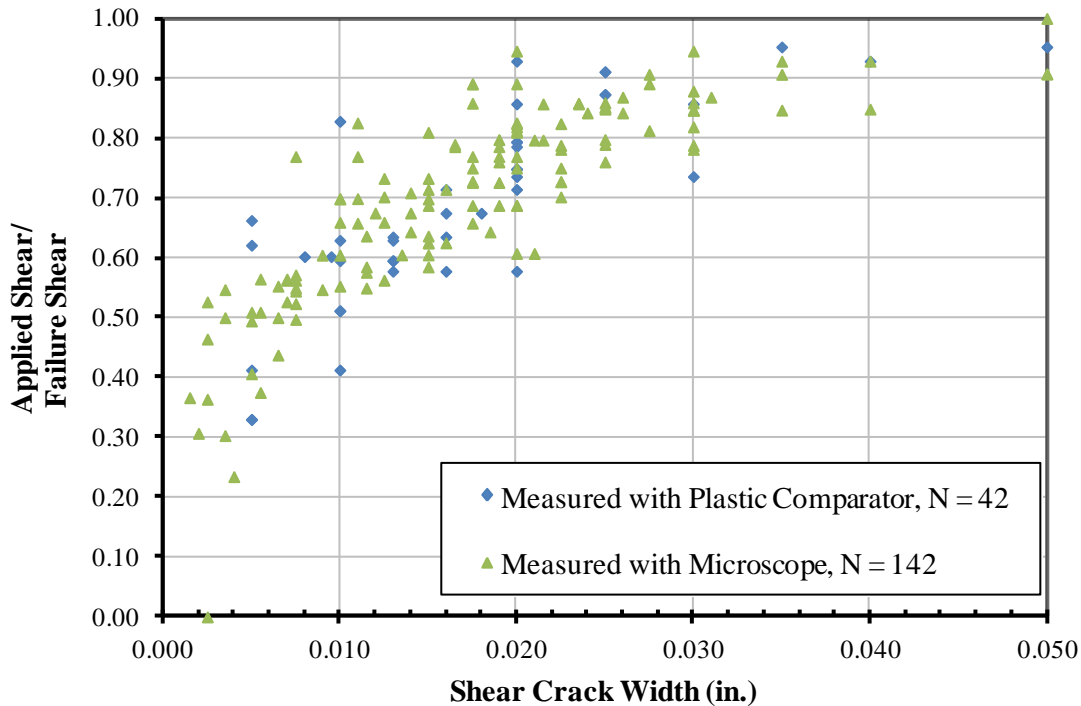
Figure 4-10: Crack width measurements for all tests grouped by measurement method.

Table 4-3: General guide based on lower bound of measured crack widths.

Maximum width of diagonal cracks (in.)	Applied Shear
0.010	Greater than 40% of failure shear
0.020	Greater than 60% of failure shear
0.030	Greater than 75% of failure shear

If crack width measurements are grouped by concrete mixture type as plotted in Figure 4-11, one can see that for the same shear level, the associated maximum crack width in beams fabricated with self-consolidating concrete is larger than in beams fabricated with conventional concrete. Also, for the same shear load, the variability in crack width measurements is higher for beams fabricated with self-consolidating beams. For example, at a shear force equal to 80% of nominal shear capacity, crack widths in conventional concrete vary from approximately 0.003 in. to 0.012 in (a 0.009-inch

range). Conversely, for self-consolidating concrete beams under a comparable shear force, measured crack widths varied from 0.003 in. to 0.020 in. (a 0.017-inch range).
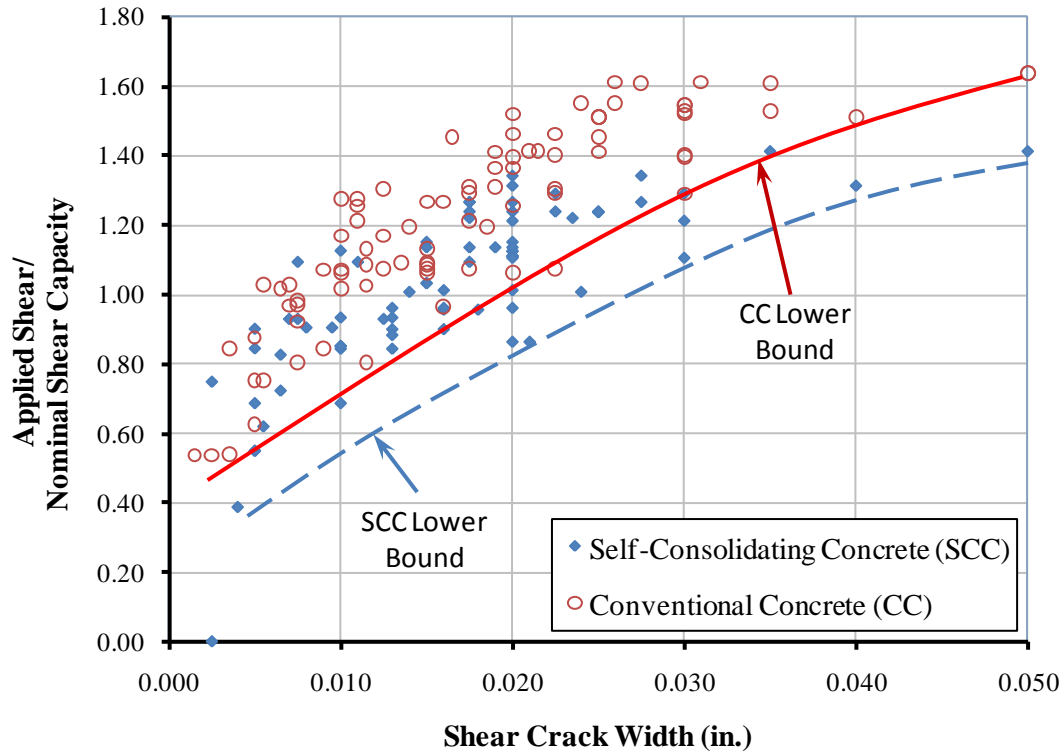
Figure 4-11: Crack width measurements for all tests grouped by concrete mixture type.

The lower bounds indicated in Figure 4-11 can be explained in two ways: an indication of the minimum shear associated with a given crack width (i.e. a lower bound for shear) or an indication of the maximum crack width for a given applied shear force (i.e. an upper bound for crack widths). Using the latter approach, one can do a similar exercise as presented in Table 4-3 to synthesize a short guideline for crack widths in both materials as presented in Table 4-4.

Table 4-4: General guide based on lower bound of measured crack widths for different concrete mixture types

Shear Force (% of Nominal Shear Capacity)	Maximum Crack Width (in.)	
	Self-consolidating concrete	Conventional Concrete
60%	0.010	0.006
80%	0.020	0.012
100%	0.025	0.020

4.3 FLEXURE AND FLEXURE-SHEAR CRACKING

In the case of web-shear cracks, significant differences were observed between the load causing diagonal cracks at each side of the beam. This was not the case for flexure and flexure-shear cracks. In the worst of all tests conducted on 4B28 box beams, the load causing flexural and flexure-shear cracks on either side of the beam differed from one another by 10 kips, which was approximately 4% of the load applied at that point in time.

To calculate the shear causing flexure-shear cracks, equations from the detailed method from ACI 318-08, previously described in Section 2.4.1 were used. The nominal shear strength provided by concrete when diagonal cracking results from combined shear and moment (V_{ci}) was calculated using Equation 2-2. Once V_{ci} was obtained, the applied load (including the self-weight of the beam, weight of the testing frame and the concentrated applied live load) that would cause this shear at a critical section located a distance $d_p/2$ away from the load point, towards the nearest support (i.e. within the test region), was calculated. The calculated load was then compared to the measured load causing flexure-shear cracks.

Similarly, the load that would cause a total moment equal to M_{cre}, exactly under the load point was found and then compared to the measured load causing flexural cracks. The cracking moment (M_{cre}) was calculated according to Equation 2-4. The ratios of the measured load to the calculated load for each test are presented in Table 4-5.

Table 4-5: Measured to Calculated ratios for applied load causing flexural and flexure-shear cracks

Test ID	Flexure-Shear Cracking Load (Measured/Calculated)	Flexural Cracking Load (Measured/Calculated)
BB-01-CC-LS-Q-1-2.9	0.79	0.99
BB-01-CC-LS-KK-2-3.4	0.98	1.11
BB-02-CC-LS-Q-1-2.9	0.73	1.09
BB-02-CC-LS-KQ-1-3.4	0.90	1.11
BB-03-CC-RG-Q-2-2.9	0.90	1.07
BB-03-CC-RG-KK-2-3.4	1.05	1.29
BB-04-CC-RG-Q-2-2.9	0.92	1.25
BB-04-CC-RG-KQ-1-3.4	1.00	1.18
BB-05-CC-RG-Q-2-2.9	0.91	1.16
BB-05-CC-RG-KH-2-3.4	0.99	1.20
BB-06-SCC-LS-Q-2-2.9	0.75	1.01
BB-06-SCC-LS-KK-1-3.4	0.77	0.87
BB-07-SCC-LS-Q-1-2.9	0.75	1.01
BB-07-SCC-LS-KQ-1-3.4	0.85	0.96
BB-08-SCC-RG-Q-1-2.9	0.69	1.02
BB-08-SCC-RG-KK-1-3.4	0.81	0.97
BB-09-SCC-RG-Q-2-2.9	0.75	1.02
BB-09-SCC-RG-KQ-2-3.4	0.86	1.05
BB-10-SCC-RG-KH-1-3.4	0.79	1.06
BB-10-SCC-RG-Q-1-3.4	0.87	1.04
Average	0.85	1.07
Minimum	0.69	0.87
Maximum	1.05	1.29
Std. Deviation	0.10	0.10
COV	12%	10%
Cases < 1.0	18/20	4/20

In general, agreement between the calculated loads causing flexure-shear cracks and flexure cracks, and the loads observed experimentally was reasonable. The same trends were present for flexure-shear and flexure cracks. The conservativeness of the load calculation varied with the different concrete mixtures. As summarized in Table 4-6 and Table 4-7, the most conservative results were obtained for tests on beams fabricated with

conventional concrete and river gravel coarse aggregate. Calculations performed for beams fabricated with self-consolidating concrete were less conservative than those fabricated with conventional concrete. Similarly, calculations performed for beams fabricated with crushed limestone aggregate were less conservative than those from beams fabricated with river gravel aggregate.

Visually; for web-shear, flexure-shear and flexure cracks, it is worth noting that beams fabricated with self-consolidating concrete exhibited more cracks of lesser width than beams fabricated with conventional concrete as has been reported for these same beams in the past by Schnittker and Bayrak (2008). The averages reported in Table 4-6 and Table 4-7 show small differences between conventional concrete and self-consolidating concrete. Small differences seen in SCC and CC behavior, in regards to flexural and flexure-shear cracking, are less than the typical variation seen in such data and are considered insignificant.

In summary, there are two final points to make regarding the differences in the experimental to calculated ratios. First, differences were modest. Secondly, and perhaps more importantly, all of the average ratios of calculated to experimental loads are reasonably close to a value of 1. This indicates acceptable accuracy of the simple methods use to calculate flexure-shear and flexure cracking loads.

Table 4-6: Average ratios of experimental to calculated flexure-shear cracking load

Flexure-Shear Cracking Load (Experimental/Calculated)	Conventional Concrete	Self-Consolidating Concrete	All Concrete Types
Crushed Limestone	0.85	0.78	0.82
River Gravel	0.96	0.80	0.88
All Aggregates	0.92	0.79	0.85

Table 4-7: Average ratios of experimental to calculated flexure cracking load

Flexure Cracking Load (Experimental/Calculated)	Conventional Concrete	Self-Consolidating Concrete	All Concrete Types
Crushed Limestone	1.08	0.96	1.02
River Gravel	1.19	1.03	1.11
All Aggregates	1.15	1.00	1.07

4.4   SIDE-TO-SIDE REACTION DISTRIBUTION

In bridge construction, 4B28 box beams are supported using three elastomeric bearing pads. Underneath one end of the beam, one larger bearing pad (14 in. wide by 6 in. long) is centered across the width of the box beam. Underneath the other end of the beam, two smaller bearing pads (7 in. wide by 6 in. long) are placed closer to the sides with a considerable separation between them. In the case of the 4B28 box beams with a 30 degree skew, the distance between the centroids of the two smaller bearing pads is more than 3 feet. This separation raises the question of whether a larger fraction of the load is flowing into one of the bearing pads

Where two bearing pads were used to support at a given beam end, each of the two bearing pads was placed on top of a load cell, allowing for the reaction at each bearing pad to be accurately measure. A total of nine tests were conducted with the tested end supported by two separated bearing pads. Five of these tests correspond to square ends and four of them correspond to skewed ends. For square beam ends, about half of the total shear was measured on either side. Given the symmetry of the beam end and the placement of the support bearing pads, equal reactions at both bearing pads can be expected. For skewed beam ends, one could expect a higher fraction of the total shear to flow towards the shorter side of the beam.

The ratio of the reaction on the short side of the beam to the sum of the reactions on both bearing pads was studied through the loading process as illustrated in Figure 4-12 and Figure 4-13. As can be seen in Figure 4-12, the reaction on the short side for square ends was around 50% of the shear plus or minus approximately 3%. On the other hand, as can be seen in Figure 4-13, the reaction on the short side (the obtuse corner) of skewed beam ends was on average 54% of the total shear plus or minus approximately 6%.

These ratios confirm that a larger fraction of the load flows towards the shorter side of skewed ends. However, in the worst case measured, 60% of the load went to the short side of the beam. This difference (± 10%) is small within the context of shear behavior. More importantly, the difference in the load flowing to each support did not result in failures of either web at a load lower than the calculated capacity. That is; even

though both webs seldom failed simultaneously, this never resulted in unconservative shear strength calculations. It is safe to say then that the unsymmetrical load distribution caused by the skewed geometry of the beam end and supports is not a cause for concern for box beams with ends skewed up to 30 degrees.
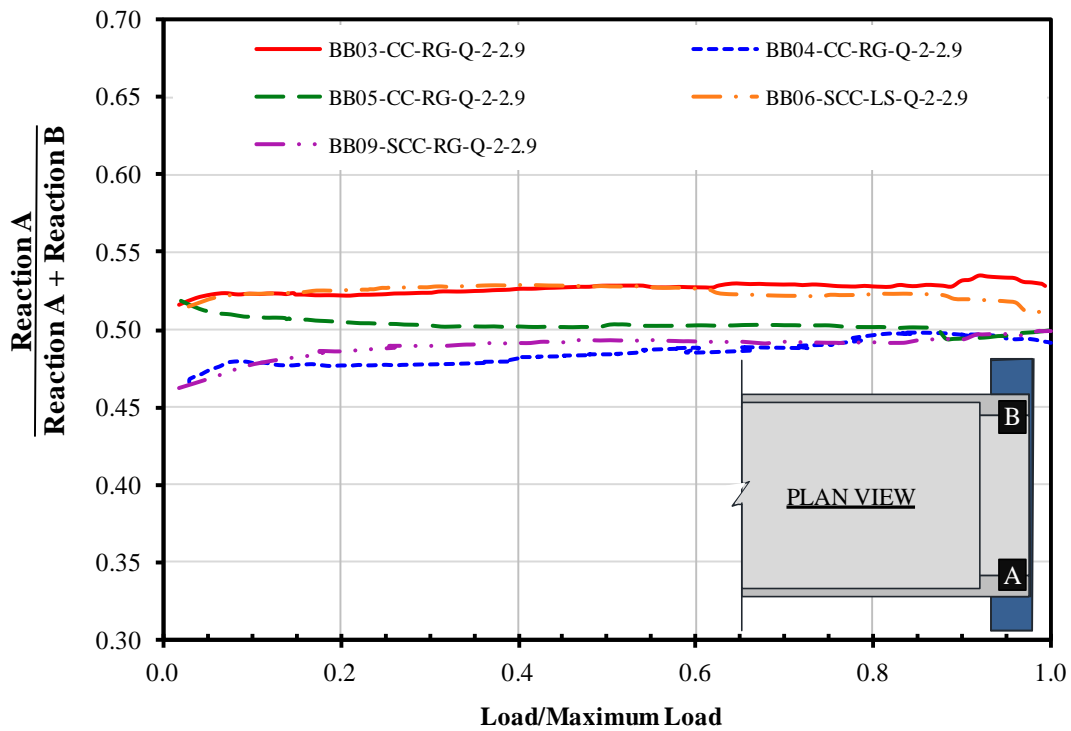
Figure 4-12: Side-to-side distribution of reactions for square ends supported by two separated bearing pads.
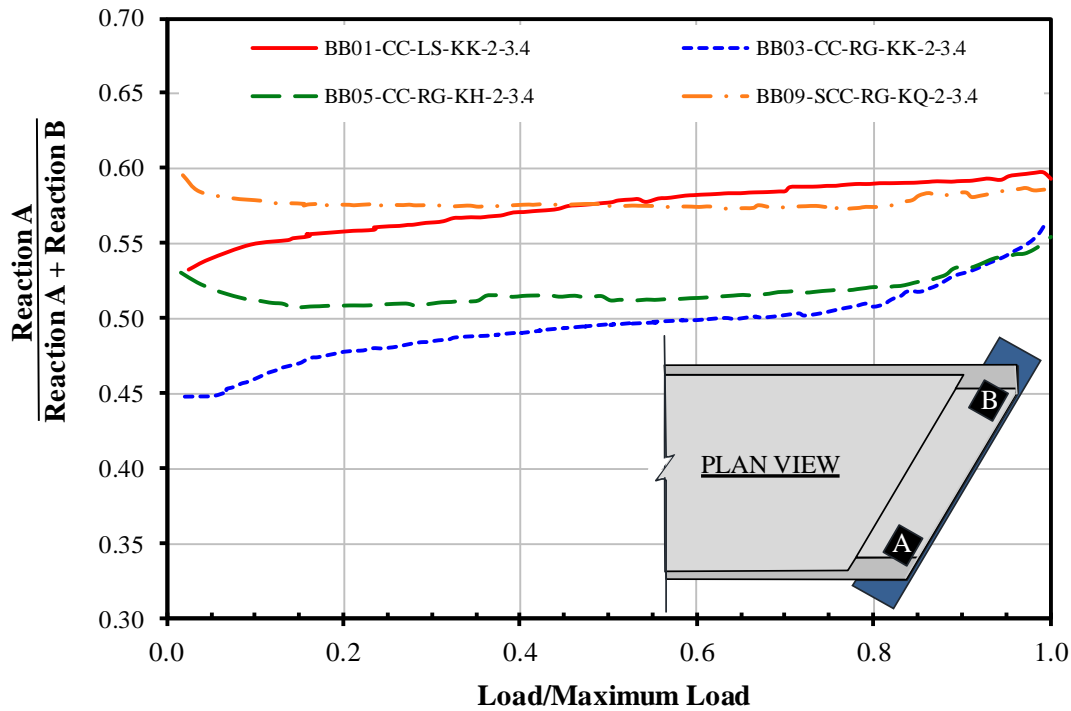
Figure 4-13: Side-to-side distribution of reactions for skewed ends supported by two separated bearing pads.

4.5 STRAND SLIP ANALYSIS

Linear potentiometers were installed to measure strand slip during testing as discussed in Chapter 3. In all tests, a total of 4 strands were monitored. In all cases, strand slip manifested itself as a consequence of failure rather than a cause. Practically no slip was measured in fully bonded strands until failure had occurred. In the following discussion and accompanying figures, a monitored strand is identified by the column number, followed by the debonding length if any. For example, strand C3D10 would be the strand in the third column from the left ("C3"), debonded through 10 ft from the end of the beam ("D10"). All monitored strands were in the bottom row of strands.

As there were many possible findings that could have come out of strand slip monitoring, different sets of 4 strands were monitored in several opportunities. In other words, not the same 4 strands were monitored in all 20 shear tests. A total of 4 different strand slip monitoring configurations were used. These configurations, identified as A

111

through D, are explained in the subsequent sections. Load-vs.-strand slip curves for the monitored strands are presented within each sub-section. The test key described in the introduction of this chapter is used. Strand slip curves for all tests can be found in Appendix C.

4.5.1 **Strands under different webs**

Configuration A was used in 15 out of 20 tests. In this configuration, 2 strands were monitored under each web; one of them fully bonded and one of them debonded through the first 10 ft of the beam. This configuration was used in an effort to determine, through strand slip, if more load found its way to one particular web and therefore, more tensile demands were present in the corresponding strands. This differentiation is of special interest in skewed ends supported on two bearing pads due to the different spans at which each web can be said to be supported.

It was seen that regardless of how many bearing pads were used (1 or 2), and regardless of the geometry of the beam end (square or skew), measured slip in the debonded strand under each web was practically the same through the whole loading process. Also in the debonded strands, a sharp change in the slope of the load-slip curve could be seen after flexural cracks had appeared. A good example of such behavior is illustrated in Figure 4-14, where it can be seen how two tested skewed ends with different supporting conditions (1 vs. 2 bearing pads) presented practically identical strand slip behavior.
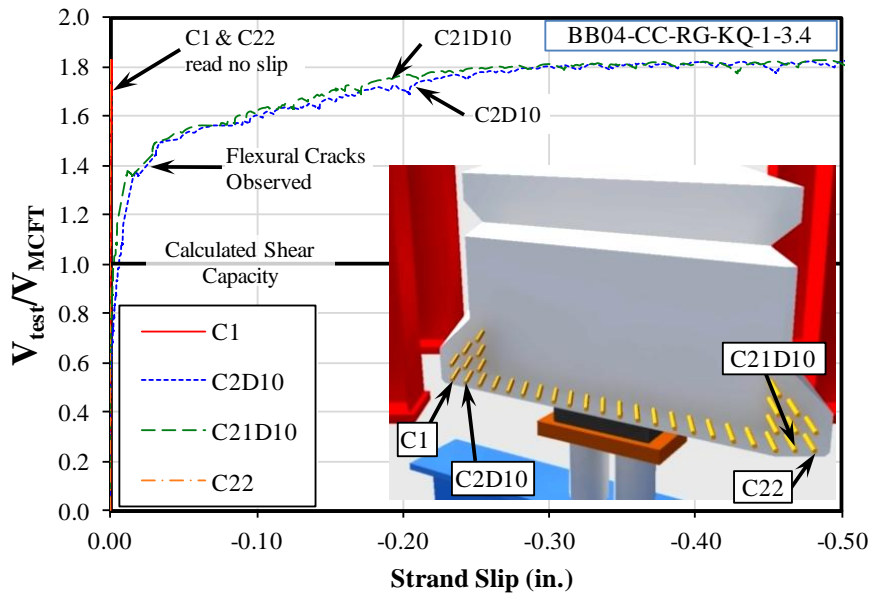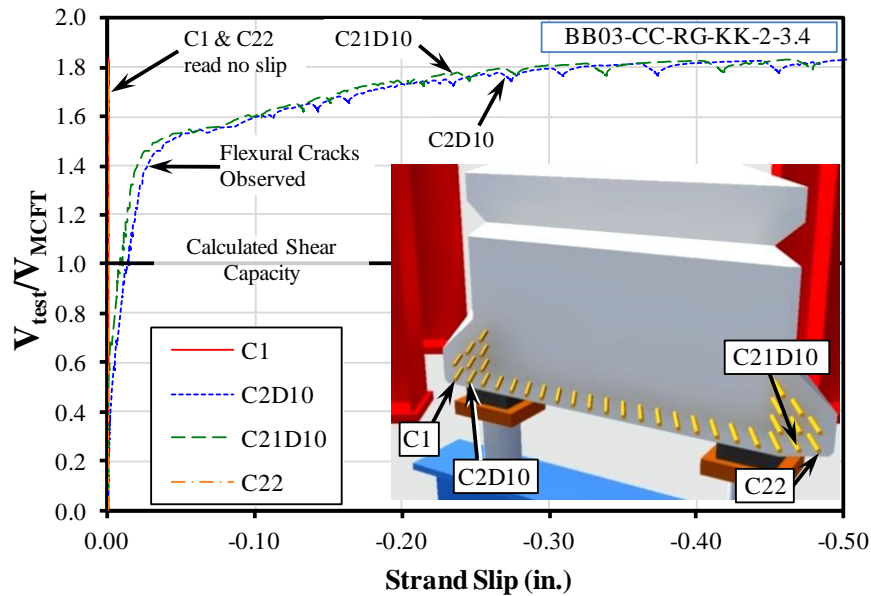
Figure 4-14: Load vs. Strand Slip curves (Instruments Configuration A)

For the bonded strands under each web, negligible strand slip was observed prior to failure, as shown in Figure 4-14. It might be worth noting that in many cases, the residual slip after the load had been removed was approximately the same in fully bonded strands as in debonded strands, suggesting that the former had effectively lost its bond to

the concrete. The best example of such behavior is illustrated in Figure 4-15, where it can be seen how the residual slip in strands C2D10 matches the slip in strand C3 and the residual slip in strand C20 matches the slip in strand C21D10.
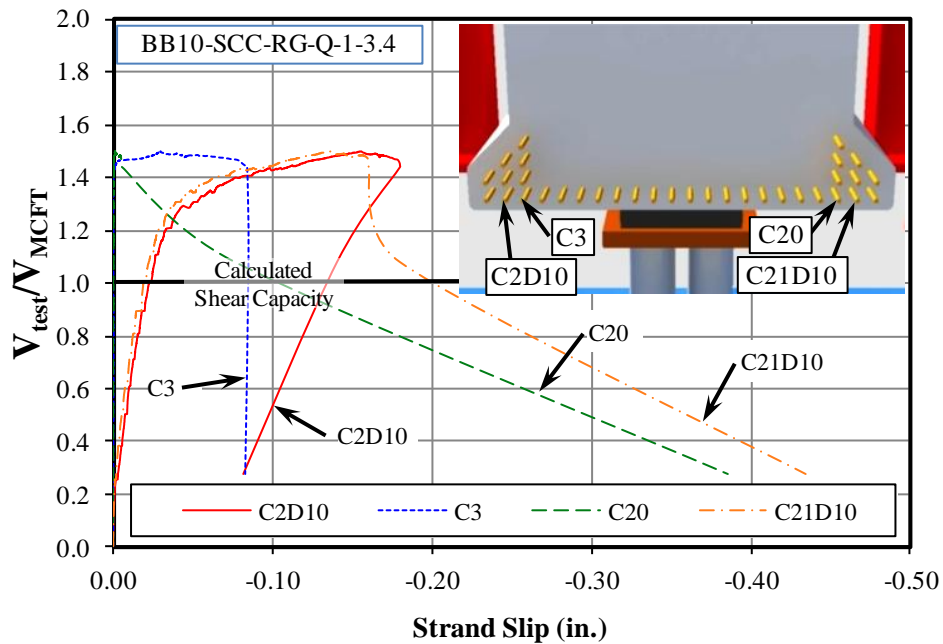
Figure 4-15: Load vs. Strand Slip curves for test BB10-SCC-RG-Q-1-3.4 (Instruments Configuration A)

4.5.2 Strand under the webs vs. strands in the middle of the beam

Configuration B, illustrated in Figure 4-16, was used in 3 of the 20 tests. In this configuration, the 4 monitored strands were fully bonded; two of them under the webs and two of them towards the middle of the beam. This configuration was used in an effort to determine, through strand slip, if the strands under the webs carry more load than those towards the middle of the beam. Results from such comparison would be relevant to optimize debonding practices (i.e. avoid debonding strands located under the web if it is determined that they carry a higher fraction of the load).

In the test BB04-CC-RG-Q-2-2.9, the strands located towards the middle of the beam exhibited significantly more slip than those strands located under the webs. The location of the bearing pads in this test is believed to be related to the difference in slip

114

measured between the groups of strands. The strands in the middle of the beam, being away from the supporting bearing pads, were not subject to a direct clamping force as the strands under the web (and above the bearing pads) were.

Test BB05-CC-RG-Q-2-2.9 yielded mixed results. Of the two strands that recorded the highest slip measurement, one was located under the web and above the bearing pad, and the other strand was closer to the middle of the beam.

In the third test in which strand slip was measured using configuration B (BB05-CC-RG-KH-2-3.4), negligible strand slip was measured in all strands.
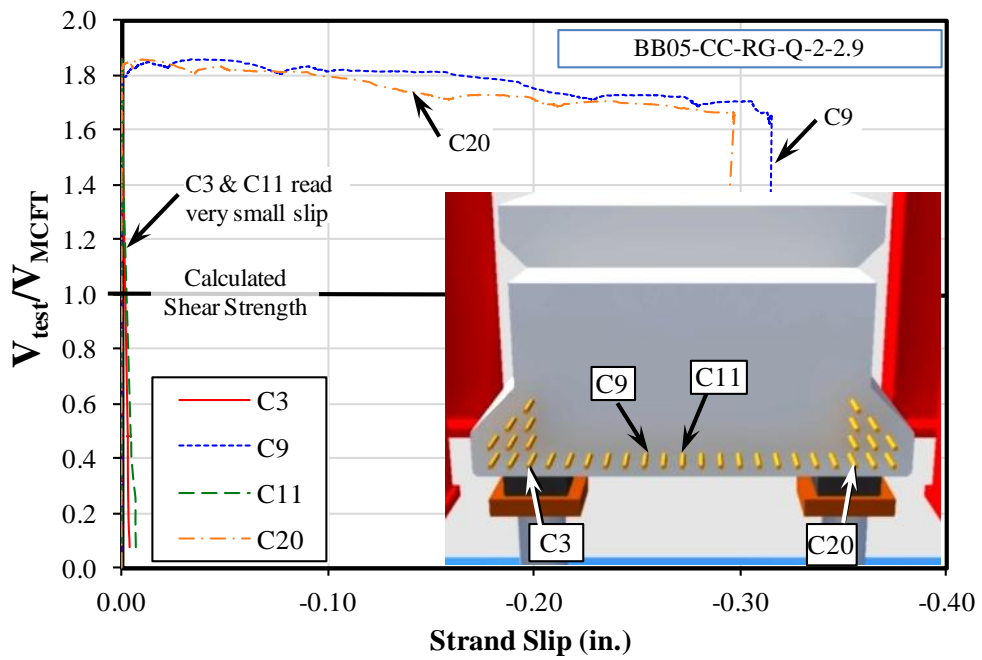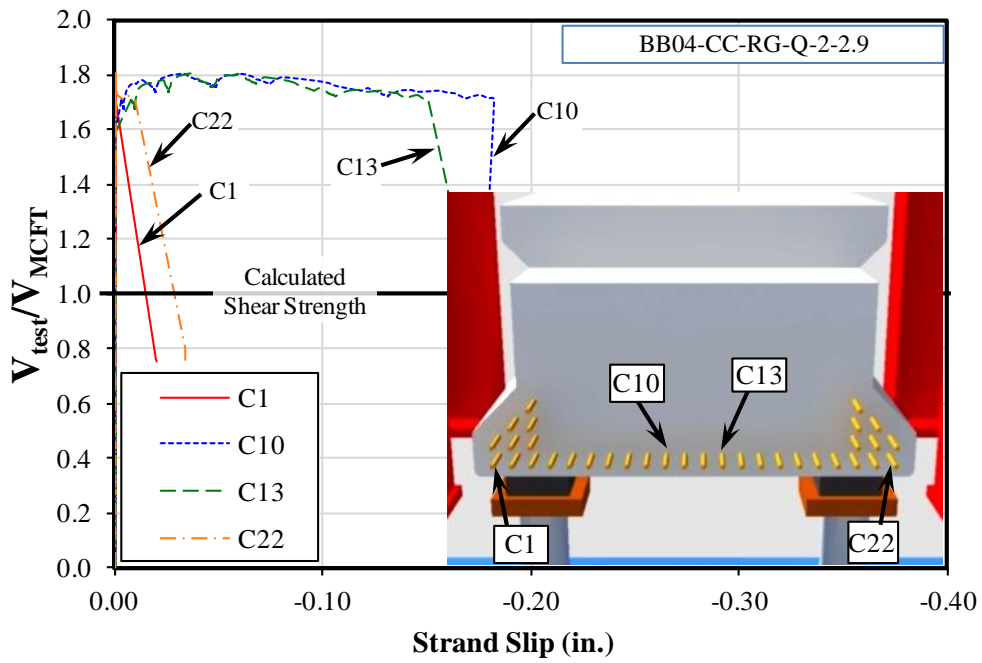
Figure 4-16: Load vs. Strand Slip curves (Instrumentation Configuration B)

4.5.3 Strands with different debonded lengths

Configuration C was used in 1 of the 20 tests, 2 of the monitored strands were debonded through 10 ft (one under each web) and the other 2 monitored strands were debonded through 4 ft (in the middle third of the beam). As could be expected, the strands debonded through 10 ft presented higher slip measurements than those debonded through 4 ft as can be seen in Figure 4-17.
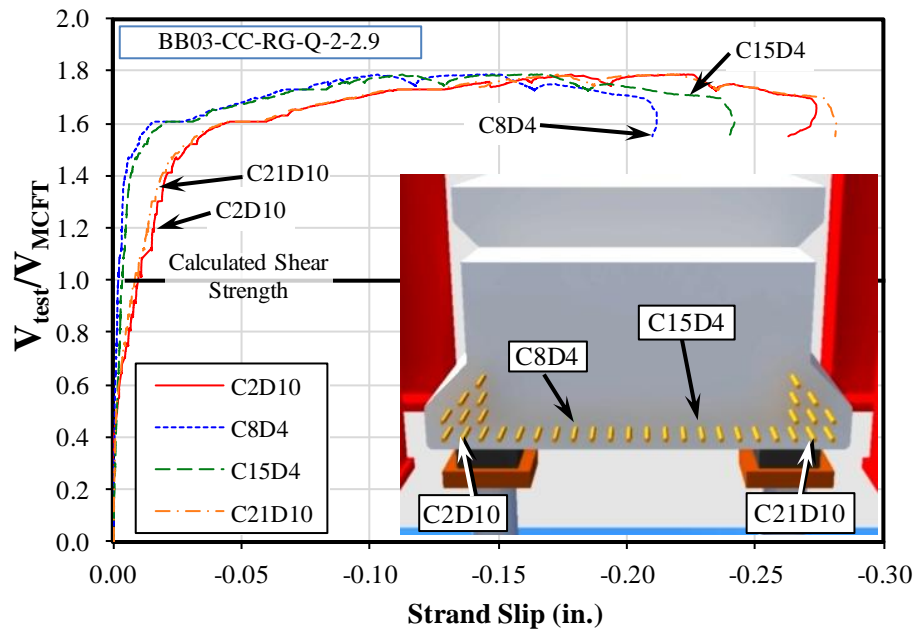
Figure 4-17: Load vs. Strand Slip curves (Instrumentation Configuration C)

4.5.4 Different bond conditions within the same side of the beam

Finally, configuration D was used in 1 of the 20 tests, as illustrated in Figure 4-18, all 4 monitored strands were on the same side of a square-ended beam; one fully bonded strand in the first column away from the middle, one strand debonded through 4 ft in the middle third of the beam, one fully bonded strand under the web and one strand also under the web but debonded through 10 ft. Coincidentally, the side of the beam with the strand slip instrumentation was the side of the beam to fail.

In this test, it was seen that residual slip was higher as the strand location was further away from the center of the beam as illustrated in Figure 4-19. This was correlated to the degree of damage to the underside of the beam and to the position of the bearing pad. As was discussed in section 4.5.2, the strands located over the bearing pad (C12 in this case) exhibited less slip due to the clamping effect.
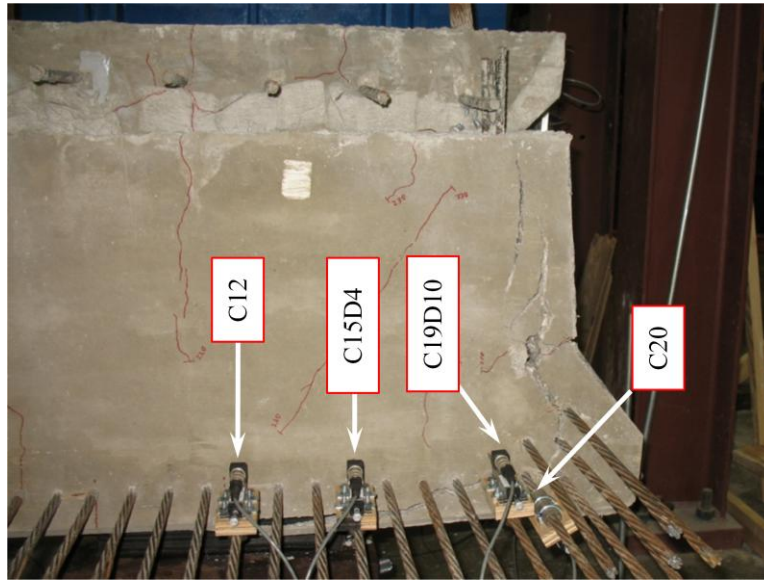
Figure 4-18: Strand slip instrumentation on test BB07-SCC-LS-Q-1-2.9
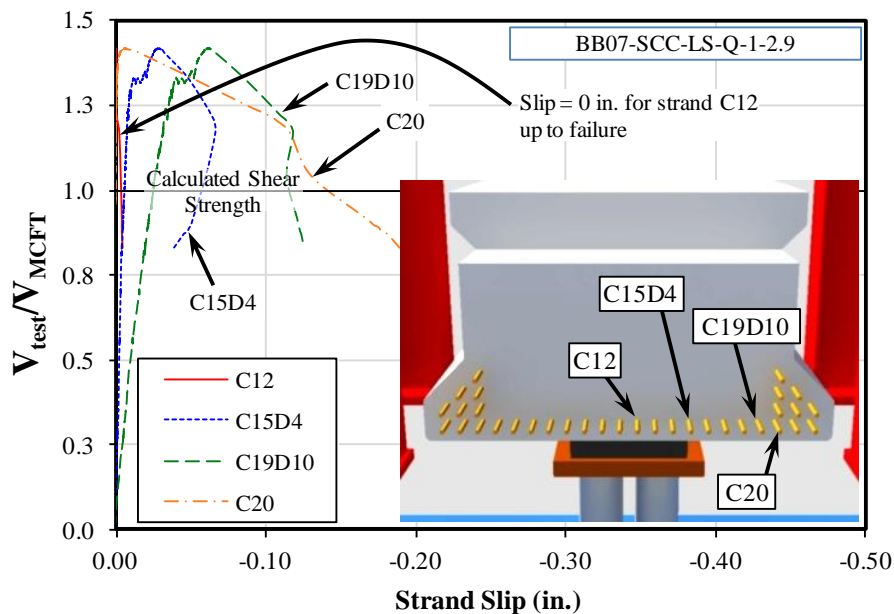
Figure 4-19: Load vs. Strand Slip curves (Instrumentation Configuration D)

4.6   FAILURE MODES

All but two tests resulted in diagonal web crushing failures. Testing of the skewed end of BB-03 resulted in flexure-shear failure and testing of the skewed end of BB-04 resulted in flexural failure (crushing of compression zone).

All web-crushing failures were accompanied by spalling of concrete cover over the re-entrant corner of the bent shear reinforcement (where the bottom of the web meets the top of the bottom flange). At failure, bent shear reinforcement was straightened out (Figure 4-20, part B), resulting in spalling of cover over that bar. The original undeformed shape of the shear reinforcement is illustrated with a dashed line in part B of Figure 4-20.

The beams fabricated with SCC failed at lower loads (18% less on average) and damage was more localized around the straightened shear reinforcement as shown in Figure 4-21. Conversely, failures in conventional concrete beams were associated with higher loads and very brittle and explosive failures of a larger portion of the web as shown in Figure 4-22.
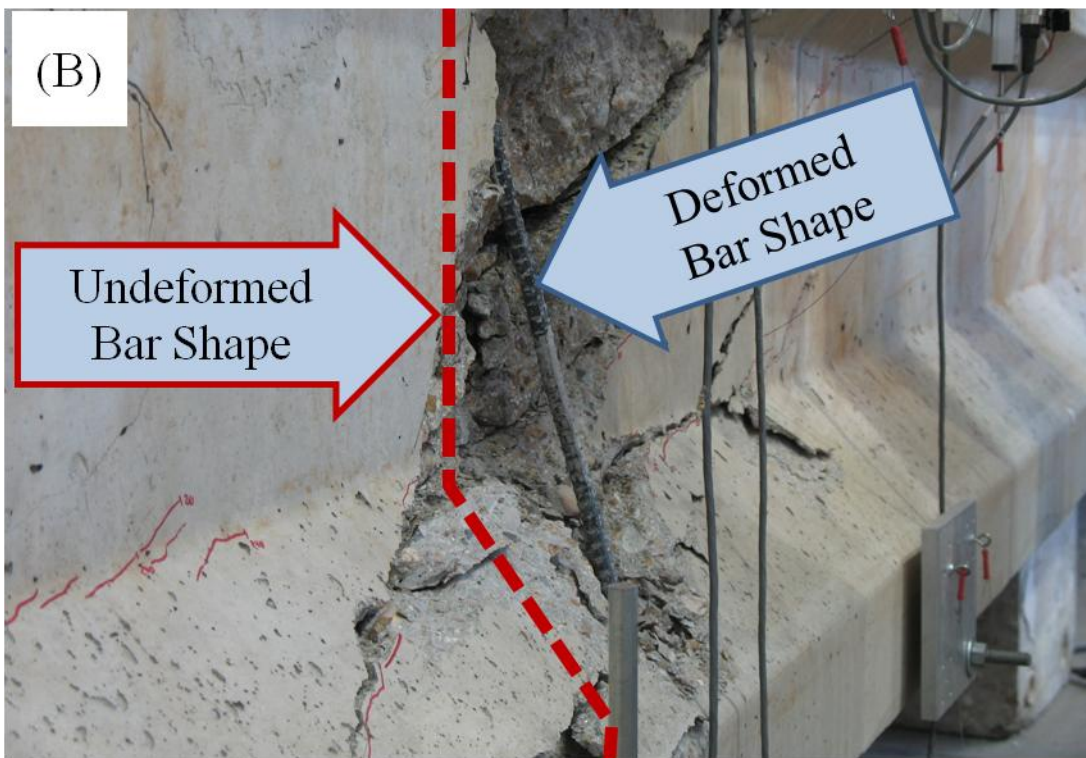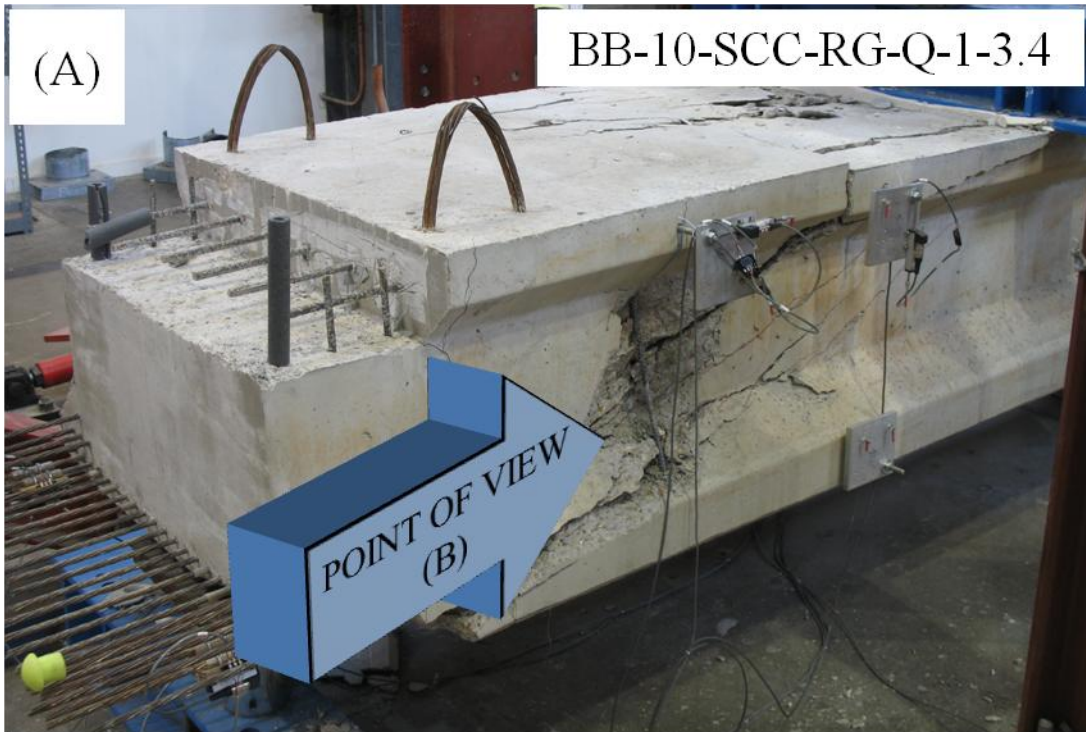
Figure 4-20: Straightened shear reinforcement after failure.

Figure 4-21: Failure of Square end of BB-09 (SCC).

Figure 4-22: Failure of skewed end of BB-02 (Conventional Concrete).

4.7 MEASURED VERSUS CALCULATED SHEAR STRENGTH

Four different provisions were used to calculate shear failure loads. Specifically:

1. The Detailed Method from ACI 318-08
2. The General Procedure from AASHTO-LRFD (2010)
3. The Simplified Procedure from AASHTO-LRFD (2010)
4. The Segmental Bridge Specifications from AASHTO-LRFD (2010).

Results from these evaluations, presented in Table 4-8, revealed that the shear strength of all box beams fabricated and tested in this experimental program was conservatively estimated by the different shear design provisions in question.

Given that the same conclusion are applicable all provisions, comparisons of the conservativeness of shear strength calculations in the subsequent sections are based on the General Procedure from AASHTO-LRFD (2010).

Table 4-8: Load test results and performance of code equations for ten 4B28 beams.

Test ID	Failure Shear (Measured/Calculated)			
	ACI 318-08	**AASHTO-LRFD (2010)**		
	Detailed Method	**General Procedure**	**Simplified Procedure**	**Segmental Bridges**
BB-01-CC-LS-Q-1-2.9	1.35	1.48	1.68	1.87
BB-01-CC-LS-KK-2-3.4	1.35	1.52	1.70	1.89
BB-02-CC-LS-Q-1-2.9	1.34	1.47	1.67	1.86
BB-02-CC-LS-KQ-1-3.4	1.37	1.55	1.73	1.92
BB-03-CC-RG-Q-2-2.9	1.63	1.78	2.02	2.26
BB-03-CC-RG-KK-2-3.4[a]	1.63	1.84	2.06	2.30
BB-04-CC-RG-Q-2-2.9	1.65	1.81	2.03	2.31
BB-04-CC-RG-KQ-1-3.4[b]	1.62	1.82	2.02	2.29
BB-05-CC-RG-Q-2-2.9	1.70	1.86	2.10	2.37
BB-05-CC-RG-KH-2-3.4	1.58	1.77	1.98	2.22
BB-06-SCC-LS-Q-2-2.9	1.24	1.36	1.50	1.77
BB-06-SCC-LS-KK-1-3.4	1.25	1.41	1.54	1.80
BB-07-SCC-LS-Q-1-2.9	1.29	1.42	1.57	1.84
BB-07-SCC-LS-KQ-1-3.4	1.31	1.48	1.62	1.89
BB-08-SCC-RG-Q-1-2.9	1.30	1.42	1.56	1.87
BB-08-SCC-RG-KK-1-3.4	1.46	1.65	1.79	2.14
BB-09-SCC-RG-Q-2-2.9	1.46	1.60	1.76	2.11
BB-09-SCC-RG-KQ-2-3.4	1.48	1.67	1.82	2.16
BB-10-SCC-RG-KH-1-3.4	1.50	1.66	1.82	2.12
BB-10-SCC-RG-Q-1-3.4	1.33	1.50	1.64	1.91
Average	1.44	1.60	1.78	2.05
Minimum	1.24	1.36	1.50	1.77
Maximum	1.70	1.86	2.10	2.37
Std. Deviation	0.15	0.16	0.19	0.20
COV	10.3%	10.3%	10.8%	9.7%
Cases < 1.0	0/20	0/20	0/20	0/20

a.   Flexure-shear failure.
b.   Flexural failure. Ratios shown for maximum load applied.

4.7.1 Influence of Concrete Type

For beams fabricated with crushed limestone aggregate, the average V_{test}/V_{calc} ratio of beams fabricated with conventional concrete was 8% greater than that ratio for beams fabricated with self-consolidating concrete.

For beams fabricated with river gravel aggregate, the average V_{test}/V_{calc} ratio of beams fabricated with conventional concrete was 23% greater than that ratio for beams fabricated with self-consolidating concrete.

Considering both types of aggregates, the average V_{test}/V_{calc} ratio of beams fabricated with conventional concrete was 17% greater than that ratio for beams fabricated with self-consolidating concrete.

More importantly, the average V_{test}/V_{calc} ratio for both concrete types was close to or above the database average for comparable sections. More discussion on the results and how they compare to previous test results included in the UTPCSDB-2011 is included in subsequent sections.

4.7.2 Influence of Coarse Aggregate Type

For beams fabricated with self-consolidating concrete, the V_{test}/V_{calc} ratio of beams fabricated with crushed limestone aggregate was, on average, 16% lower than that ratio for beams fabricated with river gravel aggregate.

For beams fabricated with conventional concrete, the V_{test}/V_{calc} ratio of beams fabricated with crushed limestone aggregate was, on average, 31% lower than that ratio for beams fabricated with river gravel aggregate.

Considering both types of concrete, the average V_{test}/V_{calc} for beams fabricated with crushed limestone was 24% lower than that ratio for beams fabricated with river gravel aggregate.

For better visualization, the comparisons between concrete types and coarse aggregate types are summarized in Table 4-9.

124

Table 4-9: Average V_{test}/V_{calc} (using the General Procedure from AASHTO-LRFD (2010)) for different concrete mixes and coarse aggregates.

V_{test}/V_{calc}	Conventional Concrete	Self-Consolidating Concrete	All Concrete Types
Crushed Limestone	1.50	1.42	1.46
River Gravel	1.81	1.58	1.70
All Aggregates	1.69	1.52	1.60

Within each set of concrete mixture and aggregate type, results had minimum variation, suggesting no influence of the remaining variables. Figure 4-23 illustrates the ratio of the experimental shear capacity to the shear capacity estimated using the General Procedure from AASHTO-LRFD (2010). It can be seen how differences in conservativeness are correlated to the respective concrete mixture and aggregate type used.
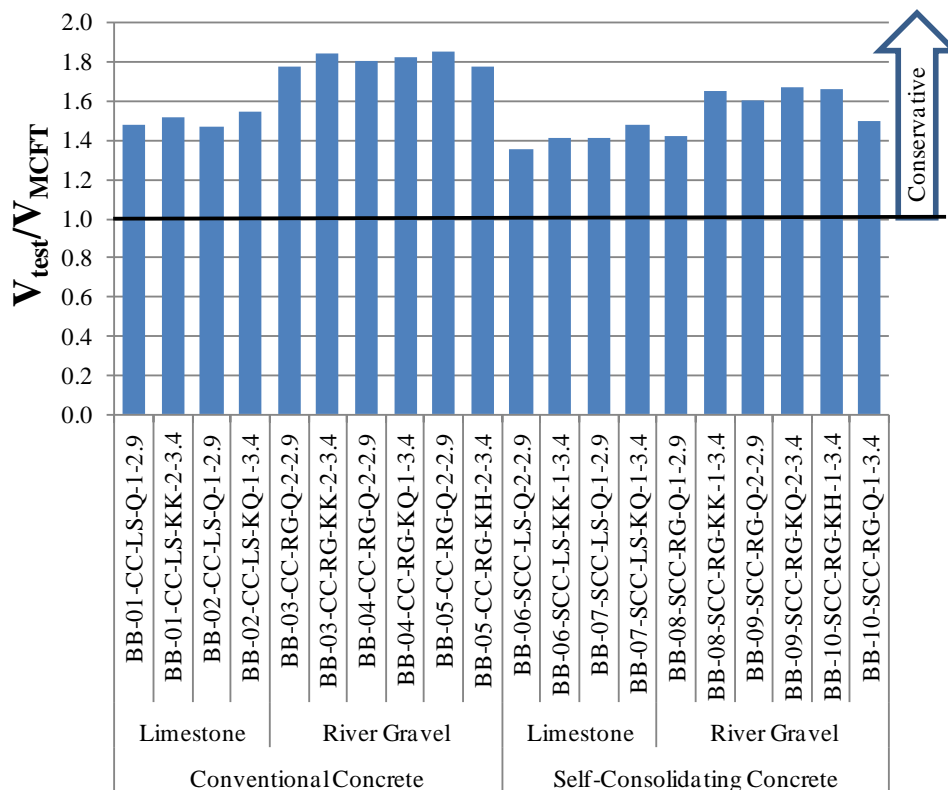
Figure 4-23: Ratio of experimental to calculated shear capacity (using the General Procedure from AASHTO-LRFD (2010)) for all 4B28 box beams

4.7.3 Influence of other variables

For the remainder test variables studied (beam end geometry, internal void geometry, shear span to depth ratio and bearing pad configuration), no definite adverse effects were observed for any variable combination. This is especially important for the case of the internal void geometry. The use of skewed and hybrid end void geometries are recommended for 4B28 box beams considering: (*i*) lower curing temperatures within skewed end blocks can be expected, thus, the potential for durability problems is reduced greatly, and (*ii*) no detrimental effects to shear performance were observed when skewed and hybrid end void geometries were used.

4.7.4 Results within the context of the UTPCSDB-2011

After the testing program was completed, results were incorporated into the UTPCSDB. Addition of these results to the UTPCSDB is extremely important considering the limited number of box beams included in the database prior to this program. With these and other additions, the UTPCSDB currently holds results from almost 1700 tests, making it the largest prestressed concrete shear database assembled to date (Nakamura, 2011).

Conservativeness and accuracy of current code equations when used to calculate the shear strength of box beams fell well within the scatter observed within the UTPCSDB for beams of similar characteristics (concrete compressive strength, shear reinforcement index and overall member depth). As can be seen in Figure 4-24 through Figure 4-26, the conservativeness and variability of the results of the shear testing program of the 4B28 box beams is comparable to that seen across the UTPCSDB.

Using the General Procedure from AASHTO-LRFD (2010) to calculate shear strength, the average ratio of the experimental maximum shear (V_{test}) to the calculated shear capacity (V_{calc}) for all tests was 1.60 with a coefficient of variation (COV) of 10.3%. More detailed statistics are shown in Table 4-10. Within the database, an evaluation sub-set of data comprised of specimens of similar characteristics has an

average shear strength ratio of 1.41 with a COV of 18%. This sub-set of data contains results for 162 specimens complying with the following criteria:

- Concrete strength was greater than 4 ksi
- Lightweight concrete was not used
- Overall member depth exceeded 12 in.
- Shear reinforcement in excess of code minimum requirements was provided
- Tests were conducted under simply supported conditions with an *a/d* ratio greater than 2
- Specimens were pretensioned, and
- A traditional mode of failure was observed

The resulting collection of results is plotted in Figure 4-24 through Figure 4-27. For comparison, all of the results from the 4B28 shear testing program are included in these plots. Results from test BB04-CC-RG-K-1-3.4 are included despite the reported failure mode being flexural. Shear capacity was cleared abundantly in the aforementioned test and the maximum load at the time the flexural failure occurred constitutes a lower bound for the shear capacity (shear capacity is at least as great as the maximum applied shear).

Table 4-10: Shear strength ratio statistics for all 4B28 box beams.

	Tests	V_{test}/V_{calc}	Standard Deviation	COV
Conventional Concrete				
Limestone Aggregate	4	1.50	0.04	2.4%
River Gravel Aggregate	6	1.81	0.03	1.8%
All Aggregates	10	1.69	0.16	9.7%
Self-Consolidating Concrete				
Limestone Aggregate	4	1.42	0.05	3.6%
River Gravel Aggregate	6	1.58	0.10	6.5%
All Aggregates	10	1.52	0.12	7.9%
All mixtures	20	1.60	0.16	10.3%
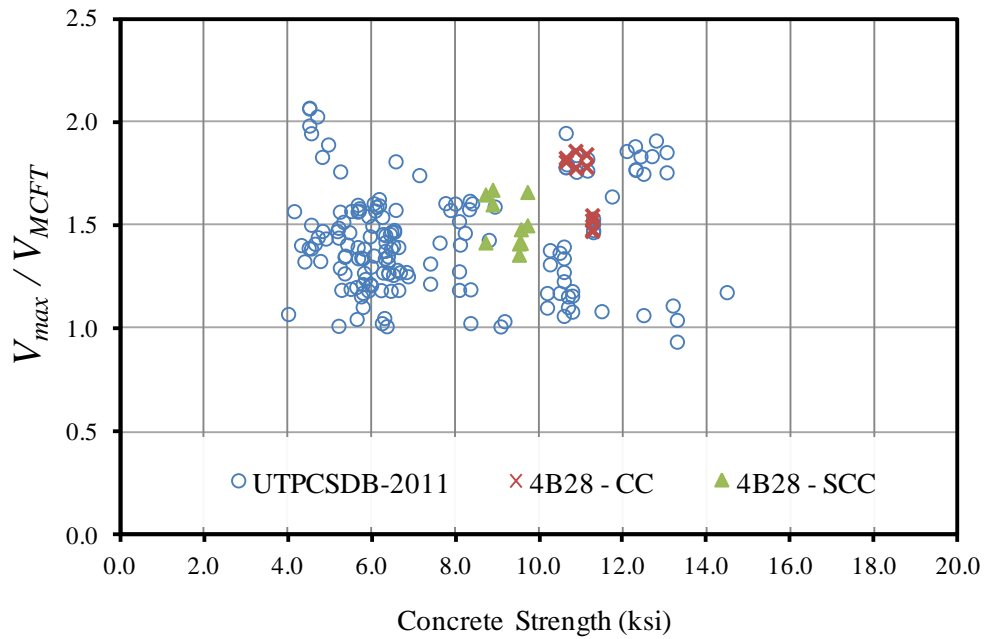
Figure 4-24: Shear strength ratios of 4B28 box beams compared to other specimens of various concrete compressive strengths in the UTPCSDB-2011. Shear strength calculated using the General Procedure from AASHTO-LRFD (2010).
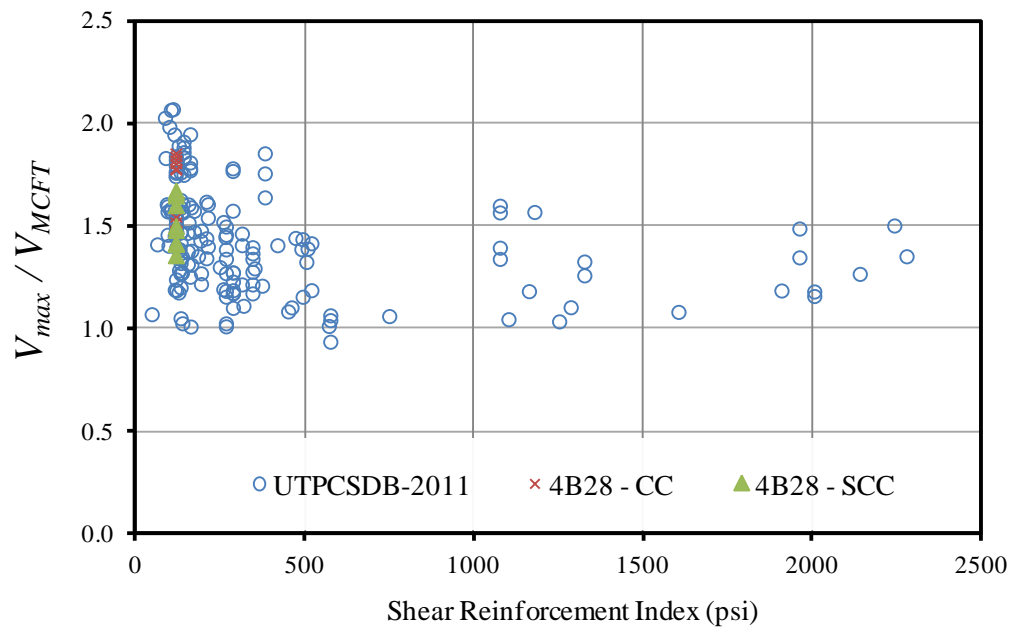
Figure 4-25: Shear strength ratios of 4B28 box beams compared to other specimens of various shear reinforcement indexes in the UTPCSDB-2011. Shear strength calculated using the General Procedure from AASHTO-LRFD (2010).

128
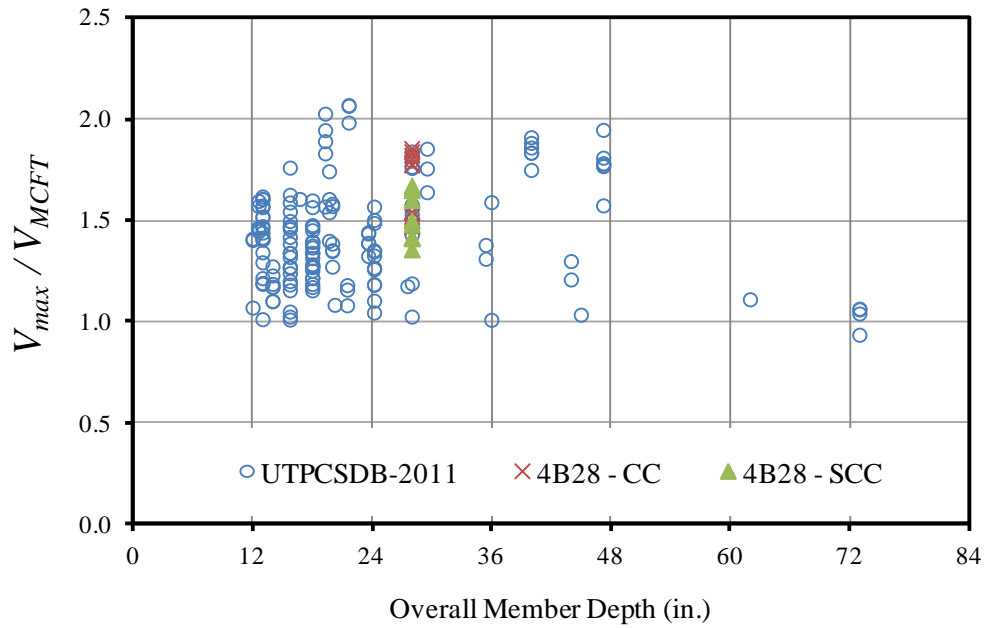
Figure 4-26: Shear strength ratios of 4B28 box beams compared to other specimens of various overall depths in the UTPCSDB-2011. Shear strength calculated using the General Procedure from AASHTO-LRFD (2010).
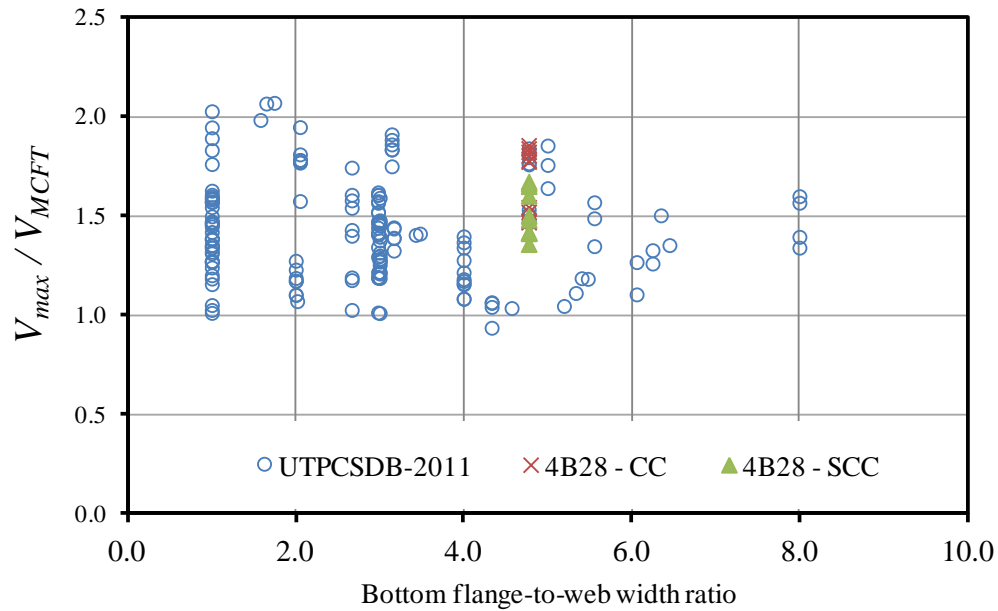
Figure 4-27: Shear strength ratios of 4B28 box beams compared to other specimens of various flange-to-web width ratios in the UTPCSDB-2011. Shear strength calculated using the General Procedure from AASHTO-LRFD (2010).

4.8   AGGREGATE DISTRIBUTION INVESTIGATION

TxDOT engineers expressed their concerns regarding the inferior performance of the beams fabricated with SCC, as reported by Schnittker and Bayrak (2008) after TxDOT Project 0-5197 and confirmed through the shear testing program described herein. This concern led to the funding of TxDOT Implementation Project 0-5197-01-1 where twenty-five cuts were made in the box beams tested through the use of a diamond wire cutting saw as illustrated in Figure 4-28. The goal was to investigate if aggregate segregation and/or poor consolidation could have adversely influenced the structural performance of the beams fabricated with SCC.

Figure 4-28: Diamond wire cutting saw cutting through 4B28 beam.

Conclusions of TxDOT Implementation Project 0-5197-01-1 indicated that the aggregate distribution and consolidation characteristics observed in the beams fabricated with SCC (Figure 4-29) was comparable to that observed in those fabricated with conventional concrete.

Figure 4-29: Cut section of beam fabricated with SCC and river gravel.

4.9   SUMMARY AND CONCLUSIONS

The results from a total of twenty shear tests conducted on ten 4B28 box beams were presented in this chapter.

First, shear cracking load was evaluated. Two different code provisions were used to calculate the shear causing diagonal cracks. The resulting calculations were then compared to the experimental values. Since each box beam had two webs, and each box beam was tested at both ends, 40 ratios of calculated to experimental diagonal cracking shear were obtained. Neither method provided consistent results; variability was high with calculations being over or under the experimental value by as much as 20%. The webs of the same box beam presented first diagonal cracks under substantially different shear forces in 15 of the 20 shear tests. This could be attributed to slight differences in the thickness of the two webs and/or the asymmetrical characteristic of the beams and their support conditions.

Shear-distortion plots were presented as a secondary means to establish the experimental cracking shear. Good agreement was found between the information gathered from the shear-distortion plots and visual observation of crack appearance. The

downside of this measurement method lied within how localized the measurements were. While shear-distortion plots rendered useful information for the region they encompassed, shear deformation instrumentation could not be relied on solely to monitor diagonal cracks as the formation of cracks was not limited to the monitored region.

Diagonal crack widths were monitored during each test. By plotting all of the measured crack widths, a general guide was created to correlate crack width to the state of demand imposed on a beam. It was found that the initial crack width was different for beams made with conventional concrete compared to beams made with SCC. Initial crack widths for SCC beams ranged from 0.0025" to 0.005" whereas for conventional concrete beams the range was between 0.005" and 0.015".

Comparisons were made between the experimental load and the calculated load that caused flexural cracks and later flexure-shear cracks. Agreement between the experimental and calculated loads was reasonable in both cases.

The side-to-side distribution of reactions, observed when two separated bearing pads were used to support a beam end, was studied. Although, in the worst case, it was found that 60% of the total end reaction was measured on the bearing pad placed near the shorter side of the beams with skewed ends, the uneven distribution of the reaction at the test end was never sufficiently large to cause unconservative shear strength estimations.

Strand slip measurements suggested that slip occurred as a consequence of failure rather than a cause of failure. Practically no slip was observed in fully bonded strands until failure had occurred. Debonded strands did present slip through the loading process and it was possible to correlate changes in the slope of the load-strand slip curve with the load corresponding to the first flexural cracks. After failure, residual slip measurements between 0.2 in. and 0.5 in. were common. Determining if either web carried a higher fraction of the load during the loading process was not possible through strand slip instrumentation.

The conservativeness of current design provisions used to estimate the shear strength of the 4B28 box beams was evaluated. Conservative failure load calculations were obtained for *all beams*, regardless of the design provision used to calculate capacity.

132

In general, beams failed by diagonal web crushing of one or both webs. Current code equations worked as well for box beams as they did for other specimens within the UTPCSDB-2011.

In an effort to explain the difference in performance between the beams fabricated with conventional concrete and those fabricated with self-consolidating concrete, 25 cross sectional cuts were obtained from the box beams described in this chapter. No difference was observed between the aggregate distribution and the consolidation characteristics of either type of concrete mixture.

CHAPTER 5

Results and Analysis: Early-age Behavior of 5B40 Box Beams

5.1 INTRODUCTION

The results from two main aspects of the early-age behavior of box beams are discussed in this chapter: *(i)* transverse stresses in the end region at the time of prestress transfer and, (ii) curing temperatures in different end block geometries.

Regarding the transverse stresses in the end region, the difference between spalling and bursting stresses was established in Chapter 2. Essentially, spalling stresses are concentrated away from the line of action of the prestressing force and close to the end of the beam. Conversely, bursting stresses are concentrated close to the line of action of the prestressing force and extend a significant distance into the beam. Figure 2-16 was used to illustrate these two different phenomena. In the present study, only bursting stresses are discussed as they proved to be more important than spalling stresses.

As discussed in Chapter 2, current design recommendations in AASHTO-LRFD require a sufficient amount of transverse reinforcement provided in the end region, within a certain distance from the end (a quarter of the height of the member), to balance 4% of the net prestressing force while not exceeding certain stress level in the reinforcement (20 ksi). These recommendations can be found in AASHTO-LRFD (2010) §5.10.10.1 – *Splitting Resistance.* While these recommendations are more suitable for spalling stresses, they are the only recommendation made to manage transverse stresses in the end regions of prestressed members. Considering that fact, the recommendations will be evaluated in their effectiveness in managing both bursting and spalling stresses.

One could divide these recommendations into three parts:

(1). A limit of 20 ksi is placed on the stresses to be experienced by the transverse reinforcement at prestress transfer

(2). A total transverse force equal to 4% of the net prestressing force is to be managed, and

(3). A length equal to $h/4$ over which such transverse reinforcement should be placed is set

Evaluating how the three aforementioned aspects of the design recommendations measure against the experimental data gathered in this testing program and gaining an understanding of the behavior of box-beam end regions at prestress transfer are the goals of this research project that are addressed in this chapter.

First, the maximum observed bursting stresses are compared to the AASHTO-LRFD (2010) limit of 20 ksi. Then, the total bursting force accumulated within the first $h/4$ of the beam is compared to the net prestressing force. Finally, the accumulation of bursting forces within and beyond the first $h/4$ of the beam is discussed.

Regarding the second aspect of early-age behavior; temperatures measured within the different end block geometries during the initial curing process are discussed.

5.2 MAXIMUM TRANSVERSE REINFORCEMENT STRAINS

Local stresses inferred from the strain measurements are presented in this section. Through these results, it was possible to evaluate the local maximum stresses, compare the maximum stresses to the 20 ksi limit imposed by AASHTO-LRFD (2010) and optimize the transverse reinforcement quantity and distribution accordingly for the beams in Phase II.

5.2.1 Phase I Beams

5.2.1.1 Description

Three beams were fabricated as part of the Phase I study: 5B40-1, 5B40-2 and 5B40-3. These beams were fabricated with reinforcement details that were very similar to those of the current TxDOT standard (December 2006). The difference between the reinforcement detail in the current TxDOT standard (December 2006) and the reinforcement detail used in the beams fabricated in Phase I was basically the addition of horizontal reinforcement across the end block as is further explained later in this section.

In terms of vertical bursting stresses, the three beams were fabricated with no changes to the standard reinforcement detail. The reinforcement detail contains, in the first $h/4$ of the beam, 92% of the area of reinforcement required to balance 4% of the net prestressing force introduced by the maximum number of strands possible (76) without the reinforcement being stressed beyond 20 ksi. This is an important fact as 76 strands were used in the beams fabricated in Phase I of this research project. In other words, the end region contains 92% of the area of vertical transverse reinforcement recommended by AASHTO-LRFD (2010) for this particular case. The aforementioned reinforcement is provided in two curtains: the first one located approximately 2.5 in. from the face of the beam and the second one located approximately 4.25 in. from the first one (6.5 in. from the end). In each of the curtains, as illustrated in Figure 5-1, 1 Bar C (#4), 6 Bars N (#4) and 2 Bars U (#4) are included. An additional reinforcement curtain is located beyond the first $h/4$ of the beam, at approximately 11 in. from the end.
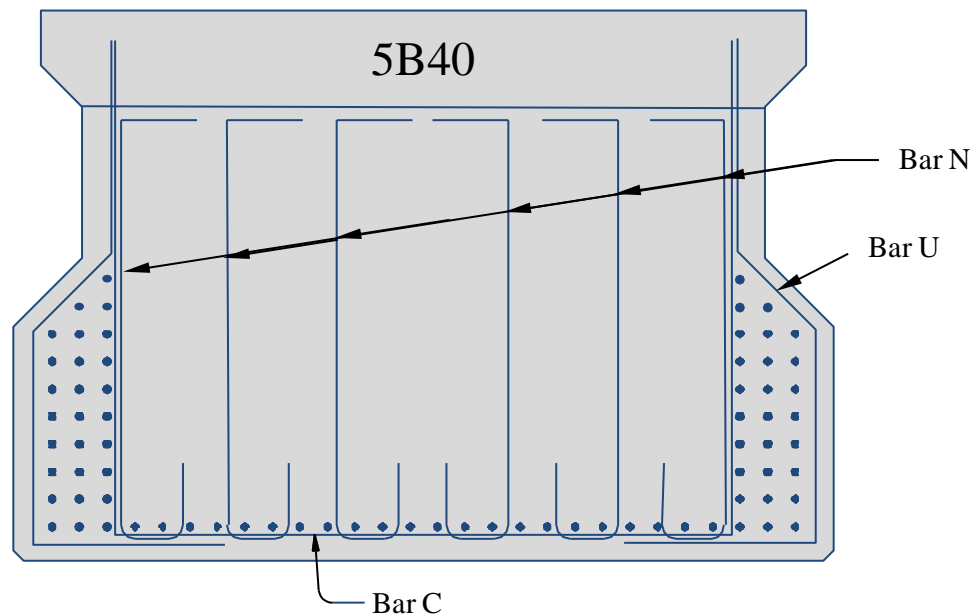
Figure 5-1: Vertical Reinforcement in Phase I Beams

In terms of horizontal bursting stresses, some additional reinforcement was added to the standard detail in the form of Bars E across the end block. This slight modification from TxDOT specifications was done to accommodate a request from the standards engineer of the TxDOT Bridge Division, in order to address recently-encountered field

136

problems at prestress transfer in beams fabricated locally. The field problems consisted of spalling of the cover on the side and end face of the beam as shown in Figure 5-2. The damage was repaired by using dowels anchored into the side of the beam and refinishing the beams end. This damage was attributed to the high number of strands used in the beam. The beam contained 60 fully bonded strands plus another 14 strands debonded in the end region as illustrated in Figure 5-3.
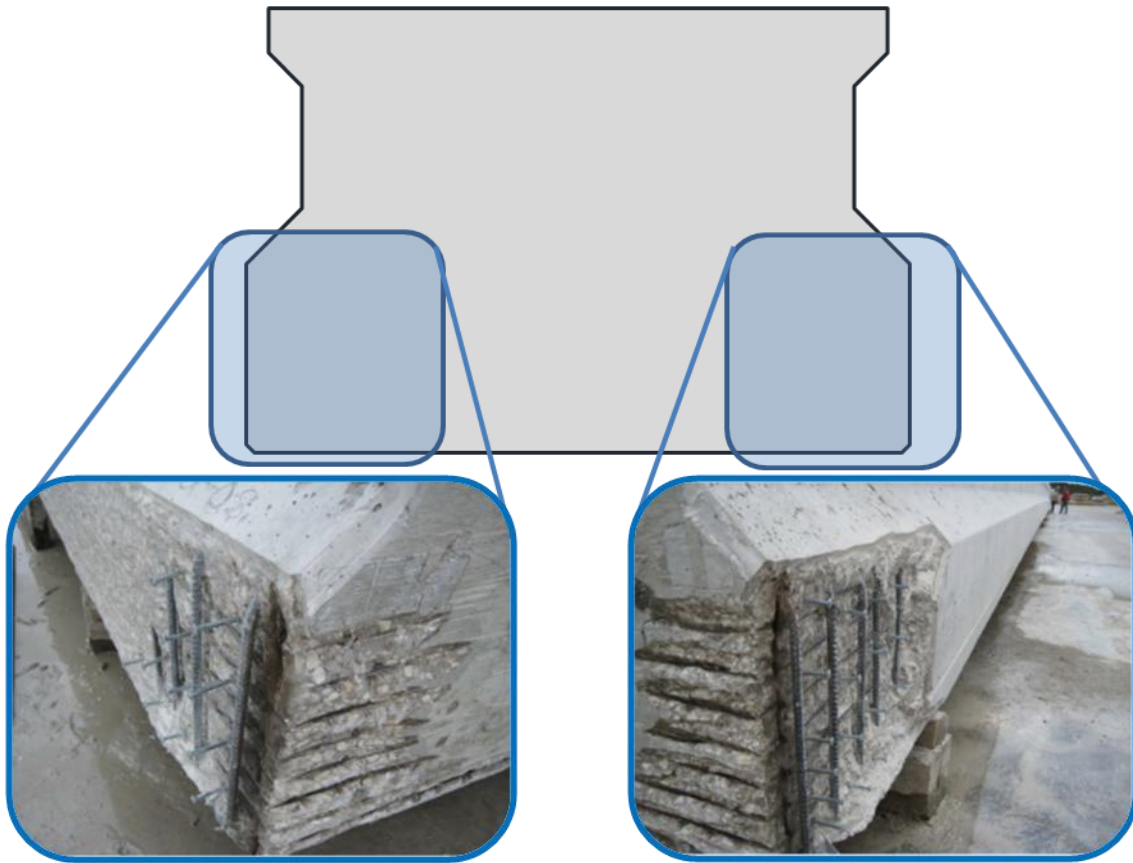
Figure 5-2: Spalling of concrete cover immediately after prestress transfer
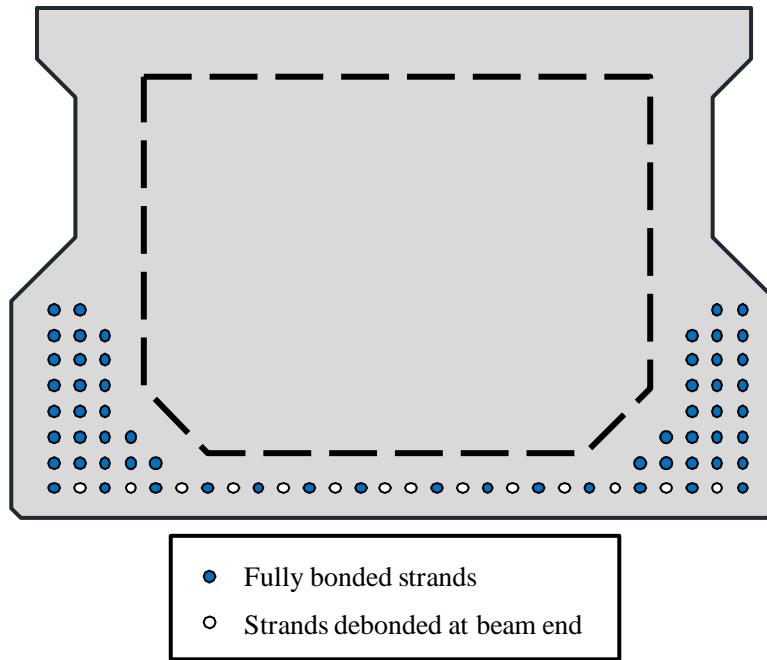
Figure 5-3: Strand Pattern used in beam presenting spalling problems

Four #5 bars (Bar E) in the three reinforcement curtains in the end block were added to the beams fabricated in Phase I. Placement and detail of these bars is shown in Figure 5-4. Complete details of the reinforcement can be found in Appendix B.
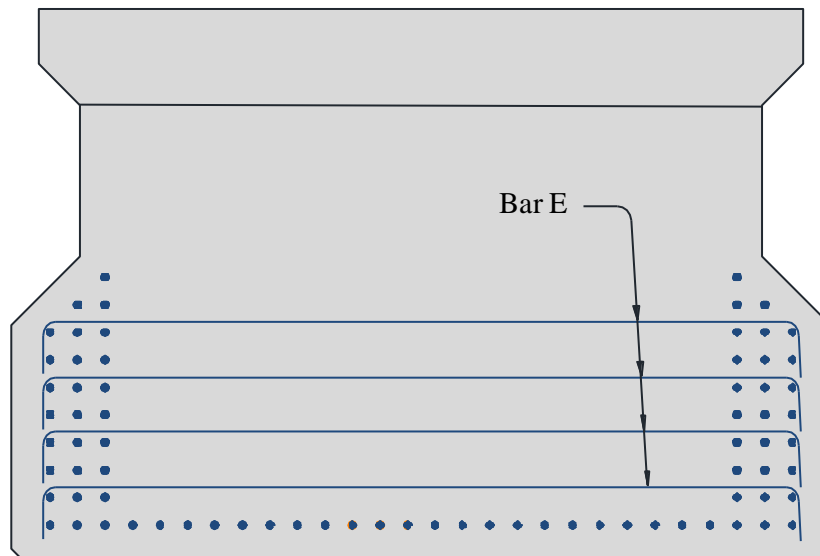
Figure 5-4: Bar E added to Phase I beams (other bars omitted for clarity)

Within the first $h/4$ of the beam, 2 curtains of reinforcement, each of them as illustrated in Figure 5-5, constituted the horizontal reinforcement provided across the end block. Each curtain contained 1 Bar C (#4), 4 Bars E (#5) and 6 Bars M (#4). These two curtains contain an area of reinforcement equal to 112% of the area recommended by AASHTO-LRFD (2010) to balance 4% of the net prestressing force within the first $h/4$ of the beam (as provided by 76, ½-in. strands). Beyond the first $h/4$ of the beam, a third reinforcement curtain provided additional transverse reinforcement, located approximately at 11 in. from the end.
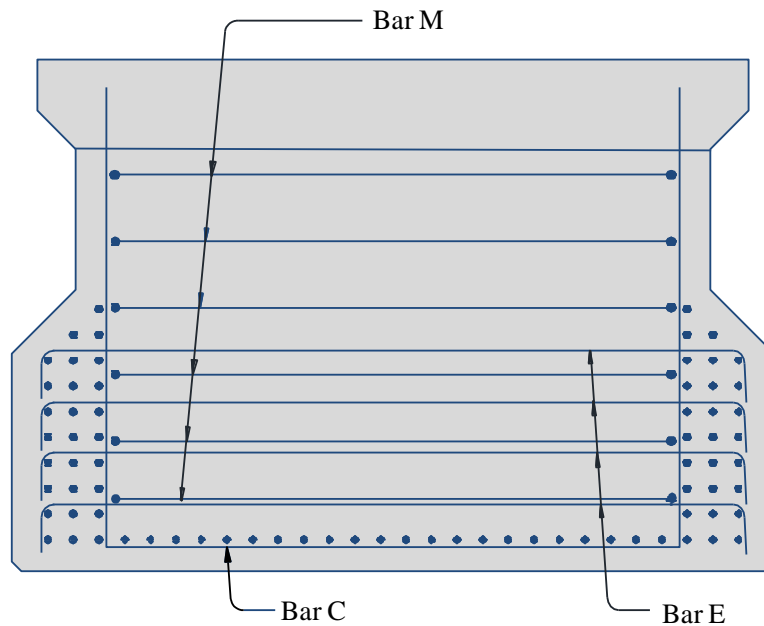
Figure 5-5: Horizontal Reinforcement in Phase I box beams.

All three beams fabricated in Phase I had concrete strengths of approximately 6400 psi at the time of prestress transfer ($f'_{ci} = 6400$ psi). As discussed in Chapter 3, strain gauge locations were initially selected based on observations of bursting cracks on 4B28 box beams and engineering judgment.

In all beams, strain gages were installed to measure vertical bursting stresses. Such measurements were obtained through strain gages aligned vertically, installed on Bars C or Bars U as pictured in Figure 5-1 and Figure 5-6. In the right portion of Figure 5-6, a simplified illustration of the strain gauge locations is given. A marker was used at

each strain gauge location, with the size of the marker being proportional to the inferred stress. The actual strain measurements at prestress transfer are discussed in the next section and illustrated in Figure 5-8 through Figure 5-10.
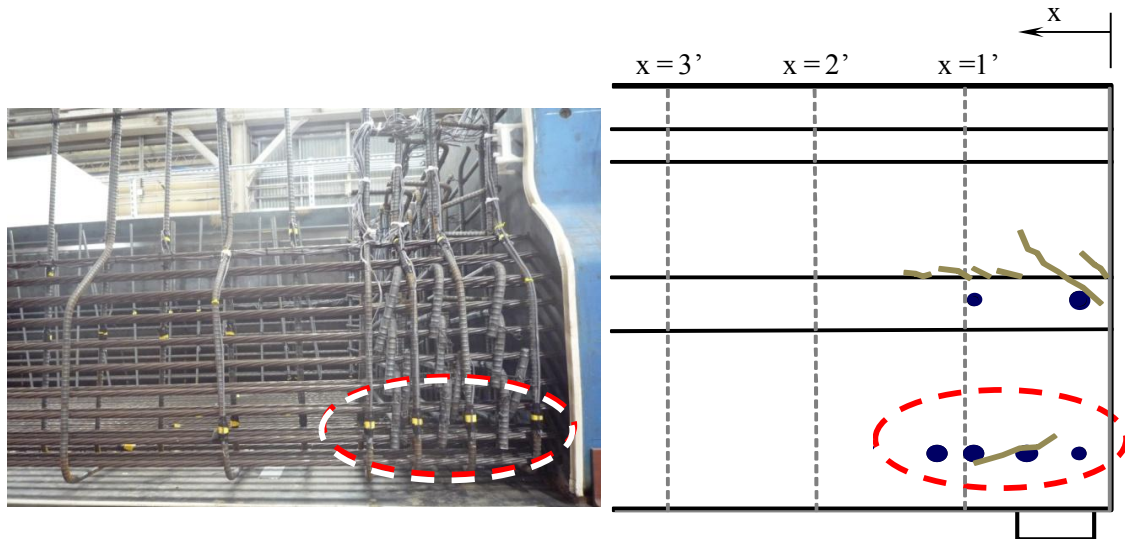
Figure 5-6: Vertical Bursting Measurements

Horizontal bursting strains were measured in all but the first beam. In this case, strain gages were aligned horizontally and installed on Bars E or Bars M as illustrated in Figure 5-5 and Figure 5-7. A simplified illustration is presented in the bottom right portion of Figure 5-7. As with vertical bursting stresses, the actual horizontal strain measurements at prestress transfer are discussed in the next section and illustrated in Figure 5-8 through Figure 5-10.
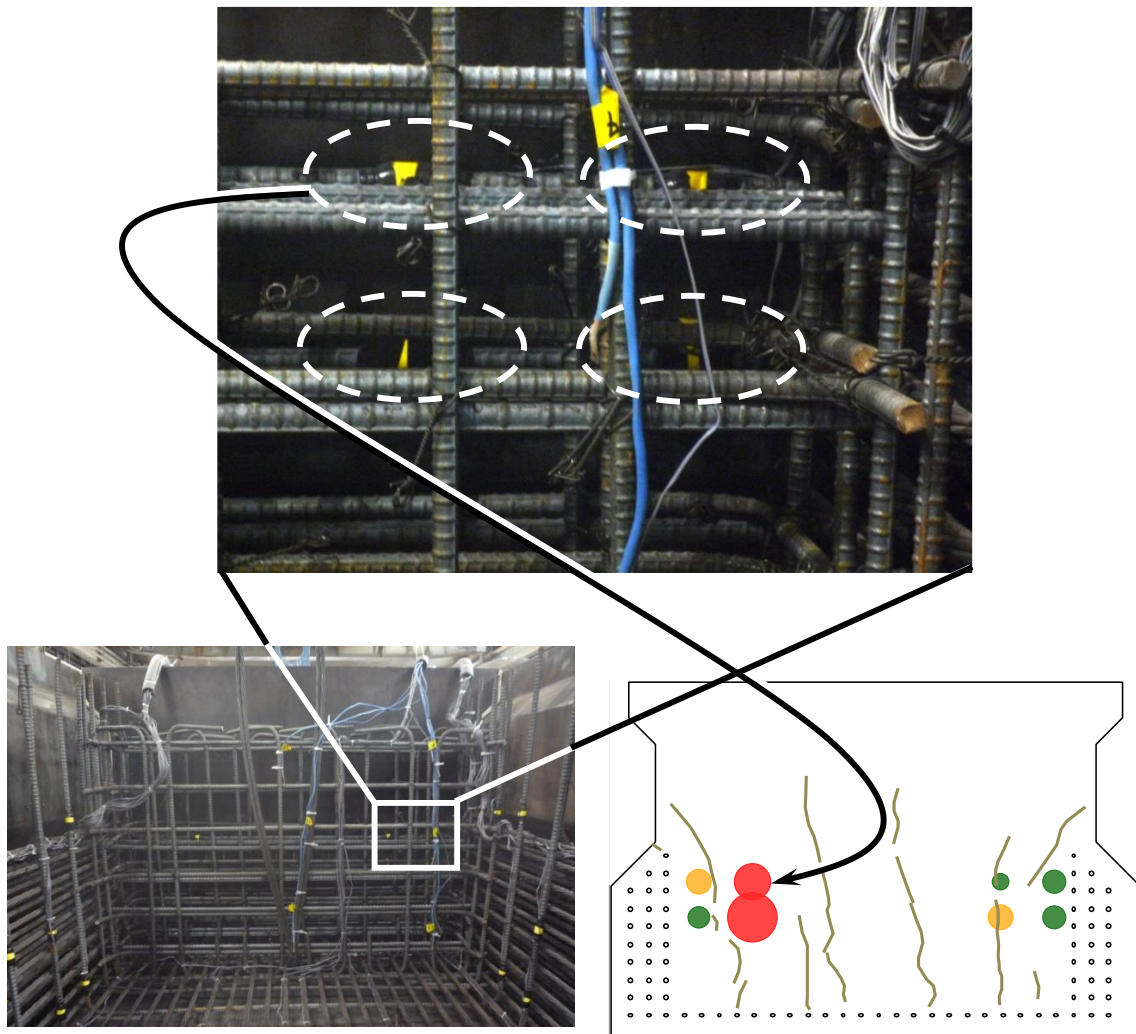
Figure 5-7: Horizontal strain Measurements

5.2.1.2 Measured Strains

The highest vertical bursting strain readings were gathered in beam 5B40-1, with strains proportional to 22.9 ksi in a Bar U; 2.5 in. from the end face of the beam and 20 in. from the bottom of the beam, as illustrated in Figure 5-8. In the same beam, strains proportional to 20.7 ksi were measured in a Bar U; 14 in. from the end face of the beam and 5.5 in. from the bottom of the beam as illustrated in Figure 5-8. As can be observed in Figure 5-8 through Figure 5-10, these were the only two instances where strains in excess to those corresponding to the maximum bursting stress (20 ksi) allowed by

141

AASHTO-LRFD (2010) were measured in vertical reinforcement. Mostly, stresses in the range of 10 ksi to 15 ksi could be inferred from the vertical strain measurements. Crack widths associated with vertical strains were generally small (0.005 in.) with very few of them being as wide as 0.016 in.

Considering that the beams fabricated within Phase I had the maximum number of strands possible in a 5B40 box beam (76), and the rarity with which stresses surpassing 20 ksi and wide crack widths were found, one can consider the performance of the current reinforcement detail satisfactory in terms of its ability to accommodate vertical stresses introduced at the time of prestress transfer.

The same cannot be said regarding horizontal bursting stresses. Beam 5B40-1 had few strain gages to monitor the horizontal bursting phenomenon compared to the beams fabricated afterwards. Only the Bars M in the third reinforcement curtain (10.75 in. into the beam) were instrumented in beam 5B40-1. Strains measured in two locations on the Bars M corresponded to stresses of 9.5 ksi.

After observing the vertical cracks in the end face of 5B40-1 as illustrated in Figure 5-8, the decision to instrument reinforcement going across the end block (Bars E and Bars M in Phase I beams) was made. For beams 5B40-2 and 5B40-3, more strain gages were placed with most of them being located in the first reinforcement curtain (~2.5 in. into the beam).

Strain measurements gathered from beams 5B40-2 and 5B40-3 (see Figure 5-9 and Figure 5-10) revealed that horizontal bursting stresses on the order of 30 ksi were present in most cases, with one isolated strain measurement corresponding to a stress of 40 ksi found in 5B40-3. Crack widths were commonly 0.007 in. and 0.009 in. with a few cracks measuring up to 0.013 in.
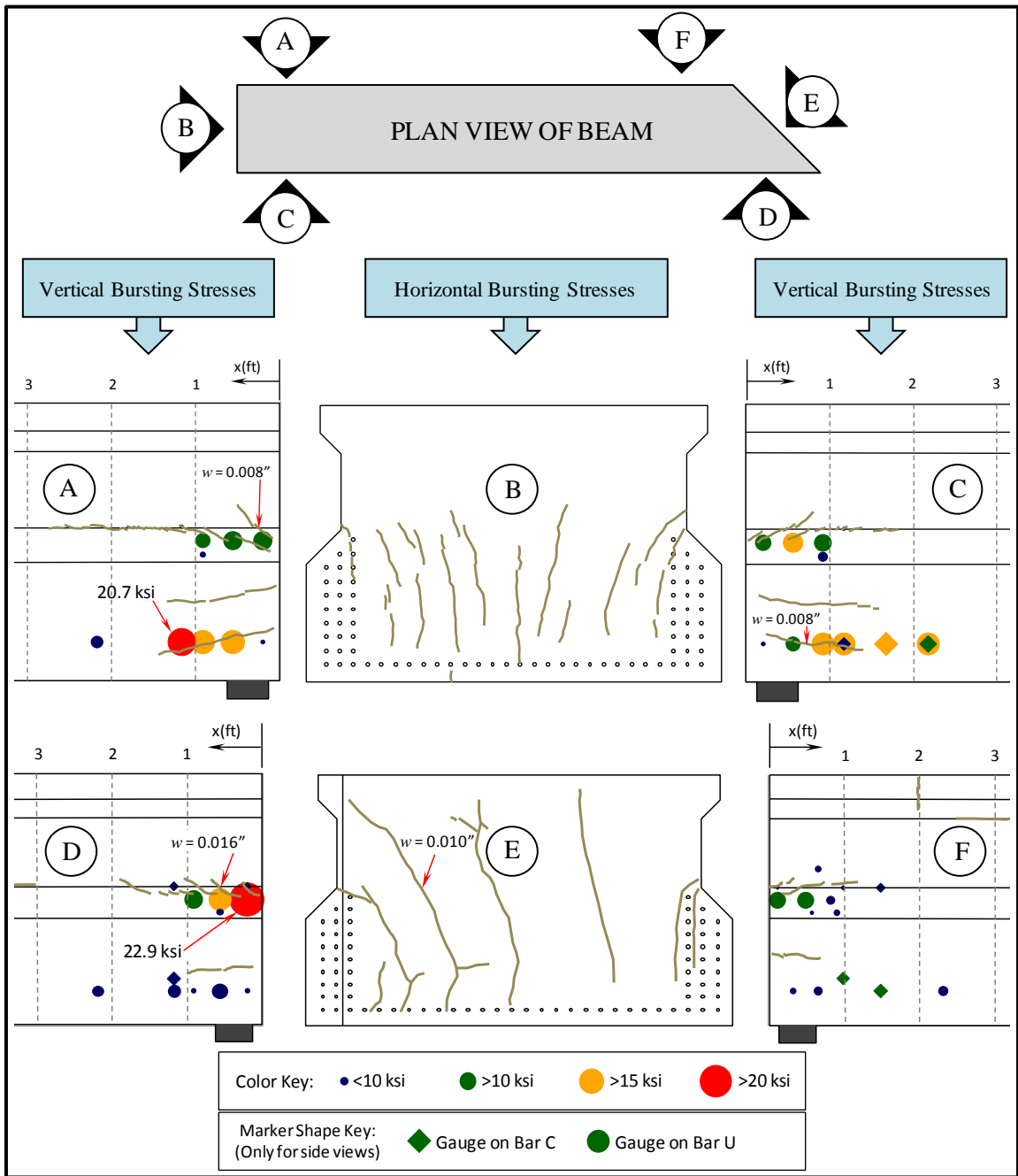
Figure 5-8: Cracks and stresses registered at the time of prestress transfer in beam specimen 5B40-1
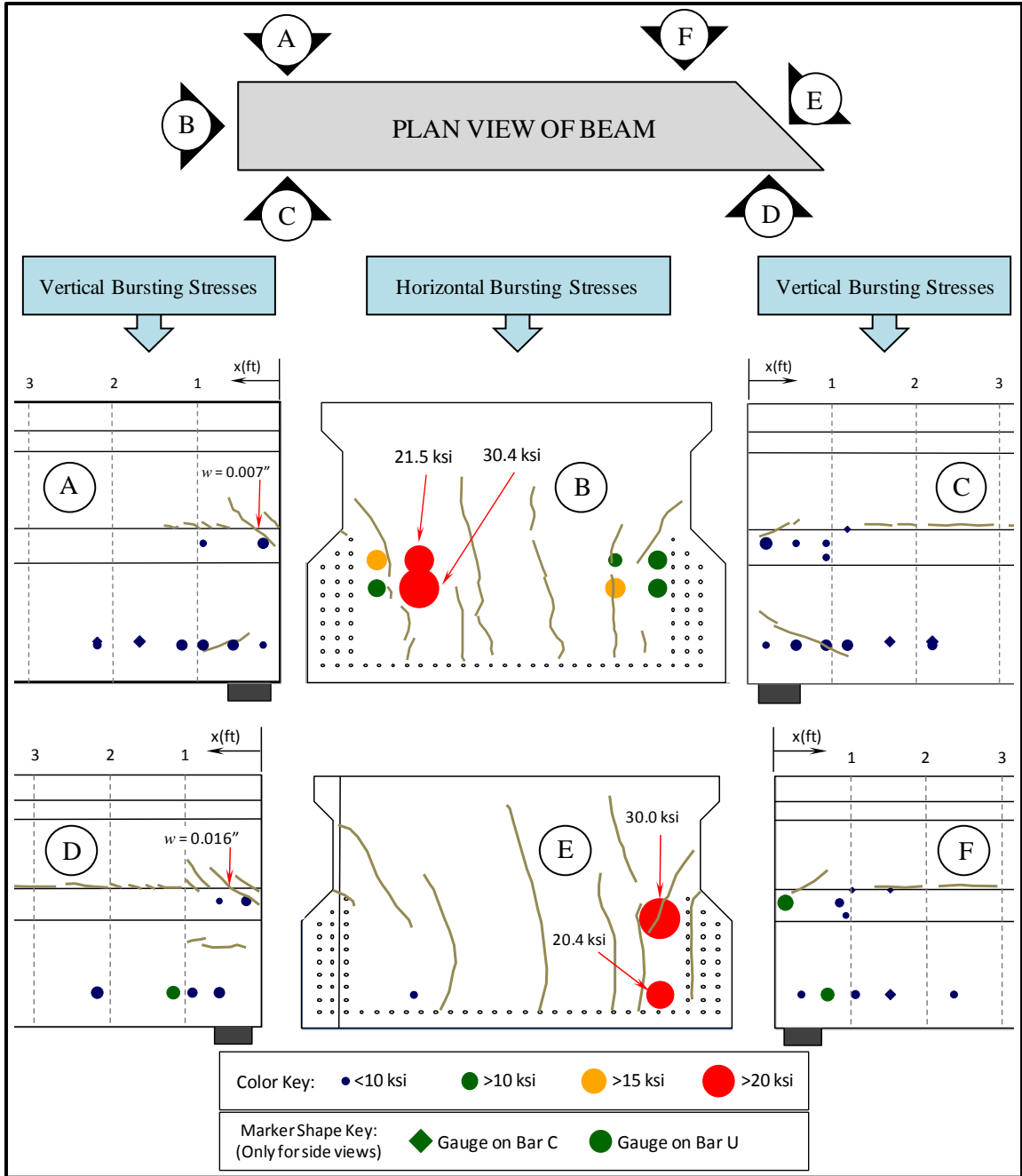
Figure 5-9: Cracks and stresses registered at the time of prestress transfer in beam specimen 5B40-2
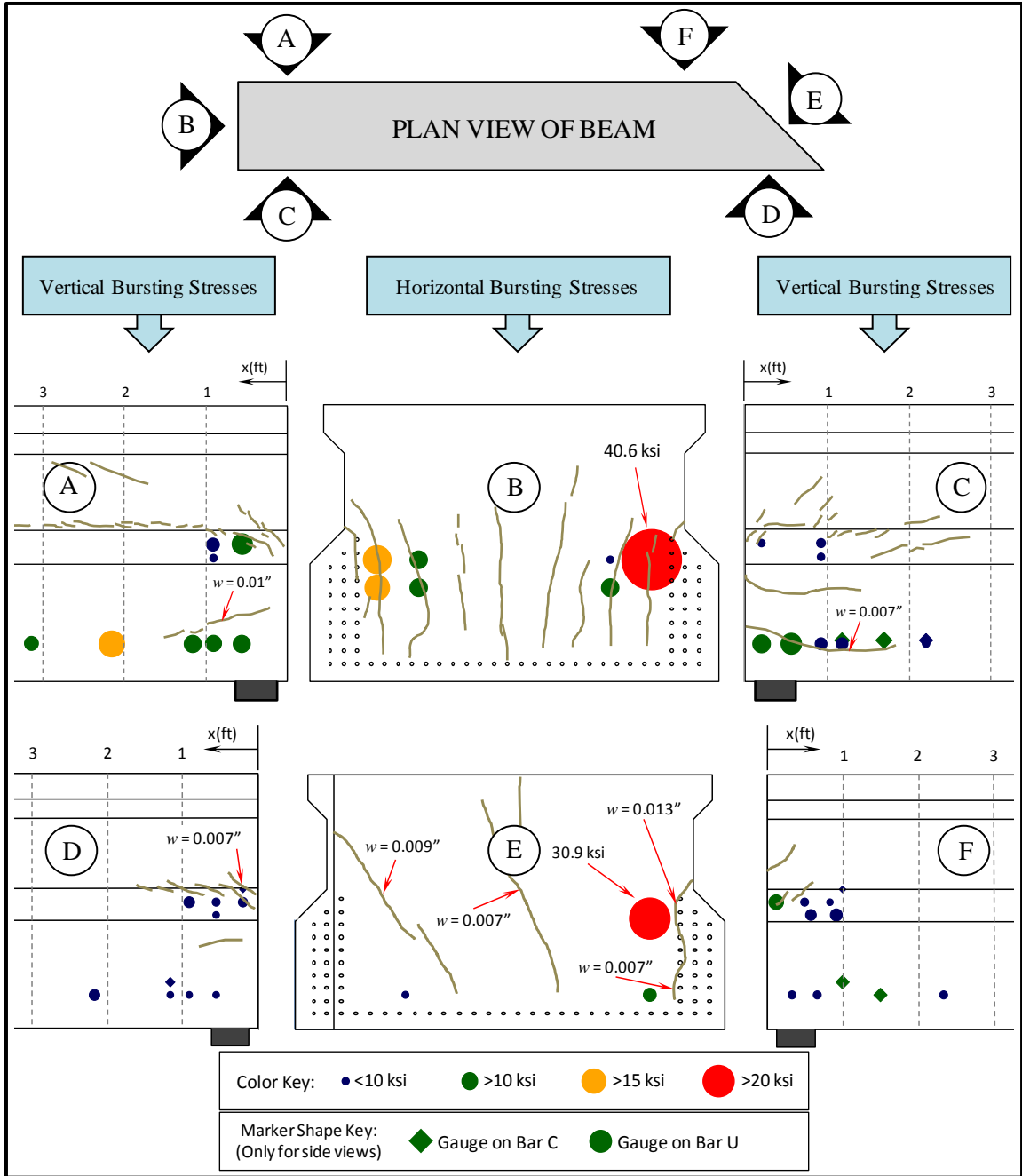
Figure 5-10: Cracks and stresses registered at the time of prestress transfer in 5B40-3-Skewed End

There is a reasonable explanation for the relatively high strain values measured on Bars E (Bar E is illustrated in Figure 5-11). The high strains measured in Bars E corresponded to locations closer to the ends of Bar M (see Figure 5-9 and Figure 5-10); where Bar M could not develop significant tensile stresses. Therefore, all of the bursting force had to be carried by Bars E and Bar C (all of these bars are illustrated in Figure 5-11). Given the strand pattern of the box beams fabricated in Phase I, one can see that a significant fraction (36%) of the strands was placed outside of each end of Bar M as illustrated in Figure 5-11. One could then expect higher stresses in Bars E in locations where Bars M could not fully participate in equilibrating the bursting force.

If only Bars E are accounted for as transverse bursting reinforcement, and the stresses inferred from the strain measurements are compared to the net prestressing force, one would find that:

$$\frac{4\,bars \cdot 3\,curtains \cdot 0.31\,in^2\!\!\big/\!bar \cdot 30ksi}{76\,strands \cdot 0.153\,in^2\!\!\big/\!strand \cdot 187ksi} = 5.1\% \qquad \textbf{Equation 5-1}$$

This ratio indicates that the bursting force in 5B40 box beams could be estimated to be more than the 4% of the total prestressing force, as recommended by AASHTO.
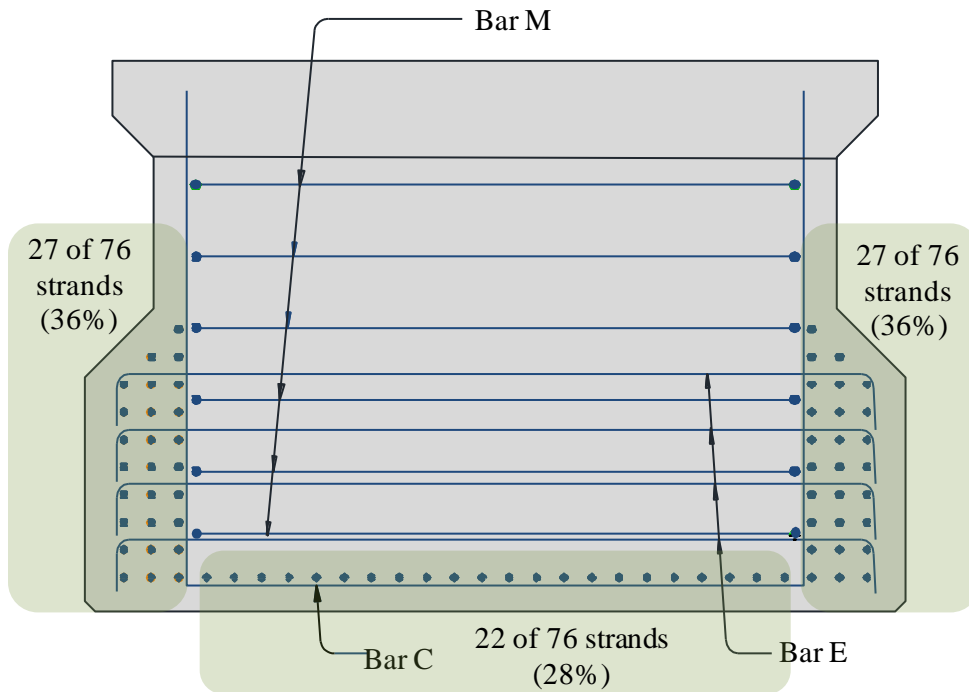
Figure 5-11: Horizontal transverse reinforcement and strand groups
(Some bars omitted for clarity)

Note that the calculation presented in Equation 5-1 was made assuming that the stress in all Bars E was constant and equal to 30 ksi as documented in Phase I. Considering that strains proportional to a stress greater than 30 ksi were only found in one location, this seems to be a reasonable estimate.

A design bursting force equal to 5.5% of the total prestressing force was used to detail the horizontal bursting reinforcement for beams fabricated in Phase II. The goals were to maintain maximum horizontal bursting stresses below the 20 ksi limit recommended by AASHTO-LRFD, and to address any other issues found during the shear testing program.

5.2.2 **Phase II Beam: 5B40-4**

5.2.2.1 Description

The first beam of Phase II, identified as 5B40-4, had the same cross sectional dimensions and strand pattern as the beams fabricated in Phase I. Transverse horizontal reinforcement was modified in order to obtain lower stresses and narrower crack widths at the time of prestress transfer. The modified end region details used in the 5B40-4 beam specimen are illustrated in Figure 5-13 through Figure 5-15. The modifications made from the details used in Phase I beam specimen can be summarized as follows:

1. In the first curtain (Figure 5-13), located 2.5 in. from the end, Bars MB (#5) and Bars MT (#4) were added. Both sets of bars had 90 degree hooks extending 30 in. into the beam. No Bars M were used in the first curtain. Bars MB and MT were meant to carry horizontal bursting forces, and provide a better connection between the two webs of the beam.

2. In the second and third curtains (Figure 5-14), located 6.5 in. and 11 in. from the end, Bars M were relocated so that they were only used in the narrowest part of the end block. Below that, Bars E were used instead. Bars M and Bars E were not used at the same location as in Phase I beams. The total number of M bars per end block was reduced from 18 in Phase I to 8 in Phase II beams.

3. A fourth curtain of Bars E only was added (Figure 5-15), located 14 in. from the end of the beam.

SIDE ELEVATION – 5B40-4

1st reinforcement curtain - Figure 5-16
(~2.25 in. from the end of the beam)

2nd reinforcement curtain – Figure 5-17
(~6.5 in. from the end of the beam)

3rd reinforcement curtain – Figure 5-17
(~11 in. from the end of the beam)

4th reinforcement curtain - Figure 5-18
(~14 in. from the end of the beam)

Internal Void
Boundary
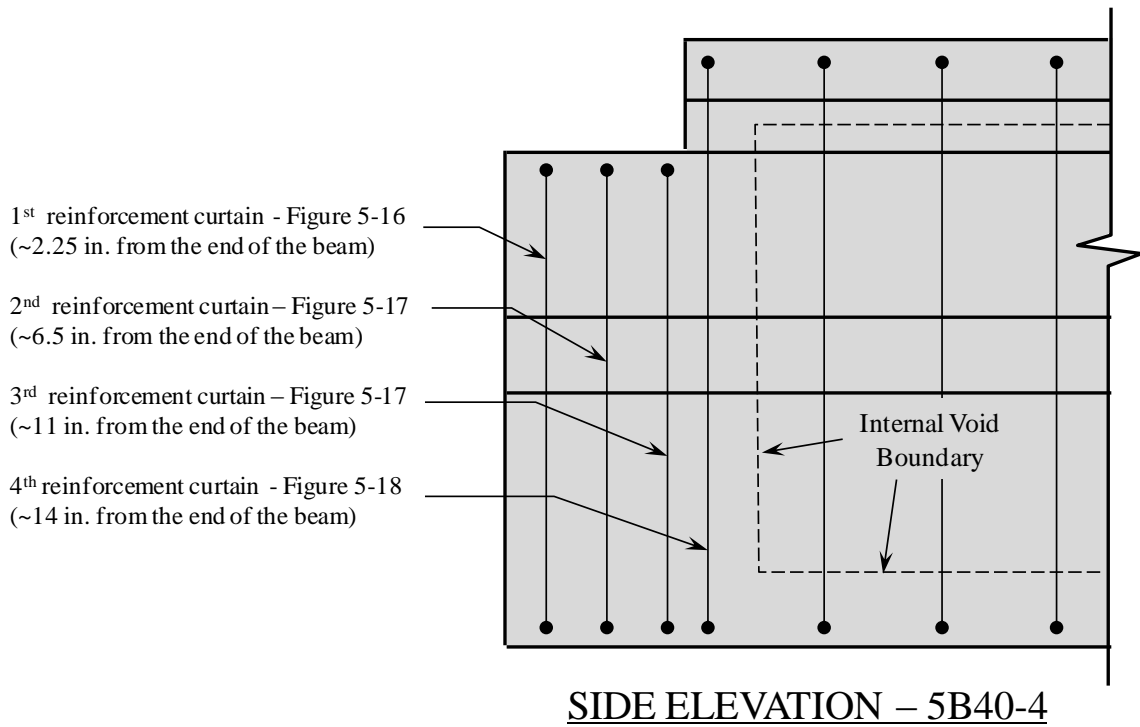
Figure 5-12: Reinforcement Curtains Locations for beam 5B40-4
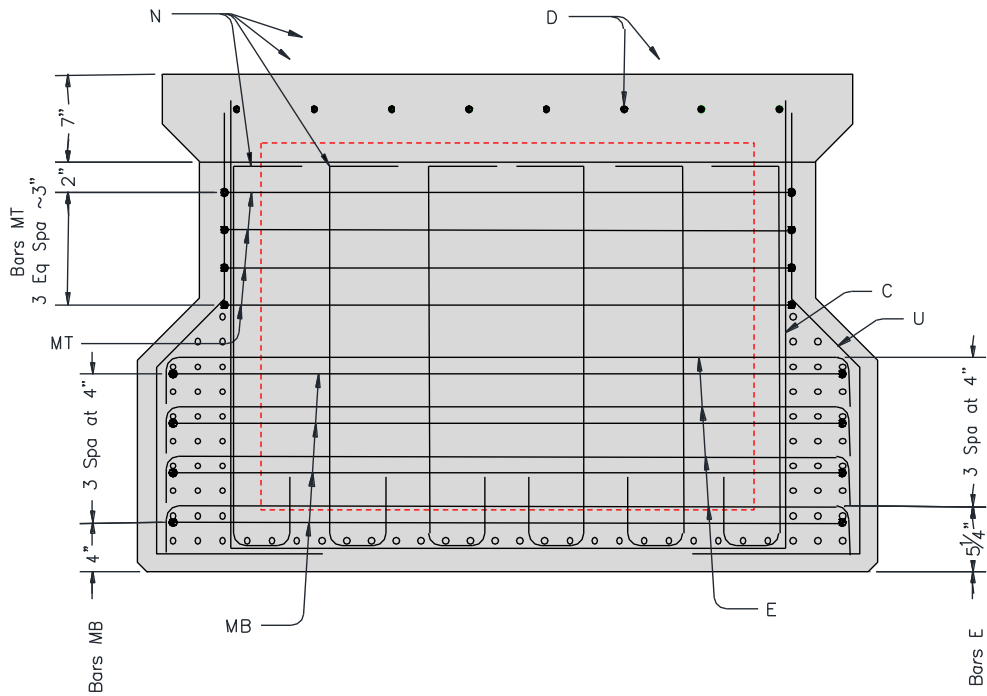
Figure 5-13: End region reinforcement used in 5B40-4. First steel curtain detail is shown.

149
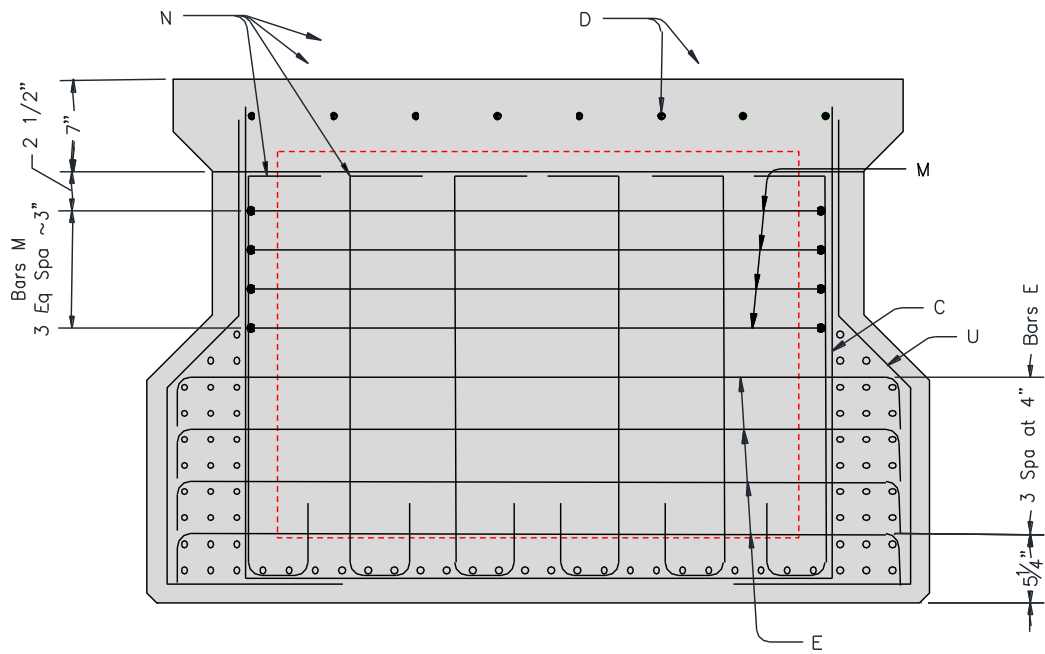
Figure 5-14: End region reinforcement used in 5B40-4. Second and Third steel curtain detail is shown.
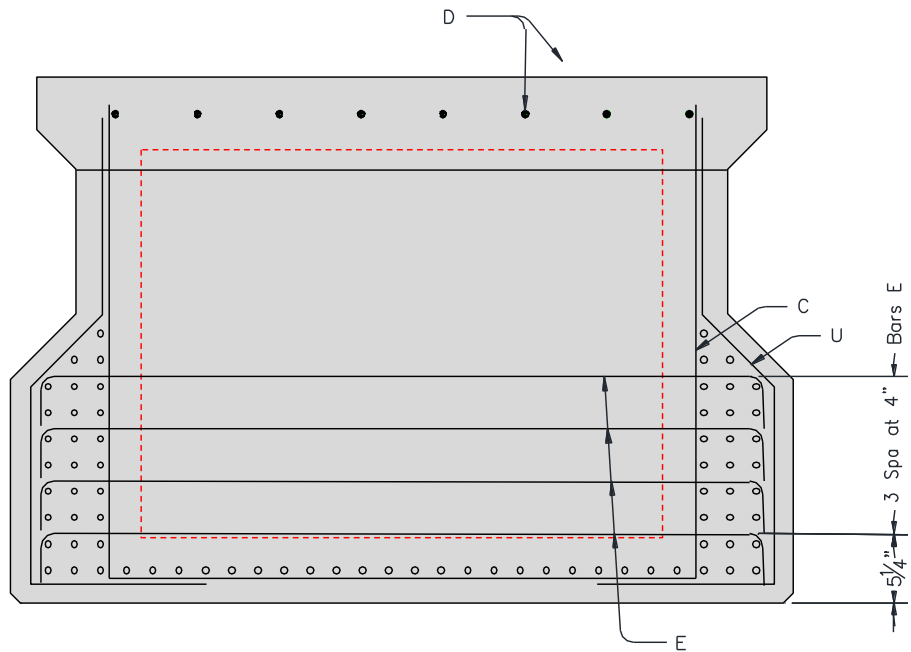
Figure 5-15: End region reinforcement used in 5B40-4. Fourth steel curtain detail is shown.

The skewed end was modified in the same manner. Full shop drawings of all beams can be found in Appendix B.

5.2.2.2 *Measured Strains*

After incorporating the aforementioned modifications, the maximum strain reading in the horizontal transverse reinforcement was proportional to a stress of 13.4 ksi. This measurement corresponds to a strain gauge located in the first Bar MB from the bottom of the beam (4 in. from the bottom), 14 in. away from the centerline of the beam as illustrated in Figure 5-16. Strains proportional to stresses between 8.7 and 12.3 ksi were measured in 9 other strain gages of the total 36 strain gages successfully monitored in the first curtain of steel. Crack widths associated with horizontal bursting were in the range of 0.002 in. to 0.005 in. Hence, it can be said that the modified end region detail used in the 5B40-4 beam successfully improved the ability of the beam to manage horizontal bursting stresses. Measured strains, stresses that can be inferred from these strain measurements and crack widths were all acceptable.

In terms of vertical bursting stresses, the maximum strain measured was proportional to a stress of 12.4 ksi. Crack widths associated with vertical bursting were comparable to those found in the beams fabricated in Phase I of this study. Since no change was made to the vertical reinforcement in the end region, this result could be expected. Once again, considering that beams 5B40-1 through 5B40-4 contained the maximum possible number of prestressing strands, they were deemed to be a worst case scenario in terms of bursting stresses. With that in mind, there was no need to modify the existing reinforcement detail in terms of its ability to manage vertical bursting stresses introduced at the time of prestress transfer.

151
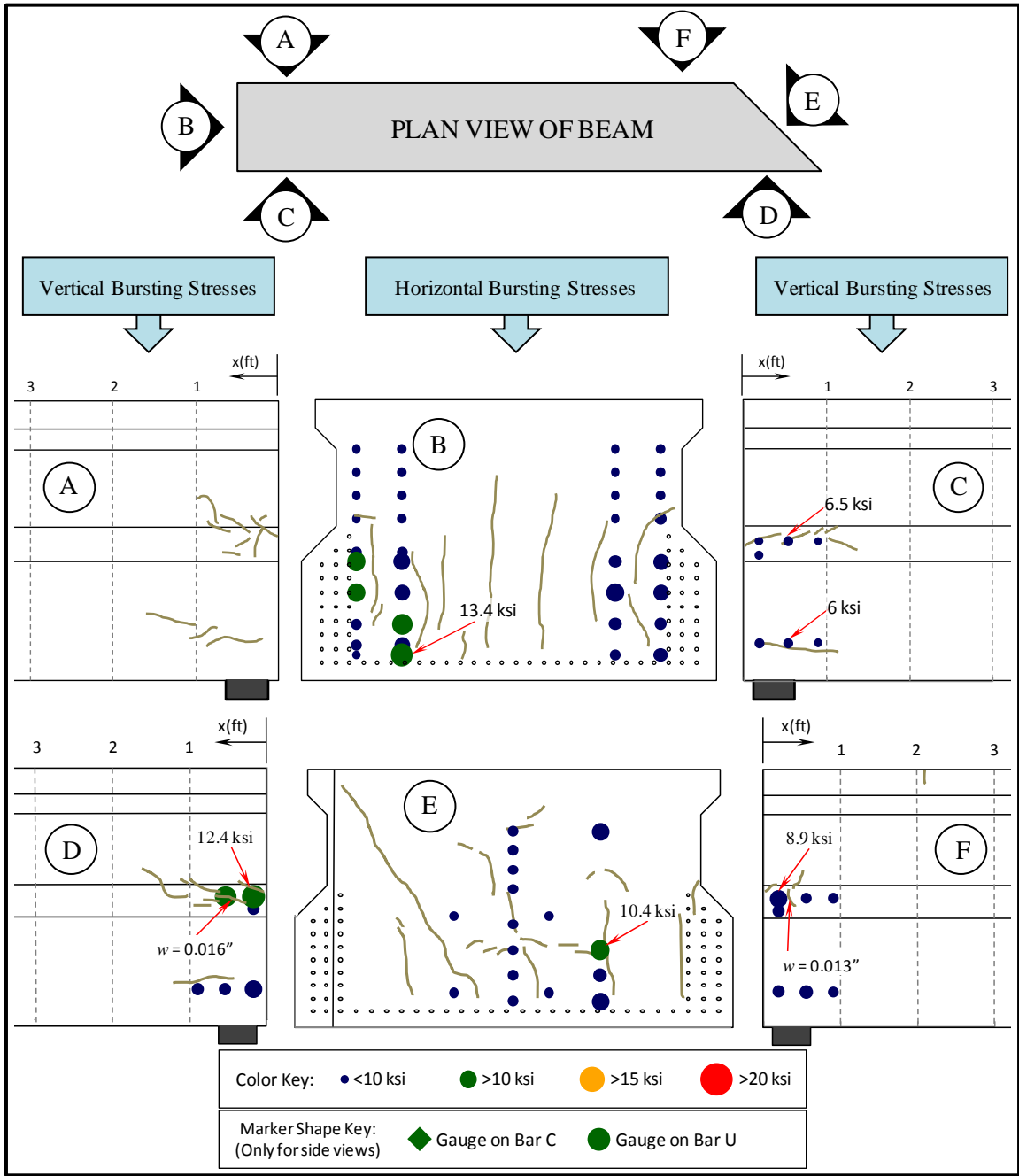
Figure 5-16: Cracks and stresses registered at the time of prestress transfer in beam specimen 5B40-4

5.2.3   **Phase II Beam: 5XB40**

5.2.3.1   Description

The last beam fabricated in this study had significant differences compared to all previous ones. The thickness of the web was increased from 5 in. to 6.5 in. The depth of the bottom slab was increased from 5 in. to 7 in. Finally, and most importantly, the placement of the strands was substantially different; with two full bottom rows of strands (28 strands per row) and only three more rows above with 6 strands each (3 per web) for a total of 74 strand positions.

Although 74 strands were used, only 66 of them were fully bonded as illustrated in Figure 5-17. Hence, bursting forces were expected to be slightly lower than in the previous beams where 76 strands were fully bonded in each beam.

Debonding had to be done in order to control the tensile stress in the extreme top fiber of the beam at the time of prestress transfer. In the 5XB40 beam, the strands were effectively lower than in the previous 5B40 beams. The centroid of the bonded strands was 4.8 in. from the bottom of the beam, compared to 8.2 in. in all previous beams. The higher eccentricity resulted in a higher prestressed-induced moment (i.e. $P \cdot e$) on the cross section, explaining the comparatively higher tensile stresses in the 5XB40 box beam and the consequent need for debonded strands.

Debonded through the
entire beam length
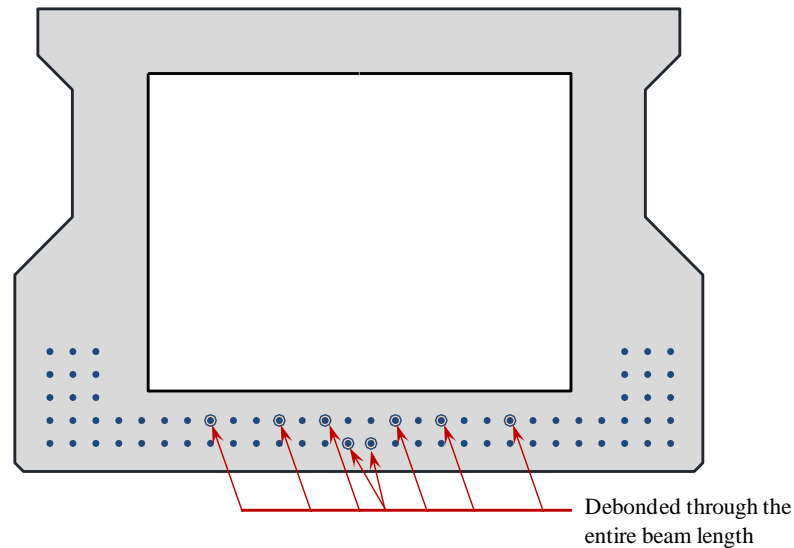
Figure 5-17: Strand pattern in 5XB40

The decision to place two full rows of strands in the bottom slab of the 5XB40 is geared towards maximizing the flexural capacity of the box beam sections. The increased flexural capacity allows 5XB40 beams to be used with space between the beams (i.e. "spread box beam" configuration) and an 8 inch thick cast-in-place deck, rather than the 2 in. asphalt overlay used occasionally when beams are placed with no space in between them. Asphalt overlays require grouted shear keys and transverse post-tensioning of the box beams. With the spread box beam configuration, there is no longer a need for the shear keys or the transverse post-tensioning.

Reinforcement through the 5XB40 end block, illustrated in Figure 5-18, is similar to that of the previous beams. Two Bars E were used in the first three reinforcement curtains (curtains located at 2.25 in., 6.25 in. and 10.25 in. from the end respectively), the bottom hook in the bottom of Bars N was changed to a 90 degree hook in order to simplify their placement, Bars M are #5 bars (previously #4) with the hooks in a vertical plane to avoid conflicts and Bars W are placed only in the outermost layer with a 90 degree hook extending 36 in. into the beam. A complete set of drawings of the fabricated beam can be found in Appendix B.

154

BarN
(#4)

BarR
(#4)

BarM
(#5)

BarY
(#5)

BarU
(#4)

BarE
(#5)

BarW
(#5)
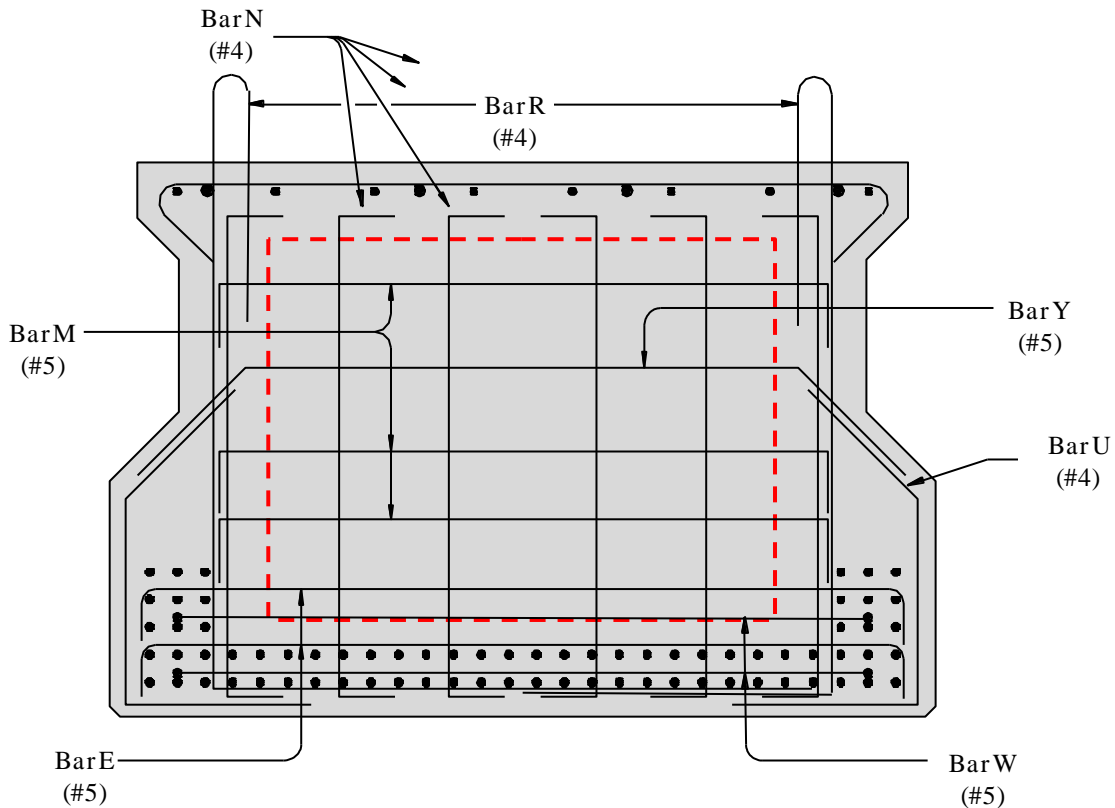
Figure 5-18: First curtain of 5XB40 end-block reinforcement

5.2.3.2 Measured Strains

Maximum measured strains were lower (approximately half of the previously measured values) than those observed in Phase I beams and the first beam of Phase II (5B40-4). The first reason for the lower strains is the lower number of bonded strands used in the 5XB40 beam (66 fully bonded strands in beam 5XB40 compared to 76 in all previous beams). Nevertheless, as was summarized in Table 5-1, the total bursting forces measured in the 5XB40 beam were proportional to approximately 2% of the net prestressing force. Hence, the reduction in the magnitude of the transverse strains measured exceeded the relative reduction in the number of bonded strands.

The second reason for lower strains and perhaps the key difference between the 5XB40 beam and all beams fabricated previously is the distribution of the strands, as opposed to the number of strands. In regards to transverse horizontal stresses, the more

155

even distribution of strands through the width of the 5XB40 beam resulted in a more even strain distribution.

Transverse strains measured in the 5XB40 were more consistent through the cross section. As shown in Figure 5-19, in the north end of the 5XB40 beam, transverse horizontal stresses in the middle of the section (8.1 ksi) were practically equal to those measured towards the webs (8.2 ksi).

While strands were more evenly distributed horizontally in the cross section, the same cannot be said about their vertical distribution (i.e. the strands had a high eccentricity). In the 5XB40 beam, strands are concentrated towards the bottom of the section. This resulted in a different crack pattern than that observed in all Phase I beams, as can be observed in Figure 5-19. Cracks were mostly horizontally oriented; in contrast with what was observed in all previous beams where cracks were mostly vertically oriented (as seen in Figure 5-16).

In terms of vertical bursting stresses, the maximum measured strains were proportional to stresses between 8 and 9 ksi.
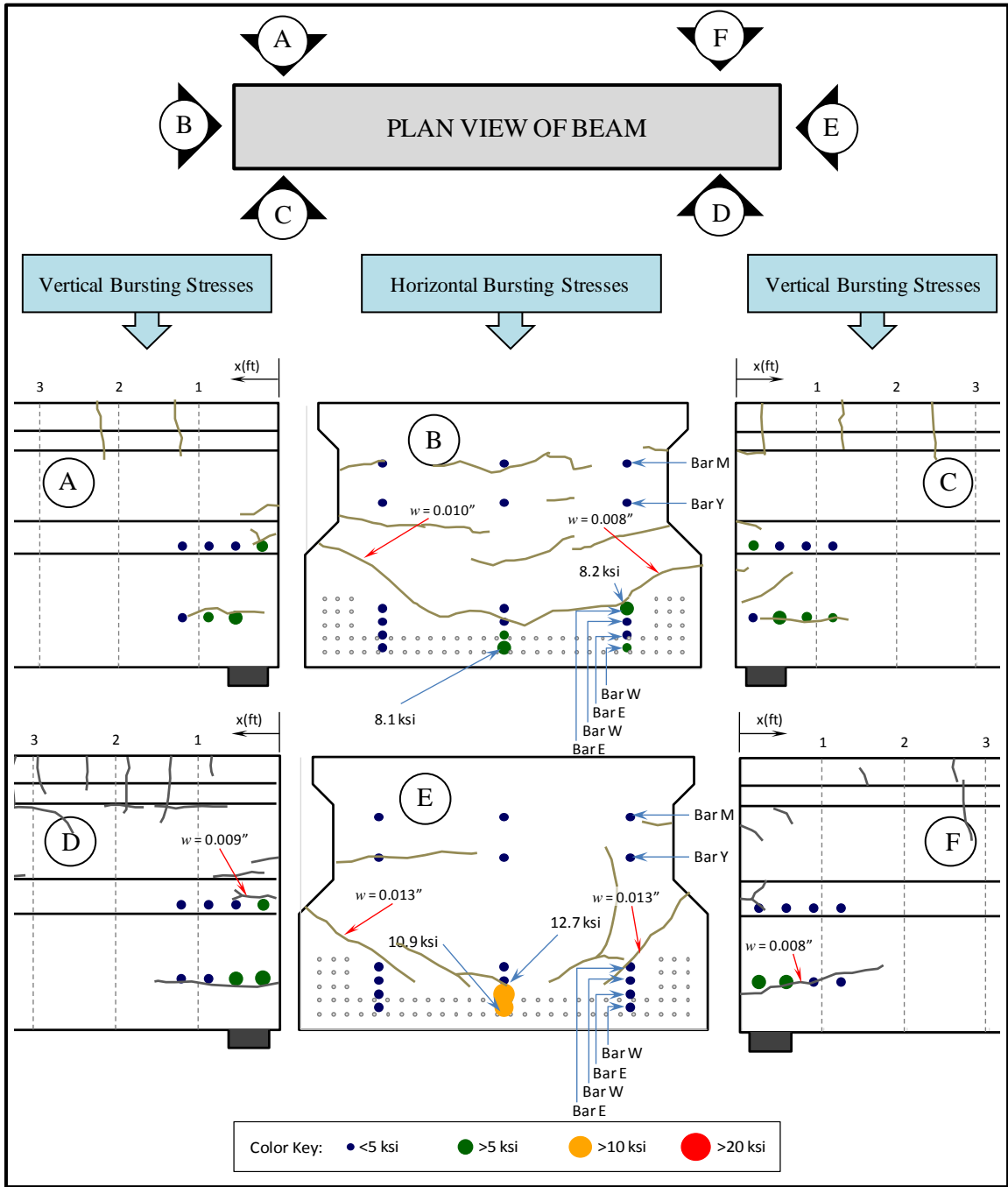
Figure 5-19: Cracks and stresses registered at the time of prestress transfer in beam specimen 5XB40

5.3 **TOTAL BURSTING FORCE**

As discussed previously, strain gages were installed in all beams to quantify strains in the reinforcement at the time of prestress transfer. From the strain readings gathered, the total transverse force was estimated. Although strain gages were not installed in every single bar, enough were installed to infer stresses for bars within close proximity of an instrumented bar. The following simplifying assumptions were made to facilitate the computation of the total bursting force:

(1). When multiple bars were bundled in one location, the strain measurement from any bar was assumed to be applicable to all bars within the bundle.

(2). Given that the strand pattern is symmetric about a vertical axis passing through the centroid of the section, the bursting forces were assumed to be symmetric as well.

(3). For beams 5B40-1,-2, -3 and -4; given that more of the strands were concentrated towards the webs, it was assumed that vertical bursting forces were of higher magnitude near the web and of lesser magnitude towards the middle of the cross section. Instrumentation in beam 5B40-1 revealed that the forces in the vertical reinforcement towards the middle of the cross section (Bars N) are approximately 50% of the magnitude of the forces measured in reinforcement bars located near the webs. This relationship was then assumed to be the same for all other beams fabricated with the same strand pattern and vertical reinforcement detail (5B40-2,-3 and -4).

Note that the use of the last two assumptions was only necessary in the absence of actual measurements. In estimating the total bursting force in the end region, approximately 80% of the calculated force was obtained through actual measurements while the remaining 20% of the force was estimated through the use of the aforementioned assumptions. Additionally, it must be appreciated that the measurements constitute lower bounds. In other words, strains of *at least* the measured magnitude were present in the reinforcement. Maximum strains would be measured if the location of the strain gages coincided exactly with a crack crossing the reinforcement.

Once the total bursting force was calculated, the result was normalized by the effective prestress force after allowing for short term losses. A summary of the normalized transverse forces in the vertical and horizontal direction per beam is presented in Table 5-1. The normalized percentage can be compared to the requirement from AASHTO-LRFD (2010) discussed in Chapter 2. In short, AASHTO-LRFD (2010) requires that transverse reinforcement be placed in the end-region of the beam, within a quarter of the height of the beam, such that a force equal to 4% of the effective prestress force after allowing for short term losses (i.e. elastic shortening) is managed without the stress in the reinforcement exceeding 20 ksi.

In Table 5-1, one can observe that the total transverse forces exceeded the 4% of the effective prestress force recommendation in two occasions. In both of these cases, the beams were fabricated with the maximum possible number of prestressing strands (76), constituting a worst case scenario in terms of the bursting forces. However, not all of the force summarized in Table 5-1 is located within the first $h/4$ of the beam as one could infer from the AASHTO recommendations. In fact, the total forces as indicated in Table 5-1 incorporate strain measurements obtained from instrumentation placed up to 26 in. into the beam. The subsequent section includes a discussion on the distribution of the total bursting force within the end region of specimens investigated in this study.

Table 5-1: Total transverse forces normalized by the effective prestressing force

Beam ID (76 bonded strands)	Vertical Force		Horizontal Force	
	Square End	Skewed End	Square End	Skewed End
5B40-1	**4.40%**	3.90%	N/A	N/A
5B40-2	2.60%	2.90%	3.80%	3.70%
5B40-3	3.20%	2.60%	**5.10%**	3.90%
5B40-4	1.90%	2.70%	3.10%	3.70%
AVERAGE (1-4)	3.03%	3.03%	4.00%	3.77%
Beam ID (66 bonded strands)	Vertical Force		Horizontal Force	
	North End	South End	North End	South End
5XB40	2.20%	2.10%	2.08%	2.16%

5.4 Location And Magnitude Of The Transverse Force In The End Region

After examining all of the data gathered in this study, it can be concluded that the transverse force within the first $h/4$ of the beam did not exceed 4% of the prestressing force. Nevertheless, it was found that significant transverse forces were concentrated beyond the region bounded by the beam end and a section located $h/4$ away from the beam end.

For the end region of each beam specimen, a large number of strain gages were monitored during prestress transfer. From the strain readings, the total transverse force in each reinforcement curtain can be inferred. The transverse force can then be divided by the net prestressing force and expressed as a percentage of the net prestressing force.

By adding the percentage forces per reinforcement curtain, starting from first curtain (closest to the end of the beam) through the *nth* curtain, the total transverse force within the end of the beam and a specific distance away from the end can be calculated. An example of such procedure is tabulated in Table 5-2 for the square end of beam 5B40-1 and the vertical bursting forces measured therein. In example, from the last column of Table 5-2, the total transverse force measured within the end of the beam and the third curtain of reinforcement (located at 11 in.) represents 3.0% of the net prestressing force.

Table 5-2: Transverse force per reinforcement curtain for end region 5B40-1-Q

Curtain	Distance from the end of the beam (in.)	Total Force in Curtain (kip)	Percentage of net prestressing force[†] per curtain	Accumulated force as percentage of net prestressing force
1	2.5	20.9	1.0%	1.0%
2	6.5	23.8	1.1%	2.1%
3	11	19.2	0.9%	3.0%
4	14	14.0	0.7%	3.6%
5	20	7.0	0.3%	4.0%
6	26	10.2	0.5%	4.4%

[†]The net prestressing force was 2139.6 kips

The accumulated force as a percentage of the net prestressing force can then be plotted versus the distance from the end of the beam. Plots for all end regions are presented in Figure 5-20. As can be seen in Figure 5-20, the total bursting force increases

beyond $h/4$. On average, the total bursting force was 50% greater than that occurring within the first quarter-height ($h/4$) of the beams. Note that bursting forces were accumulated within the first 26 in. of the beams, which is close to the transfer length of the used strands (~30 in. for ½ in. strands). These findings resonate with those of O'Callaghan and Bayrak (2008) discussed in chapter 2. O'Callaghan and Bayrak (2008) found significant bursting stresses up to the transfer length of the specimens in his study.
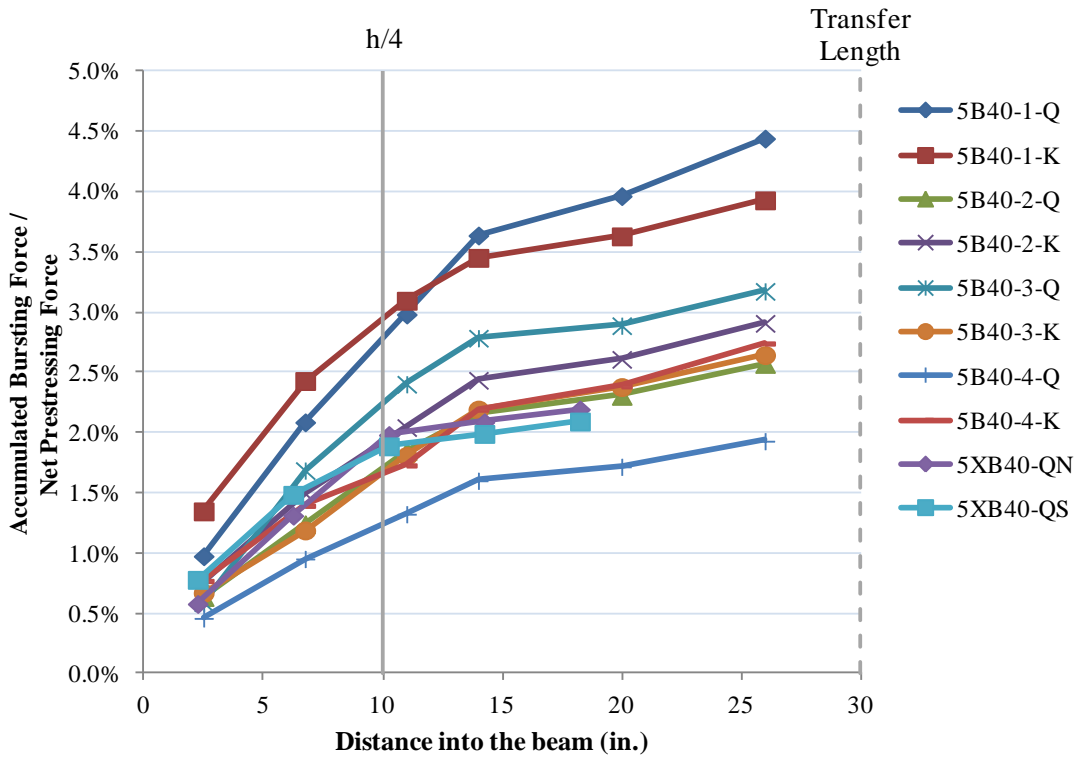
Figure 5-20: Accumulated vertical bursting force versus distance into the beam

The results of the present study indicate that providing reinforcement to equilibrate 4% of the prestressing force within the first $h/4$ length of the beam is a conservative design practice. That can be said since 4% of the prestressing force has, once again, been proven to be a conservative upper bound for the bursting force within the first $h/4$ of the beam.

Nevertheless, the bursting forces occurring in the region bounded within $h/4$ from the end of the beam and the transfer length are not addressed by the current AASHTO-

LRFD specifications. O'Callaghan and Bayrak (2008) recommended that reinforcement be provided in the region bounded within $h/4$ from the beam end and the transfer length to equilibrate 4% of the prestressing force without the stress in the reinforcement steel exceeding 20 ksi. Within the present experimental program, bursting forces equal to as much as 1.7% of the prestressing force were found in the mentioned region. Based on these results, it can be concluded that the design recommendations of O'Callaghan and Bayrak (2008) are adequate and necessary. The inclusion of such recommendations in future design specifications is recommended.

5.5   RESULTS WITHIN THE CONTEXT OF PREVIOUS RESEARCH

Previous work regarding the magnitude of the transverse force in the end region of pretensioned beams was presented in Chapter 2. In this experimental program, data from 10 box beam end regions was gathered. Comparing the gathered data to previously obtained results is useful in establishing if the behavior of box beams is similar to that of more typical I-shaped girders. It is important to note that besides the tests reported by Dunkman (2009) and Hovell (2011), where U-beams were instrumented, all previous work consisted on single-webbed beams.

Dunkman (2009) gathered the results of his work and five other relevant publications regarding bursting stresses in a database. By examining the database, Dunkman (2009) found that using 4% of the prestressing force as a design force was a conservative upper bound. Later results added to the bursting database by Hovell (2011) support such finding.

After incorporating the results of the present experimental program into the bursting stresses database, as plotted in Figure 5-21, one can see that the vertical bursting forces observed in box beams are comparable to those observed in T-beams, I-beams and U-beams. For consistency with previous work, only the data gathered for vertical bursting was incorporated into Figure 5-21.
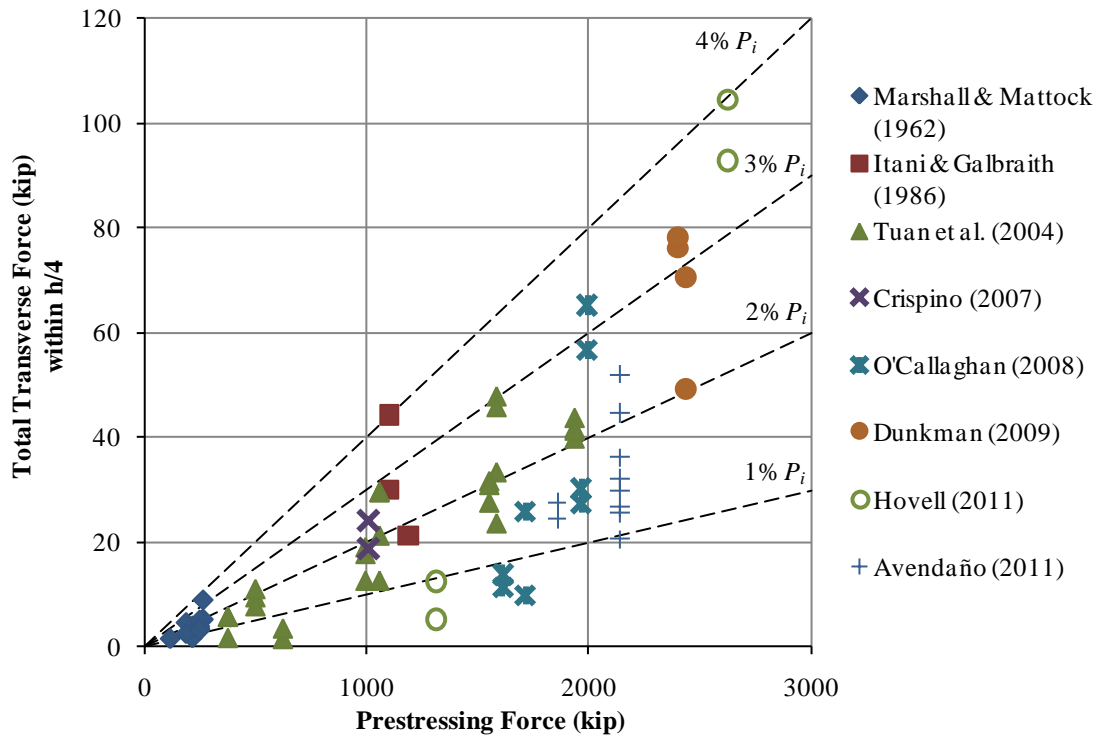
Figure 5-21: Total transverse forces versus total prestressing force for the current and past studies.

5.6 CURING TEMPERATURES

High curing temperatures can lead to durability problems. In box beams, the presence of an end block creates a concentrated mass of concrete that can reach higher temperatures than other beam geometries. This issue is aggravated in skewed end blocks due to the higher volume of concrete in the end block, compared to a square end block. For these reasons, it was of interest to measure the curing temperatures within end blocks of different geometries.

The absolute maximum temperature in each end block and the maximum temperature differential within the end block are of interest. Comprehensive studies (Day, 1992 and Lawrence, 1994) have shown that once the maximum temperature in the end block exceeds 158 °F for a few hours, the potential for Delayed Ettringite Formation (DEF) increases drastically. Recently, research results have shown that replacing 20% of the cementitious material with fly ash can reduce the heat of hydration and therefore

diminish the potential for DEF. Nevertheless, TxDOT restricts maximum curing temperatures to 170 °F, for concrete mixtures containing at least 20% fly ash as a cementitious material, in order to prevent durability problems. TxDOT also restricts the maximum temperature differential within the section to 35 °F in order to prevent thermal cracking. More importantly, the use of fly ash is now mandatory for all precast prestressed concrete beams.

All beams were fabricated using metal forms. The form surface consisted of a 3/8-in. plate. Forms were kept in place at least until prestress transfer took place. The top of the beam was covered with 20 mil plastic sheeting until the forms were removed.

5.6.1 Description of gathered data

Each end block was instrumented with at least 6 thermocouples spread through a cross section parallel to the end face of the beam and approximately 10 in. from the end face. A typical thermocouple arrangement is illustrated in Figure 5-22. Three thermocouples were placed along a vertical line through the middle of the section. The same was done in a line closer to the side of the beam. In square end blocks, temperature gradients were assumed symmetric (side to side) and a temperature profile through the section could be obtained as illustrated in Figure 5-23. For a skewed end block, three vertical lines of thermocouples are used: one through the middle of the section and one towards each side of the beam to incorporate the variation across the asymmetric geometry as illustrated in Figure 5-24. As expected, the measured temperature profiles were not symmetric. The asymmetry of a temperature profile can be observed in Figure 5-25.

SECTION A

LOC
1,2,3

LOC
4,5,6

~10 in.

A

A

VOID BOUNDARY

PLAN VIEW
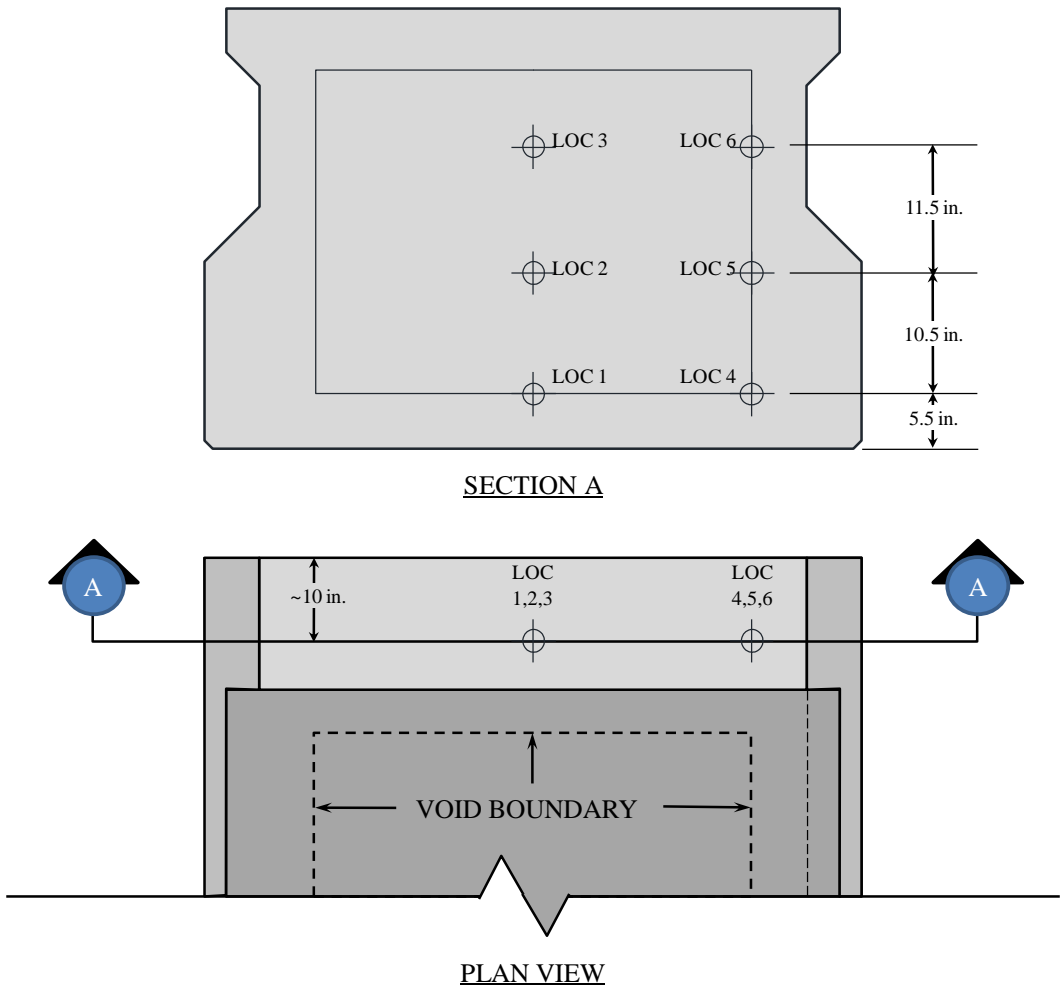
Figure 5-22: Typical thermocouple locations at square end block
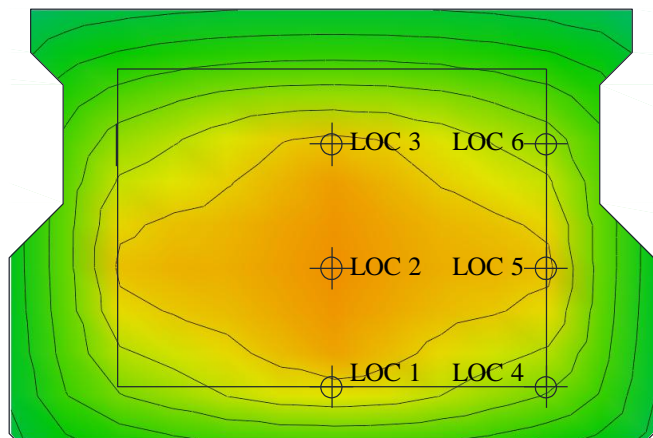
Figure 5-23: Temperature Profile of a square end block

165

SECTION B

LOC 9   LOC 3   LOC 6

LOC 8   LOC 2   LOC 5

LOC 7   LOC 1   LOC 4

11.5 in.

10.5 in.

5.5 in.

B

LOC 4,5,6

LOC 1,2,3

~10 in.

LOC 7,8,9

B

SKEWED VOID BOUNDARY

SQUARE VOID BOUNDARY

PLAN VIEW
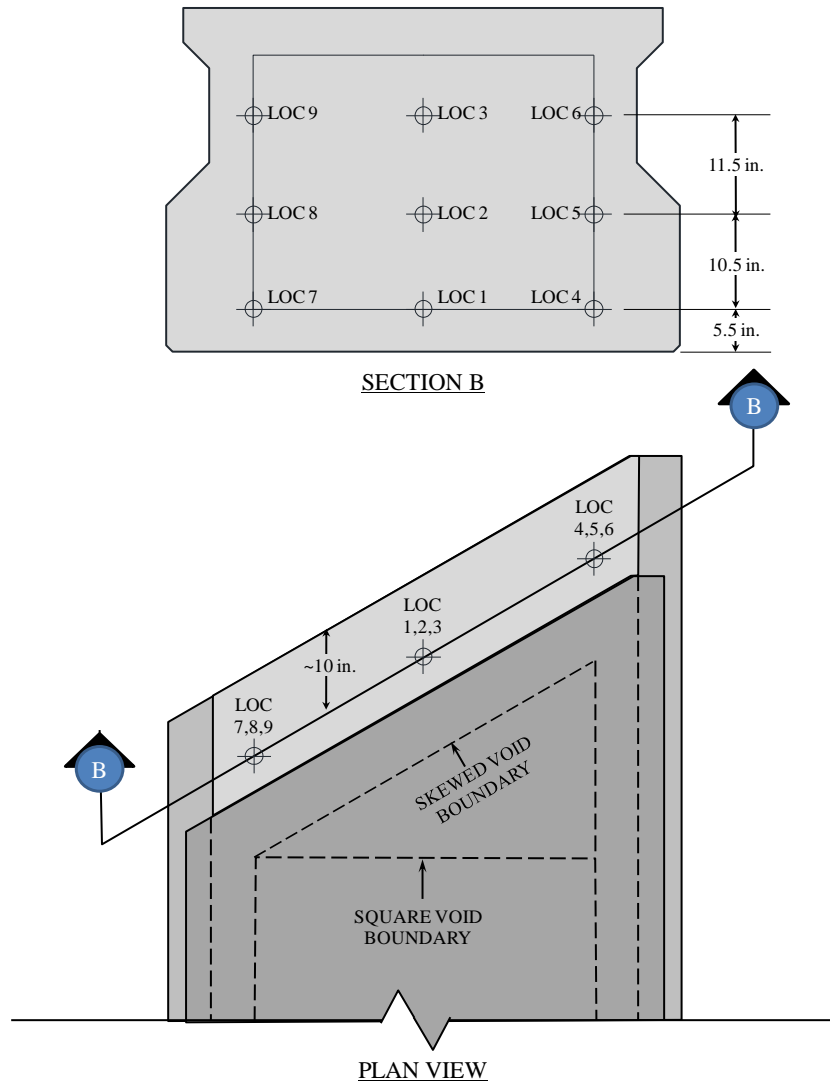
Figure 5-24: Typical thermocouple locations at skewed end block

LOC 9   LOC 3   LOC 6

LOC 8   LOC 2   LOC 5

LOC 7   LOC 1   LOC 4
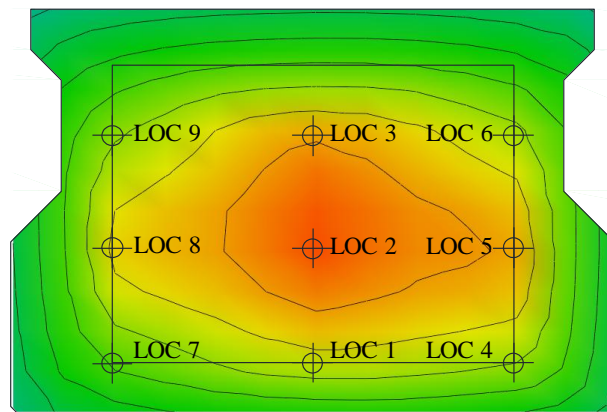
Figure 5-25: Temperature Profile of a skewed end block

166

Temperatures were recorded every 6 minutes during the curing process and for more than 24 hours after the initial placement of concrete took place. The temperature history for the square end of beam 5B40-1 is plotted in Figure 5-26.
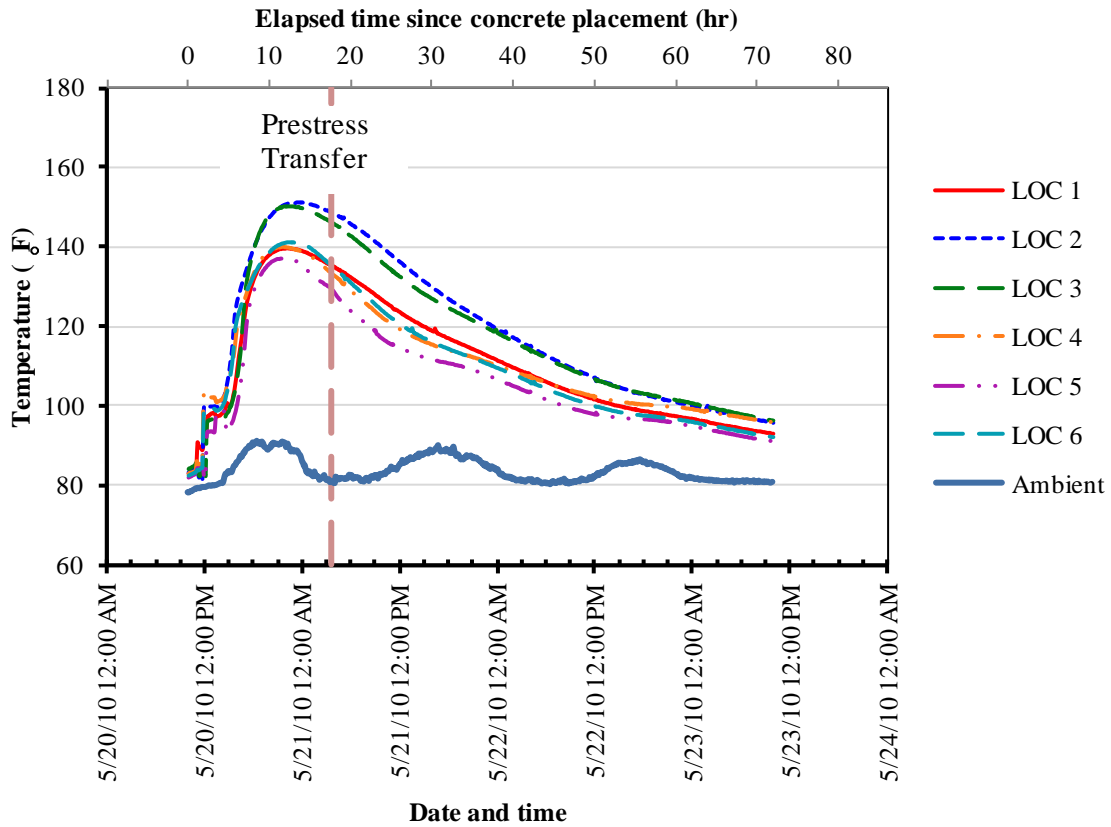
Figure 5-26: Temperature History for square end of beam 5B40-1

5.6.2 Data Analysis

After the temperature histories for all thermocouples, end blocks and beams were analyzed, it was possible to compare maximum temperatures and differentials across different end block geometries. For most of this analysis, the temperatures gathered from beams 5B40-4 and 5XB40 were not used given the uncharacteristically cold temperatures (40 °F) that the concrete was exposed to during its travel from the batching plant to FSEL (approximately 30 minutes). Nevertheless, the end block geometries used and instrumented in the first three beams allowed for the comparisons through the intended variables. The results from all beams are summarized in Table 5-3 and Table 5-4.

167

Table 5-3: Summary of temperature measurements: square end blocks

Square end block temperatures		5B40-1	5B40-2	5B40-3	5B40-4	5XB40
	Concrete Placement Date	5/20/10 10:00 AM	7/22/10 10:00 AM	9/7/10 10:00 AM	1/18/11 12:00 PM	5/2/11 10:00 AM
At time of Maximum Temperature	Maximum (°F)	151.4	149.1	151.6	124.2	138.8
	Ambient (°F)	88.6	88.6	84.3	68.2	70.4
	Date &Time (Elapsed Time (hr))	5/20/10 11:30 PM (13.5)	7/23/10 3:54 AM (17.9)	9/8/10 1:00 AM (15)	1/19/11 5:00 AM (17)	5/3/11 4:00 AM (18)
At time of Maximum Temperature Differential within the section	Maximum (°F)	126.7	144.8	143.3	120.8	134.1
	Minimum (°F)	100.5	124.7	115	98.5	116.1
	Differential (°F)	26.5	20.1	28.3	22.3	18
	Ambient (°F)	85.8	85.1	82.6	70.7	71.2
	Date &Time (Elapsed Time (hr))	5/20/10 4:00 PM (6)	7/23/10 9:06 AM (23.1)	9/8/10 9:30 AM (23.5)	1/19/11 10:54 AM (22.9)	5/3/11 12:06 PM (26.1)
At time of Prestress Transfer	Maximum (°F)	148.9	148.8	150.7	87.9	90.5
	Minimum (°F)	129.4	132	125.5	79.8	88.9
	Differential (°F)	19.5	16.8	25.2	8.0	1.6
	Ambient (°F)	80.8	87.6	84.1	69.4	88.1
	Date &Time (Elapsed Time (hr))	5/21/10 3:30 AM (17.5)	7/23/10 5:00 AM (19)	9/8/10 2:42 AM (16.7)	1/21/11 2:48 AM (62.8)	5/9/11 3:17 PM (173.3)

168

Table 5-4: Summary of temperature measurements: skewed end blocks

Skewed end block temperatures		5B40-1	5B40-2	5B40-3	5B40-4
Void Geometry at skewed end		Square	Skewed	Skewed	Square
Concrete Placement Date		5/20/10 10:00 AM	7/22/10 10:00 AM	9/7/10 10:00 AM	1/18/11 12:00 PM
At time of Maximum Temperature	**Maximum** (°F)	155.5	138.5[*]	154.8	124.0
	Ambient (°F)	81.8	86.8	81.1	73.7
	Date &Time (Elapsed Time (hr))	5/21/10 2:10 AM (16.2)	7/23/10 12:50 AM (14.9)	9/08/10 1:20 AM (15.4)	1/19/11 4:30 AM (16.5)
At time of Maximum Temperature Differential within the section	**Maximum** (°F)	147.7	129.8[*]	151.7	121.1
	Minimum (°F)	113.6	107.5	123.3	98.8
	Differential (°F)	34.1	22.2	28.4	22.3
	Ambient (°F)	82.5	84.4	79.5	74.5
	Date &Time (Elapsed Time (hr))	5/21/10 11:00 AM (23)	7/23/10 10:20 AM (24.4)	9/08/10 6:30 AM (20.5)	1/19/11 10:18 AM (22.3)
At time of Prestress Transfer	**Maximum** (°F)	155.3	135.3[*]	154.6	87.9
	Minimum (°F)	127.8	114.4	129.2	79.8
	Differential (°F)	27.5	20.9	25.4	8.0
	Ambient (°F)	80.8	87.6	84.1	69.4
	Date &Time (Elapsed Time (hr))	5/21/10 3:30 AM (17.5)	7/23/10 5:00 AM (19)	9/8/10 2:42 AM (16.7)	1/21/11 2:48 AM (62.8)

Notes: [*]In the skewed end of beam 5B40-2, the thermocouple placed at "LOC 2" was damaged during concrete placement and no temperature readings were obtained from it. The temperature shown corresponds to "LOC 1". The comparable temperatures measured at "LOC 1" at the time of maximum temperature for beams 5B40-1,-3 and -4 were 141.2 °F, 140.8 °F and 116.5 °F respectively.

Temperature profiles and temperature histories for all end blocks are included in Appendix D.

Maximum temperatures and temperature differentials can be compared for three different end block geometries:

     i. a square void in a square end,

     ii. a square void in a skewed end, and

     iii. a skewed void in a skewed end

The average temperature measurements for the three different end block geometries are summarized in Table 5-5. One can observe that the maximum temperatures measured in skewed ends (~155 °F) were slightly higher than the maximum temperatures observed in square ends (~150 °F). The maximum temperatures observed in end blocks formed with square voids in skewed ends and skewed voids in skewed ends were practically the same. The difference between the two skewed end void geometries was mostly in the temperature differential. When a square void was used in a skewed end, the maximum temperature differential was 34 °F. Conversely, when a skewed void was in a skewed end, the maximum temperature differential was 28 °F. Both of these differentials were greater than that observed in square ends, which averaged to be 25 °F.

Table 5-5: Average end block temperature measurements in different end blocks

	Square void in a square end	Square void in a skewed end	Skewed void in a skewed end
Maximum Temperature (°F)	150	155	155
Maximum Temperature Differential (°F)	25	34	28

It can be seen that in all cases, the maximum temperature did not approach the 170 °F limit set by TxDOT. This was partly due to the relatively mild ambient temperatures measured during the fabrication days (~88°F). It is usual to have much higher ambient temperatures in precast plants during summer days in Texas. However, the positive results seen through the use of fly ash in precast plants make higher curing

temperatures less of a concern in terms of the occurrence of Delayed Ettringite Formation. Regarding the maximum temperature differential, the use of the skewed end void geometry in skewed ends is recommended as a measure to control the temperature differential.

5.7 SUMMARY AND CONCLUSIONS

Bursting strains were measured in the end regions of three box beams reinforced according to the current TxDOT standard for 5B40 box beams. The maximum vertical bursting strain measured was proportional to a stress equal to 22 ksi. Considering that the beams in this study contained the maximum possible number of bonded strands in the end region (76 strands), and that a vertical stress in excess of the 20 ksi AASHTO-LRFD (2010) limit was measured only in one occasion, it was concluded that vertical bursting stresses from a worst-case scenario can be controlled through the current reinforcement details. Crack widths associated with vertical bursting stresses were as much as 0.016 in. but the extension of such wide cracks was very small (3 in. to 4 in.).

The total vertical bursting force measured in the end regions of the 5B40 box beams was as much as 4.4% of the net prestressing force. More specifically, the maximum vertical bursting force measured *within the first h/4* was around 3% of the net prestressing force. Significant vertical bursting forces were measured beyond the first *h/4* (10 in.) of the beam all the way to a point located 26 in. from the end of the beam (there was no instrumentation beyond that point). The forces located in the aforementioned region were also managed adequately through the current standard reinforcement detail used in 5B40 box beams. Nevertheless, a recommendation to amend the current AASHTO-LRFD design recommendations for bursting stresses, based on the results from O'Callaghan (2008) and supported by the results of the present study, was made. Different conclusions were made from the study of horizontal bursting stresses in the end regions of box beams. Horizontal bursting stresses as high as 40 ksi and frequently equal to 30 ksi were measured in the box beams built according to the current TxDOT standard reinforcement detail for 5B40 box beams (Phase-I beams). In the box beams studied

through Phase I, the total measured horizontal bursting force was consistently higher that the vertical bursting force in the same end region and was as much as 5.1% of the net prestressing force. This was attributed to the large fraction of the strands that were placed in the web regions, creating highly eccentric forces and prestress differentials within the section. Crack widths associated with horizontally transverse bursting forces were always over 0.007 in. A significant portion of the cracks as widths ranged between 0.009 in. and 0.010 in. and extended through the depth of the end face as can be seen in Figure 5-8, Figure 5-9 and Figure 5-10. Crack widths of 0.013 in. were measured in few ocassions.

A modified end region reinforcement detail was used in the first beam of Phase II (i.e. beam 5B40-4). The modified detail managed the horizontal bursting force much better, with the maximum bursting stresses being around 13 ksi. The implementation of the modified end region reinforcement detail is recommended for future box beam standards. In terms of vertical bursting stresses, the first beam of Phase II was equivalent to the beams fabricated in Phase I. In terms of horizontal bursting stresses, much lower stresses and smaller crack widths were observed in the end face of beam 5B40-4.

The second beam of Phase II (i.e. beam 5XB40) was a modified box beam cross section with a higher flexural capacity and great potential to be used in a *spread box beam* configuration. The end region of the modified box beam was detailed incorporating the knowledge gathered from the beams fabricated in Phase I and the first beam of Phase II. The bursting stresses reported in this chapter revealed that both vertical and horizontal bursting stresses can be controlled adequately through the reinforcement details used in beam 5XB40. It was concluded that the more even distribution of prestressing strands used in the 5XB40 box beam resulted in smaller horizontal bursting forces in the end of the beam.

Finally, important comparisons were made regarding maximum temperatures and maximum temperature differentials across different end block geometries. The alternative skewed void geometry in skewed ends proved to be an effective way to reduce the temperature differentials within the end block. Very little benefit was observed in its ability to reduce the maximum temperature within the end block.

172

CHAPTER 6

Results and Analysis: Shear Performance of 5B40 Box Beams

6.1 INTRODUCTION

The results from a total of 9 shear tests performed on 5B40 box beams are presented in this chapter. Five of the nine shear tests correspond to beams fabricated within Phase I of the experimental program. The remaining four tests were performed on beams fabricated within Phase II.

Phase I of this study included beams fabricated with the current standard reinforcement details used by TxDOT. Based on the knowledge acquired during Phase I, the reinforcement details of the end regions of box beams were improved for the fabrication of Phase-II beams. The last beam of Phase II incorporated a modified cross section and a different strand pattern designed to maximize flexural strength when used in a "spread box beam" configuration.

The main variables studied within this part of the experimental program were the beam end geometry (square or skewed), the internal void geometry at skewed ends and how both of these variables affected shear performance. Joining the results of the 9 shear tests presented within this chapter and the 20 shear tests presented in Chapter 4, it was possible to study how the shear strength of box beams was influenced by different beam depths and different bottom flange-to-web width ratios.

Crack patterns and crack widths are presented in an effort to assess the serviceability of 5B40 box beams. Then, the maximum shear sustained during each test is compared to the calculated shear capacity. The results of the 20 box beam tests described in Chapter 4 plus the 9 box beam shear tests presented in this chapter are evaluated within the context of the University of Texas Prestressed Concrete Shear Database.

Finally, descriptions of the damage types observed during shear tests are given. Data gathered from internal and external instrumentation were analyzed as they relate to the different types of damage.

6.2　GENERAL INFORMATION

General information for the 9 tests conducted on 5B40 box beams is summarized in Table 6-1. The five beams associated with the results presented in this chapter were all fabricated within the Ferguson Structural Engineering Laboratory. All beams were 30 feet long and had internal measurement instruments. The data gathered from the internal instruments were paramount for a better understanding of the shear behavior and load transfer mechanism of box beams.

Table 6-1: Shear testing program results summary

	Phase I						Phase II			
	5B40-1		5B40-2		5B40-3		5B40-4		5XB40	
Beam End	Q	KQ	Q	KK	Q	KK	Q	KQ	Q	Q
Bearing Pads underneath test end	1	1	1	1	1	1	1	1	1	2
Beam - f_c' (ksi)	11.8		9.4		11.2		10		10.5	
Coarse Aggregate	Crushed Limestone									
Deck - f_c' (ksi)	NDA		NDA		NDA		NDA		7.5	
f_{yt} (ksi)	65		65		65		65		66	
Spacing (in.)	6		6		6		6		6	
A_{ps} (in.^{2})	11.6		11.6		11.6		11.6		10.1	
y_{ps} (in.)	8.24		8.24		8.24		8.24		4.8	
f_{pjack} (ksi)	202.5		202.5		202.5		202.5		202.5	
f_{peff} (ksi)	163.5		163.5		163.5		163.5		167.8	
Clear Span (ft)	28.1	23.0	27.9	NT	27.9	23.0	27.9	23.0	29	22
Shear Span "a" (ft)	7.5	7.5	7.5	NT	7.5	7.5	7.5	7.5	10	10
d (in.)	31.76	31.76	31.76	NT	31.76	31.76	31.76	31.76	43.2	43.2
a/d	2.83	2.83	2.83	NT	2.83	2.83	2.83	2.83	2.78	2.78
$Vn_{(ACI)}$ (kip)	433	433	420	NT	430	430	423	423	526	526
$Vn_{(MCFT)}$ (kip)	443	443	431	NT	440	440	434	434	602	602
P_{max} (kip)	583	856	727	NT	700	973	791	880	1006	1287
V_{max} (kip)	438	585	543	NT	523	664	590	601	675	710
V_{max}/V_{ACI}	1.01	1.35	1.29	NT	1.22	1.55	1.39	1.42	1.28	1.35
V_{max}/V_{MCFT}	0.99	1.32	1.26	NT	1.19	1.51	1.36	1.38	1.12	1.18

Notes: Q = Square End, KQ = Skewed End with square internal void, KK = Skewed End with skewed internal void, NDA = No deck added, NT = Not tested (interior void former floated)

During the shear tests conducted on the 4B28 box beams described in Chapter 4, it was observed that, when the test end of the beam was supported on one central bearing pad, more damage (more and wider cracks) was visible in end region of the beam. This fact led to the decision of conducting the tests on 5B40 box beams with the test end supported on a single central bearing. By doing so, a more critical load condition was imposed on the beam.

Only the last specimen, beam 5XB40, was topped with a composite deck. The composite deck was 8 in. thick and 53.75 in. wide.

6.3   DIAGONAL CRACKS AND SERVICEABILITY

Wide diagonal cracks in an operational bridge are not appealing to public. In most cases, motorists cannot observe diagonal cracks (or any other cracks) on a bridge over which they are traveling. The same cannot be said about overpasses which are in the line of sight of travelers such as that pictured in Figure 6-1.

Figure 6-1: Diagonal cracks in box beams over central bent cap in bridge over IH35.

In the case portrayed above, diagonal cracks are clearly visible from the road below. Perception of a deteriorating infrastructure makes the general public feel uneasy and, in extreme cases, can prompt costly restorations. This section is meant to aid inspection practices in determining the relevance of diagonal cracks to shear loads.

6.3.1 Crack Width Measurements

During each test, diagonal crack widths were documented at each load step. The maximum diagonal crack width at each step was of special interest as proximity to failure can be inferred from it. From the nine shear tests and all the load steps in each test, 72 crack width measurements were gathered and plotted in Figure 6-2. By plotting the crack width versus the ratio of the applied shear to the failure shear, it is possible to obtain a general idea of what the maximum crack width for a given shear level would be.

Basic assumptions can be made to establish a relationship between the ordinates in Figure 6-2 and service load levels. From the UTPCSDB, one can assume an average ratio between the failure shear and the calculated nominal capacity. From Table 2-2, using the General Procedure from AASHTO-LRFD,

$$V_{failure} = 1.43 V_n \qquad \textbf{Equation 6-1}$$

where the factor 1.43 can be defined as an average shear strength ratio ($\overline{SSR}$). Similarly, an average strength reduction factor ($\phi = 0.9$) can be used to establish ratios between the ultimate shear and the nominal shear capacity as shown in Equation 6-2. An average load factor (L.F. = 1.5) can be used to relate the ultimate shear with service level shear as shown in Equation 6-3.

$$V_u = \phi V_n \qquad \textbf{Equation 6-2}$$

$$V_u = L.F. \cdot V_{service} \qquad \textbf{Equation 6-3}$$

Substituting V_n from Equation 6-1 into Equation 6-2, one can establish:

$$V_u = \phi \left(\frac{V_{failure}}{SSR} \right) \qquad \textbf{Equation 6-4}$$

Equating V_u from Equation 6-3 and Equation 6-4 and solving for $V_{service}$, it can be said that:

$$V_{service} = \left(\frac{\phi}{\overline{SSR} \cdot L.F.} \right) V_{failure} \qquad \textbf{Equation 6-5}$$

or

$$\frac{V_{service}}{V_{failure}} = \left(\frac{\phi}{\overline{SSR} \cdot L.F.} \right) = \frac{0.9}{1.43 \cdot 1.5} = 0.43 \qquad \textbf{Equation 6-6}$$

The ratio obtained in Equation 6-6 is a reasonable estimate of what the relationship between service level shear and failure shear is. A range centered on the ratio obtained in Equation 6-6 is illustrated in Figure 6-2. Within the illustrated service shear level range, the maximum width of diagonal crack widths ranged from 0.008 in. to 0.016 in. On average, the maximum width of a diagonal crack at service level shears can be expected to be around 0.012 in. As discussed in Chapter 2, a crack width of 0.012 in. is often taken as an upper limit of acceptability. That is, cracks wider than 0.012 in. are deemed unacceptable.
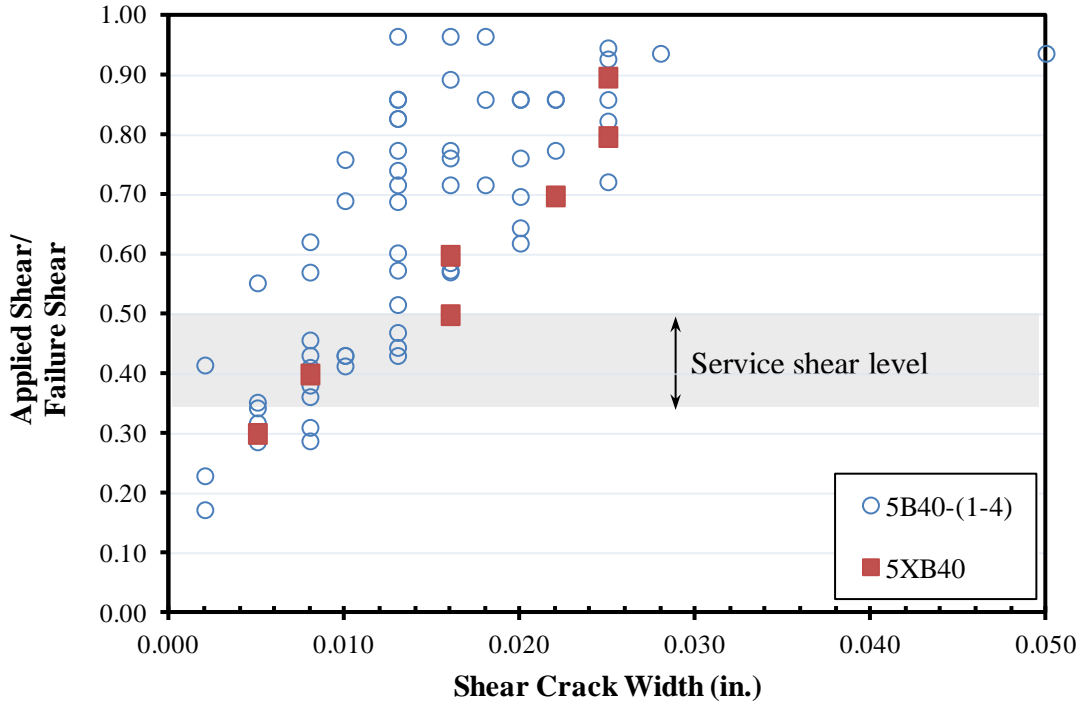
Figure 6-2: Crack Width measurements for 5B40 box beam series

As was provided for the 4B28 box beams in Chapter 4, a general guideline for the 5B40 box beam series is provided in Table 6-2. The first two shear levels in these tables (Table 4-2 and Table 6-2) are identical. The highest shear level is slightly different. At higher shear levels, crack width is slightly smaller in the 5B40 series. This is due to the smaller spacing of the stirrups in 5B40 beams (6 in.) compared to the stirrup spacing in 4B28 beams (20 in.). The fact is that closely spaced stirrups restrain crack growth more efficiently.

Table 6-2: General guide based on lower bound of measured crack widths.

Maximum width of diagonal cracks (in.)	Applied Shear
0.010	Greater than 40% of failure shear
0.020	Greater than 60% of failure shear
0.025	Greater than 70% of failure shear

6.3.2 **Diagonal Crack Maps**

In addition to crack widths, crack maps can provide a visual aid in assessing the state of distress that a beam is subject to. While it is obvious to state that more cracks correspond to a higher state of distress, it would be difficult to try to estimate the state of distress of a beam based on its unique crack pattern.

Crack maps for 8 of the 9 tests are presented in Figure 6-3 through Figure 6-10. The region tested in the 9th test was extensively cracked during the 8th test. Therefore, useful crack width and crack pattern information was hard to obtain from the 9th test. For each test, crack maps are presented for five load steps. The maximum width of diagonal cracks in the web (w_{max}) is indicated in each crack map. In the first step, the cracks existing prior to the application of any load are drawn. Cracks included in this map are resulting from bursting/spalling stresses and concrete shrinkage. Three intermediate load steps before the failure shear are mapped, including a crack map at a shear approximately equal to the calculated shear capacity using the general procedure from AASHTO-LRFD. Finally, cracks existing after failure are drawn and spalled concrete is indicated as shaded areas.

6.3.2.1 *Beams 5B40-1 through 5B40-4*

As explained earlier, beams fabricated during Phase I of this study (5B40-1 through 5B40-3) were reinforced according to the current TxDOT standards. After the Phase I beams were tested, no need to improve on their shear performance was justified. Hence, the first beam of Phase II (5B40-4) was only modified in the end region reinforcement detail to address excessively high bursting stresses as discussed in Chapter 5. Having the same shear properties, the crack maps for beams 5B40-1 through 5B40-4 are presented together in this section. A summary of the load steps for each test is presented in Table 6-3.

Based on all crack maps and crack width measurements presented earlier, it is possible to synthesize a general description of the crack map at different stages:

- *At approximately 30% of the beam's shear capacity,* diagonal cracks widths did not exceed 0.010 in. Diagonal cracks were concentrated within the main web region and did not extend into the top or bottom flange or the transitions areas. A linear foot of web was crossed by only one diagonal crack.

- *At approximately 60% of the beam's shear capacity,* diagonal cracks widths did not exceed 0.020 in. Diagonal cracks were concentrated within the main web region and some extension into the bottom flange transition existed. A linear foot of web was crossed by two diagonal cracks.

- *At approximately 80% of the beam's shear capacity,* diagonal cracks of 0.025 in. in width were present. Diagonal cracks extended through the main web region; there was extension into the bottom flanges and possibly the top flange as well. A linear foot of web was crossed by three diagonal cracks.

Table 6-3: Summary of crack map load steps for each test. Beams 5B40-1 through 5B40-4.

V/V_{max} (V/V_{MCFT})	5B40-1		5B40-2	5B40-3		5B40-4	
End (Figure)	**Square** (Fig. 6-3)	**Square** (Fig. 6-4)	**Square** (Fig. 6-5)	**Square** (Fig. 6-6)	**Skewed** (Fig. 6-7)	**Square** (Fig. 6-8)	**Skewed** (Fig. 6-9)
Zero Load	0.00 (0.00)	0.00 (0.00)	0.00 (0.00)	0.00 (0.00)	0.00 (0.00)	0.00 (0.00)	0.00 (0.00)
Intermediate Load Steps	0.36 (0.36)	0.36 (0.47)	0.42 (0.53)	0.30 (0.36)	0.37 (0.55)	0.31 (0.42)	0.18 (0.25)
	0.61 (0.60)	0.59 (0.78)	0.63 (0.79)	0.58 (0.69)	0.52 (0.78)	0.56 (0.76)	0.46 (0.64)
	0.78 (0.77)	0.76 (1.01)	0.83 (1.04)	0.86 (1.02)	0.62 (0.94)	0.81 (1.09)	0.74 (1.03)
Failure Load	1.00 (0.99)	1.00 (1.32)	1.00 (1.26)	1.00 (1.19)	1.00 (1.51)	1.00 (1.36)	1.00 (1.38)

Crack widths and spacing between cracks can be influenced by factors such as the level of applied prestressing, different concrete mixtures, curing conditions and type and spacing of web reinforcement among others. While we believe the aforementioned descriptions and crack maps can be useful in an inspection setting, they are not a substitute for sound engineering judgment.

$V = 0\,kip$	$V/V_{max} = 0$	$V/V_{MCFT} = 0$	$w_{max} = 0.000$ in.

$V = 158\,kip$	$V/V_{max} = 0.36$	$V/V_{MCFT} = 0.36$	$w_{max} = 0.010$ in.

$V = 268\,kip$	$V/V_{max} = 0.61$	$V/V_{MCFT} = 0.60$	$w_{max} = 0.013$ in.

$V = 341\,kip$	$V/V_{max} = 0.78$	$V/V_{MCFT} = 0.77$	$w_{max} = 0.022$ in.

$V = 438\,kip$	$V/V_{max} = 1.00$	$V/V_{MCFT} = 0.99$	$w_{max} = 0.025$ in.
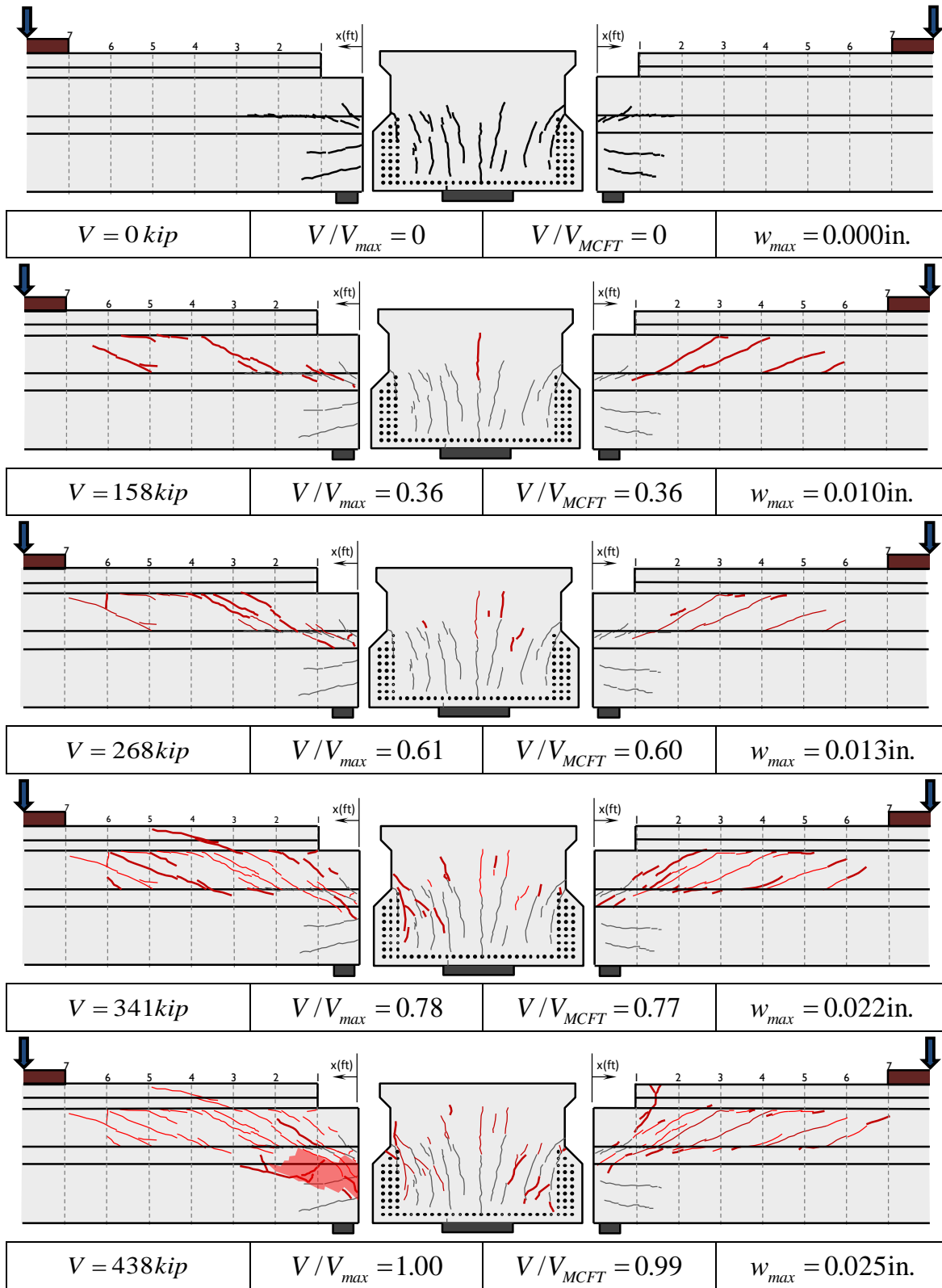
Figure 6-3: Crack Maps for 5B40-1 Square End Shear Test

$V = 0\,kip$	$V/V_{max} = 0$	$V/V_{MCFT} = 0$	$w_{max} = 0.000$in.
$V = 210\,kip$	$V/V_{max} = 0.36$	$V/V_{MCFT} = 0.47$	$w_{max} = 0.005$in.
$V = 345\,kip$	$V/V_{max} = 0.59$	$V/V_{MCFT} = 0.78$	$w_{max} = 0.016$in.
$V = 446\,kip$	$V/V_{max} = 0.76$	$V/V_{MCFT} = 1.01$	$w_{max} = 0.020$in.
$V = 585\,kip$	$V/V_{max} = 1.00$	$V/V_{MCFT} = 1.32$	$w_{max} = 0.050$in.
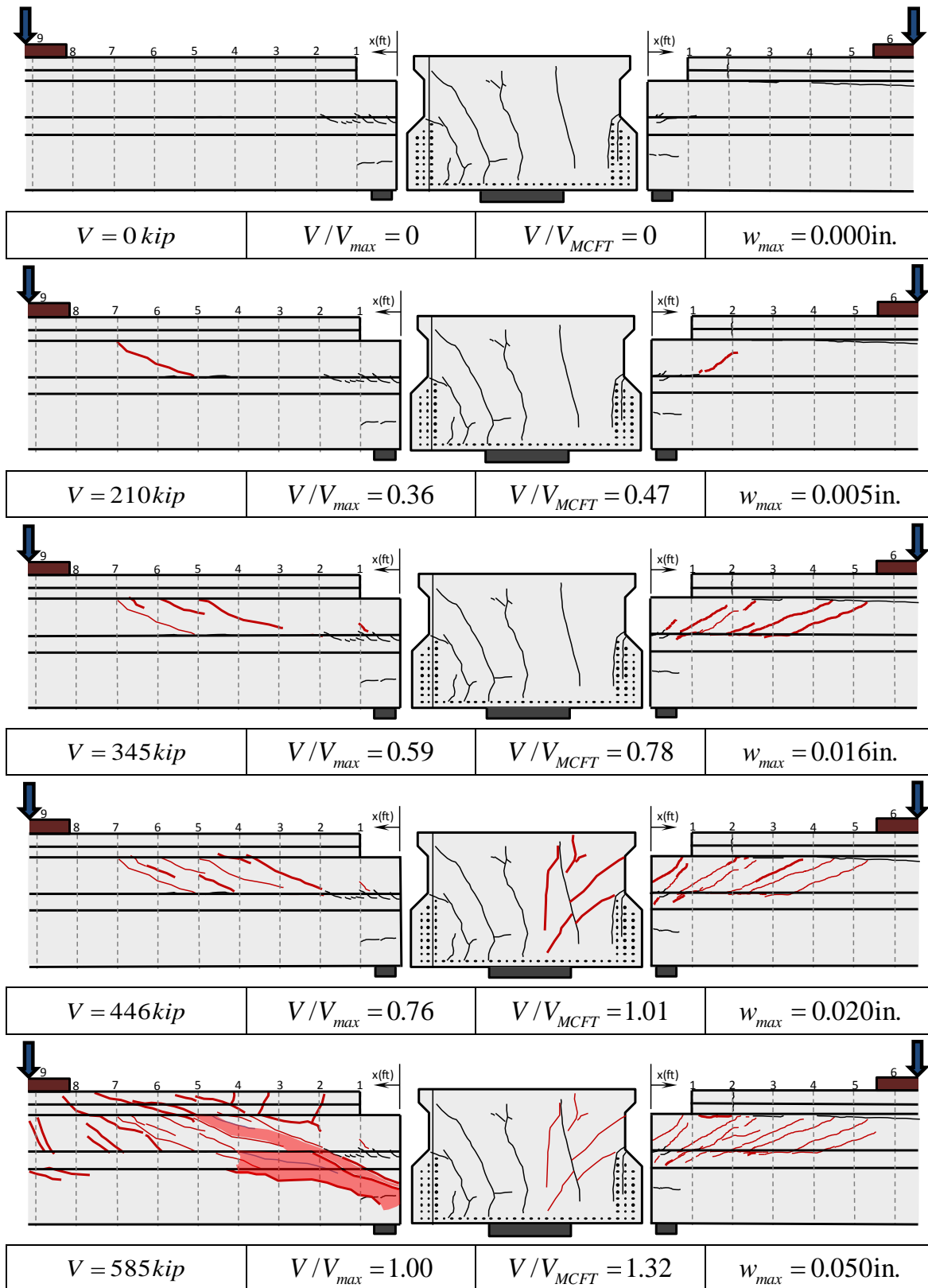
Figure 6-4: Crack Maps for 5B40-1 Skewed End Shear Test

182

$V = 0\,kip$	$V/V_{max} = 0$	$V/V_{MCFT} = 0$	$w_{max} = 0.000$in.
$V = 230\,kip$	$V/V_{max} = 0.42$	$V/V_{MCFT} = 0.53$	$w_{max} = 0.002$in.
$V = 340\,kip$	$V/V_{max} = 0.63$	$V/V_{MCFT} = 0.79$	$w_{max} = 0.008$in.
$V = 450\,kip$	$V/V_{max} = 0.83$	$V/V_{MCFT} = 1.04$	$w_{max} = 0.013$in.
$V = 543\,kip$	$V/V_{max} = 1.00$	$V/V_{MCFT} = 1.26$	$w_{max} = 0.018$in.
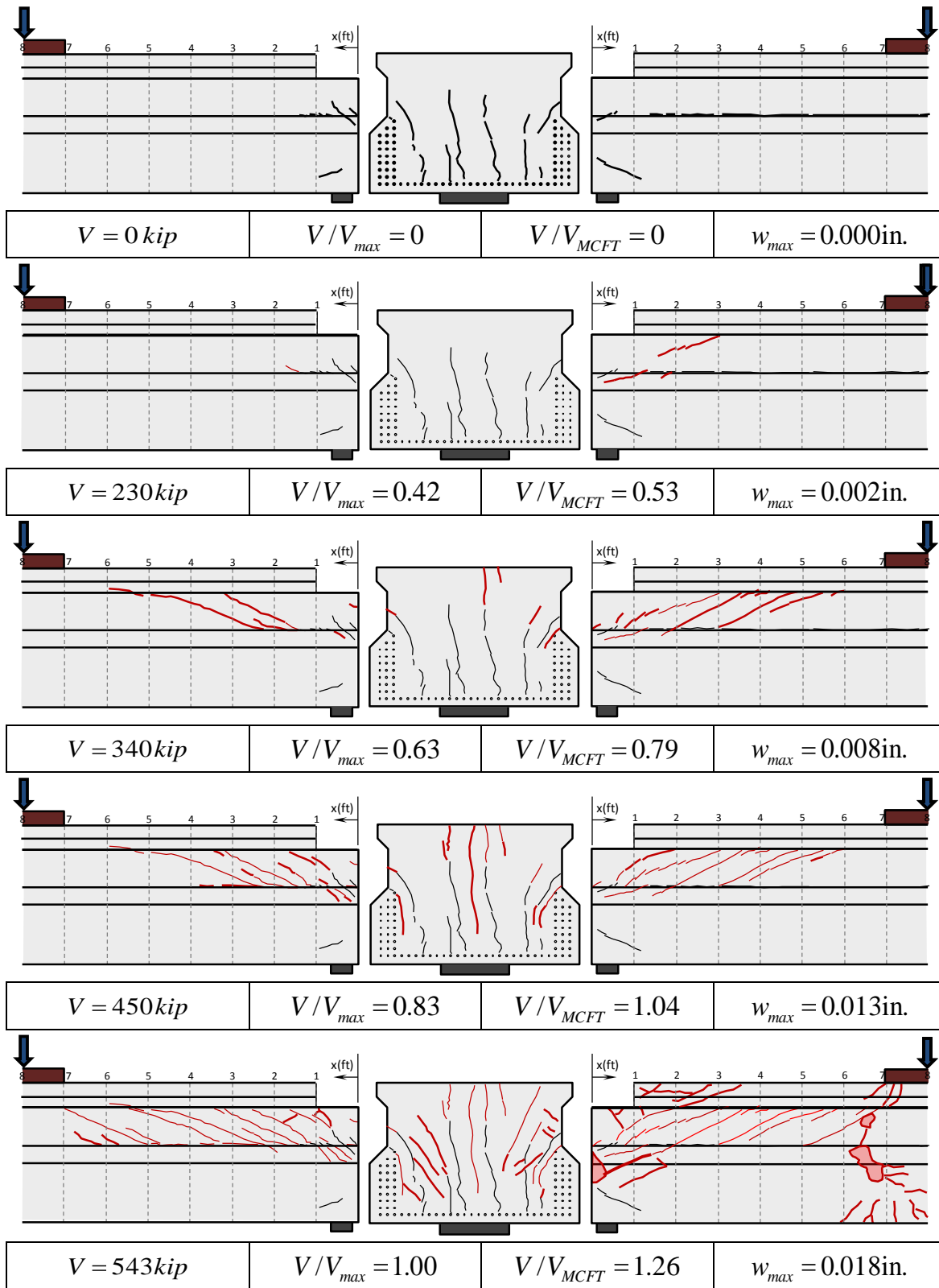
Figure 6-5: Crack Maps for 5B40-2 Square End Shear Test

183

$V = 0\,kip$	$V/V_{max} = 0$	$V/V_{MCFT} = 0$	$w_{max} = 0.000$in.

| $V = 157\,kip$ | $V/V_{max} = 0.30$ | $V/V_{MCFT} = 0.36$ | $w_{max} = 0.008$in. |

| $V = 304\,kip$ | $V/V_{max} = 0.58$ | $V/V_{MCFT} = 0.69$ | $w_{max} = 0.016$in. |

| $V = 450\,kip$ | $V/V_{max} = 0.86$ | $V/V_{MCFT} = 1.02$ | $w_{max} = 0.025$in. |

| $V = 523\,kip$ | $V/V_{max} = 1.00$ | $V/V_{MCFT} = 1.19$ | $w_{max} = 0.025$in. |
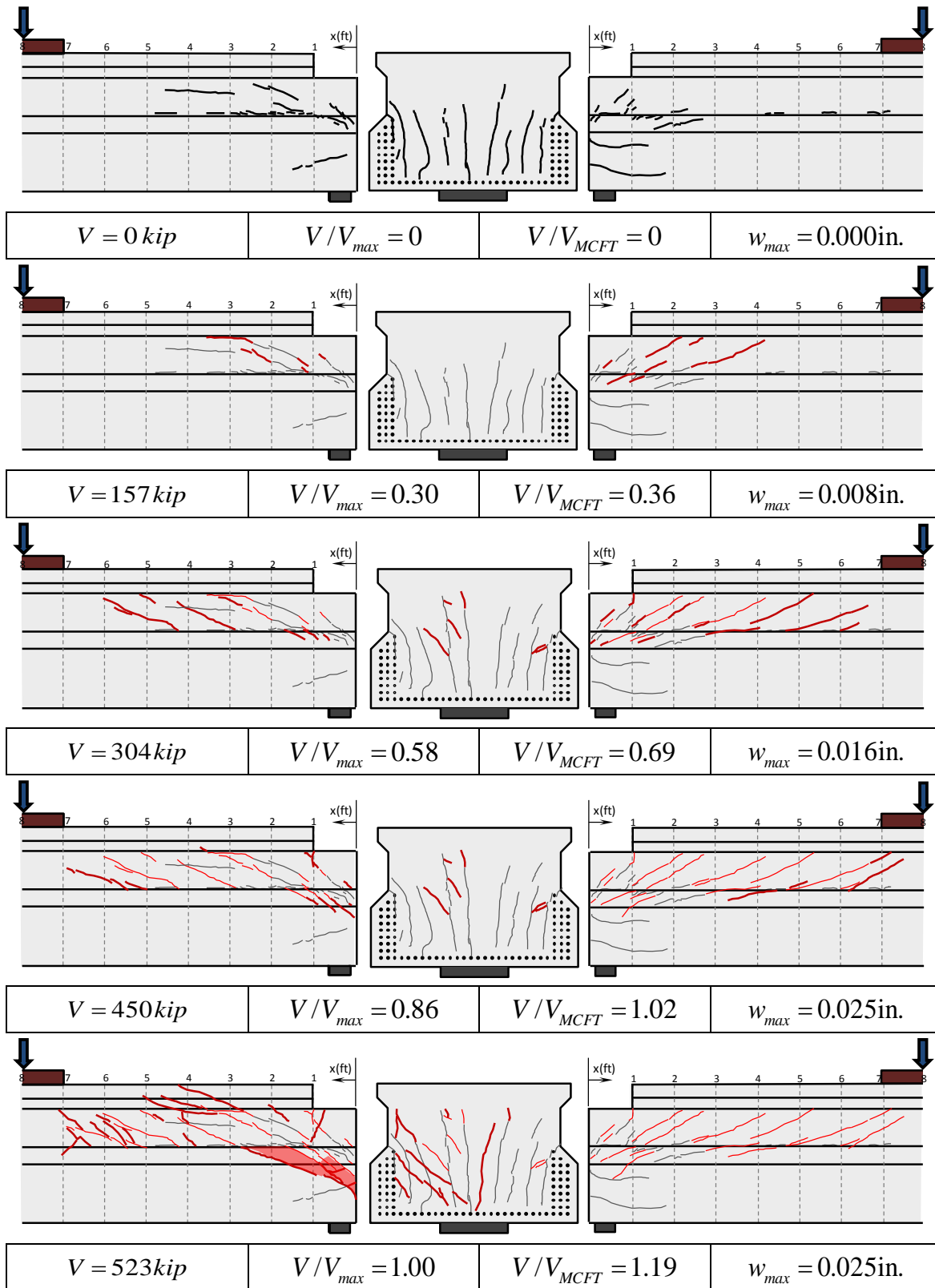
Figure 6-6: Crack Maps for 5B40-3 Square End Shear Test

$V = 0 \, kip$	$V/V_{max} = 0$	$V/V_{MCFT} = 0$	$w_{max} = 0.000 \text{in.}$
$V = 244 \, kip$	$V/V_{max} = 0.37$	$V/V_{MCFT} = 0.55$	$w_{max} = 0.008 \text{in.}$
$V = 345 \, kip$	$V/V_{max} = 0.52$	$V/V_{MCFT} = 0.78$	$w_{max} = 0.013 \text{in.}$
$V = 412 \, kip$	$V/V_{max} = 0.62$	$V/V_{MCFT} = 0.94$	$w_{max} = 0.020 \text{in.}$
$V = 664 \, kip$	$V/V_{max} = 1.00$	$V/V_{MCFT} = 1.51$	$w_{max} = 0.025 \text{in.}$
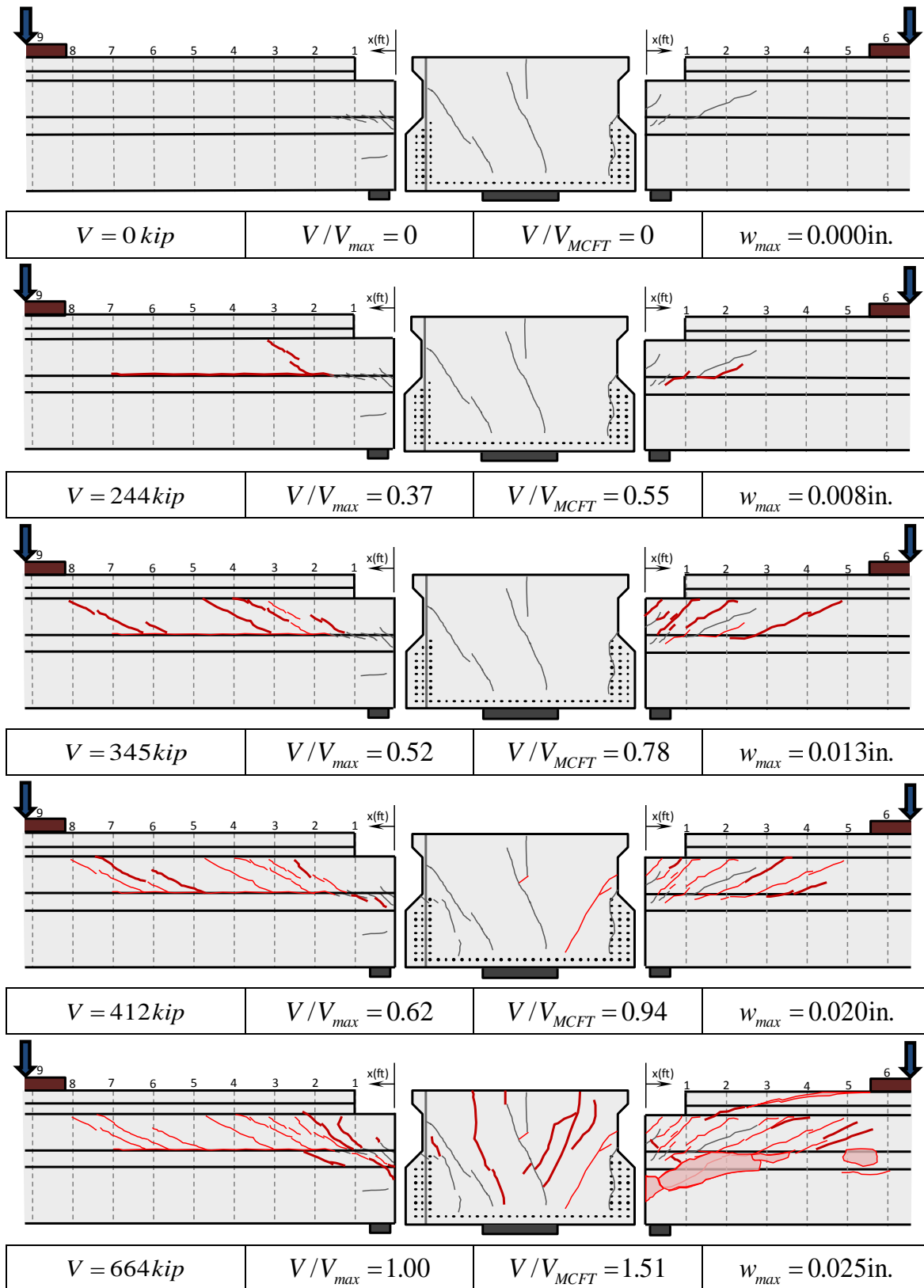
Figure 6-7: Crack Maps for 5B40-3 Skewed End Shear Test

185

| $V = 0\,kip$ | $V/V_{max} = 0$ | $V/V_{MCFT} = 0$ | $w_{max} = 0.000$in. |

| $V = 182\,kip$ | $V/V_{max} = 0.31$ | $V/V_{MCFT} = 0.42$ | $w_{max} = 0.005$in. |

| $V = 329\,kip$ | $V/V_{max} = 0.56$ | $V/V_{MCFT} = 0.76$ | $w_{max} = 0.016$in. |

| $V = 475\,kip$ | $V/V_{max} = 0.81$ | $V/V_{MCFT} = 1.09$ | $w_{max} = 0.025$in. |

| $V = 590\,kip$ | $V/V_{max} = 1.00$ | $V/V_{MCFT} = 1.36$ | $w_{max} = 0.025$in. |
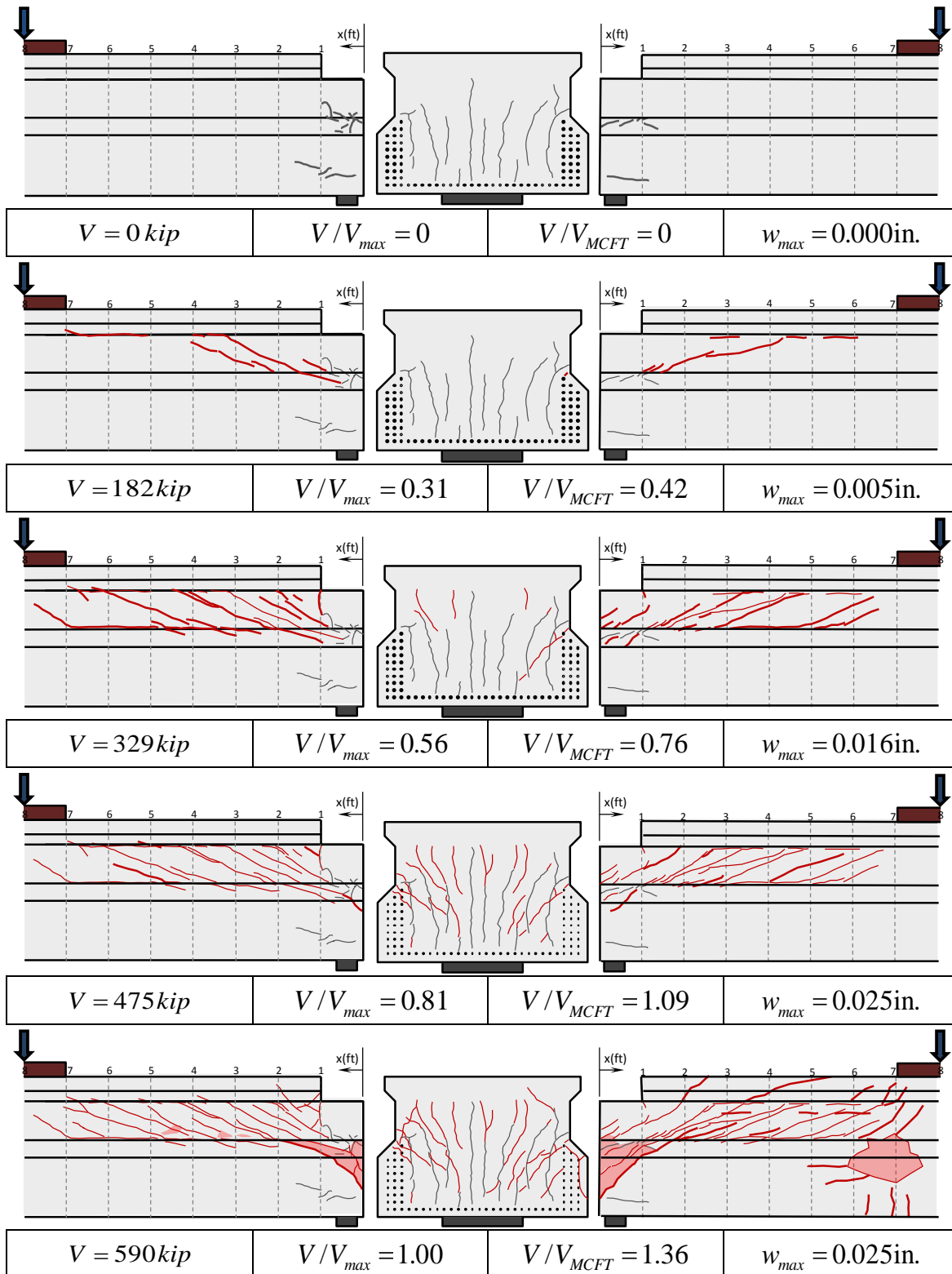
Figure 6-8: Crack Maps for 5B40-4 Square End Shear Test
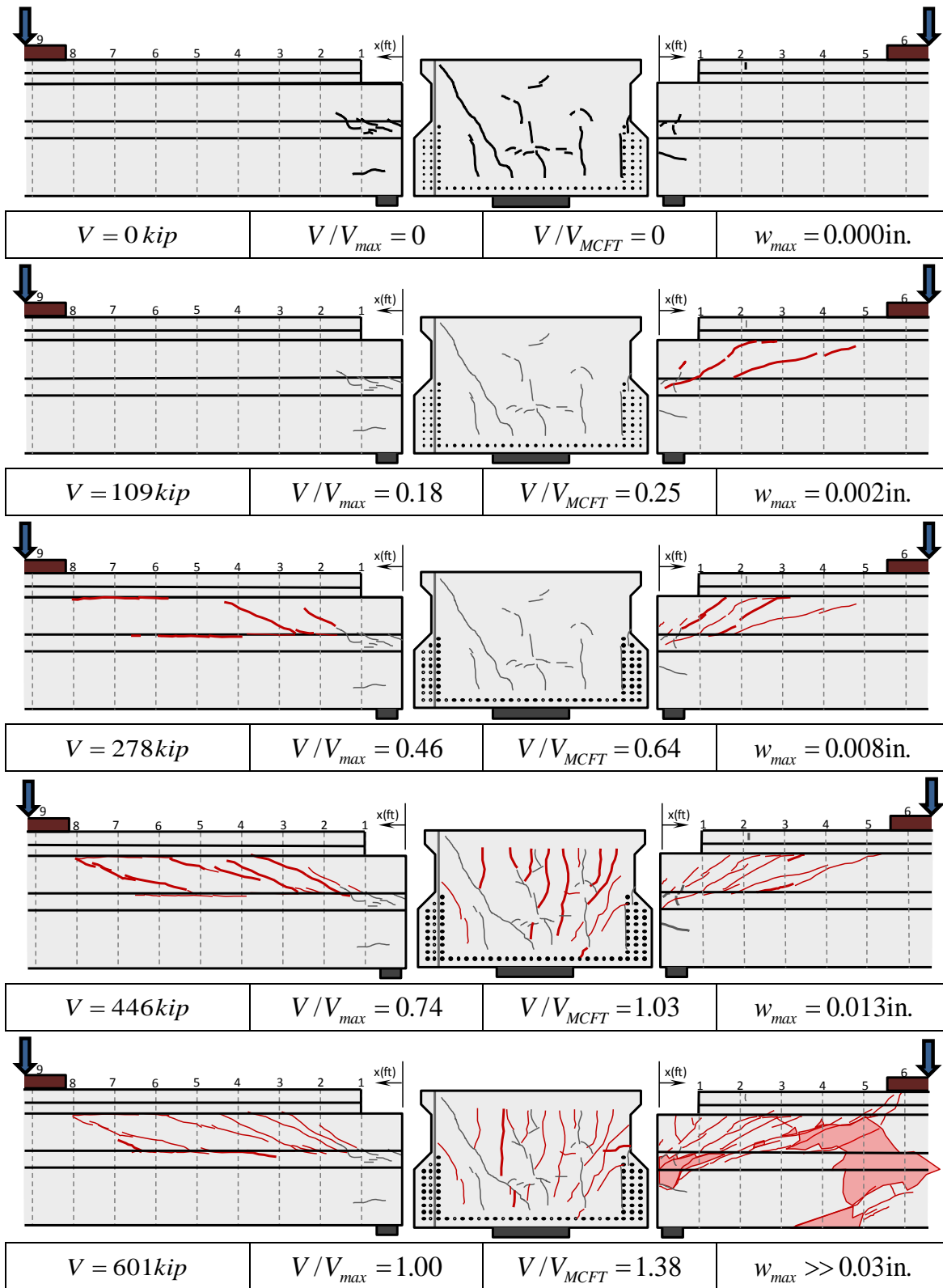
Figure 6-9: Crack Maps for 5B40-4 Skewed End Shear Test

$V = 0\,kip$	$V/V_{max} = 0$	$V/V_{MCFT} = 0$	$w_{max} = 0.000\,\text{in.}$
$V = 109\,kip$	$V/V_{max} = 0.18$	$V/V_{MCFT} = 0.25$	$w_{max} = 0.002\,\text{in.}$
$V = 278\,kip$	$V/V_{max} = 0.46$	$V/V_{MCFT} = 0.64$	$w_{max} = 0.008\,\text{in.}$
$V = 446\,kip$	$V/V_{max} = 0.74$	$V/V_{MCFT} = 1.03$	$w_{max} = 0.013\,\text{in.}$
$V = 601\,kip$	$V/V_{max} = 1.00$	$V/V_{MCFT} = 1.38$	$w_{max} \gg 0.03\,\text{in.}$

6.3.2.2 5XB40 - Square End - Single Bearing Pad

The second beam of Phase II incorporated modifications into the cross section of typical box beams. The width of each web was increased from 5 in. to 6.5 in. Also, the bottom slab was two in. thicker to allow for a full second row of strands.

The relatively lower position of the strands influenced the shear behavior. Due to the higher eccentricity, the bending component of the prestressing force increased, resulting in less pre-compression applied to the centroid of the beam section. This was evident through a relatively early occurrence of diagonal cracks in the web, at a lower fraction of the total shear capacity. Higher strand eccentricities were optimal for flexural behavior, but that was not the case for shear strength. Nevertheless, while shear performance was not optimized, it was still possible to achieve excellent results as observed in this experimental program.
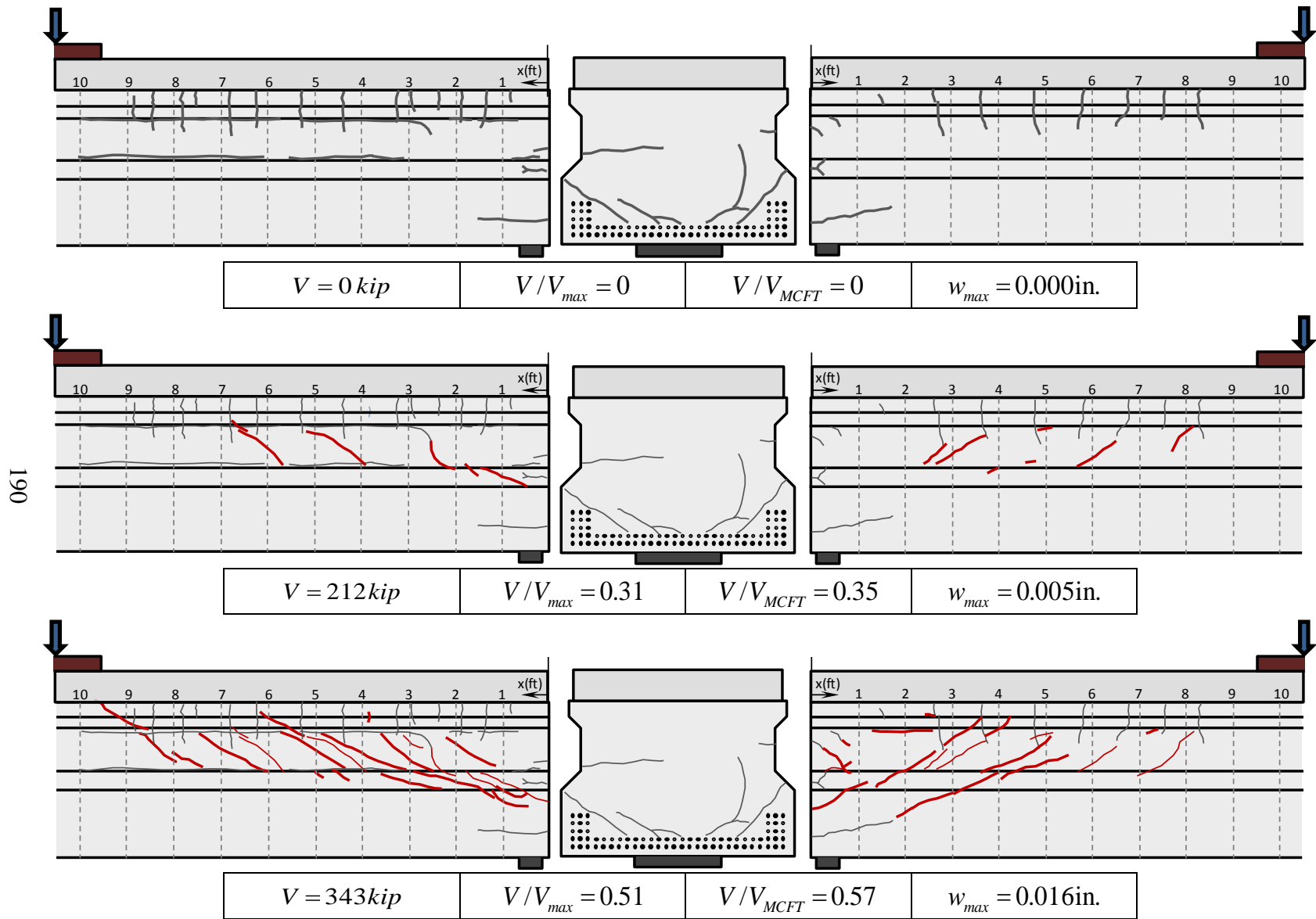
Two tests were conducted on the 5XB40 box beam. However, crack maps are only presented for the first of the two tests. The second test region included shear cracks that formed during the first test, hindering any significant interpretation of the cracks observed (or not observed) during the second test.

Based on the crack maps in Figure 6-10 and the crack width measurements presented earlier, we are able to synthesize a general description of the crack maps at different stages of loading for the 5XB40 box beam:

- *At approximately 30% of the beam's shear capacity,* diagonal crack widths did not exceed 0.005 in. Diagonal cracks were concentrated within the main web region and did not extend into the top or bottom flange or the transition areas. A linear foot of web was crossed by only one diagonal crack.

- *At approximately 60% of the beam's shear capacity,* diagonal crack widths did not exceed 0.020 in. Diagonal cracks were concentrated within the main web region and some extension into the top and bottom flanges existed. A linear foot of web was crossed by three diagonal cracks.

- *At approximately 80% of the beam's shear capacity,* diagonal cracks of 0.025 in. in width were present. Diagonal cracks extended through the main web region,

188

well into the bottom flange and possibly the top flange. A linear foot of web was crossed by three or more diagonal cracks.

The main difference between the cracks observed in the 5XB40 box beam and previous 5B40 beams lied in the extension of cracks, more so than the crack widths.

| $V = 0\,kip$ | $V / V_{max} = 0$ | $V / V_{MCFT} = 0$ | $w_{max} = 0.000\,\text{in.}$ |

| $V = 212\,kip$ | $V / V_{max} = 0.31$ | $V / V_{MCFT} = 0.35$ | $w_{max} = 0.005\,\text{in.}$ |

| $V = 343\,kip$ | $V / V_{max} = 0.51$ | $V / V_{MCFT} = 0.57$ | $w_{max} = 0.016\,\text{in.}$ |

Figure 6-10: Crack Maps for 5XB40 Square End supported on a single bearing pad

| $V = 474\,kip$ | $V/V_{max} = 0.70$ | $V/V_{MCFT} = 0.79$ | $w_{max} = 0.022\,\text{in.}$ |

| $V = 605\,kip$ | $V/V_{max} = 0.90$ | $V/V_{MCFT} = 1.01$ | $w_{max} = 0.025\,\text{in.}$ |

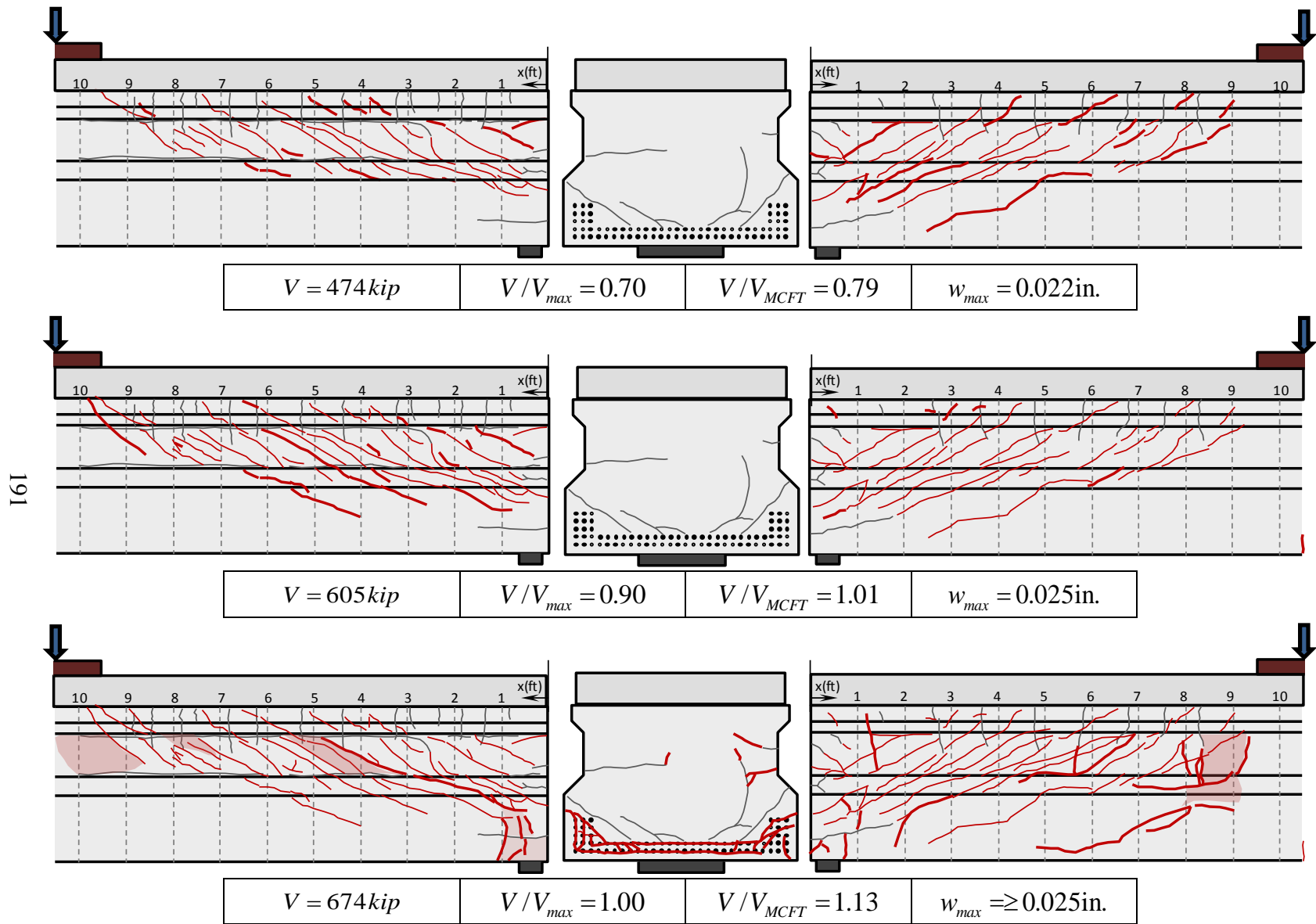| $V = 674\,kip$ | $V/V_{max} = 1.00$ | $V/V_{MCFT} = 1.13$ | $w_{max} = \geq 0.025\,\text{in.}$ |

Figure 6-10 (continued): Crack Maps for 5XB40 Square End supported on a single bearing pad

6.4 **MEASURED VERSUS CALCULATED SHEAR STRENGTH**

There are several sets of shear strength equations available to the bridge designer. Nakamura (2011) conducted an evaluation of shear strength equations from around the world, including those typically used in the United States. Among other provisions, Nakamura evaluated the accuracy and conservativeness of shear strength provisions included in ACI 318-08 and several AASHTO Bridge Design Specifications editions. Nakamura found that the best equations were those of the *General Procedure* from AASHTO-LRFD (2010). These MCFT-based equations did best in maintaining a consistent degree of accuracy and conservativeness through a wide spectrum of all possible variables. The general procedure is based on the Modified Compression Field Theory (MCFT). Hence, the nominal shear capacity calculated with this procedure is abbreviated through this document as $"V_{MCFT}"$.

As a measure of performance of a given beam, the ratio of the maximum applied shear (V_{max}) to the calculated capacity (V_{MCFT}) is obtained. This ratio is often called a "shear strength ratio". It is desired that a beam can support shear forces in excess of its calculated shear capacity. As such, if failure is caused by high shear demands on the web, the shear strength ratio should be greater than one.

For the beams discussed in this chapter, the observed shear strength ratios were mostly greater than one, with the lowest case having a shear strength ratio equal to 0.99. All skewed ends resulted in higher shear strength ratios than the square ends of the same beam. The shear strength ratios for all tests are summarized in Figure 6-11.
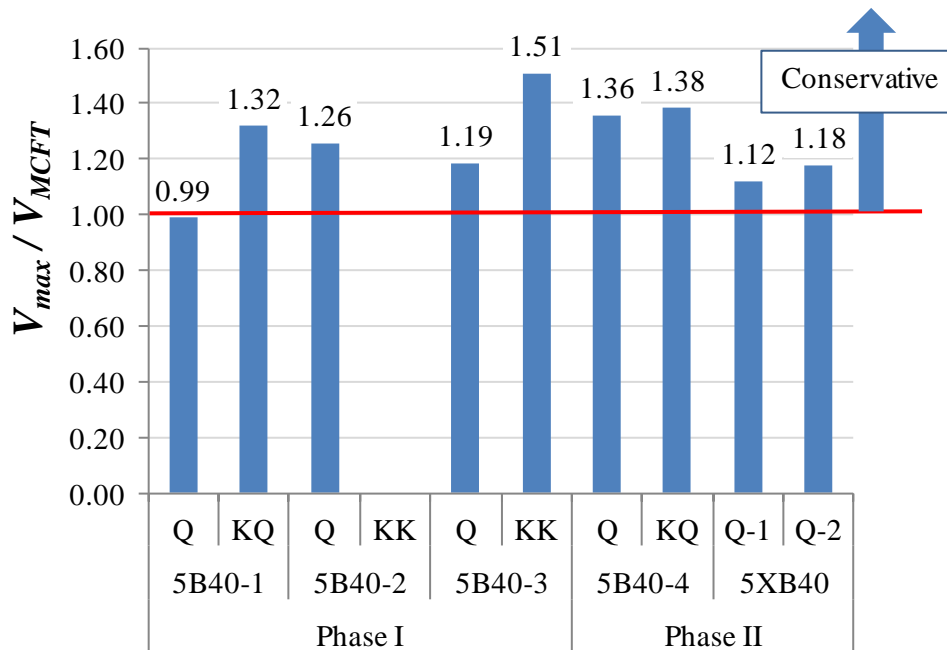
Figure 6-11: Shear Strength Ratios for 5B40 box beam series

6.4.1 Results within the context of the UTPCSDB

As was done for the tests on the 4B28 series of box beams, results from the tests on 5B40 box beams were incorporated into the UTPCSDB. Accounting for all the tests reported in Chapter 4 and the present chapter, a total of 29 box beam tests were added to the UTPCSDB.

At the time Nakamura published the results of his analysis on the database; partial results from this experimental project had been incorporated to the database. For shear strength evaluation purposes, Nakamura defined a set of specimen as an "Evaluation Database – Level II" (EDB-II). This selection of specimens contained results from 171 tests, including results from 9 tests on box beams that are a part of this experimental program, complying with the following criteria:

- Concrete strength was greater than 4 ksi
- Lightweight concrete was not used
- Overall member depth exceeded 12 in.

193

- Shear reinforcement in excess of code minimum requirements was provided (both ACI 318-08 and AASHTO-LRFD-2010)
- The test specimens were simply supported and the *a/d* ratio was greater than 2
- Specimens were pretensioned, and
- A traditional shear failure mode was observed

The objective was to compare the conservativeness and variability observed in other prestressed concrete sections to that observed with the box beam in this experimental program. Therefore, the 9 test results from this experimental program incorporated into the database by Nakamura must be subtracted from the EDB-II, leaving a sample of 162 test results. The shear strength ratio for the sample of 162 test results and the 29 box beam test results obtained from this experimental program was obtained by using three distinct sets of equations:

1. The detailed method from ACI 318-08
2. The general procedure from AASHTO-LRFD (2010)
3. The segmental bridge specifications from AASHTO-LRFD (2010), modified per the recommendations of Avendaño and Bayrak (2008).

As can be seen in Table 6-4, the Evaluation Database-Level II sample and the box beam test results observed in this experimental program have similar degrees of conservativeness and variability.

Table 6-4: Shear strength ratio statistics for the Evaluation Database Level-II and all box beam tests.

| SSR Statistics	ACI 318-08 Detailed Method		AASHTO-LRFD General Procedure (2010)		AASHTO-LRFD Segmental Procedure (2010)	
	EDB-II (N=162)	Box Beams (N=29)	EDB-II (N=162)	Box Beams (N=29)	EDB-II (N=162)	Box Beams (N=29)
Average	1.38	1.40	1.41	1.50	1.71	2.03
COV	21%	11%	18%	15%	21%	12%
Minimum	0.82	1.01	0.94	0.99	0.86	1.59
Maximum	2.32	1.70	2.07	1.86	2.73	2.44

The results from this experimental program must also be examined for bias against a range of variables. Trends (or lack thereof) must be compared to those observed in the much greater EDB-II sample.

The EDB-II sample from the UTPCSDB (162 test results) and the box beam data are plotted in Figure 6-12 through Figure 6-15 with the shear capacity calculated using the general procedure from AASHTO-LRFD (2010). Once more, conservativeness and variability of current code equations when used to calculate the shear strength of box beams fell well within the expectations of the UTPCSDB for beams of comparable characteristics (concrete compressive strength, shear reinforcement index, overall member depth and flange-to-web width ratio).

Furthermore, some similar trends are observed between the EDB-II sample and the box beam results. Focusing on the shear capacity calculated using the general procedure from AASHTO-LRFD (2010) and analyzing Figure 6-12 through Figure 6-15, it is possible to observe that the results from the box beam experimental program fall within the scatter of tests gathered in the EDB-Level II.

As can be seen in Figure 6-12; considering the range of concrete strengths measured in the present study, the results fall within the same range of ratios of V_{max} to V_{calc} (SSR) as the EDB-II sample.

As can be seen in Figure 6-13, the test results from the group of box beams with the lowest shear reinforcement index (4B28 − SCC and 4B28 − CC) exhibited a considerably higher scatter than the rest of the box beam sample. The same trend is observed through the EDB-Level II.
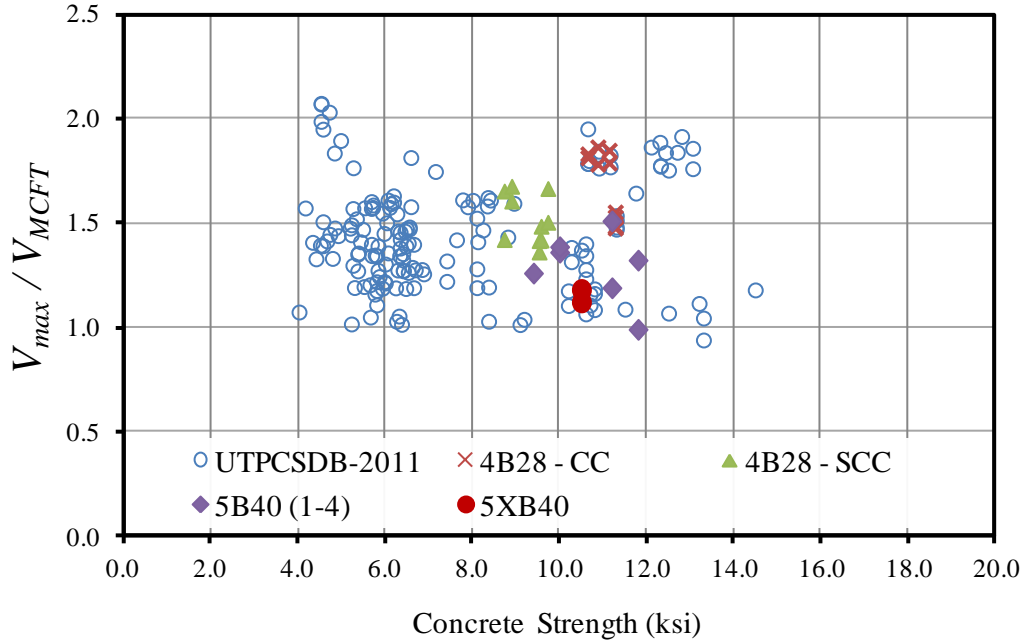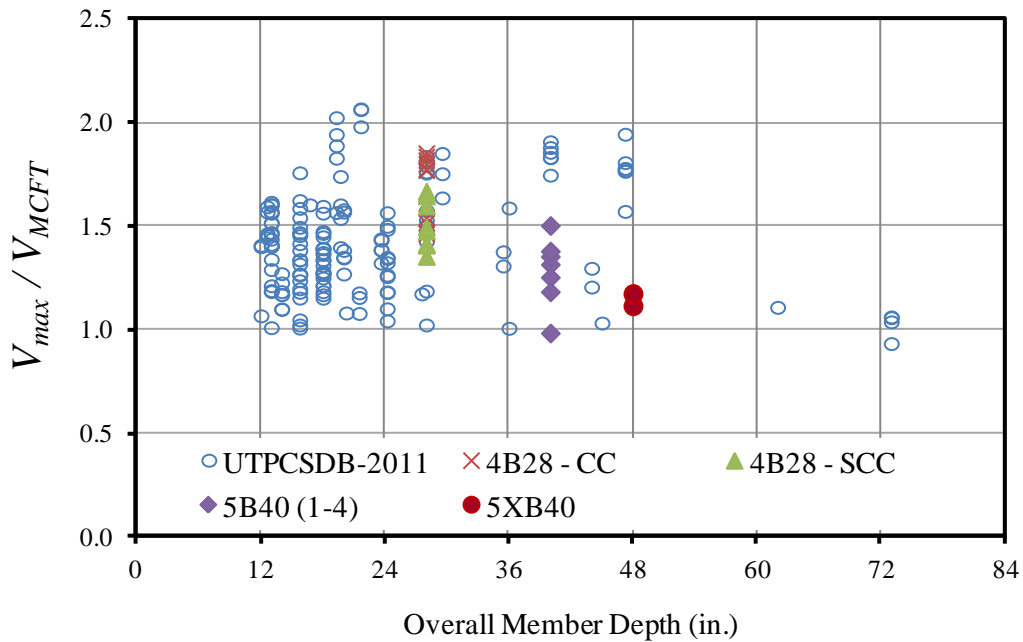
Figure 6-12: Box beam shear strength ratios (capacity calculated using the general procedure from AASHTO-LRFD (2010)), compared to other UTPCSDB-2011 data points with varying concrete strengths.
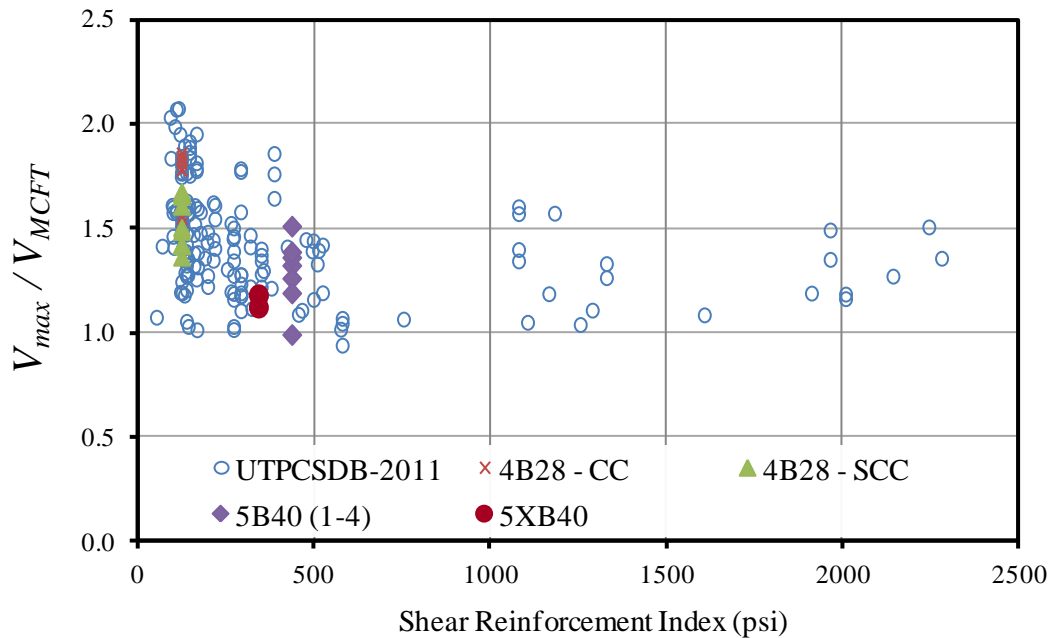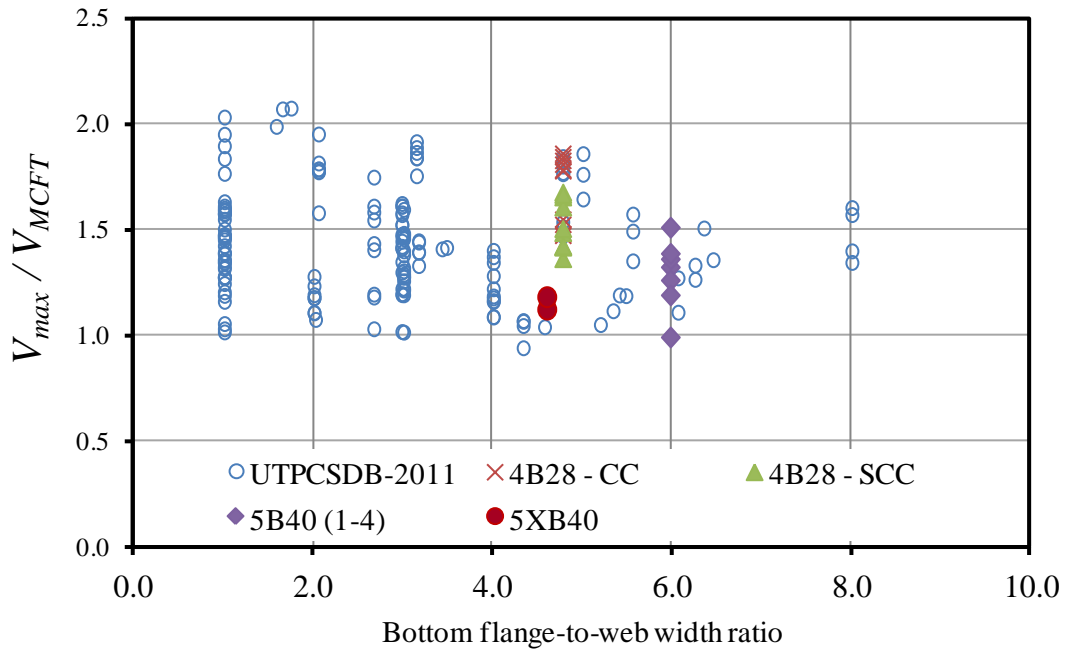

Figure 6-13: Box beam shear strength ratios (capacity calculated using the general procedure from AASHTO-LRFD (2010)), compared to other UTPCSDB-2011 data points with varying shear reinforcement index.

As can be seen in Figure 6-14, on average, box beam shear strength ratios exhibit a decreasing trend with increasing overall member depth. The same trend is observed through the EDB-Level II. Beam specimens with overall member depths equal or greater than 48 in. exhibit shear strength ratios between 1.0 and 1.1.

Figure 6-14: Box beam shear strength ratios (capacity calculated using the general procedure from AASHTO-LRFD (2010)), compared to other UTPCSDB-2011 data points with varying overall depths.

Previous literature discussed in Chapter 2 suggests that as the bottom flange-to-web width ratio gets larger, the load transfer mechanism of box beams can be affected. The flexibility of the bottom slab was said to come into consideration once the bottom flange-to-web width ratio increases. Beams of three different flange-to-web width ratios were tested. While a slight decrease in the conservativeness of the shear capacity calculations was observed in Figure 6-15, there were no visual signs of deterioration or excess flexibility of the bottom slab during all shear tests. One can safely say that the flange-to-web width ratio of the box beams tested in this program should not be an issue of concern.

Figure 6-15: Box beam shear strength ratios (capacity calculated using the general procedure from AASHTO-LRFD (2010)), compared to other UTPCSDB-2011 data points with varying bottom flange-to-web width ratios.

6.5 FAILURE MODES

All shear failures were brittle. After the peak load was reached, extensive damage caused substantial load drops of at least 30% of the peak load. It was difficult to classify any of the shear failures within a typical failure mode description. In general, shear failures were characterized by a combination of several modes of failure, described in detail in the following sections.

6.5.1 Observed Damage

The different types of damage observed through this experimental program are summarized in Table 6-5. As can be seen in this table, few of the damage descriptions are constant through the program.

Table 6-5: Observed damage summary

	5B40-1		5B40-2		5B40-3		5B40-4		5XB40	
	Q	KQ	Q	KK	Q	KK	Q	KQ	Q-1	Q-2
V_{max} / V_{MCFT}	0.99	1.32	1.26		1.19	1.51	1.36	1.38	1.12	1.18[†]
Spalling of cover at re-entrant corner of Bars U at beam end (Section 6.5.1.1)	✓	✓	✓		✓	✓	✓	✓		
Web crushing (Section 6.5.1.2)		✓					✓	✓	✓	
Strain greater than yield strain was measured in the shear reinforcement (Section 6.5.1.3)		✓	✓		✓	✓	Not measured			
Signs of Horizontal Shear Distress(Section 6.5.1.4)		✓	✓		✓		✓			
Sheared through end block along inner face of web (Section 6.5.1.5)			✓		✓			✓		
Sheared through top flange (Section 6.5.1.6)		✓				✓	✓	✓		
Sheared through bottom flange (Section 6.5.1.6)								✓		
Splitting Crack through second row[1] of strands (6.5.1.7)									✓	
Test Region did not fail										✓
Not tested				✓						

[1] Second row of strands counting from the bottom of the beam

[†] Test region did not fail. Ratio reported for the maximum shear.

6.5.1.1 *Spalling of cover on side of beam end*

Spalling of the concrete cover on the side of the beam at the beam end, as pictured in Figure 6-16, was observed in all beams fabricated with the current detail of reinforcement.

Figure 6-16: Spalling of cover at end of beam. Square end of 5B40-1 is shown.

This damage was concentrated on top of the re-entrant corner of Bars U in the end block. As load is applied, tension is introduced to Bars U. The geometry of Bars U makes them prone to have a tendency to straighten as they carry higher tensile forces. This tendency governed the shear capacity of 4B28 box beams as discussed in Chapter 4. In the case of standard reinforced 5B40 box beams, the extent of this damage was confined to the end region.
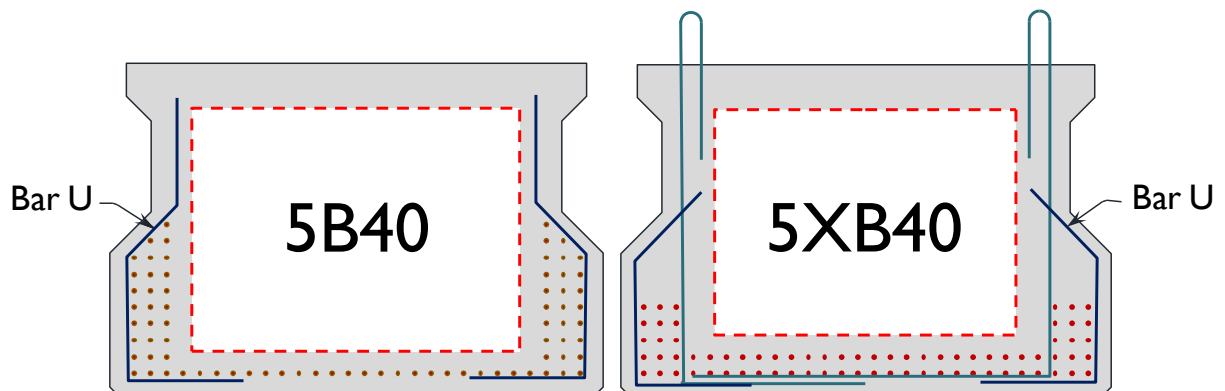
Figure 6-17: Detail of Bar U

Nevertheless, it was found that in addition to being a local problem of the end region, straightening of Bars U could control the capacity of box beams. The following phenomena likely exacerbated straightening of Bars U:

i. Bars U in the end region are subject to high bursting stresses, leaving less available capacity to sustain additional shear demands

ii. The behavior caused by a single centered bearing pad not being under the web as in typical I-girders.

The first item listed was most evident in the first test (5B40-1-Q). In this beam end, the highest vertical bursting stresses were recorded as detailed in Chapter 5 and the test region sustained the lowest maximum shear as seen in Table 6-1. Note that in this case, the maximum shear sustained was still equal to 99% of the calculated capacity.

The second item can be validated by observing the strain readings gathered from the shear tests on the two ends of beam 5XB40. For beam 5XB40, one end was tested while supported on a single centered bearing pad. The opposite end was tested while supported on two smaller bearing pads located practically centered under each web. In both cases, the first four stirrups from the end of the beam had strain gages installed about 7.5 in. from the bottom of the beam (half an inch above the top of the bottom flange).

When the end of the beam was supported on a single central bearing pad, the stirrups (Bar R) near the end of the beam acted as hangers. One can observe in Figure 6-18 how tensile strains increased as the applied shear increased beyond about 50% of the maximum applied shear. Going back to Figure 6-10, one can observe that the first cracks in the region surrounding the gages were documented at an applied shear equal to 51% of the maximum shear.
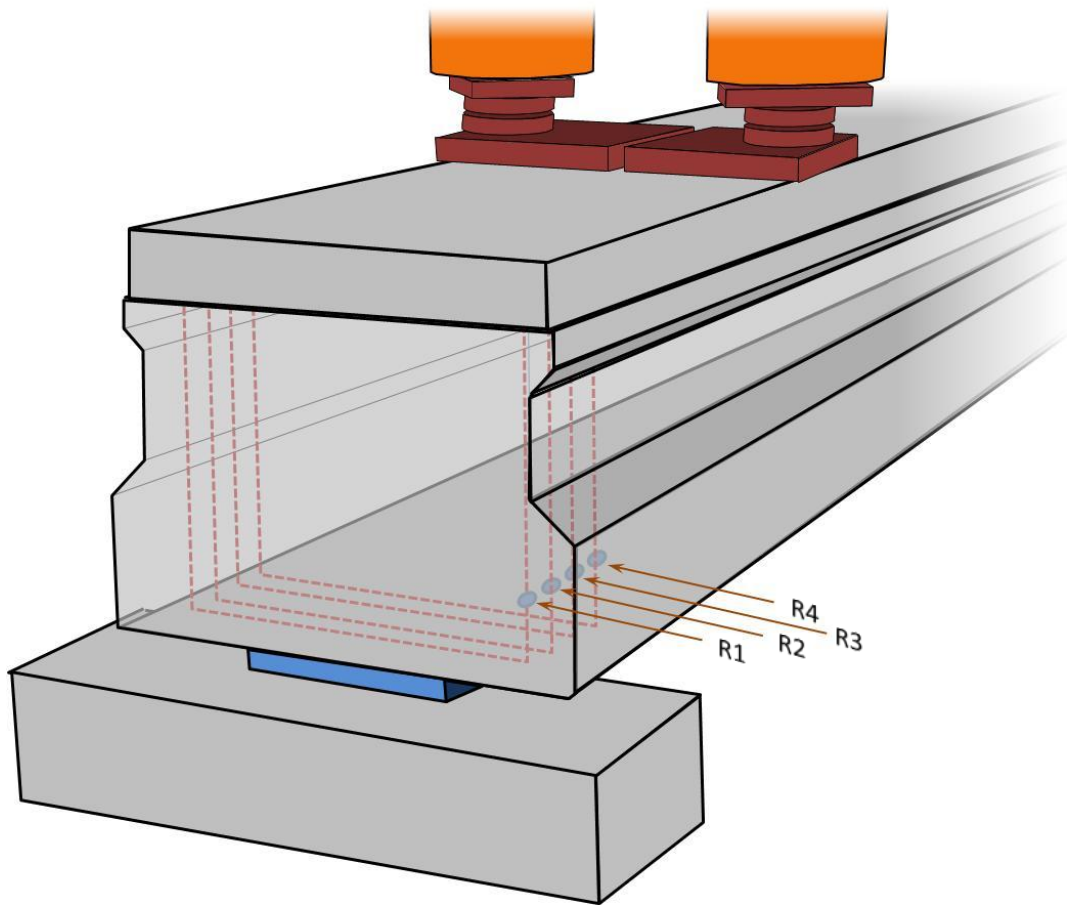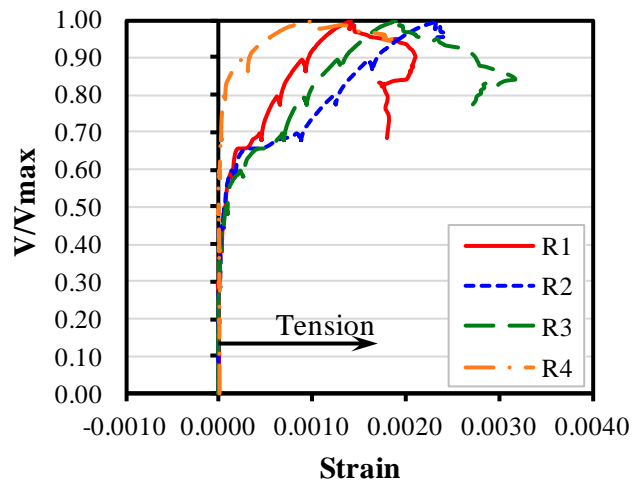
Figure 6-18: Strain readings in first four Bars R when beam is supported in a single bearing pad (Test 5XB40-Q-1)

When the end of the beam was supported on two smaller bearing pads located under the webs, the stirrups were mostly in compression, registering compressive strains proportional to 14.5 ksi. This behavior can be observed in Figure 6-19. It is worth noting that under this support condition, the beam endured a maximum shear 5% greater than that endured while supported on a single bearing pad while, at the same time, exhibiting far less damage to the end region. Some evidence of this behavior was seen in the shear testing program of the 4B28 box beams described in Chapter 4. This led to the decision of conducting most tests described in the present chapter supporting the tested end under a more demanding single bearing pad condition.
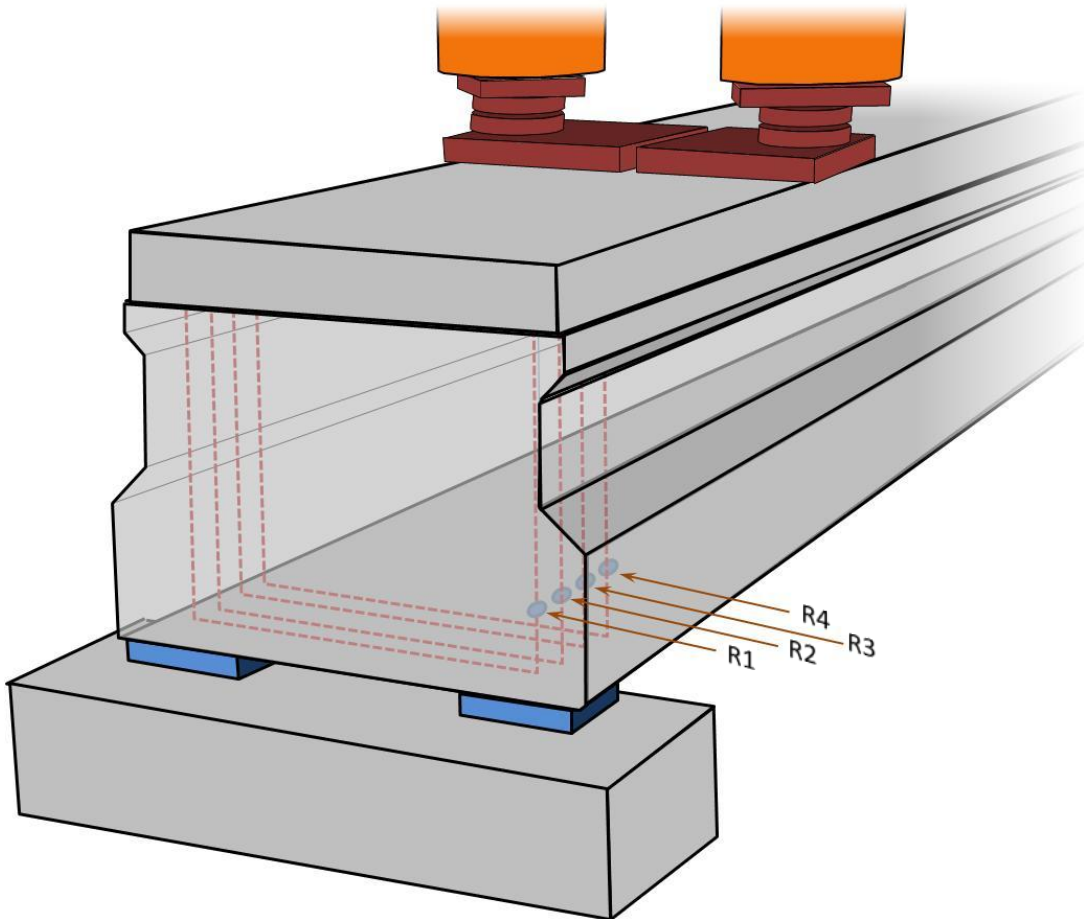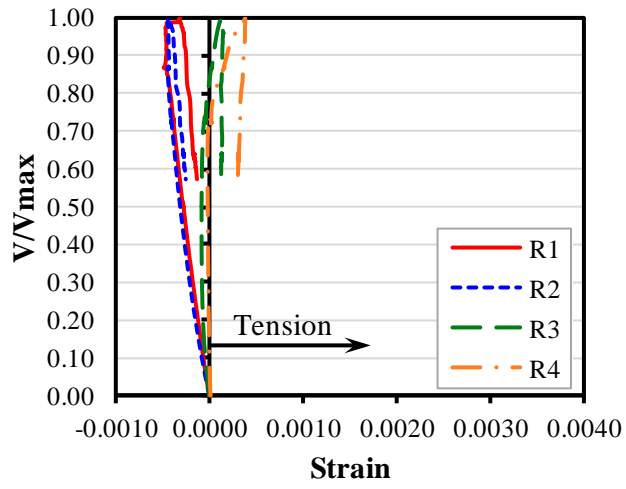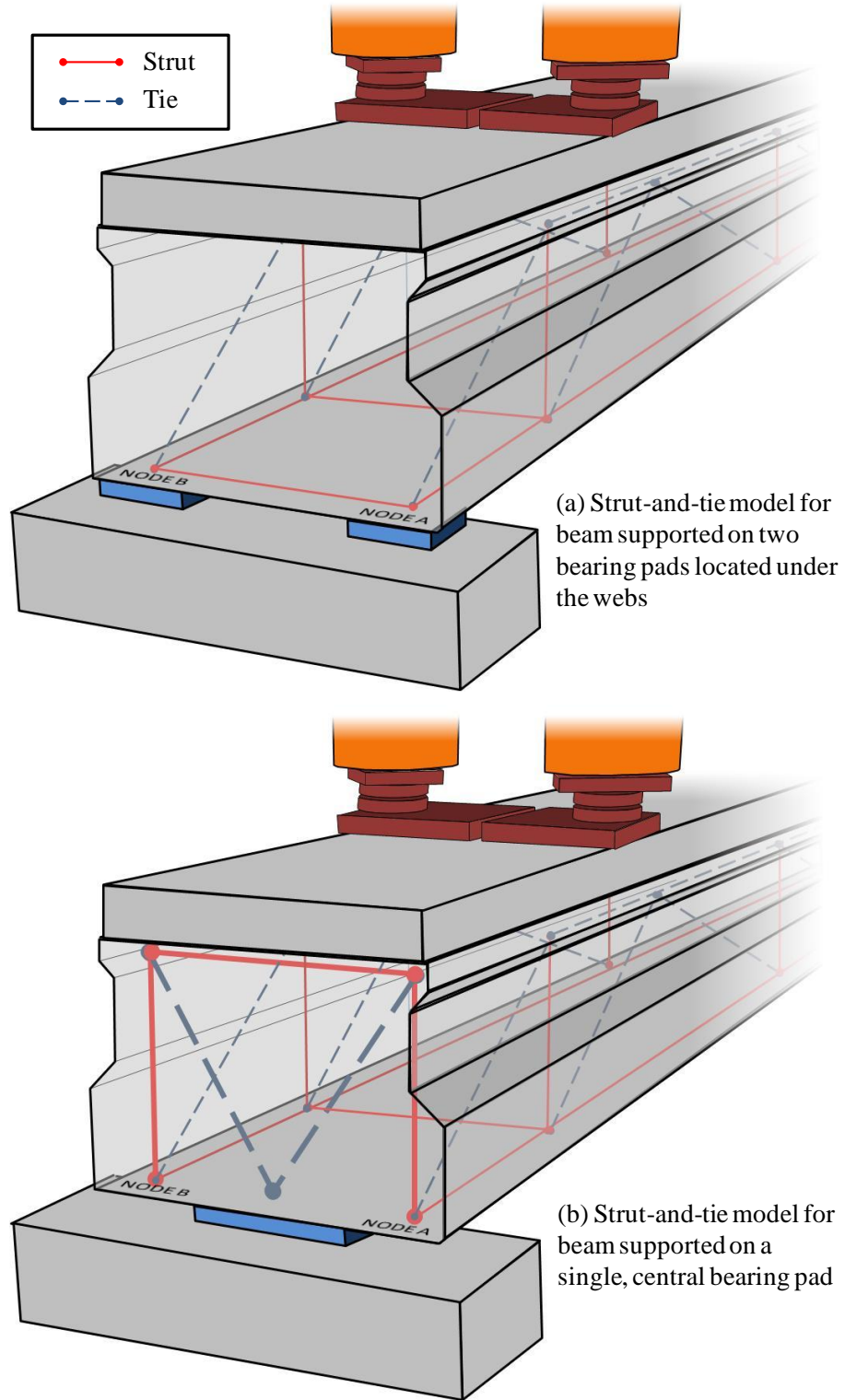
Figure 6-19: Strain readings in first four Bars R when beam is supported in two spaced bearing pads (Test 5XB40-Q-2)

Having said all of the above, it was expected that the behavior of the 5XB40 box beam would not be influenced by the Bars U in the end region. The different bar geometry used in the 5XB40 beam, illustrated in Figure 6-17, is not prone to straightening as the previous geometry was. One can see in Table 6-5 that spalling of the cover on the side of the beam near the end region was not an issue when the new Bar U geometry was used in the 5XB40 beam.

The flow of forces is in the end regions of box beams is a three-dimensional problem. The difference between the equilibrium conditions corresponding to the beam's end supported on two versus one bearing pad can be viewed through a three-dimensional strut-and-tie model (Figure 6-20). When the beam's end is supported on two bearing pads, the strut-and-tie model is equivalent to two typical beam models in each web, almost independent of each other as illustrated in Figure 6-20 – Part (a). Conversely, when the beam is supported on a single bearing pad, as illustrated in Figure 6-20 –Part (b), the load comes down through the web onto nodes A and B. Then, the load is picked up by the hangers formed by the end region reinforcement. Finally, inclined struts formed within the end block, allowing the load transfer to the central bearing pad.

While the strut-and-tie model illustrated in Figure 6-20 – Part (b) is quite simple, the vertical reinforcement in the end block was not sufficient to *hang* all the load in Nodes A and B. Other load paths were present and can be represented through other strut-and-tie models such as the one illustrated in Figure 6-21– Part (a). The combination of multiple superimposed strut-and-tie models, illustrated in Figure 6-21– Part (b), is the best representation of what the actual flow of forces was like.

(a) Strut-and-tie model for beam supported on two bearing pads located under the webs

(b) Strut-and-tie model for beam supported on a single, central bearing pad

Figure 6-20: Strut-and-tie models for different support conditions

206

(a) Secondary strut-and-tie model for beam supported on a single, central bearing pad

(b) Superimposed strut-and-tie models for beam supported on a single, central bearing pad
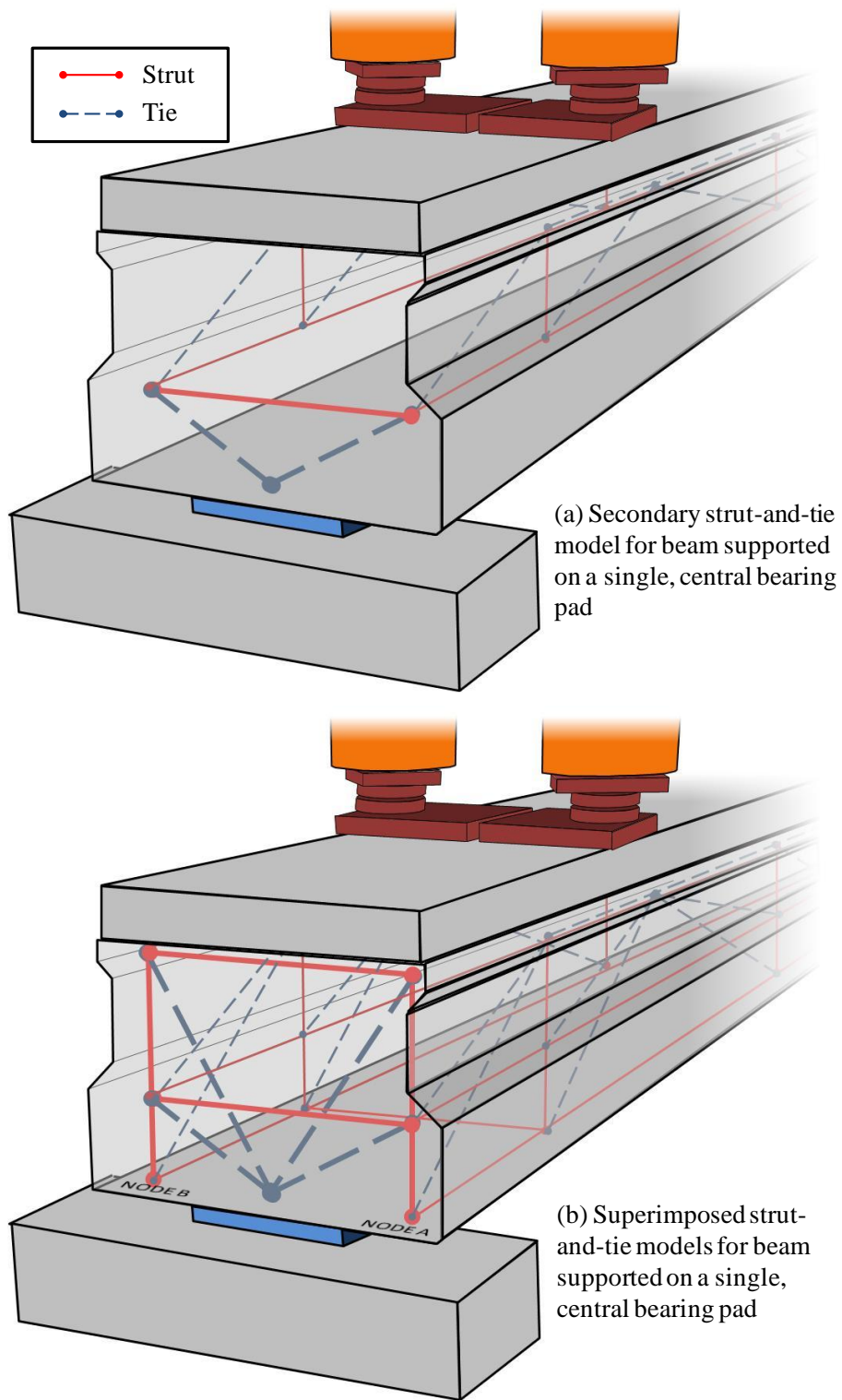
Figure 6-21: Other strut-and-tie models for the single bearing pad support condition

207

Additional evidence of such behavior was found in the shear test on the square end of beam 5B40-4. In the top half of the end block, bars MT were instrumented and monitored during the application of load. As can be seen in Figure 6-22, the gages registered strains proportional a stress as high as 33 ksi (Gauge on Bar MT1). The sudden increases in the readings of the gages can be correlated with the first observations of vertical cracks in the end face of the beam as illustrated earlier in Figure 6-8. The tensile stresses measured in bars MT correspond to the tension tie going across the end block in the strut-and-tie models.
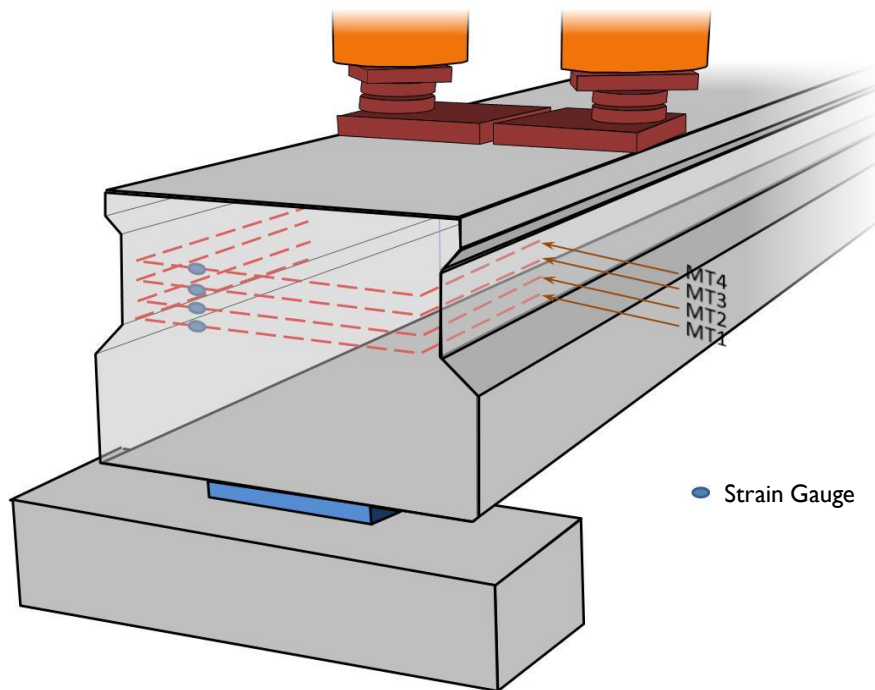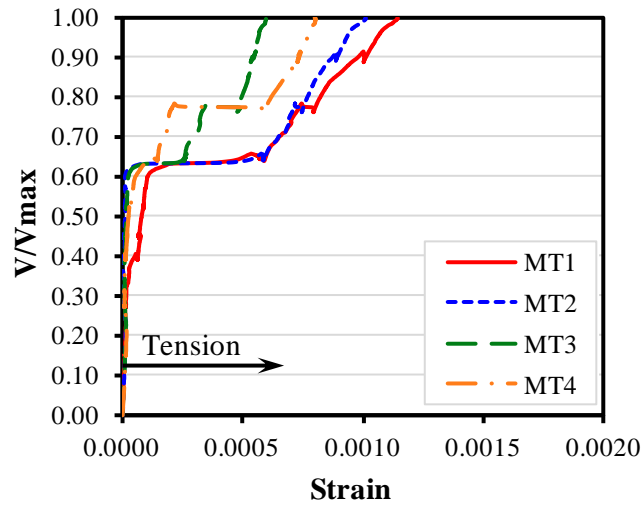
Figure 6-22: Strain readings in Bars MT during shear test on the square end of 5B40-4

6.5.1.2 *Web crushing*

Typical web crushing was observed in some cases with well defined diagonal compression struts in the web through the shear span. When present, web crushing was accompanied by bulging of the web and spalling of concrete.

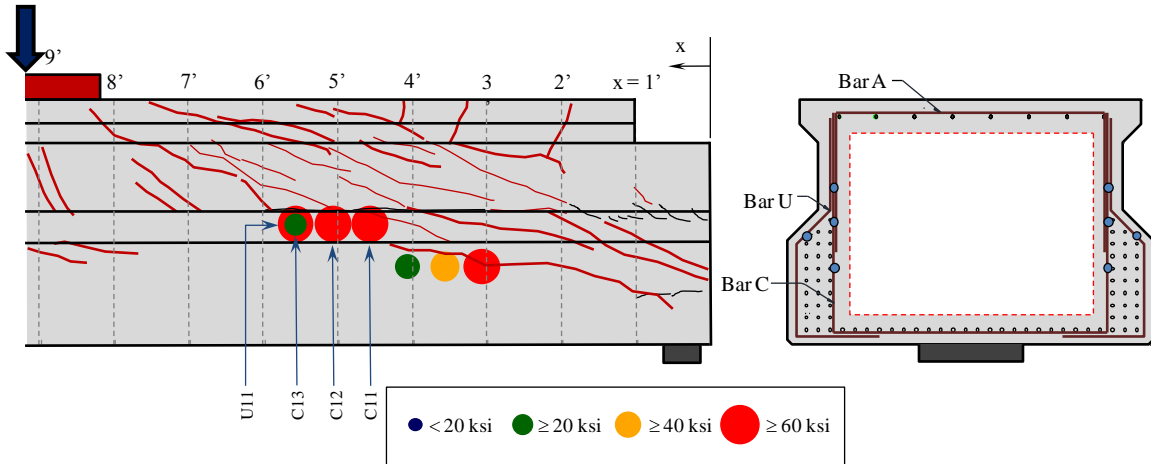### 6.5.1.3 *Yielding of the shear reinforcement*

As explained in Chapter 3, strain gages were installed in the shear reinforcement in potential areas of high tensile stress during shear tests. These gages were installed in all the beams part of Phase I of this study. The measured data revealed that the shear reinforcement was highly strained at the time of failure.

As summarized in Table 6-5, the square end of beam 5B40-1 was the only test region where strains in the reinforcement did not exceed the yield strain. This observation can be related to the comparatively lower shear endured by this test region. The maximum shear applied was equal to 99% of the calculated capacity using the general procedure from AASHTO-LRFD. As was discussed earlier, failure of this test region was characterized by a localized spalling of the cover near the end of the beam as pictured in Figure 6-16. As illustrated in Figure 6-23, the maximum strain measured in the shear reinforcement in this test region was proportional to a stress of 40 ksi.
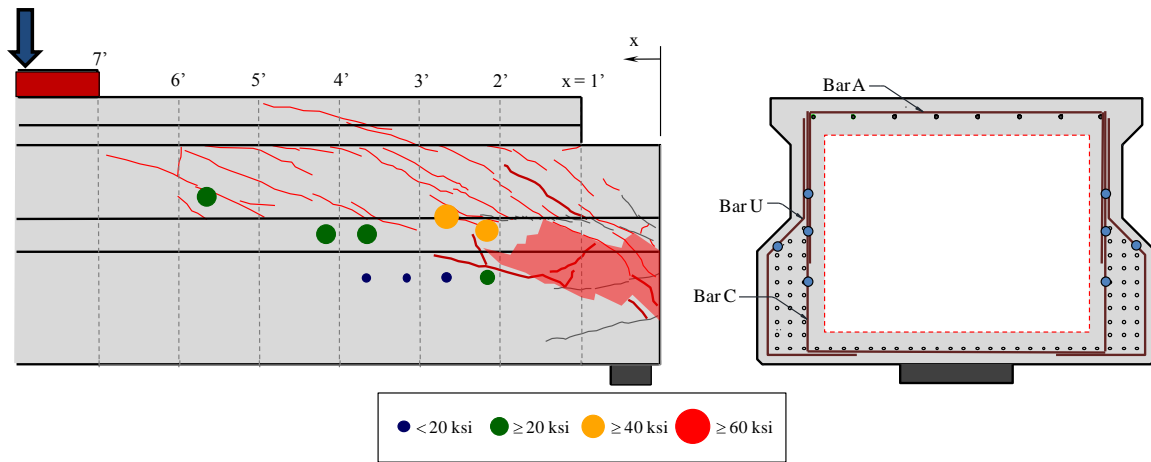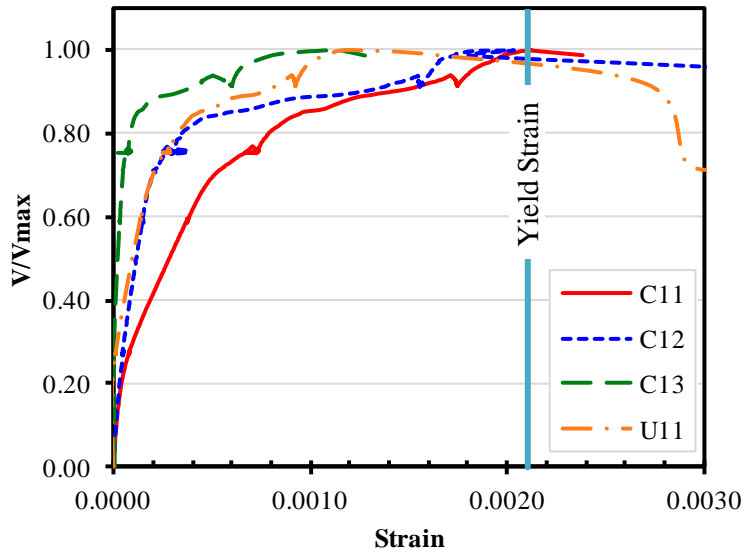

Figure 6-23: Stress in the shear reinforcement at failure for shear test of the square end of beam 5B40-1

In all other tests, the maximum sustained shear was much higher. The second lowest shear force carried within the shear tests of Phase I was 20% greater than that sustained in the square end of beam 5B40-1. An example of high measured strains can be observed in Figure 6-24 for the skewed end of beam 5B40-1. The strain versus applied shear plot for four of the strain gages marked in Figure 6-24 is shown in Figure 6-25.

Figure 6-24: Stress in the shear reinforcement at failure for shear test of the skewed end of beam 5B40-1

Figure 6-25: Strain vs. V/Vmax for strain gages in the transverse reinforcement for shear test of the skewed end of beam 5B40-1

The fact that shear reinforcement was yielding prior to shear failure is a good indication of the failure mechanism being in agreement with the shear capacity calculation method used. The general procedure from AASHTO-LRFD assumes that shear reinforcement yields at the time of shear failure. Although the strains in the shear

reinforcement were not measured during Phase II, similar crack widths and crack patterns were observed, suggesting a similar strain level in the reinforcement.

### 6.5.1.4   *Signs of horizontal shear distress*

Although failure was never controlled by horizontal shear, some horizontal shear distress could be observed at the time of failure. As part of the testing protocol, when the shear applied was approximately 80% of the calculated shear capacity, lines crossing the critical horizontal shear interface were drawn. Upon failure, it was possible to observe a shift in the crossing marks characteristic of horizontal shear distress as the top of the beam slides along the bottom flange-to-web interface. In general, sliding was small and around a quarter of an inch as illustrated in Figure 6-26.

Figure 6-26: Signs of horizontal shear distress. Square end of 5B40-3 is shown.

6.5.1.5 *Shearing through the end block*

When one web of a box beam was strained more than the other, the end block was not be able to accommodate the difference in deformation demands. Once this difference reached a certain threshold, the end block lost its integrity and the web sheared through the end block. As can be seen in Figure 6-27, a vertical crack lined up with the projection of the inner face of the web.
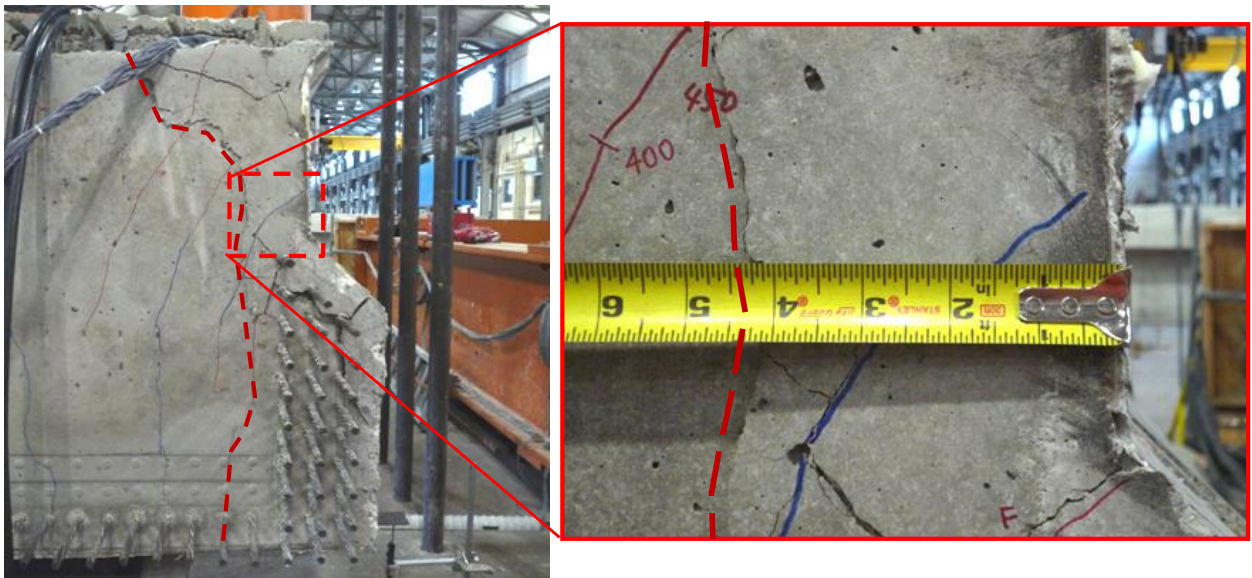
Figure 6-27: Shearing through end block. Square end of 5B40-2 is shown.

6.5.1.6   *Shearing through top and/or bottom flange*

Shearing through the top flange, as illustrated in Figure 6-28, is less likely to occur in situations where a cast-in-place composite deck is added over the box beams. Nowadays, composite decks are added in most cases, suggesting that this type of damage is not of concern for future bridges. More importantly, beams sustaining this type of damage carried a shear force at least 32% greater than the calculated shear capacity of the box beams in this study.

Figure 6-28: Shearing through top flange. Skewed end of 5B40-3 is shown.

On the other hand, shearing through the bottom flange was not observed in most cases. This observation can be attributed to the relatively high location of the centroid of the strands (8.24 in. from the bottom of the beam). In the beams where the centroid of the strands was this high, damage rarely extended into the bottom flange. The only case where damage extended into the bottom flange can be observed in Figure 6-28.

Figure 6-29: Shearing through bottom flange. Skewed end of 5B40-4 is shown.

When the centroid of the strands was lower, as was the case in beam 5XB40, damage extended well into the lower portion of the bottom flange, although, failure did not include shearing through the bottom flange.

6.5.1.7   *Splitting crack through a row of strands*

This type of damage, pictured in Figure 6-30, was only observed at failure in the test of one of the ends of beam 5XB40. In the aforementioned case, the beam was supported on a single bearing pad. The sudden way in which this damage presented itself suggested that it was more a consequence rather than a cause of failure.
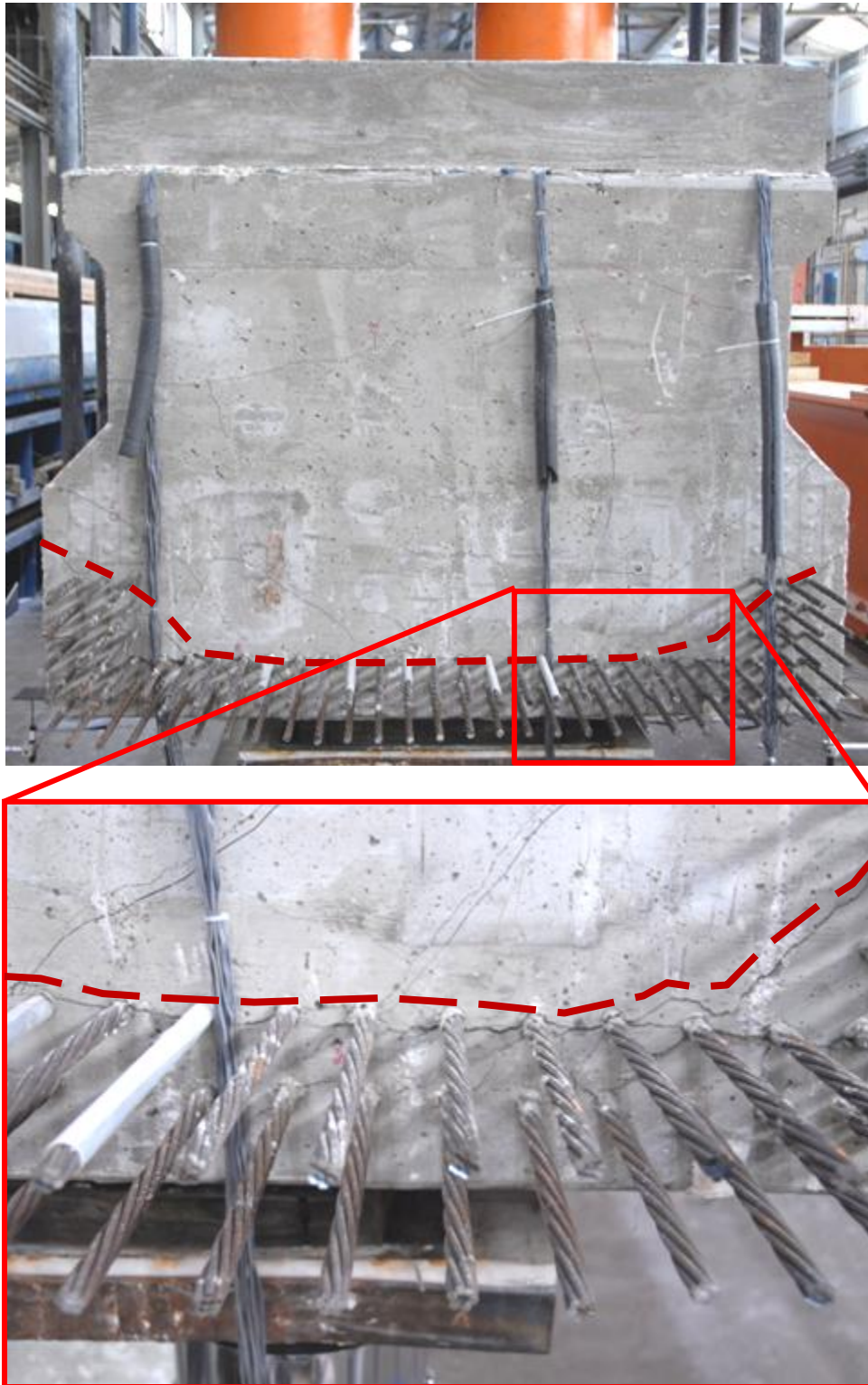
Figure 6-30: Splitting crack through second row of strands. Beam 5XB40 is shown.

6.5.1.8   Other damage observations

A failure of both webs of the beam was only on seen in the square end of beam 5B40-4. This can be attributed to the modified end region detail described in Chapter 5. One of the main goals of the modified reinforcement was to improve the ability of the end block to redistribute load, from the end of one web to the other, as damage worsened.

In all previous beams, failure was localized in one of the two webs. After failure, experimental evidence suggested that the web that did not fail endured further shear but the web that failed first was not able to sustain enough additional shear force and accommodate the additional deformation demand required to reach the failure of the second web.

Figure 6-31: Symmetric failure of both webs in 5B40-4-Q

217

6.6   SUMMARY AND CONCLUSIONS

The results from 9 shear tests conducted on 5B40 and 5XB40 box beams were discussed in this chapter. Overall, shear performance of the box beams was acceptable. On average, the ratio of the maximum applied shear to the calculated shear capacity was 1.26. The lowest ratio was 0.99 and the highest was 1.51. These results fell within the scatter observed for beams of similar characteristics included in the University of Texas Prestressed Concrete Database (UTPCSDB-2011, Evaluation Database - Level II; from Nakamura, 2011).

Phase I beams; fabricated with the current TxDOT standard reinforcement detail, performed well in shear, no changes to the proportions of shear reinforcement were justified. The reinforcement details of the first beam of Phase II were improved to reduce the magnitude of the horizontal bursting stresses and associated crack widths measured in Phase-I beams. No changes were made to the beam design in terms of web shear strength. The second beam of Phase II incorporated a new box beam section optimized for flexural strength in a spread box beam configuration. Shear performance of this beam was also deemed acceptable.

Test specimens exhibited damages on different regions and to different extents. Nevertheless; the crack widths, the number of diagonal cracks and the strains measured in the shear reinforcement suggested that shear reinforcement yielded prior to failure. Typical shear capacity calculation equations agree well with this mechanism and yielded conservative results.

The presence of skew did not affect the conservativeness of the shear capacity calculations. Even though failures in skewed were usually concentrated in the end of the beam at the short side of the beam, failure occurred at a shear higher than the calculated capacity of the two webs considered as one. The use of two internal void geometries at the skewed end and its implications on shear strength was investigated. It was found that both end block geometries were able to preserve their integrity through the shear test process.

Different load transfer mechanisms were identified for different support conditions. Specifically, when the end of the beam is supported on a single large central bearing pad or when the end of the beam is supported on two smaller bearing pads placed under the webs. It was found that supporting the beam on a single large central bearing pad creates a more demanding condition for the end block. In such case, the vertical reinforcement in the web near the end of the beam is stressed in tension, increasing the potential for spalling of the cover on the side of the beam.

CHAPTER 7

Summary, Conclusions and Recommendations

7.1 SUMMARY

In order to improve the end-region reinforcement of box beams, a thorough understanding of their behavior at the time of prestress transfer and under shear dominated loads was required.

A thorough literature review, presented in Chapter 2, was conducted. In comparison to the research conducted on single-webbed beams, the need for research regarding box beam behavior became apparent. The significance of this research study became even more apparent, after seeing that box beams represent a significant fraction (12%) of all highway bridges built in the last decade. An experimental program, presented in Chapter 3, was tailored to fill the gaps in the literature identified in Chapter 2.

In the first part of the experimental program, ten 4B28 box beams (28 in. deep and 48 in. wide) were tested under shear loads. A total of 20 shear tests were conducted. The testing program involved several variables which allowed for comparisons between different concrete mixtures, beam end geometries, internal void geometries and support conditions. The results from the first part of the testing program, presented in Chapter 4, established the basis for the next stage of the experimental program which included the fabrication and testing of 5B40 box beams (40 in. deep and 60 in. wide).

The second part of the experimental program included the in-house fabrication and testing of five 5B40 box beams. In-house fabrication allowed the research team to place internal instrumentation in the beams in order to better understand its behavior. First, at the time of prestress transfer, internal instruments were monitored and crack patterns were studied. Results related to box beam behavior at the time of prestress transfer were presented in Chapter 5. Later, a total of nine shear tests were conducted on

the in-house fabricated beams. The load carrying capacity, shear crack patterns and overall behavior was studied. The corresponding results were presented in Chapter 6.

7.2 CONCLUSIONS

The following conclusions are based on the literature review and the experimental program conducted in the present study. Current design practices, codes and specifications have been developed based on data from much simpler prestressed concrete I-beams. Comparative evaluation of box beams and I-beams were performed to put conclusions into context.

7.2.1 Behavior of Box Beams at Prestress Transfer

Conclusions presented in this section are based on the results from the experimental program conducted on the in-house fabricated beams.

7.2.1.1 Vertical forces in the end region of box beams at prestress transfer

Measured vertical strains at the time of prestress transfer revealed that the vertical forces induced by the prestressing strands at prestress transfer can be controlled successfully through the current standard reinforcement detail suggested by TxDOT.

The magnitude, location and distribution of vertical forces in the end region of box beams was found to be comparable to that of I-beams reported in previous research.

After comparing the end-region reinforcement detail suggested in the TxDOT standards to the AASHTO-LRFD Bridge Design Recommendations (2010) and studying the calculated forces in the end region, it was found that:

- Placing transverse steel, within the end $h/4$ of the beam, so as to equilibrate 4% of the net prestressing force without being stressed beyond 20 ksi, was found to be good design recommendation.
- Stresses in the reinforcement located in the region between the end $h/4$ (10 in.) length and the transfer length of the strands (30 in.) were found to be

comparable to those in the end $h/4$ length. The demands in the region between the end $h/4$ length and the transfer length of the strands were controlled well (without the reinforcement being stressed beyond 20 ksi) through the reinforcement detail used by TxDOT. Currently, there is no reinforcement requirement for the region between the end $h/4$ length and the transfer length of the strands in the AASHTO LRFD Bridge Design Specifications.

7.2.1.2 *Horizontal forces in the end region of box beams at prestress transfer*

Measured horizontal strains at the time of prestress transfer revealed that the horizontal transverse forces cannot be resisted by the current box beam standard reinforcement detail used by TxDOT without exceeding the 20 ksi limit recommended by AASHTO. Horizontal stresses as high as 30 ksi were found in several occasions.

As opposed to I-beams where strands are clustered in one region in the bottom flange; strands are spread through the width of box beams. In the box beams studied, a large fraction of prestressing strands is located within the webs. The placement of such strands magnifies the horizontal stresses induced at the time of prestressed transfer.

7.2.2 **Shear Behavior of Box Beams**

Conclusions presented in this section are based on the results from the experimental programs conducted on both the 4B28 and the 5B40 box beams.

7.2.2.1 *Square ends versus skewed ends*

In square ends of box beams, it was found that approximately half of the total shear is carried by each web. Shear performance of square-ended box beams was comparable to that of typical I-beams. Shear tests on box beams with square ends yielded conservative results with a similar scatter and degree of conservatism to that of

comparable I-beams observed in the University of Texas Prestressed Concrete Shear Database.

In skewed ends of box beams, it was found that as much as 60% of the total shear is carried by the web corresponding to the obtuse corner of the skewed end. This uneven load distribution resulted in this web controlling the failure of the test region. The uneven distribution of the shear to the webs was not sufficiently large to cause unconservative shear capacity calculations. In other words, in all tests conducted on the skewed ends of box beam specimens, the measured shear capacity was greater than the calculated shear capacity. The observed degree of conservatism of the shear strength equations when applied to the skewed end of box beams was comparable to that observed in the square end of each corresponding beam.

Shear capacities were calculated by adding the thicknesses of the two webs of box beams and assuming that shear is carried through a single equivalent web. This assumption resulted in conservative shear capacity estimations even when the load was unevenly distributed in the skewed ends of the box beams tested.

7.2.2.2   Influence of the internal void geometry at skewed ends

Varying the geometry of the internal void at skewed ends of box beams had no discernible effect on their shear strength. A slight reduction (-6°F) in the internal temperature differential within the end block was observed when a skewed internal void was used.

7.2.2.3   Influence of bearing pad configuration

Two different load transfer mechanisms were identified for the two possible bearing pad configurations as discussed in chapter 6. Having two bearing pads; placed underneath the webs of the beam, was found to be a more favorable support condition than the larger bearing pad centered under the bottom slab. For the box beams of this study, both bearing pad configurations were suitable for the shear demands imposed on the section. In other words, the strength of the test specimens supported by both bearing

pad configurations was conservatively estimated by the shear strength calculation methods described in Chapter 2. A good representation of the flow of forces created by either support condition was possible through simple strut-and-tie models.

7.2.2.4 Influence of the ratio of the bottom flange width to the web width

Although three different bottom flange-to-web width ratios were tested through this study, no difference in behavior was observed among the specimens. The shear transfer capacity of the beam along the interface of the bottom flange and the web was adequate in all cases. Furthermore, the relative flexibility of the bottom flange played no role in the overall shear behavior of the box beam sections.

7.2.2.5 Applicability of current shear strength design methodologies

Shear capacities were calculated using the general procedure from the AASHTO LRFD Bridge Design Specifications (2010), the detailed method from ACI 318-08, the simplified procedure from the AASHTO LRFD Bridge Design Specifications (2010) and the segmental bridge specifications from the AASHTO LRFD Bridge Design Specifications (2010).

Comparing the maximum applied shear to the shear capacity calculated by any of the aforementioned methods, and observing the results within the context provided by the UTPCSDB, revealed that the shear strength of box beams can be assessed with an equal degree of scatter and conservatism to that found in typical I-beams.

7.3 RECOMMENDATIONS

7.3.1 End-Region Reinforcement Details

For standard 5B40 box beams, the modified end region reinforcement details used in beam 5B40-4 are recommended. Both vertical and horizontal stresses introduced at prestress transfer were controlled adequately through the modified reinforcement details used in beam 5B40-4. The key difference between the current TxDOT Standard

reinforcement details and the recommended reinforcement detail can be observed in Figure 7-1. The additional reinforcement in the recommended details extends into the bottom portion of the webs, where a large fraction of the strands can be located. In doing so, horizontal forces in the end region introduced at prestress transfer, and additional horizontal forces in the end region due to superimposed loads can be resisted and redistributed to the whole end block. Additionally, crack control is greatly improved.

As previously recommended by O'Callaghan and Bayrak (2008), it is recommended that transverse reinforcement be placed in the region bound between the last $h/4$ of the beam and the transfer length of the strands. Reinforcement in the aforementioned region should be sufficient to resist a transverse force equal to 4% of the net prestressing force without being stress beyond 20 ksi. The inclusion of this recommendation in the AASHTO-LRFD requirements is recommended.
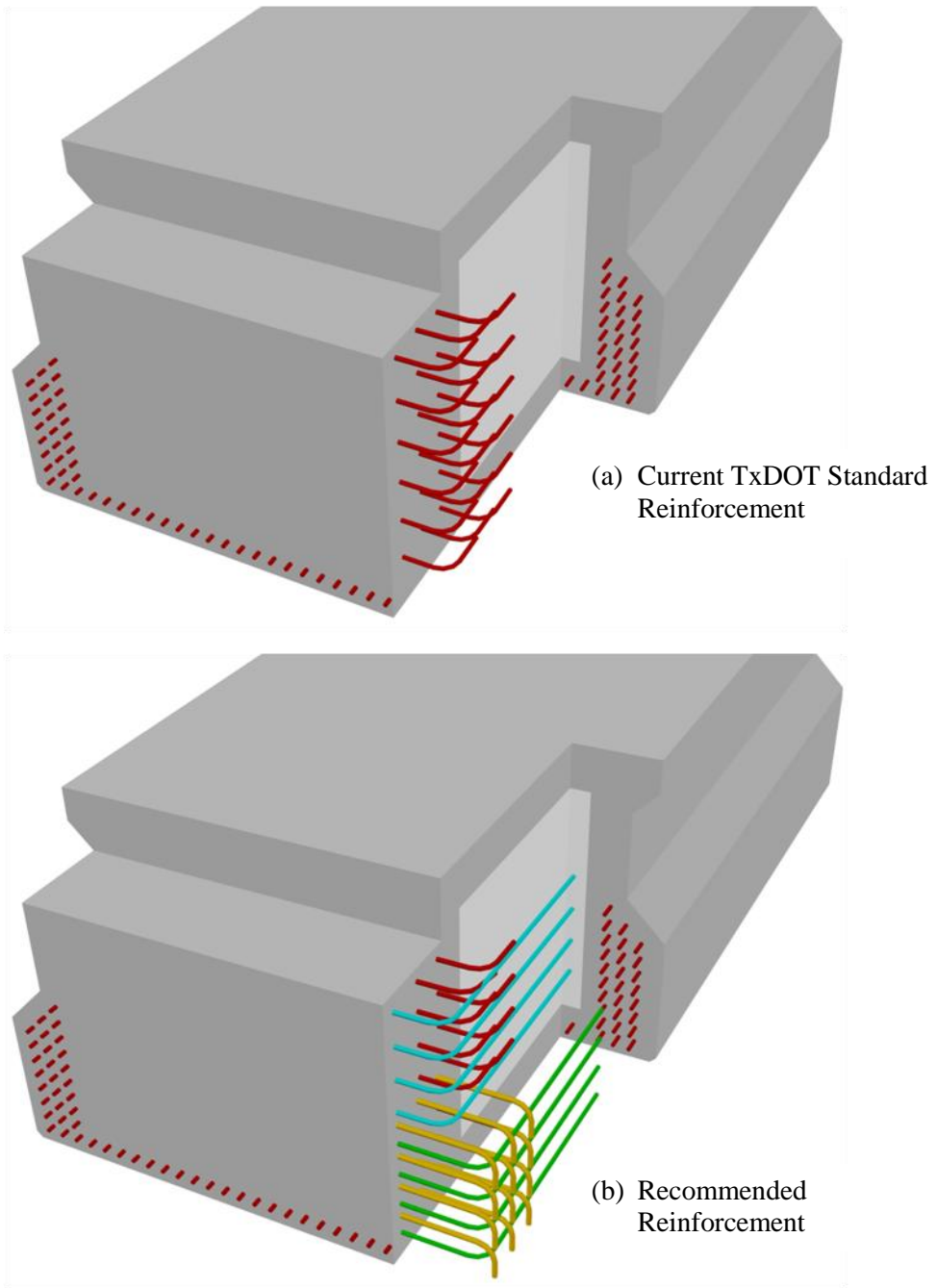
Figure 7-1: Key differences between the current TxDOT standard reinforcement details and recommended reinforcement details

A full-scale model, illustrated in Figure 7-2, was built to illustrate the proposed changes to the end-region reinforcement details. In Figure 7-2, the added reinforcement can be observed highlighted in blue (Bars MT), green (Bars MB) and red (Bars E).

Figure 7-2: Full-scale model of the improved end-region reinforcement used in beam 5B40-4

For 5XB40 box beams, the end region reinforcement details used in this study are recommended. Both vertical and horizontal stresses introduced at the time of prestress transfer were resisted by the aforementioned detail while exhibiting narrow cracks in the end region.

A complete set of drawings of reinforcement details for both types of beams can be found in Appendix B.

7.3.2 **Shear Strength Design Procedures**

The use of the following four shear strength design methodologies is recommended for prestressed concrete box beam applications:

(1). The General Procedure from the AASHTO-LRFD Bridge Design Specifications (2010)

(2). The Simplified Procedure from the AASHTO-LRFD Bridge Design Specifications (2010)

(3). The Segmental Bridge Specifications from the AASHTO-LRFD Bridge Design Specifications (2010), and

(4). The Detailed Method from ACI 318-08.

APPENDICES

APPENDIX A
Material Properties

Table 7-1: Prestressing strands elastic modulus

Beam	Modulus along wire (ksi)	Modulus along strand (ksi)
5B40-1	31127.3	28803.3
5B40-2	30124.0	28573.0
5B40-3	30693.3	28787.0
5B40-4	30332.0	28607.7
5XB40	30084.0	28283.7

Table 7-2: Mild Reinforcement Yield Strengths

Beams	Average Yield Strength (ksi)
5B40-1 and 5B40-2	64.7
5B40-3 and 5B40-4	65.0
5XB40	66.0

Table 7-3: Concrete mixtures for beams of type 4B28

Material	Details	Quantity				Units
		Casting 1 8/21/08	Casting 2 7/22/08	Casting 3 8/25/08	Casting 4 8/26/08	
		BB01-BB02	BB03-BB05	BB06-BB07	BB08-BB10	
Cementicious Material	Alamo Gray Type III	599		545	560	lb/yd^3 concrete
	Alamo Type I/II LA		658			
	Class F Fly Ash	200	165	136	140	
Coarse Aggregate	¾ in. Crushed Limestone	1839		1541		lb/yd^3 concrete
	TXI River Gravel		1923		1511	
Fine Aggregate	Manufactured Sand			871	791	lb/yd^3 concrete
	Natural Sand	1197	1055	680	751	
Water	–	173	222	193	194	lb/yd^3 concrete
Water /CM	–	0.22	0.27	0.28	0.28	–
Water Reducers	Sika Viscocrete 2100		6.43			oz./hundred weight cement
	Sika Viscocrete 4100	2.25		4.76	6.24	
Retarder	Sika Plastiment	3.25	0.85	1.29	1.52	oz./hundred weight cement

Table 7-4: Concrete mixtures for beams of type 5B40 and 5XB40

Material	Details	Quantity					Units
		5B40-1	**5B40-2**	**5B40-3**	**5B40-4**	**5XB40**	
		05/20/10	07/22/10	09/07/10	01/18/11	05/02/11	
Cementicious Material	Alamo Gray Type III	600	500	600	600	600	lb/yd^3 concrete
	Type F Fly Ash	200	300	200	200	200	
Coarse Aggregate	3/8 in. Crushed Limestone	1,457	1,385	1,385	1,385	1385	lb/yd^3 concrete
Fine Aggregate	River Sand	1,386	1,460	1,480	1544	1526	lb/yd^3 concrete
Water	–	184	184	170	276	207	lb/yd^3 concrete
Water/CM	–	0.23	0.23	0.21	0.35	0.26	–
Water Reducers	Sika Viscocrete 2110	40	40	35	40	40	oz./hundred weight cement
Retarder	Sika Plastiment	33	33	28	20	33	oz./hundred weight cement

233

APPENDIX B

Shop Drawings

BARS A #4

2'-8¾"

1'-10"

BARS C #4

5½"   2'-8¾"   5½"

7 3/4"

1'-3"

5½"

3"

1'-11½"

3'-7¾"

BARS M #4

2'-7½"

6"

BARS B #4

3'-4"

BARS D #5

APPROXIMATELY 40' (VARIES – SEE PLAN)

2'-0" MIN. SPLICE

SPLICE TO BE IN MIDDLE THIRD OF
BEAM. STAGGAR SPLICES IN ADJACENT
BARS, MIN. 4'-1" BETWEEN SPLICES

BARS MM #4

30°

6"

3'-0⅜"

BARS AA & CC #4

3'-1 7/8"

2'-0" CC

1'-10" AA

BARS AL & CL #4

2'-8 3/4" MAX.

1'-6" MIN.

2'-0" CL

1'-10" AL

BARS U #4

6 3/8"

8 3/8"

1'-3"

8 1/2"

3"

1'-1½"

BARS N #4

5½"

1'-6¼"

5½"

4½"

GENERAL NOTES.

1.   CONCRETE SHALL BE CLASS 'H'

2.   REINFORCING STEEL SHALL BE GRADE 60

3.   DIMENSIONS RELATING TO REINFORCEMENT ARE TO
     CENTERLINE OF STEEL

4.   NO SPECIAL FINISH WORK REQUIRED FOR TOP OF
     BEAM

5.   ALL EXPOSED CORNERS SHALL BE CHAMFERED ¾"

6.   REINFORCING STEEL SHALL HAVE A MINIMUM 1–¼"
     CLEAR COVER UNLESS NOTED OTHERWISE

7.   EXTEND PRESTRESSING STRANDS A MINIMUM OF 6"
     BEYOND FACE OF BEAM

8.   CUT BARS AL AND CL AS REQUIRED TO MAINTAIN
     1" CLEAR COVER BETWEEN BARS

9.   BARS M MAY BE ADJUSTED VERTICALLY AS
     REQUIRED TO AVOID PRETENSIONING STRANDS IN
     WEB

10. BLOCKOUT REQUIRED AT ENDS OF ALL BEAMS.
     EXTEND BEAM REINFORCEMENT INTO BLOCKOUTS

11. PLACE DRAIN HOLES (1" DIA. PVC SCH 40 PIPES)
     AS SHOWN IN ALL BEAM VOID CORNERS.

Figure B-1: Reinforcement bars for all 4B28 box beams.
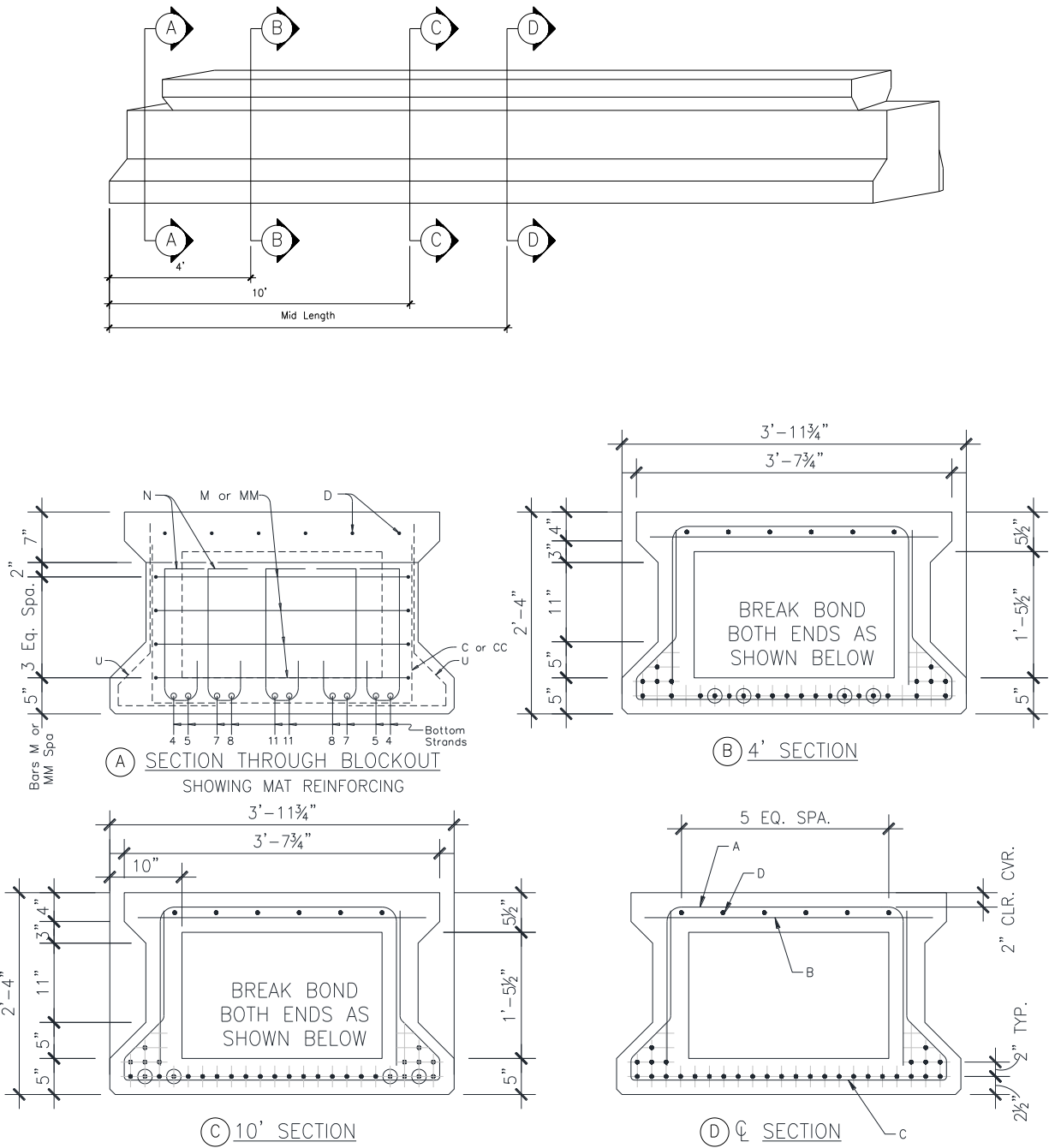
Figure B-2: Cross sections for all 4B28 box beams.
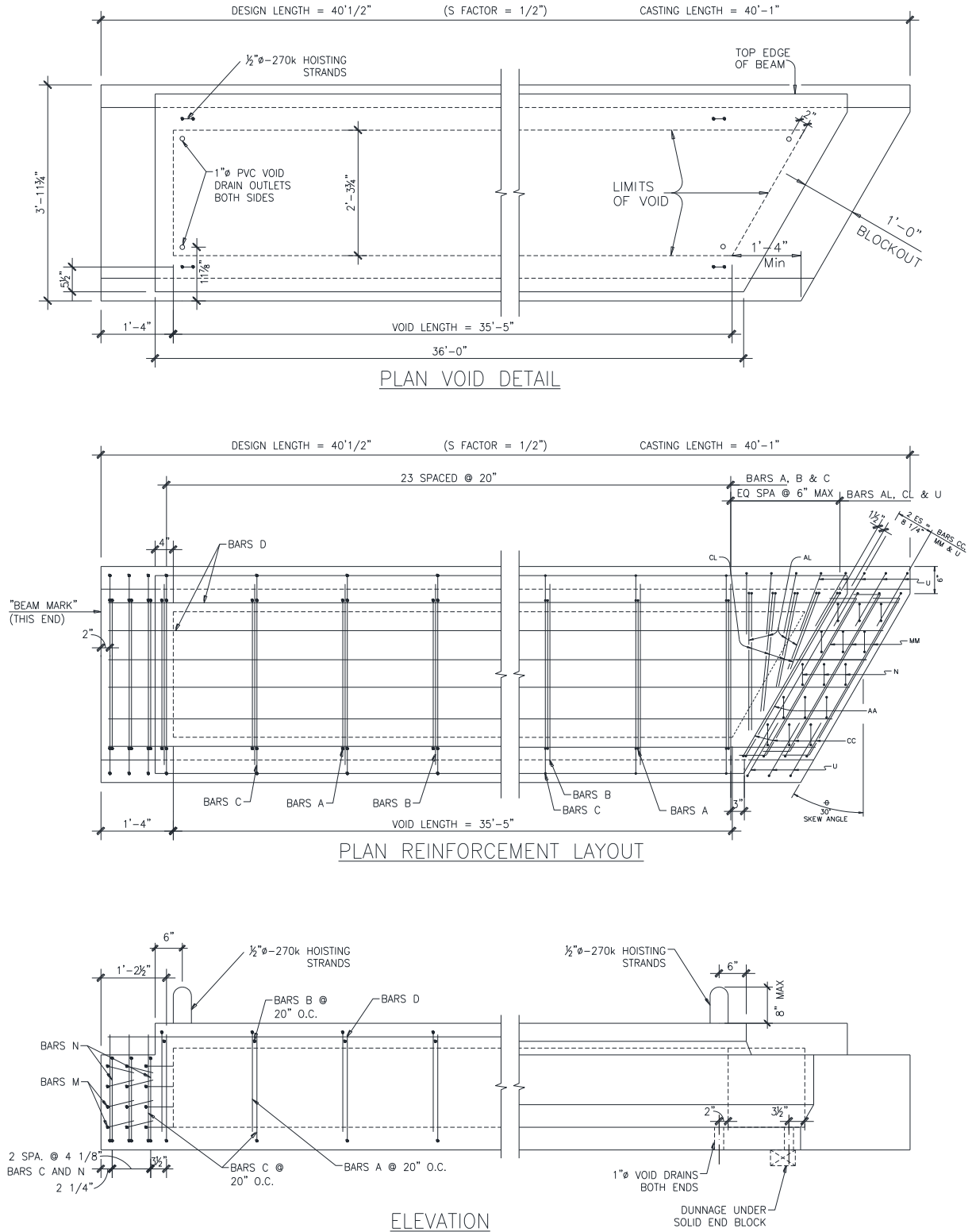
Figure B-3: Plan and Elevations for 4B28 box beams: BB-01, BB-03, BB-06 and BB-08.

237
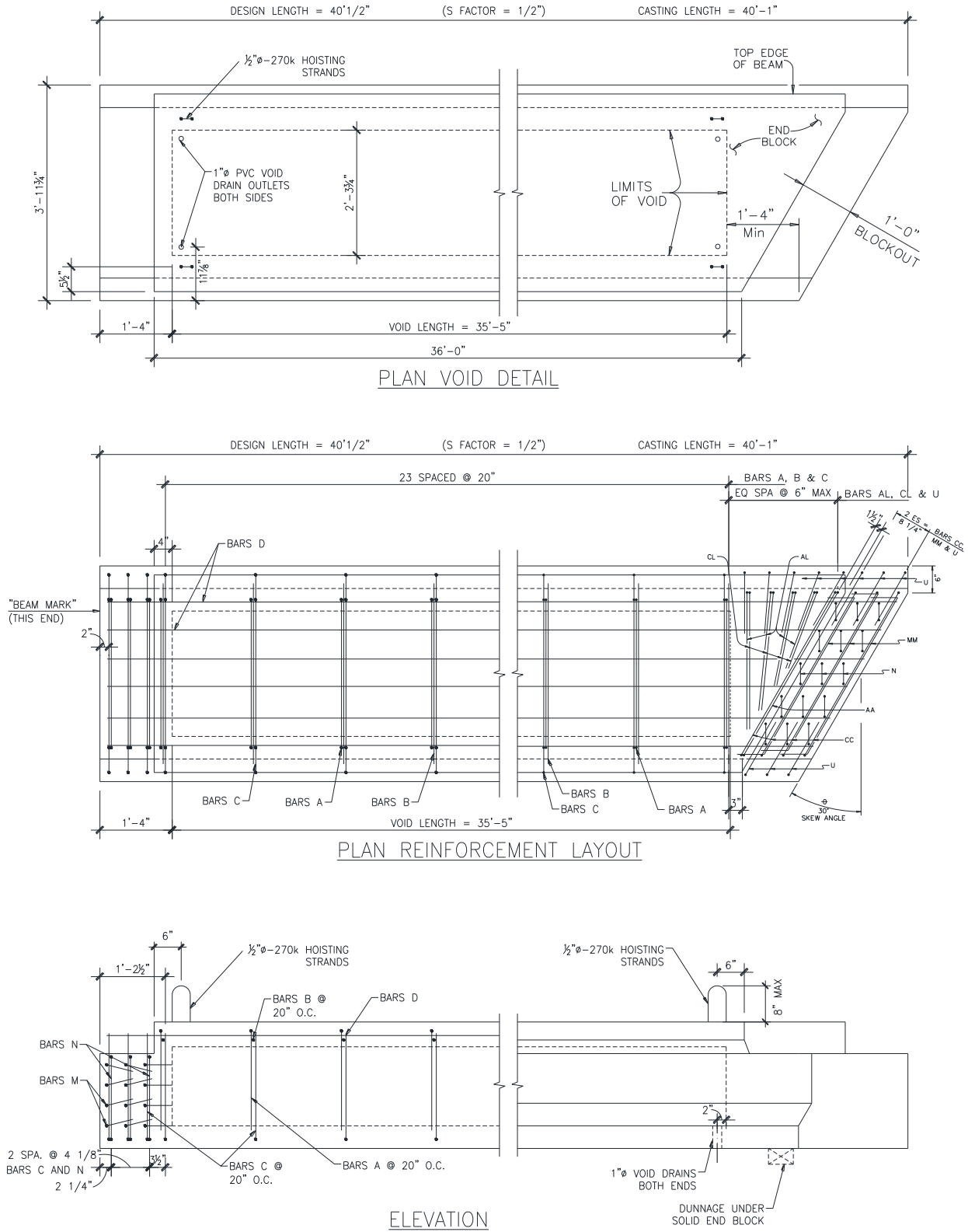
Figure B-4: Plan and Elevations for 4B28 box beams: BB-02, BB-04, BB-07 and BB-09.

238
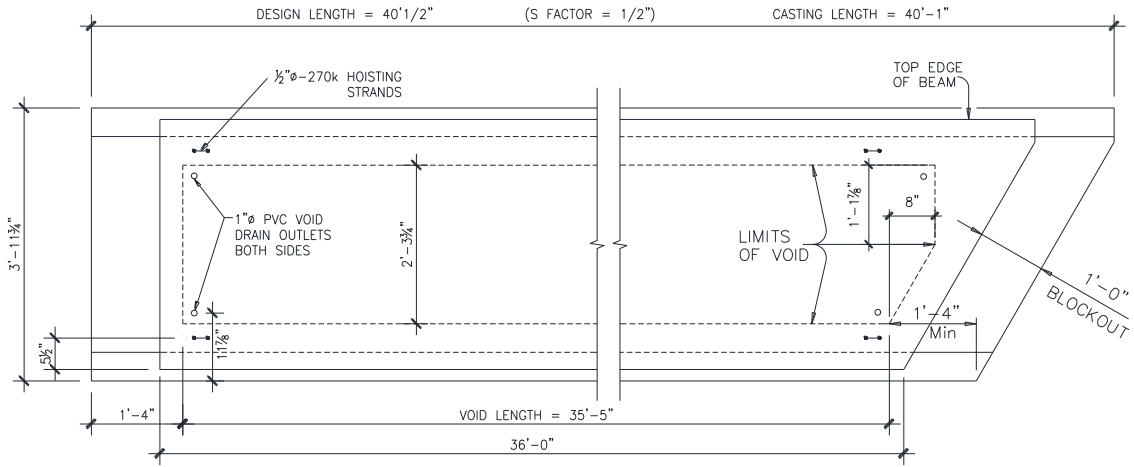
PLAN VOID DETAIL
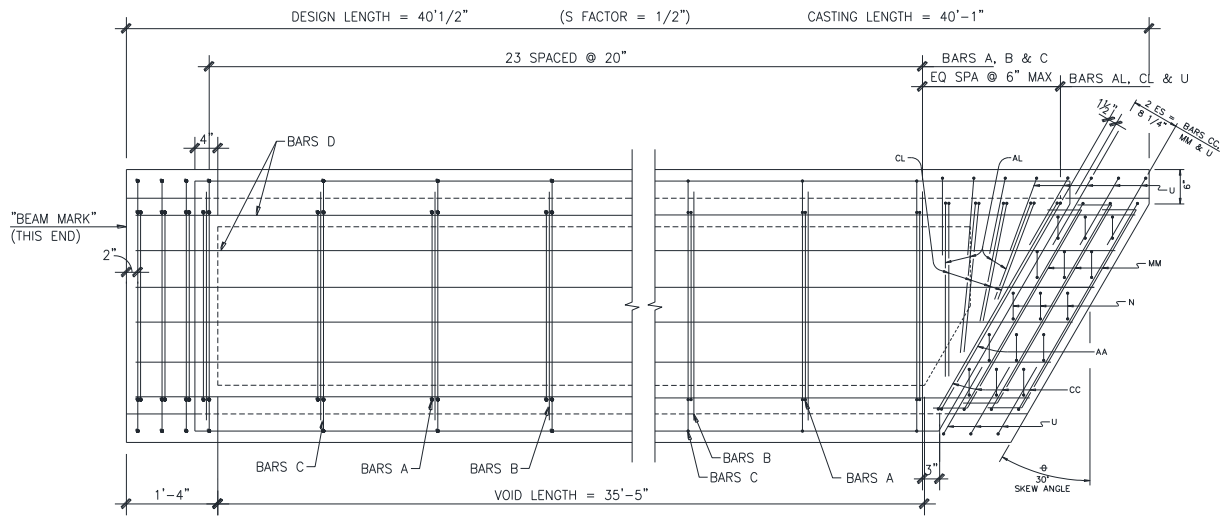
PLAN REINFORCEMENT LAYOUT
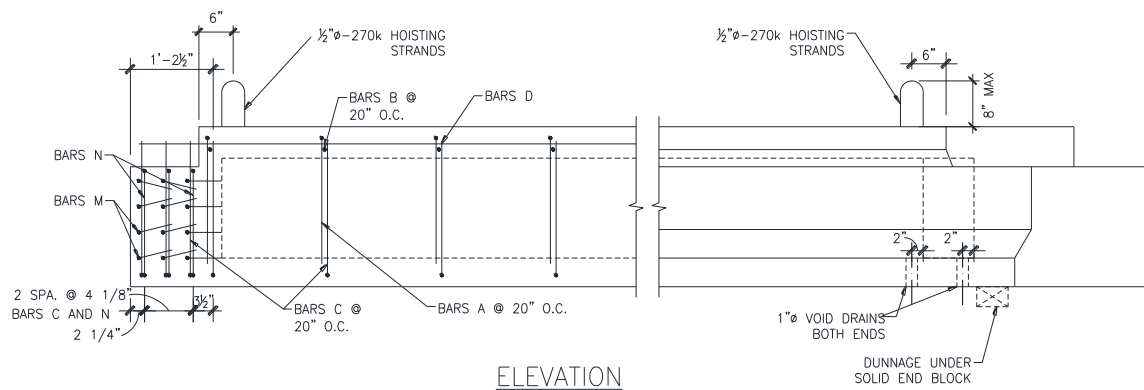
ELEVATION

Figure B-5: Plan and Elevations for 4B28 box beams: BB-05 and BB-10.

239

Bars A & B

1'-2"

6" Max Spa

Bars C ~ 2 1/4"   2 ES = 8 1/4"   3½"   6" Max Spa

Bars U ~ 2 1/4"   2 ES = 8 1/4"   3½"   12" Max Spa

Bars E ~ 2 1/4"   2 ES = 8 1/4"

Bars N ~ 2 1/4"   2 ES = 8 1/4"

Bars M ~ 2 1/4"   2 ES = 8 1/4"

U

M

D

E

A

C

N

U

B

TOTAL LENGTH = 30'
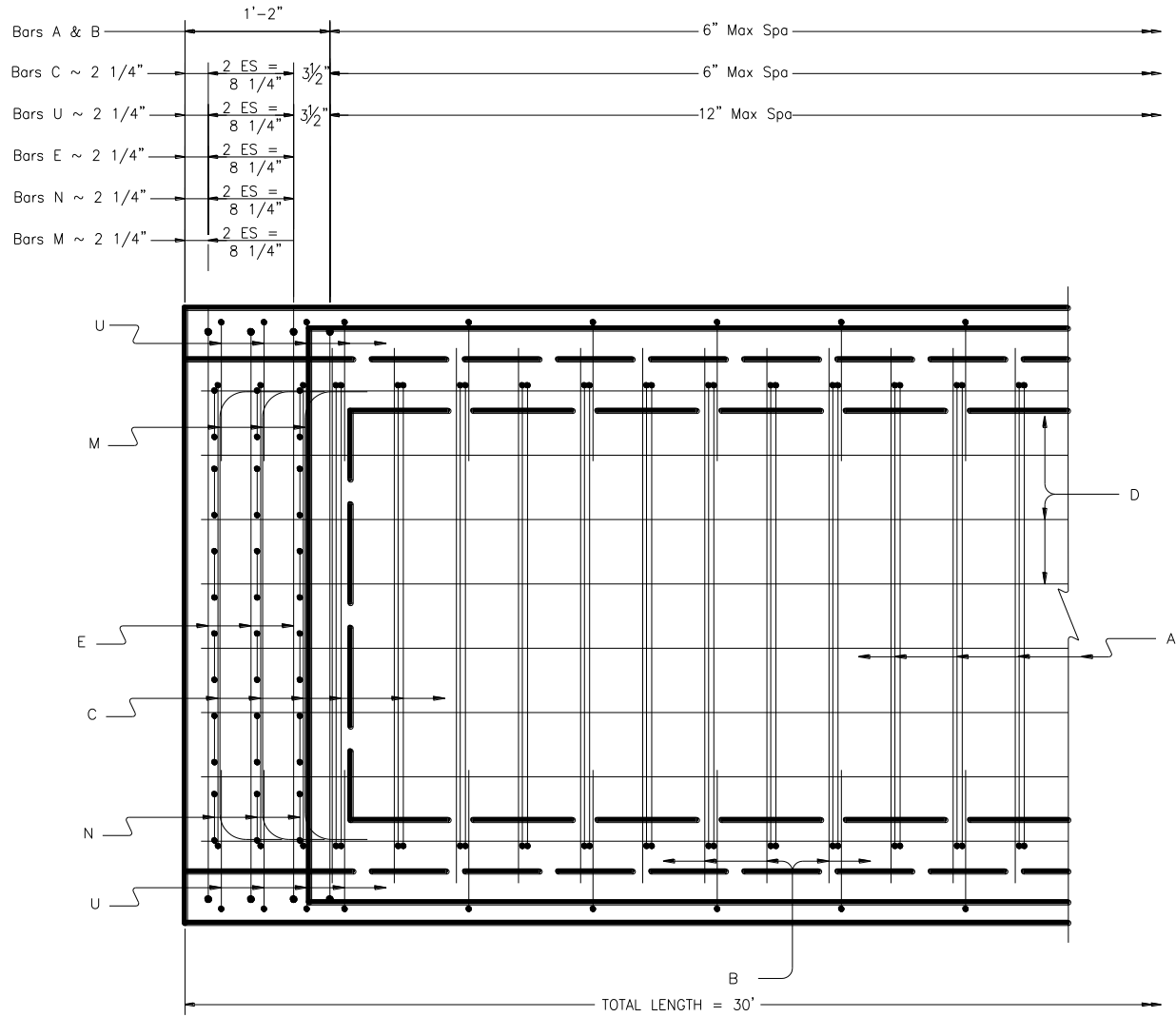
Figure B-6: Partial Plan – Square End. Beams 5B40-1, 5B40-2 and 5B40-3
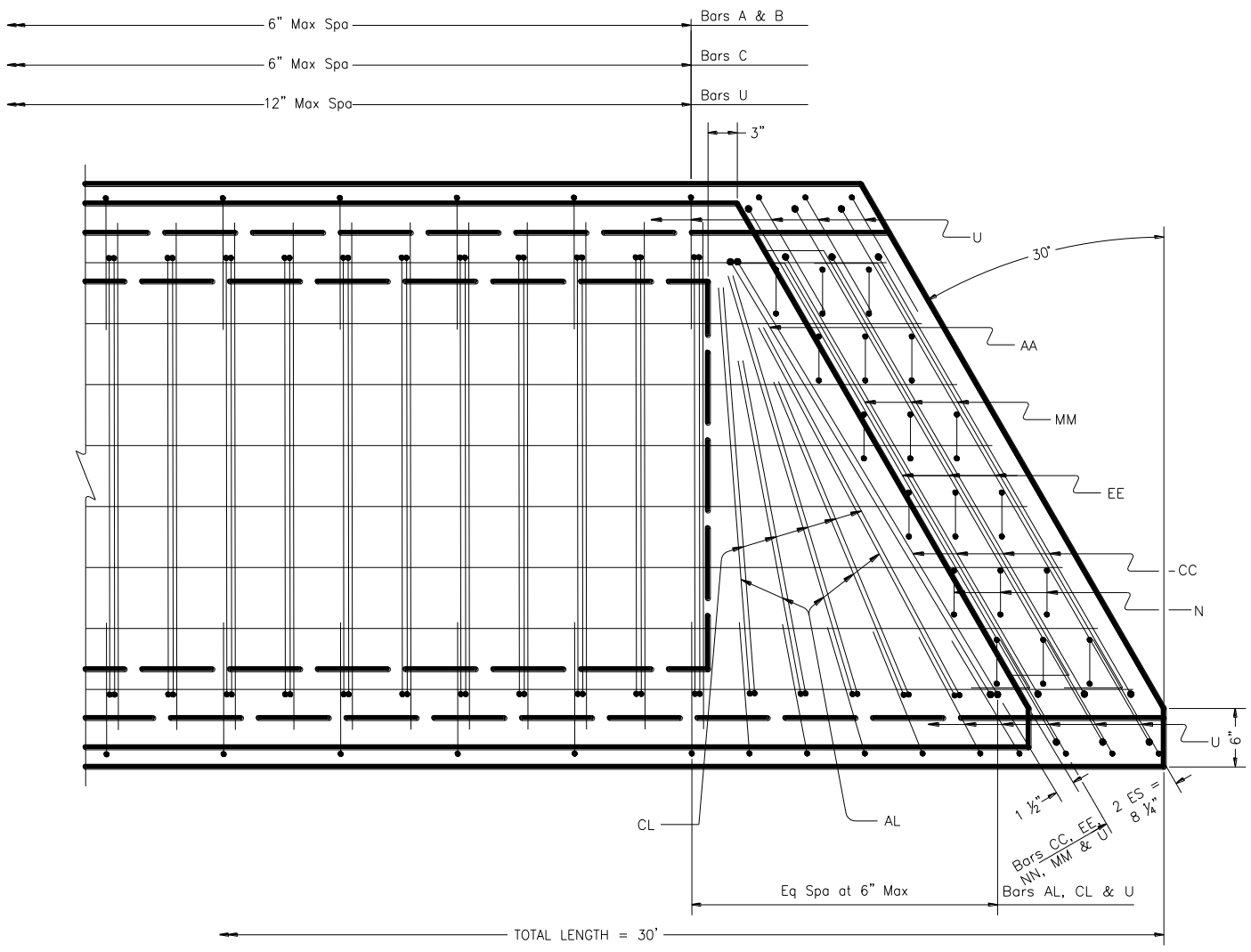
Figure B-7: Partial Plan – Skewed End. Beam 5B40-1
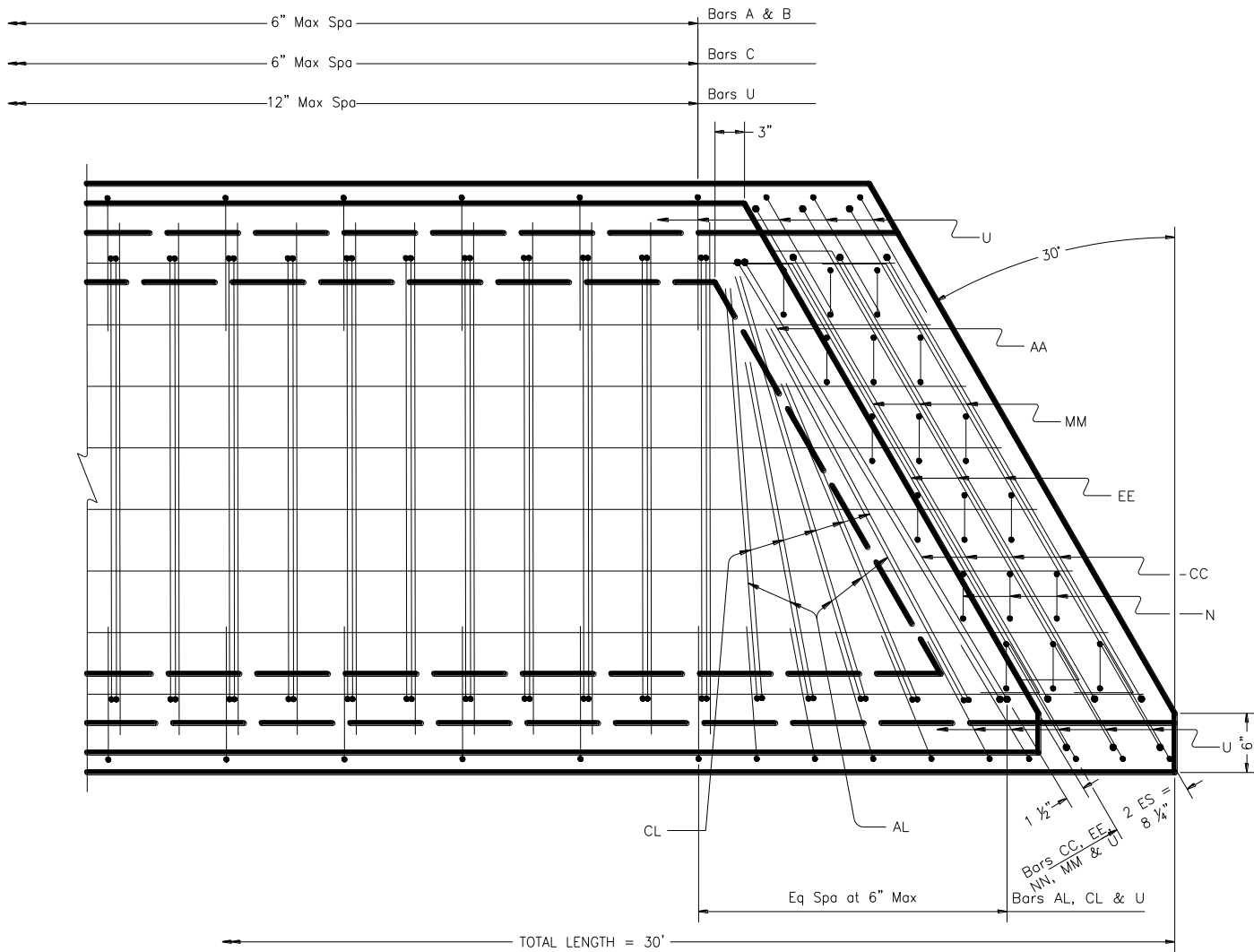
Figure B-8: Partial Plan – Skewed End. Beams 5B40-2 and 5B40-3
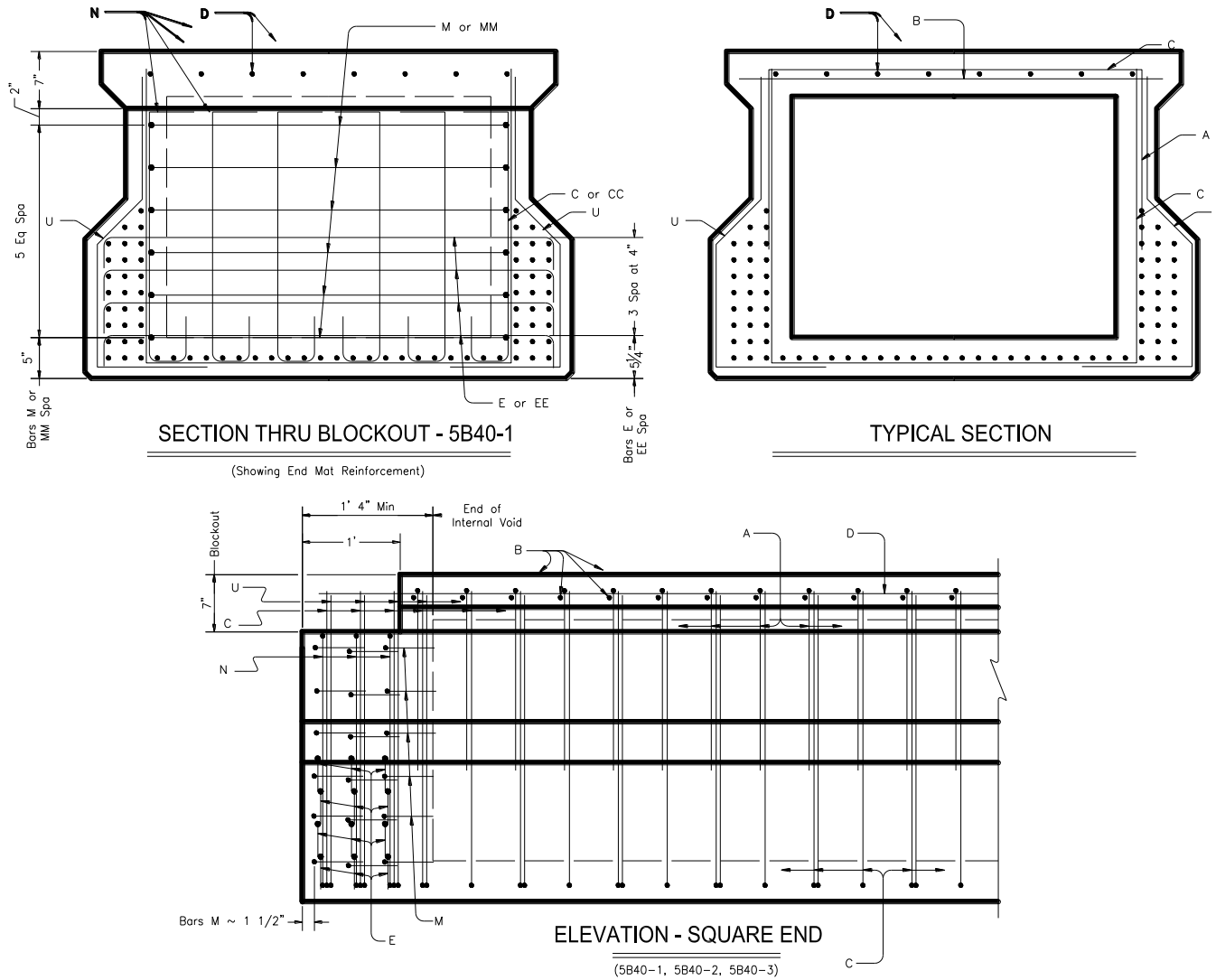
Figure B-9: Cross sections and elevations. Beams 5B40-1, 5B40-2 and 5B40-3

BARS A (# 4)

BARS AA (# 4)

BARS AL (# 4)

BARS C (# 4)

BARS CC (# 4)

BARS CL (# 4)

BARS M (# 4)

BARS MM (# 4)

BARS N (# 4)

BARS U (# 4)

BARS E (# 5)

BARS EE (# 5)
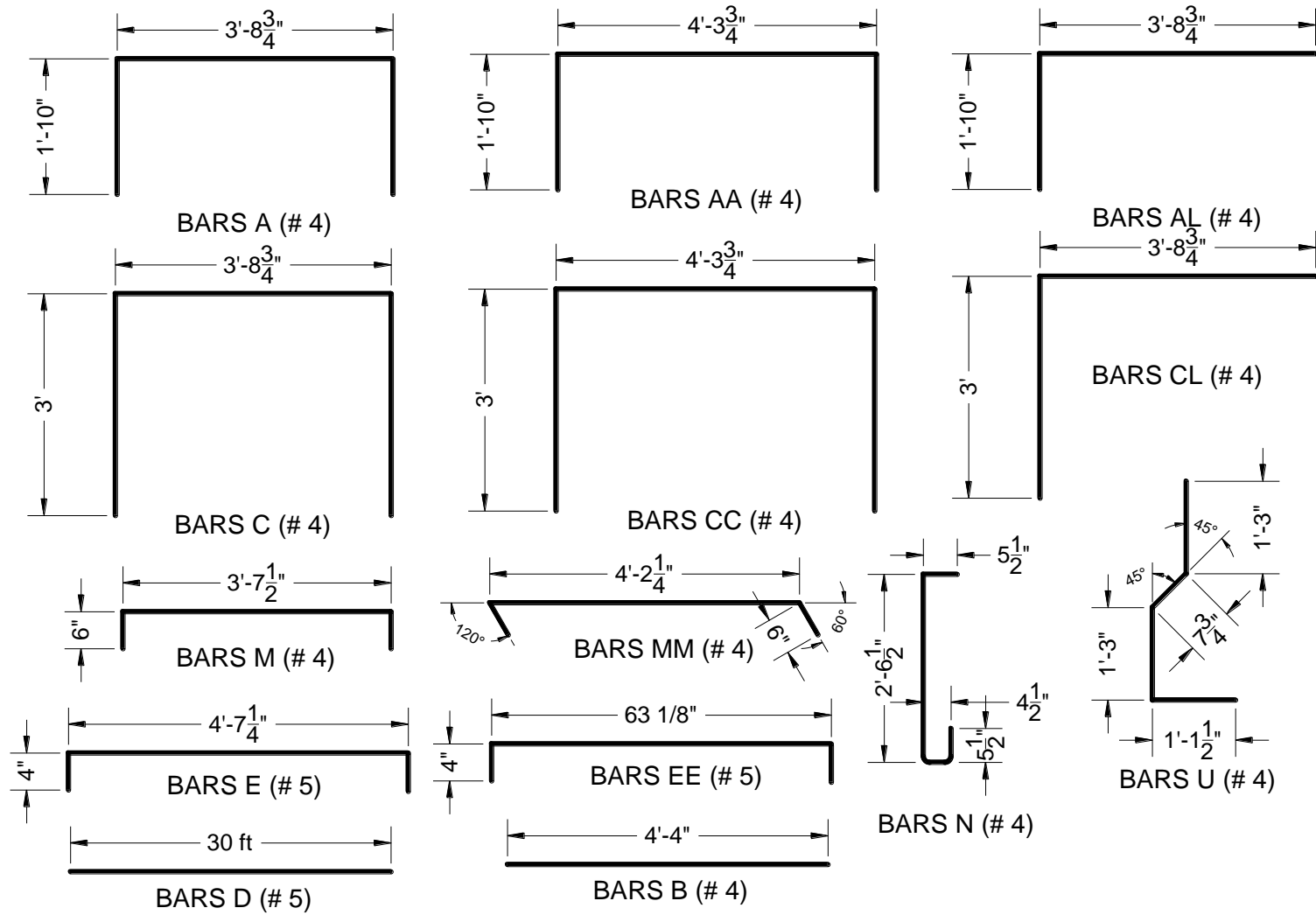
BARS D (# 5)

BARS B (# 4)

Figure B-10: Reinforcement Bars. Beams 5B40-1, 5B40-2 and 5B40-3

244

Bars A & B

1'-2"

6" Max Spa

Bars C ~ 2 1/4"

$\frac{2 \text{ ES} =}{8 \text{ 1/4}}$

3½"

39 Spaces at 6" = 19'-6"

12" Max Spa

Bars U ~ 2 1/4"

$\frac{2 \text{ ES} =}{8 \text{ 1/4}}$

3½"

12" Max Spa

Bars E ~ 2 1/4"

$\frac{2 \text{ ES} =}{8 \text{ 1/4}}$

3½"

Bars N ~ 2 1/4"

$\frac{2 \text{ ES} =}{8 \text{ 1/4}}$

Bars M ~ 6 1/2"

~4"

Bars MB & MT ~ 2 1/4"

U

M

D

E

A

C

N

U

MB

MT

B
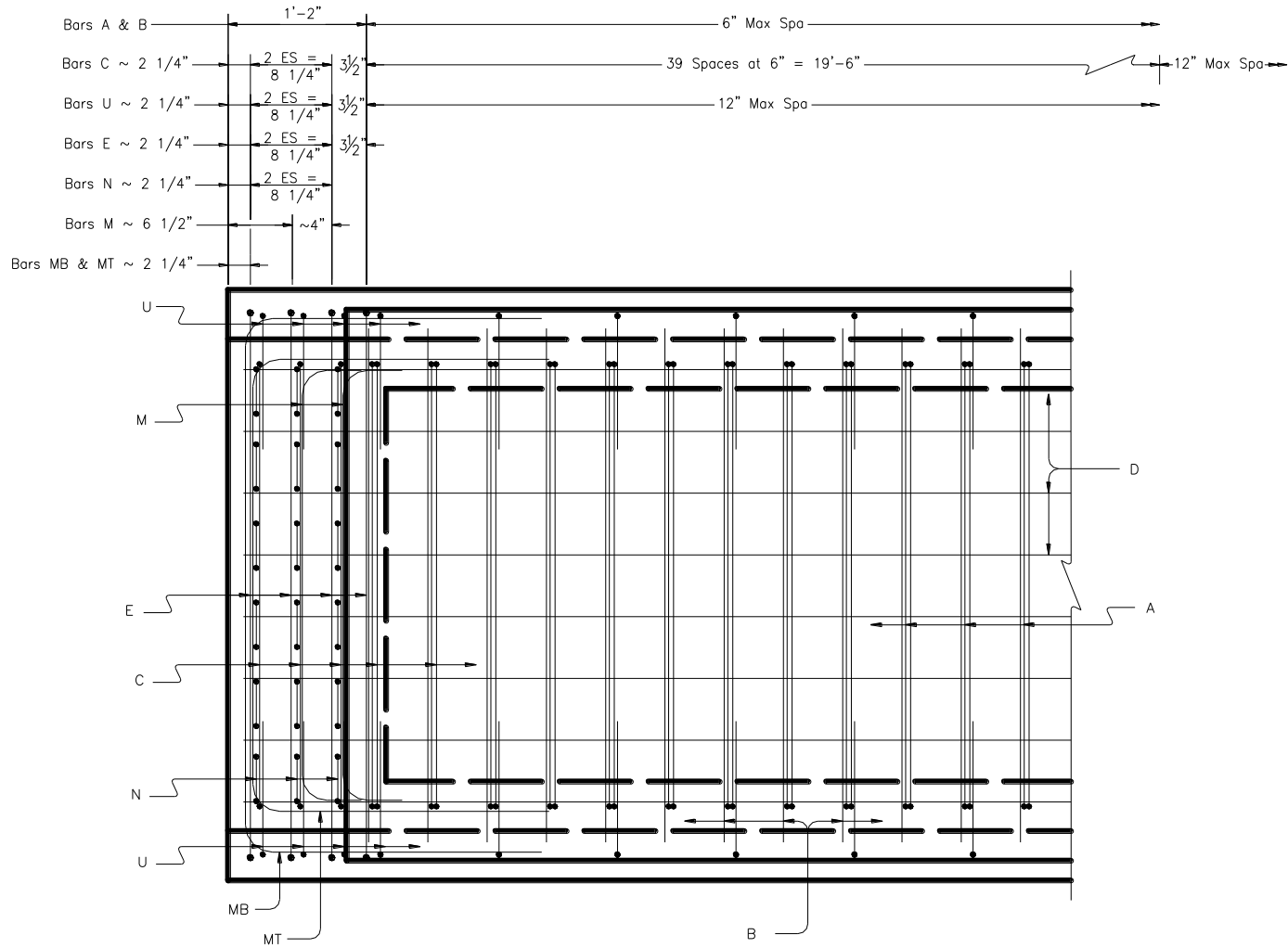
Figure B-11: Partial Plan – Square End. Beam 5B40-4
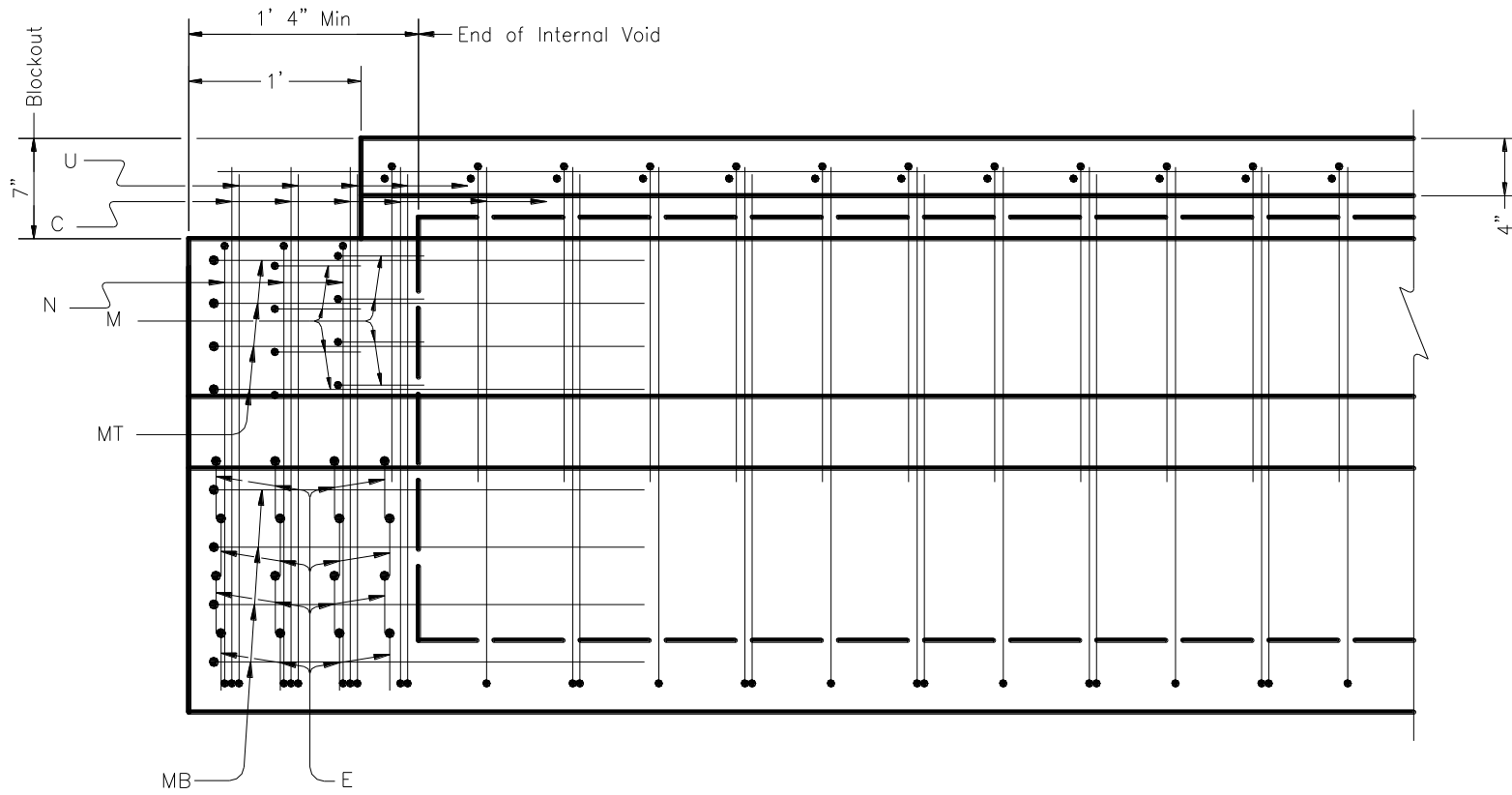
Figure B-12: Elevation – Square End. Beam 5B40-4
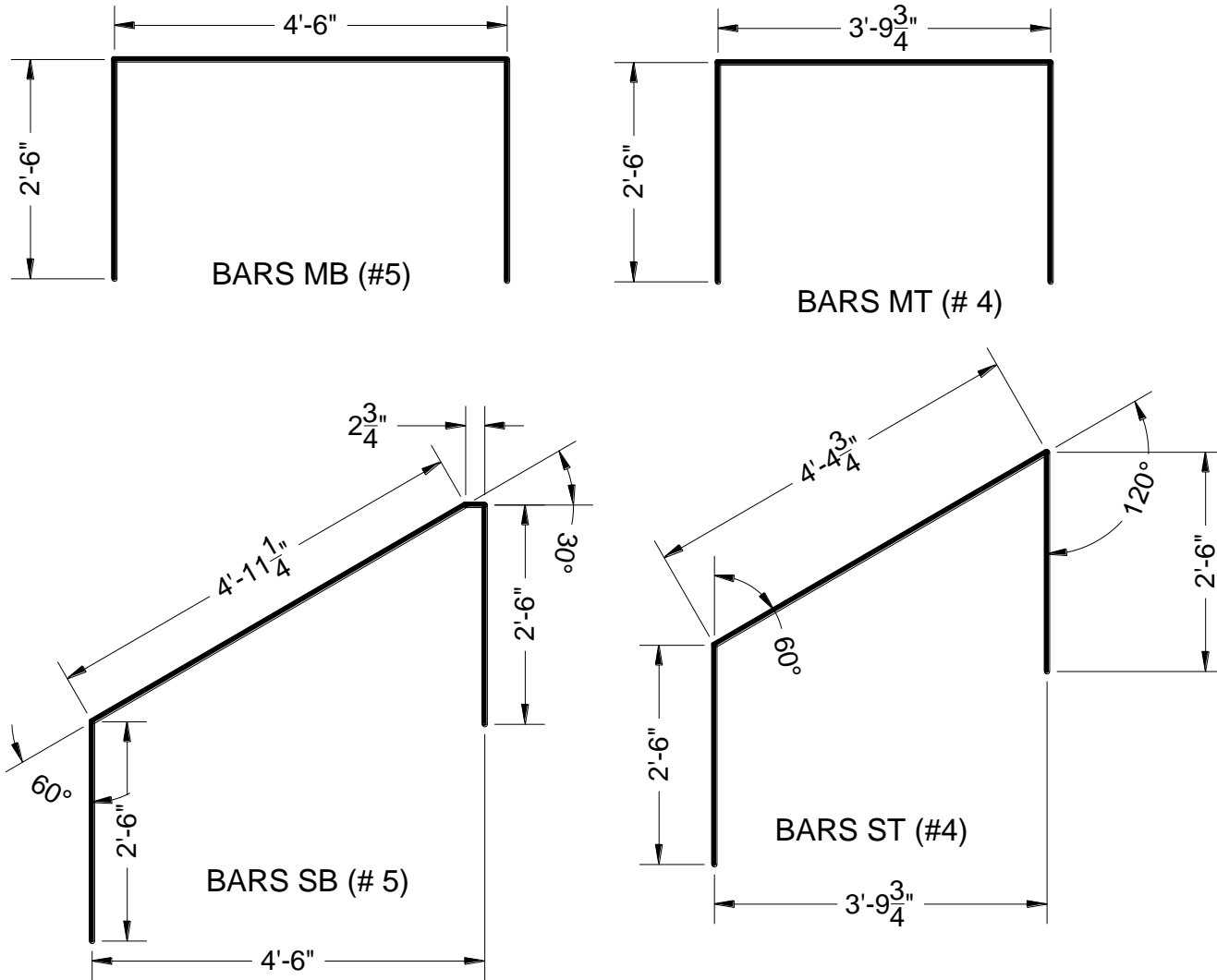
Figure B-13: New Reinforcement Bars Details. Beam 5B40-4

Figure B-14: Cross Sections. Beam 5XB40
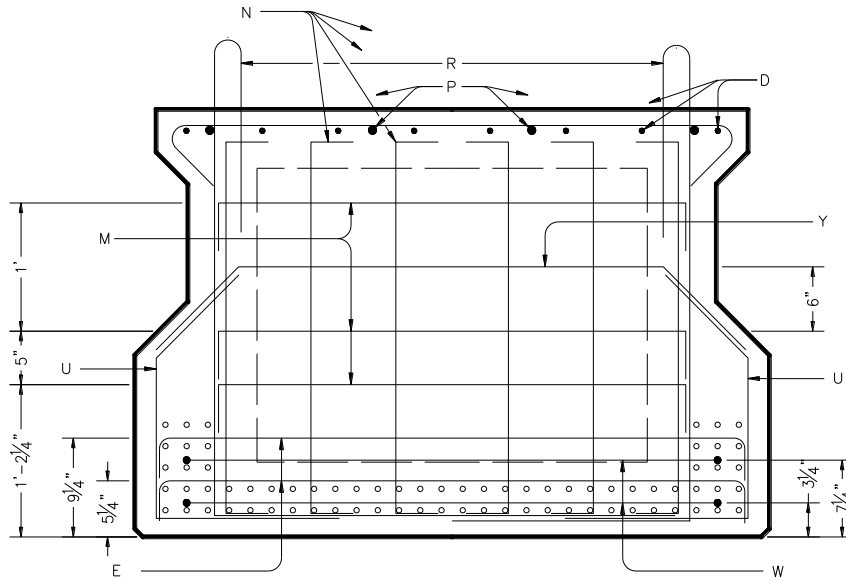
SECTION THRU BLOCKOUT ~ TYPE 5XB40
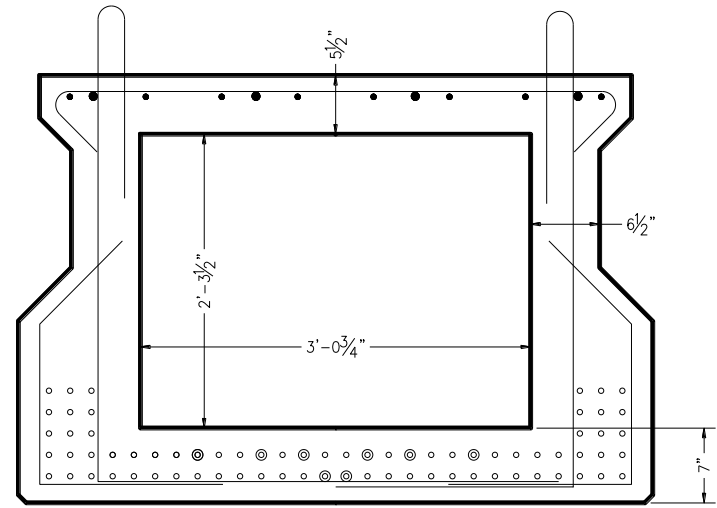
SECTION THRU MIDSPAN ~ TYPE 5XB40

(Strand Pattern throughout beam)

248
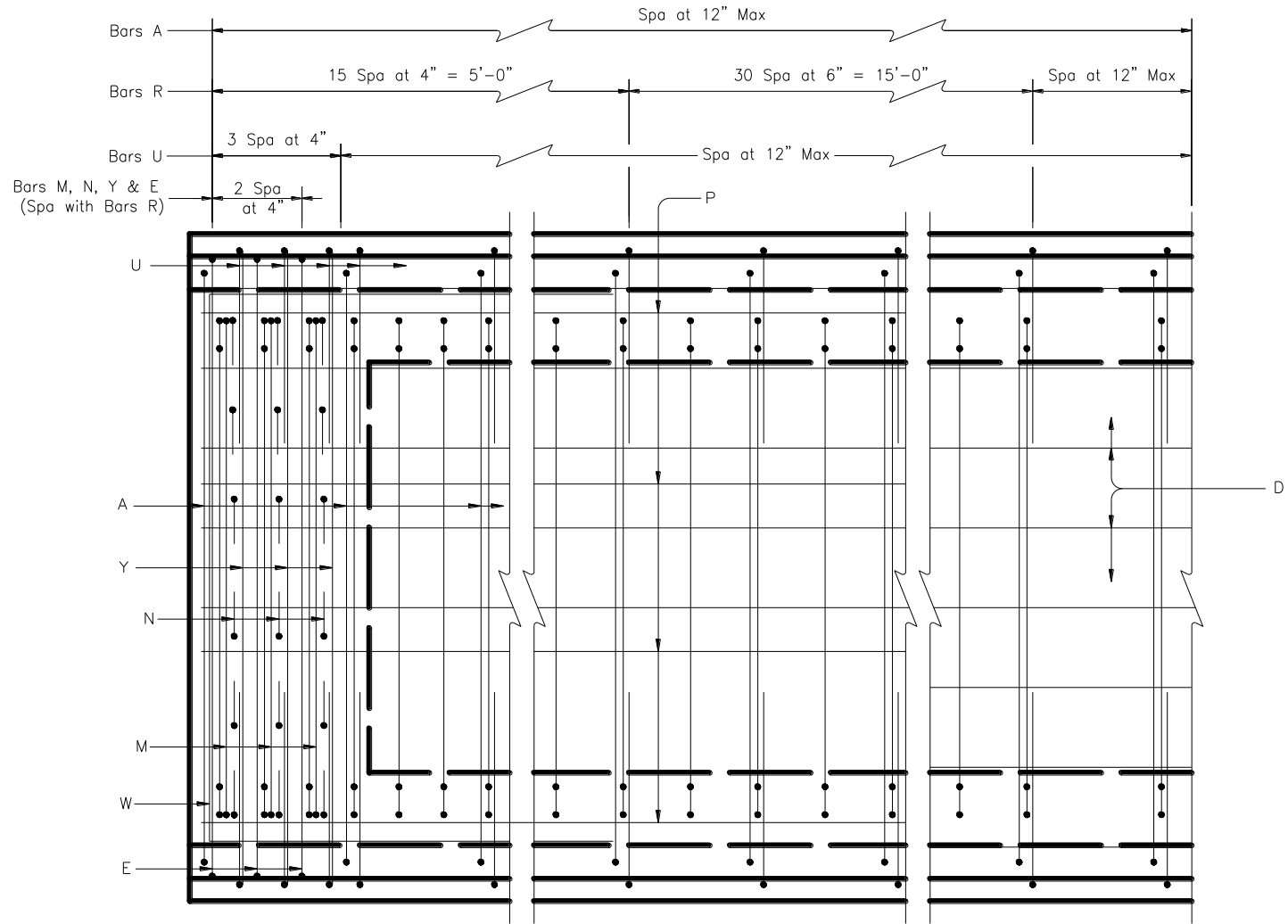
Figure B-15: Partial Plan – Square End. Beam 5XB40

Bars A

Bars R

Bars U

Bars M, N, Y & E
(Spa with Bars R)

Spa at 12" Max

15 Spa at 4" = 5'−0"   30 Spa at 6" = 15'−0"   Spa at 12" Max

3 Spa at 4"

Spa at 12" Max

2 Spa
at 4"

U

P

A

D

Y

N

M

W

E
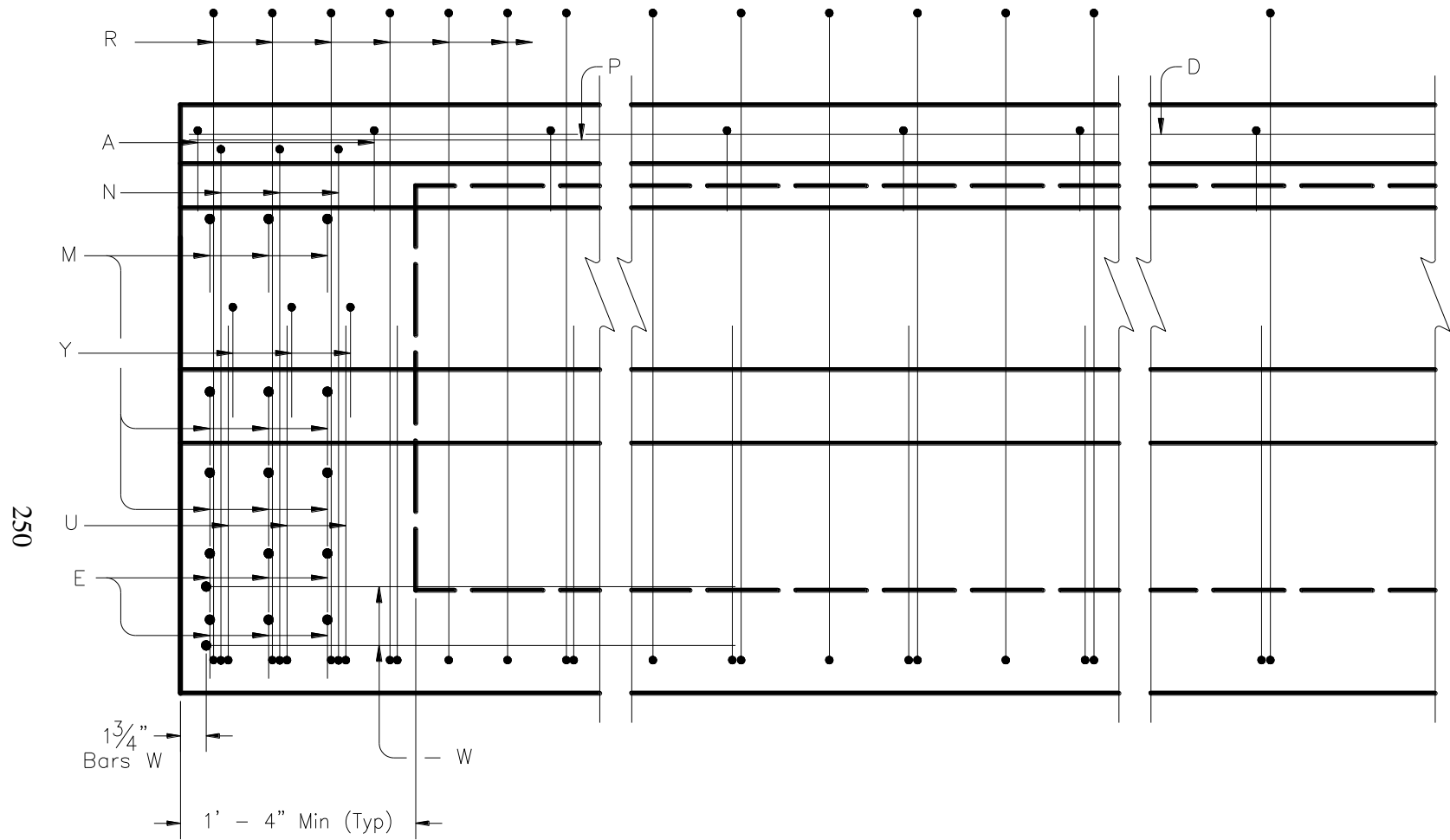
Figure B-16: Elevation – Square End. Beam 5XB40

BARS W (#5)

4'-2"

3'

BARS M (# 5)

3'-8$\frac{3}{4}$"

5"

5"

BARS N (# 4)

4"

2'-10$\frac{3}{4}$"

BARS U (#4)

45°

11"

1'-3"

1'-5$\frac{1}{4}$"

BARS Y (#5)

45°

11"

3'-4"

11"

BARS R1 AND R2 (#4)

1'-6"

3'-8$\frac{1}{2}$"

2$\frac{1}{2}$"

3'-7$\frac{1}{2}$" for Bar R1 (#4)

1'-10 1/2" for Bar R2 (#4)

251

BARS A (# 4)

4'–8¼"

4'-4$\frac{3}{4}$"

8"

45°

5¾"

BARS P (# 6)

20 ft

BARS D (# 5)

20 ft

BARS E (# 5)

4'-7$\frac{1}{4}$"

4"
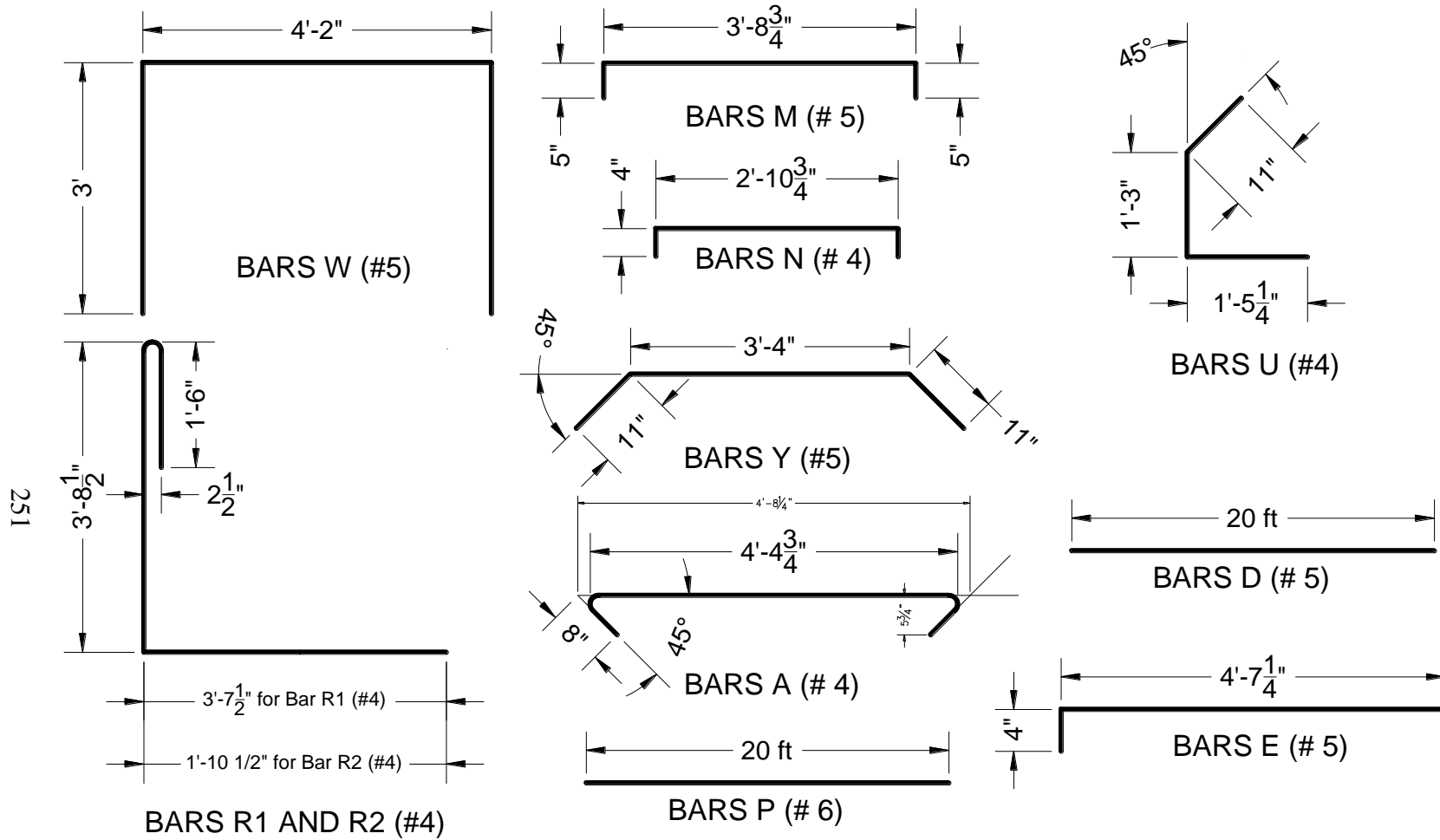
Figure B-17: Reinforcement Bars Details. Beam 5XB40

APPENDIX C

Detailed Outputs: 4B28 Box Beams

C.1 Shear-Distortion Plots
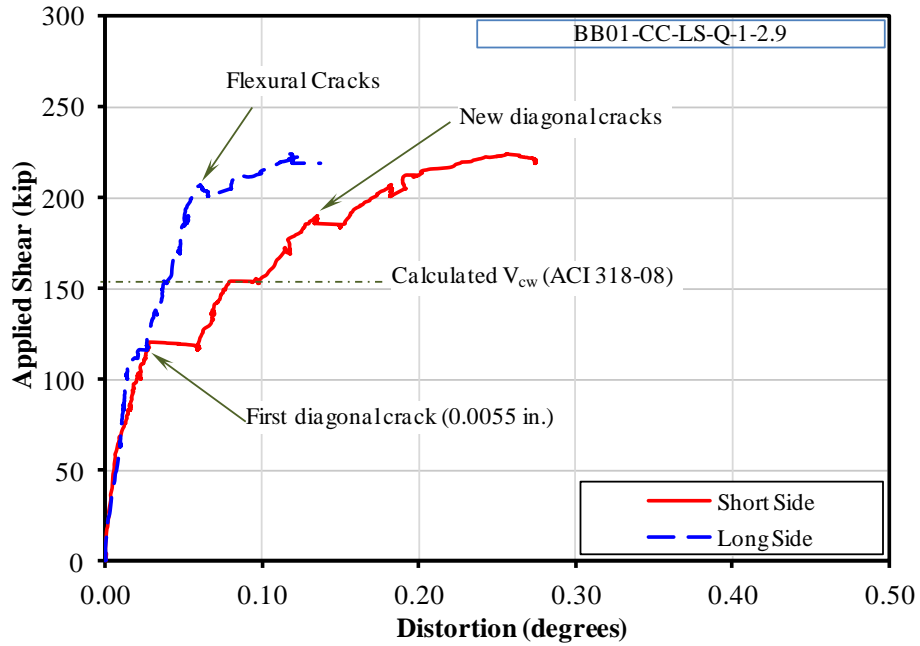
Figure C-1: Shear-distortion plot for test BB01-CC-LS-Q-1-2.9
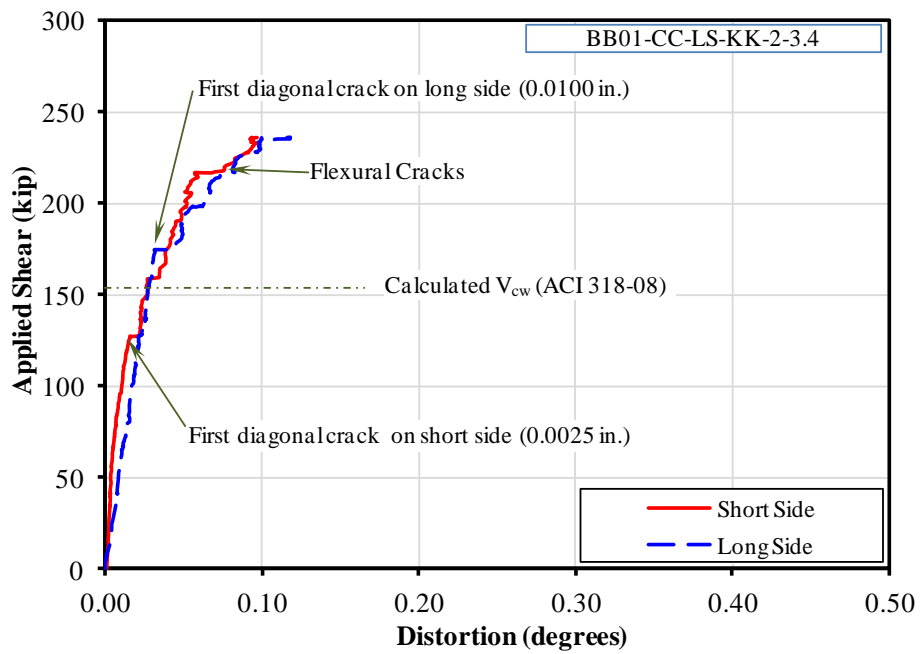
Figure C-2: Shear-distortion plot for test BB01-CC-LS-KK-2-3.4

253
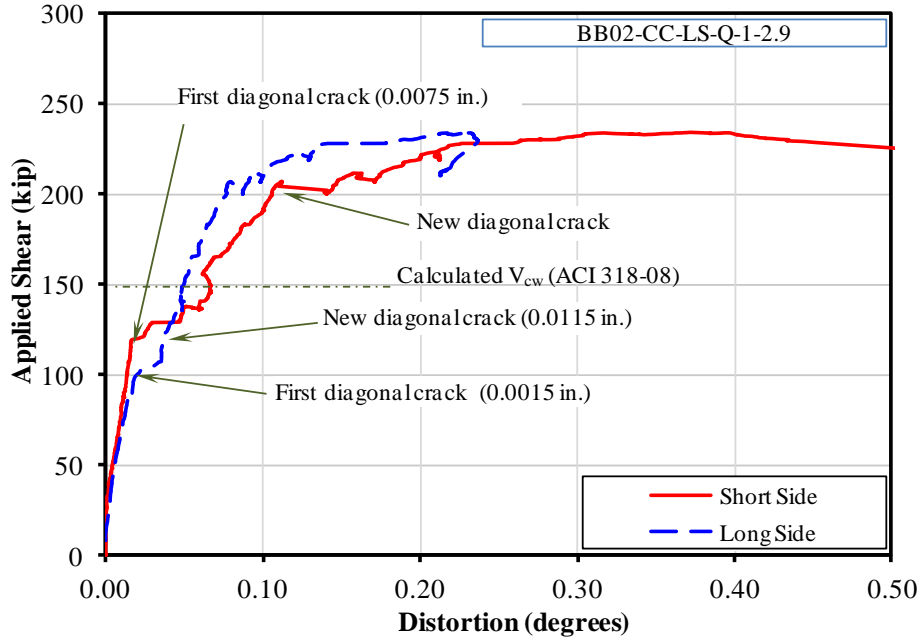
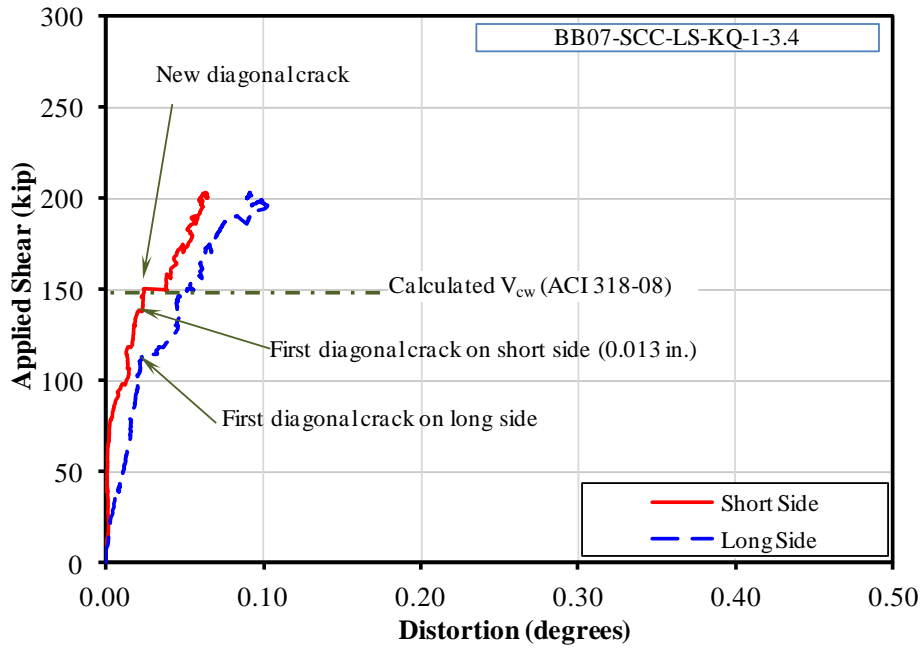**Figure C-3: Shear-distortion plot for test BB02-CC-LS-Q-1-2.9**
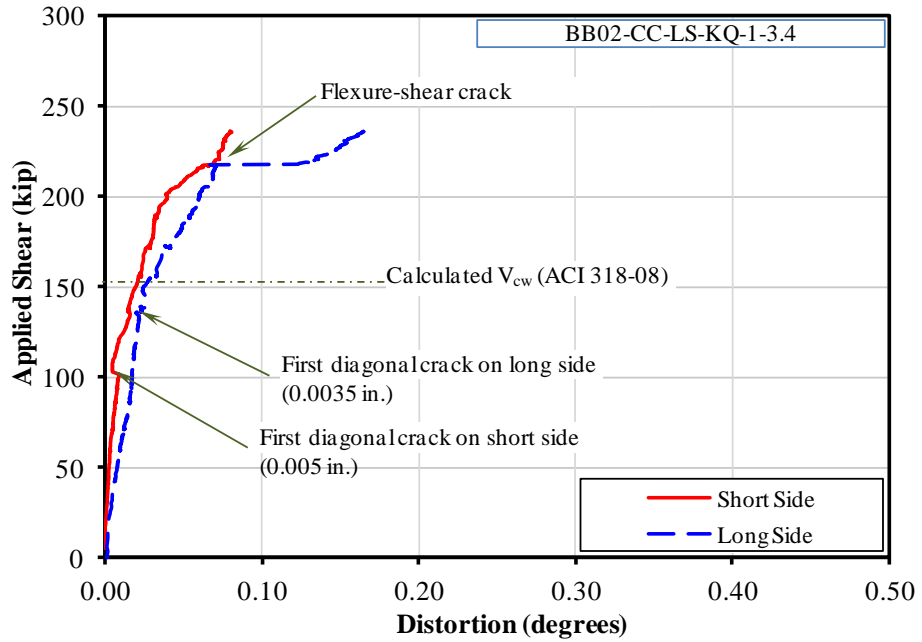
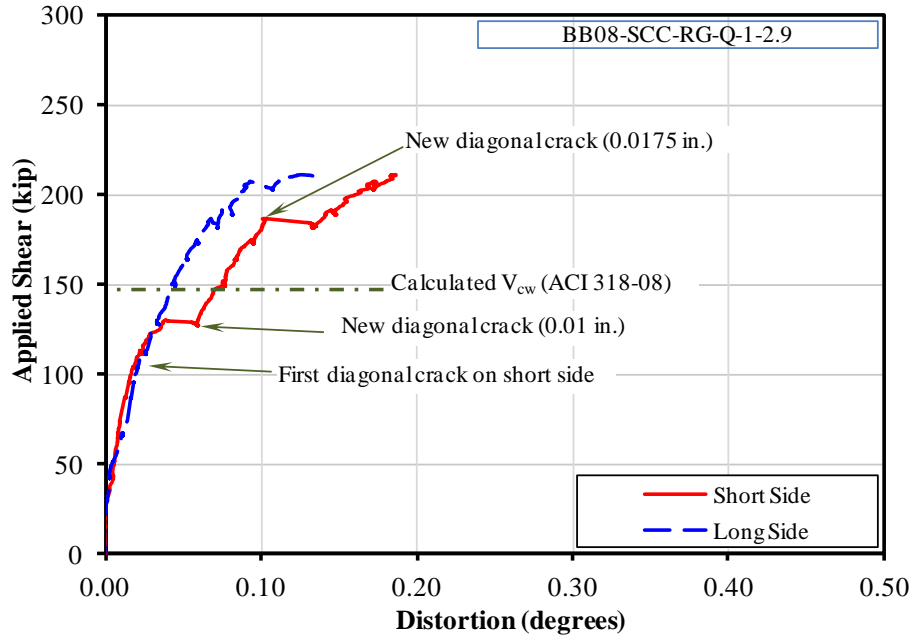**Figure C-4: Shear-distortion plot for test BB02-CC-LS-KQ-1-3.4**

254
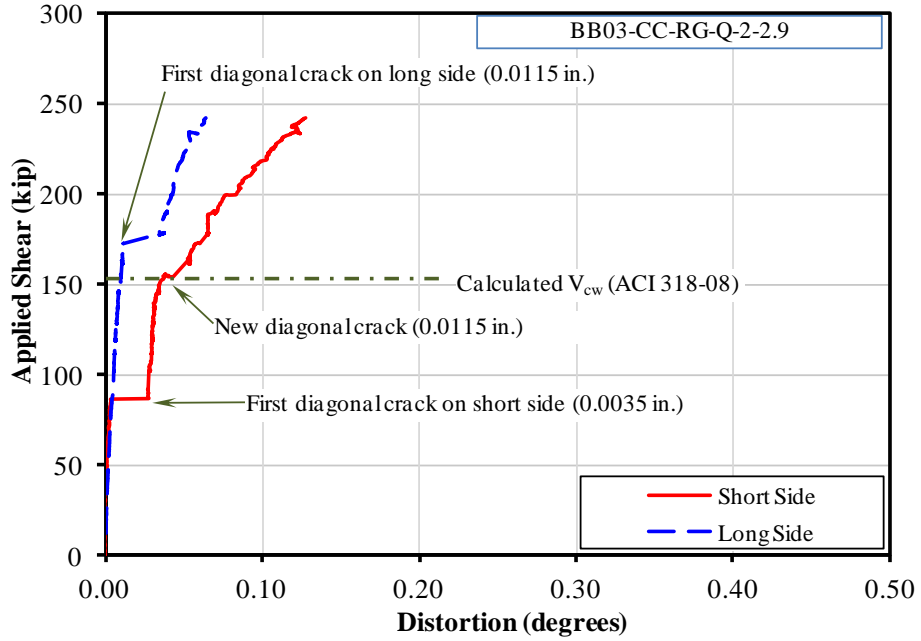
Figure C-5: Shear-distortion plot for test BB03-CC-RG-Q-2-2.9
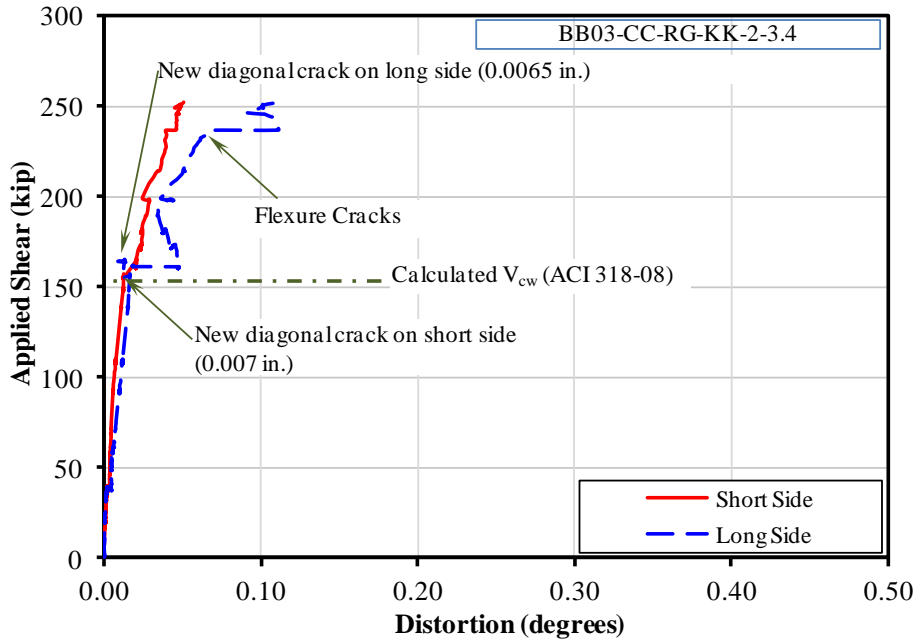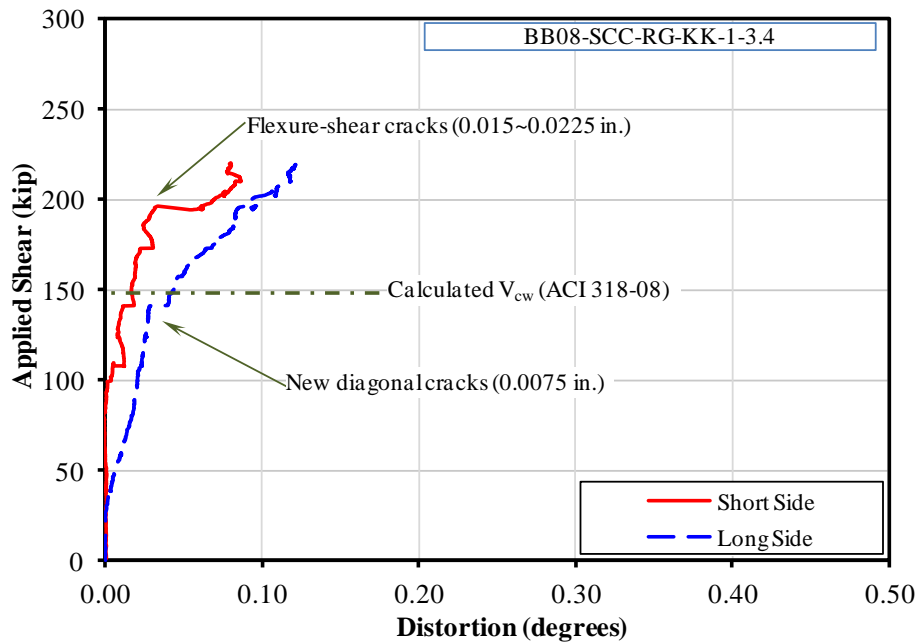

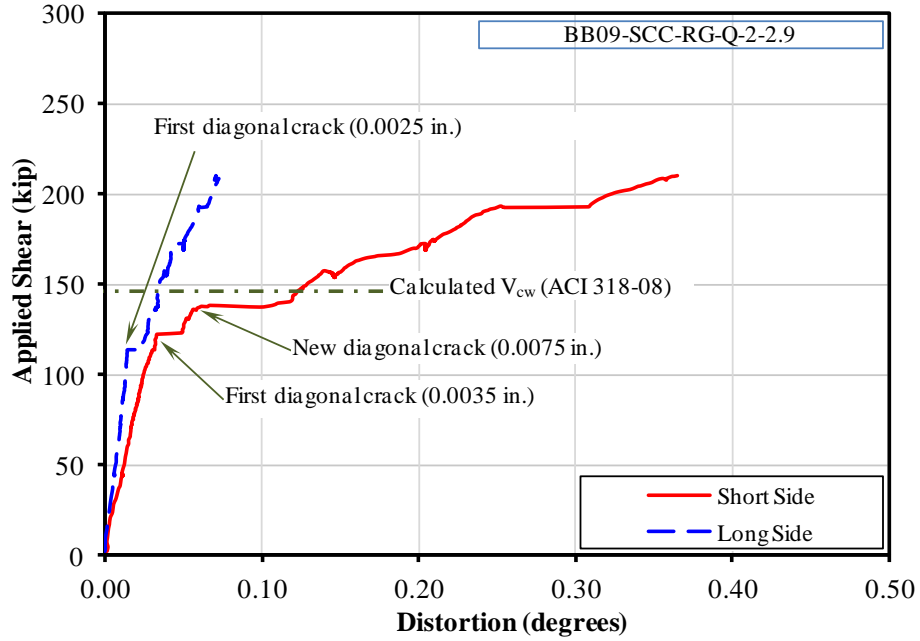**Figure C-6: Shear-distortion plot for test BB03-CC-RG-KK-2-3.4**

255
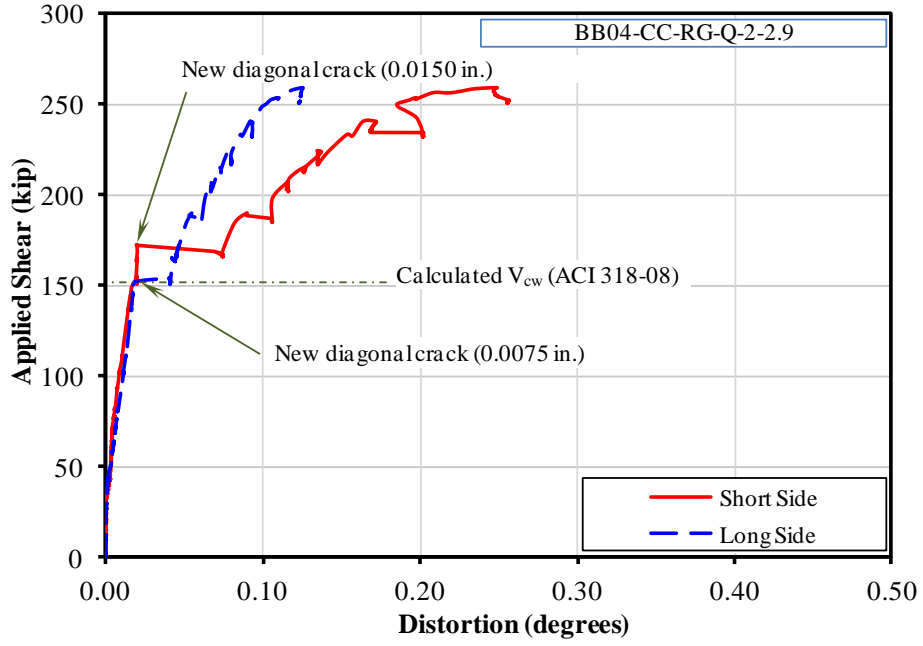
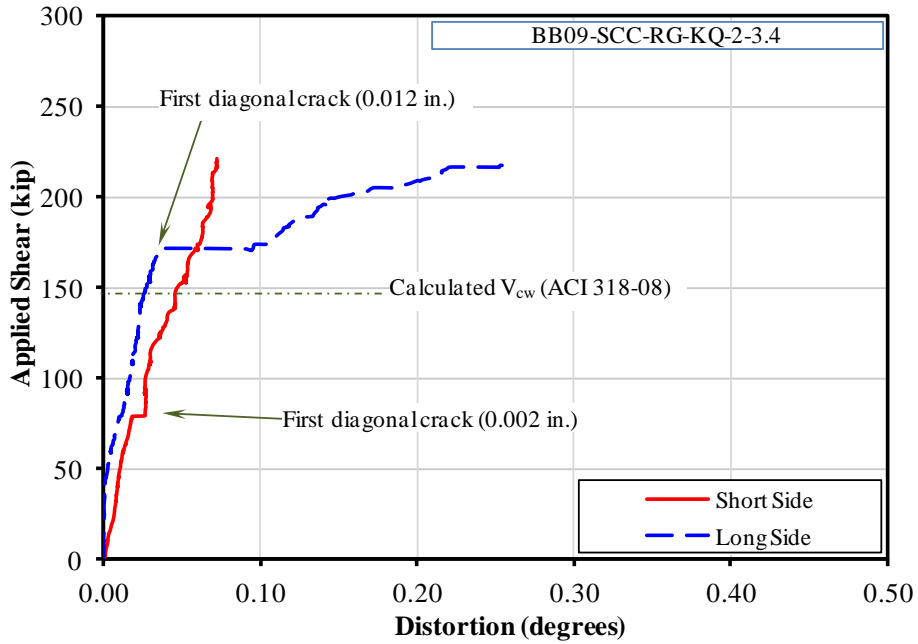**Figure C-7: Shear-distortion plot for test BB04-CC-RG-Q-2-2.9**
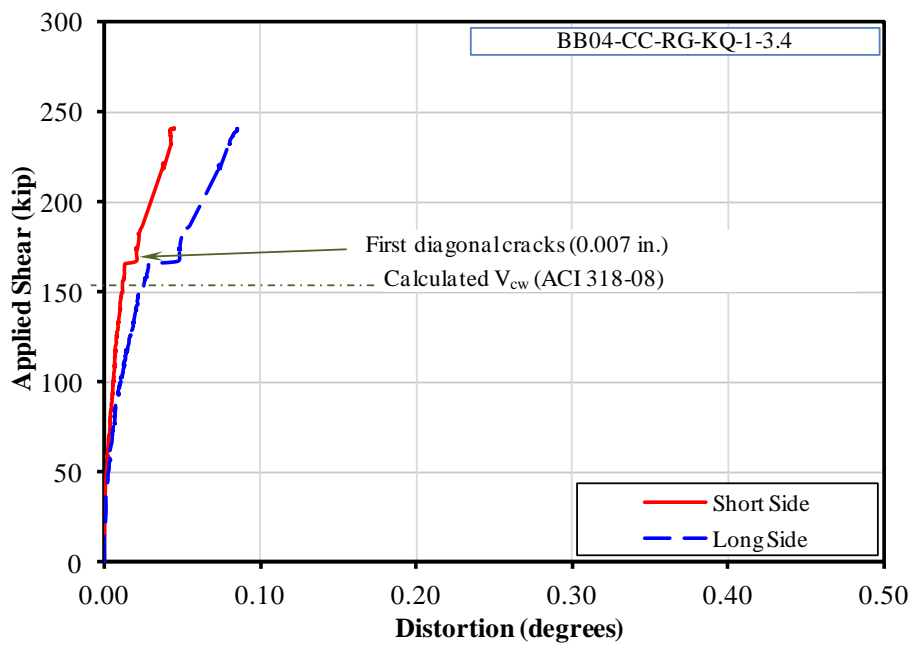
Figure C-8: Shear-distortion plot for test BB04-CC-RG-KQ-1-3.4
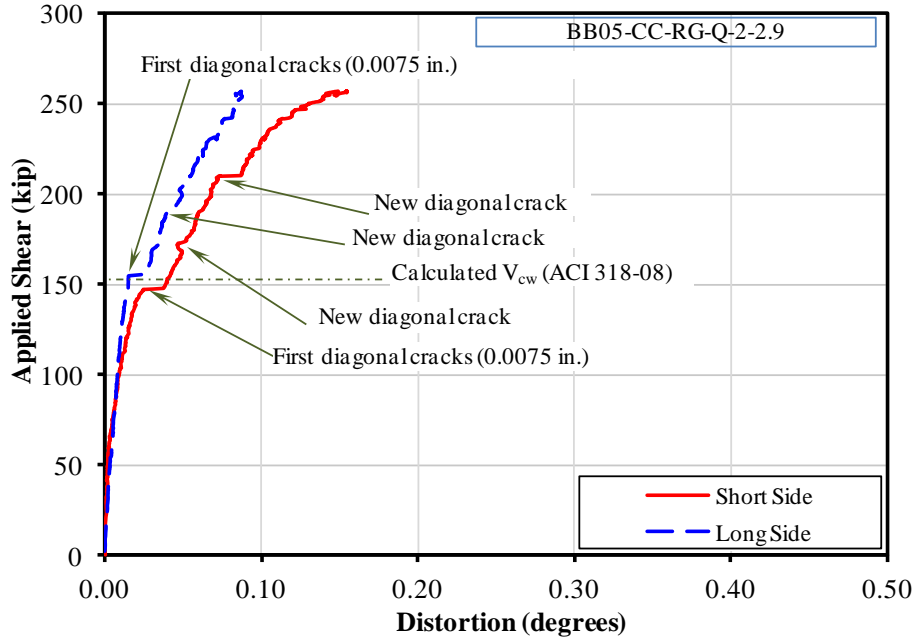
Figure C-9: Shear-distortion plot for test BB05-CC-RG-Q-2-2.9
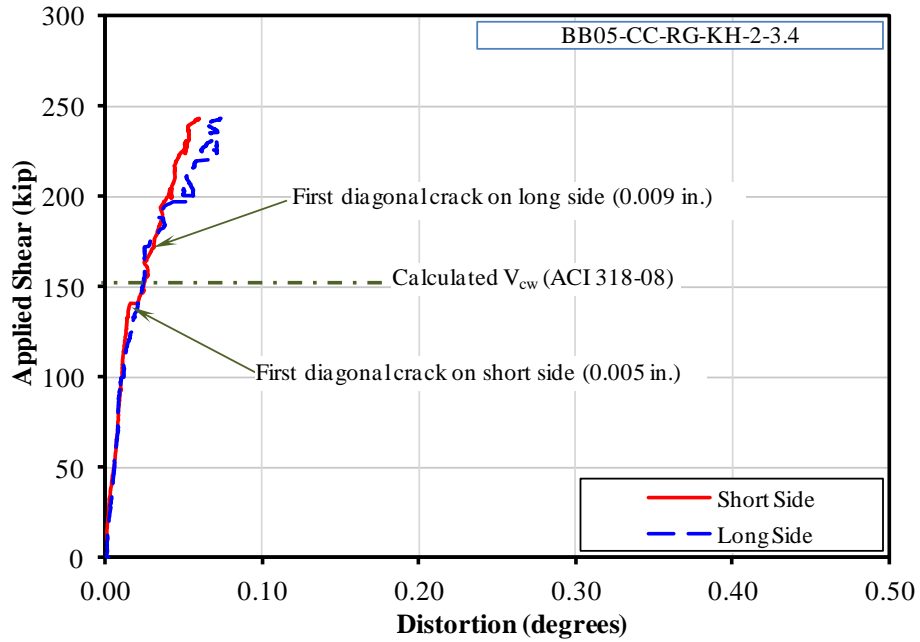
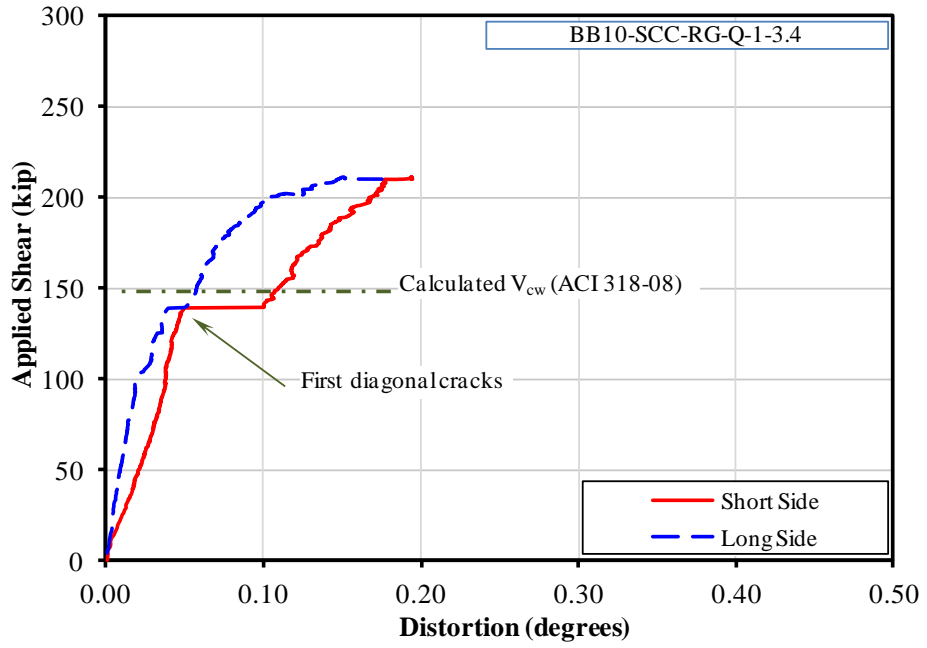**Figure C-10: Shear-distortion plot for test BB05-CC-RG-KH-2-3.4**

257
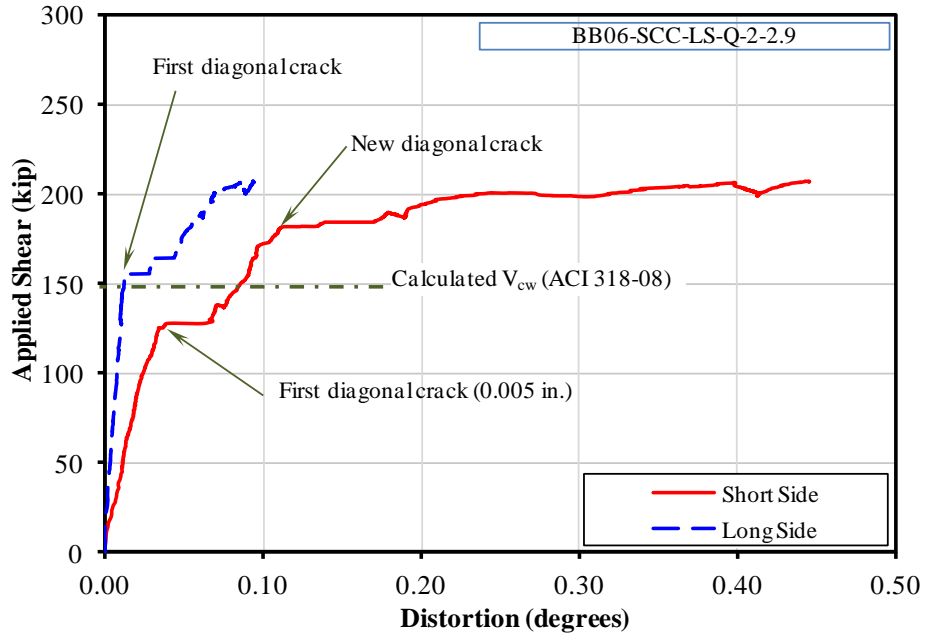
Figure C-11: Shear-distortion plot for test BB06-SCC-LS-Q-2-2.9
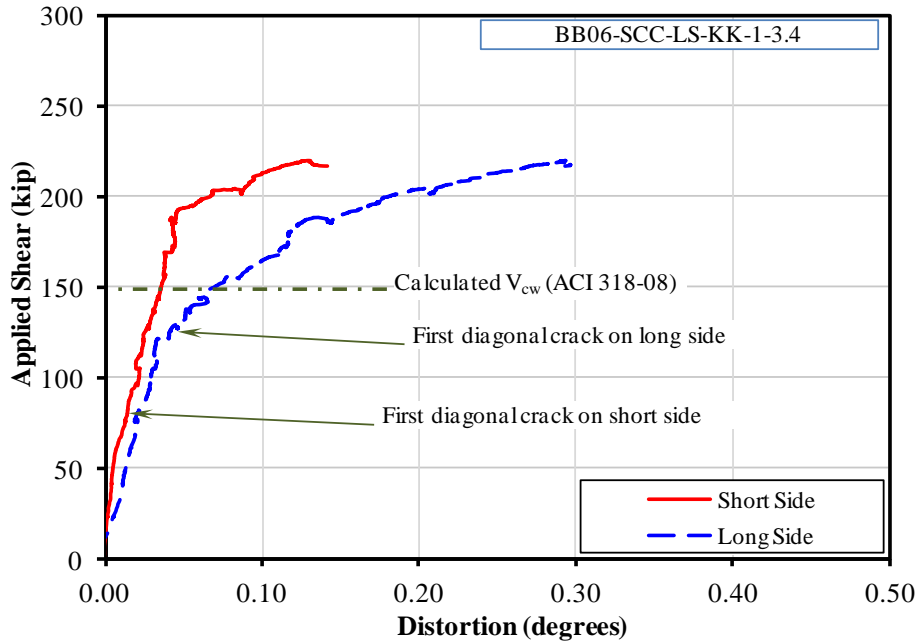
Figure C-12: Shear-distortion plot for test BB06-SCC-LS-KK-1-3.4

258
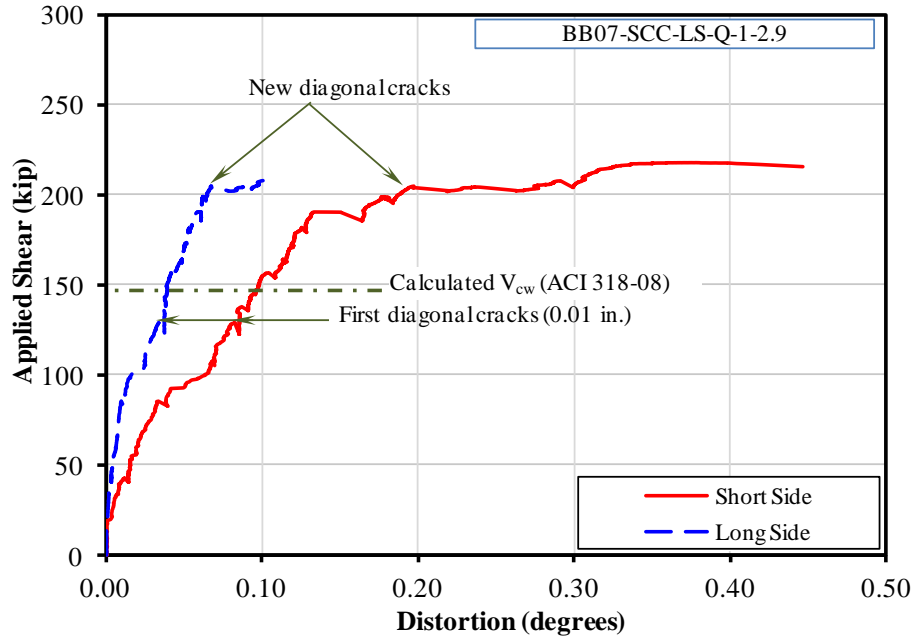
Figure C-13: Shear-distortion plot for test BB07-SCC-LS-Q-1-2.9

Figure C-14: Shear-distortion plot for test BB07-SCC-LS-KQ-1-3.4

259

Figure C-15: Shear-distortion plot for test BB08-SCC-RG-Q-1-2.9

Figure C-16: Shear-distortion plot for test BB08-SCC-RG-KK-1-3.4

Figure C-17: Shear-distortion plot for test BB09-SCC-RG-Q-2-2.9

Figure C-18: Shear-distortion plot for test BB09-SCC-RG-KQ-2-3.4

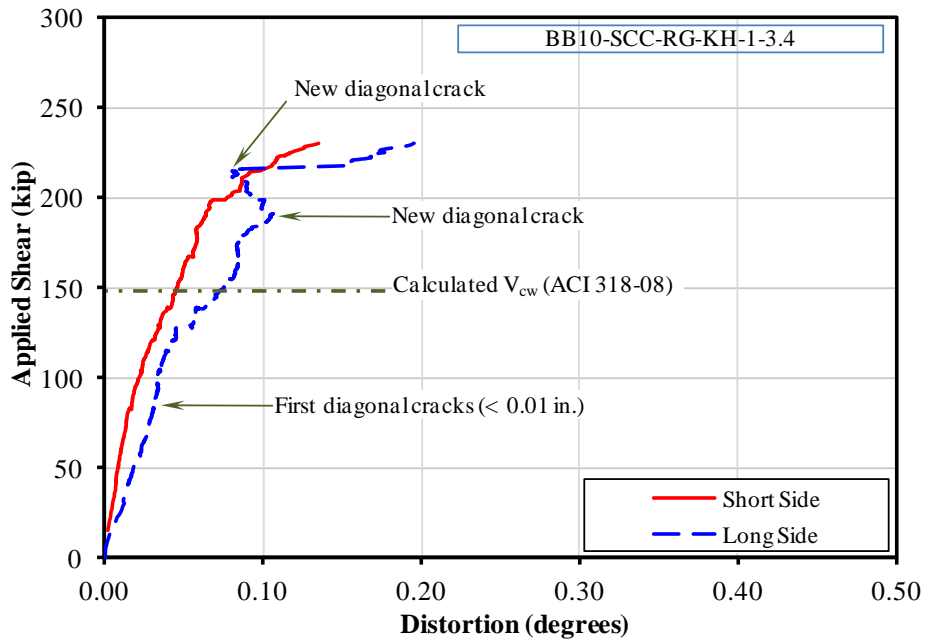**Figure C-19: Shear-distortion plot for test BB10-SCC-RG-Q-1-3.4**

Figure C-20: Shear-distortion plot for test BB10-SCC-RG-KH-1-3.4
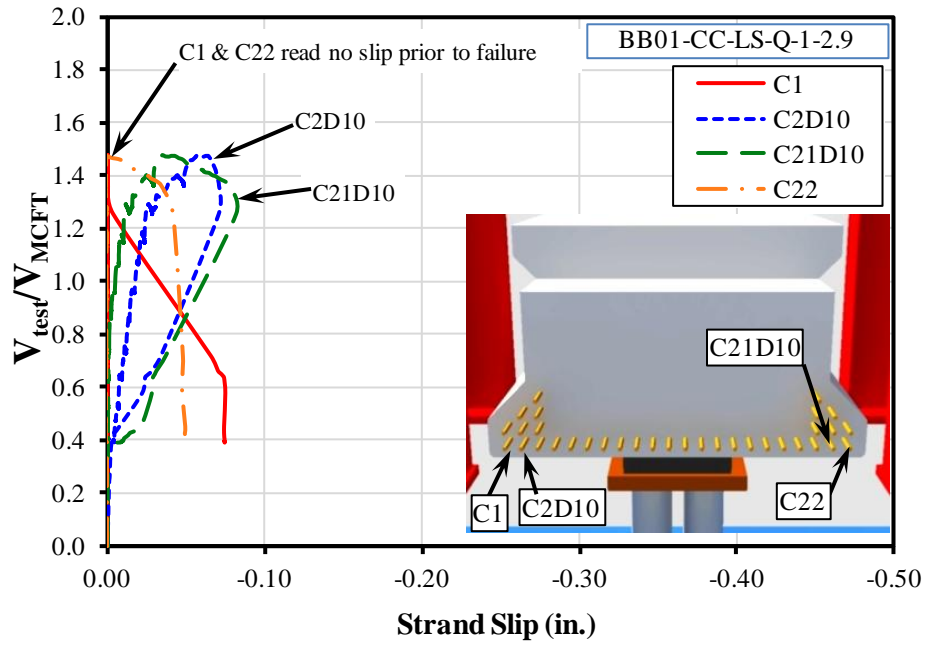
C.2 Strand Slip Plots

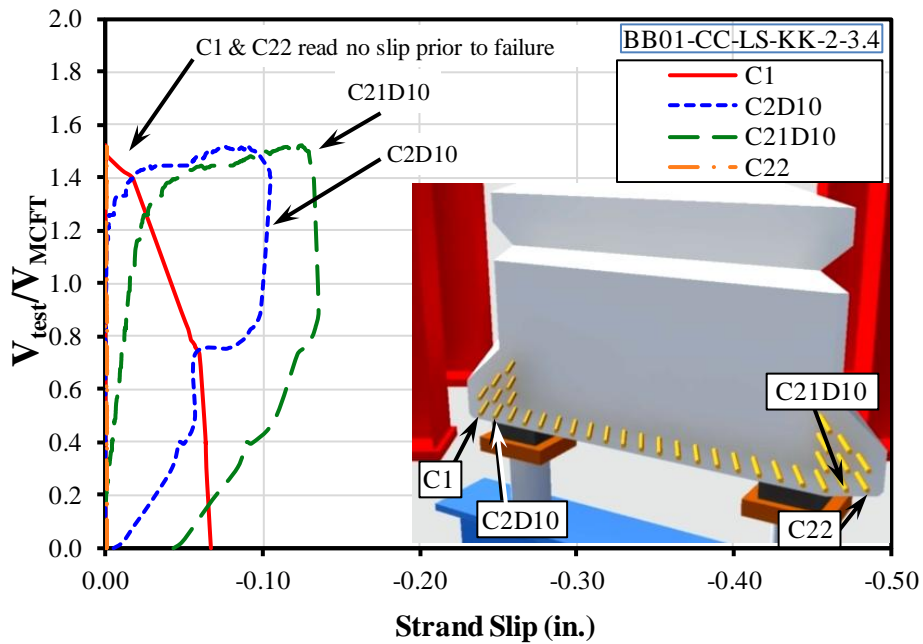**Figure C-21: Strand slip plot for test BB01-CC-LS-Q-1-2.9**

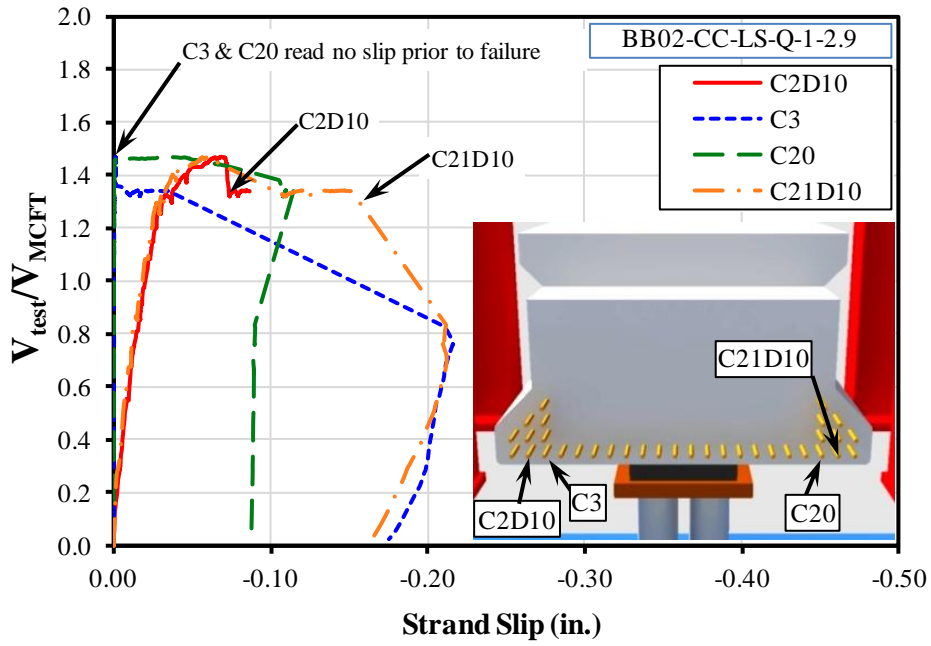**Figure C-22: Strand slip plot for test BB01-CC-LS-KK-2-3.4**

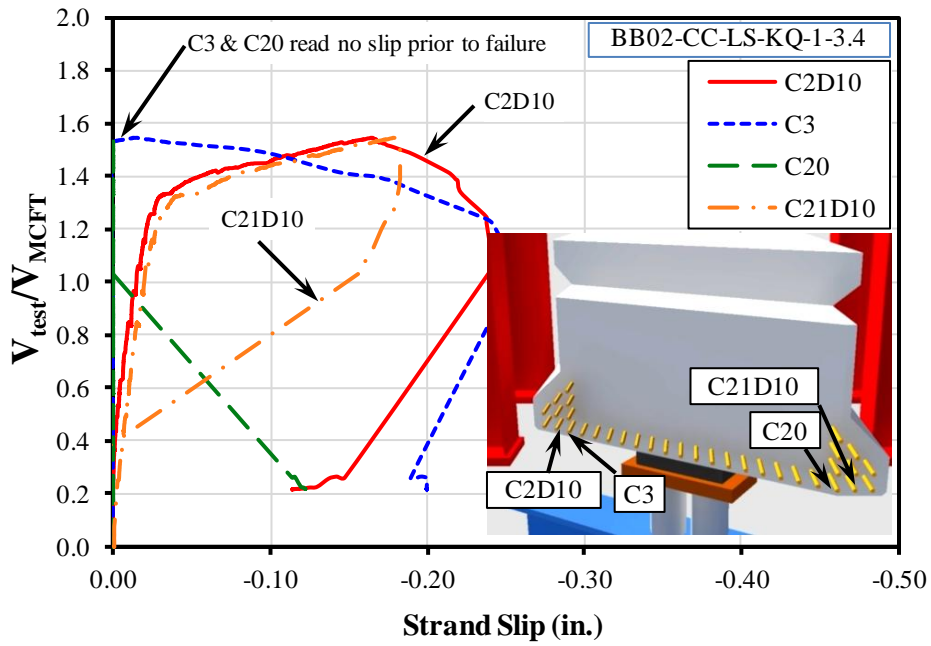**Figure C-23: Strand slip plot for test BB02-CC-LS-Q-1-2.9**

Figure C-24: Strand slip plot for test BB02-CC-LS-KQ-1-3.4
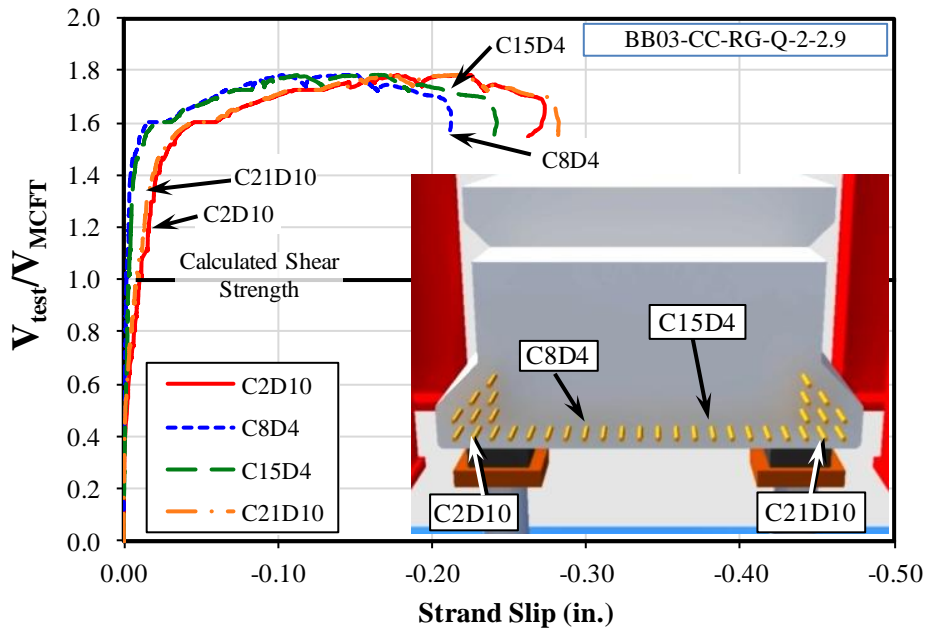
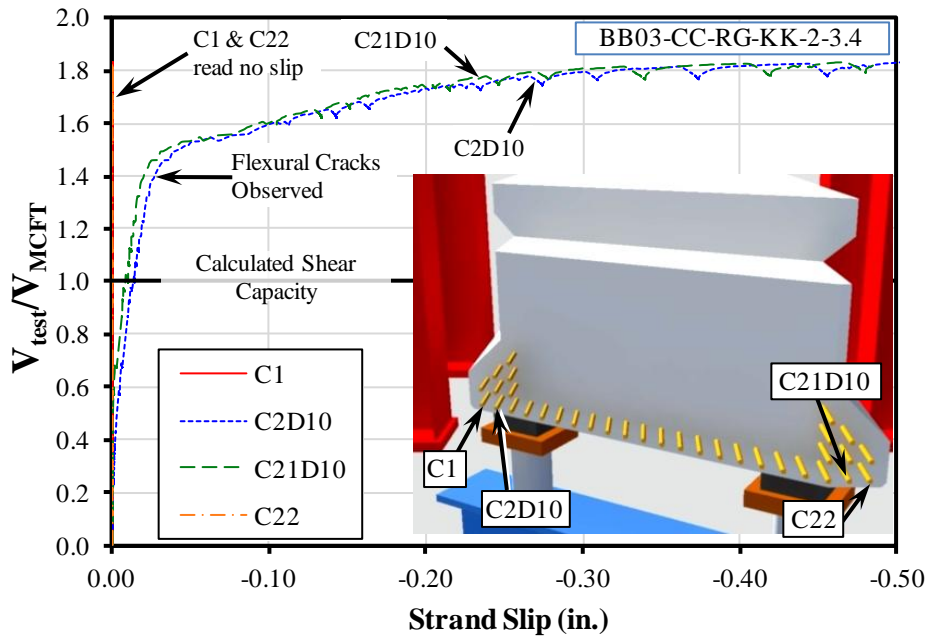**Figure C-25: Strand slip plot for test BB03-CC-RG-Q-2-2.9**

Figure C-26: Strand slip plot for test BB03-CC-RG-KK-2-3.4

Figure C-27: Strand slip plot for test BB04-CC-RG-Q-2-2.9

Figure C-28: Strand slip plot for test BB04-CC-RG-KQ-1-3.4

Figure C-29: Strand slip plot for test BB05-CC-RG-Q-2-2.9

Figure C-30: Strand slip plot for test BB05-CC-RG-KH-2-3.4

267
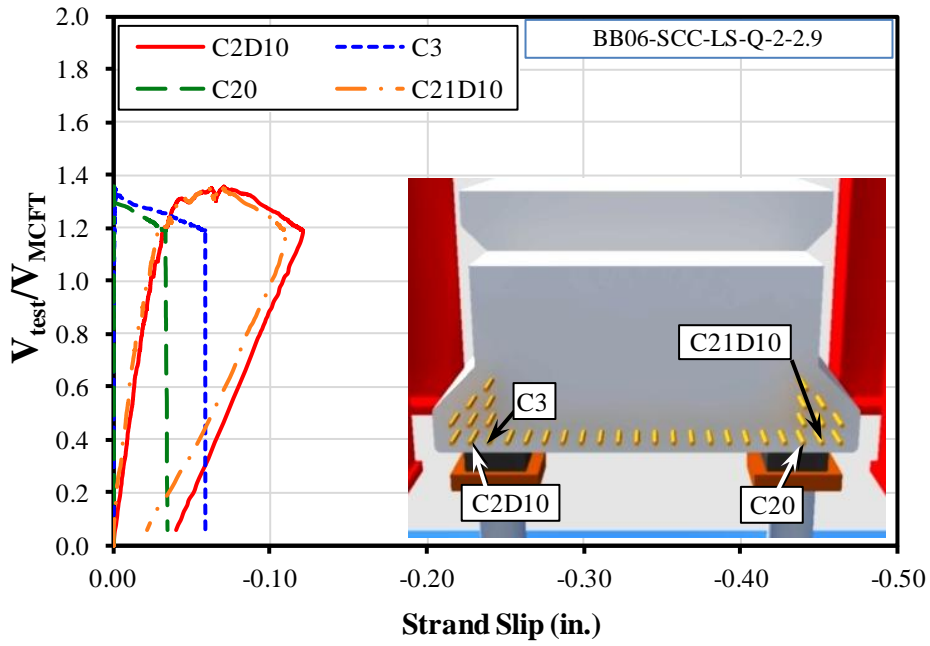
Figure C-31: Strand slip plot for test BB06-SCC-LS-Q-2-2.9
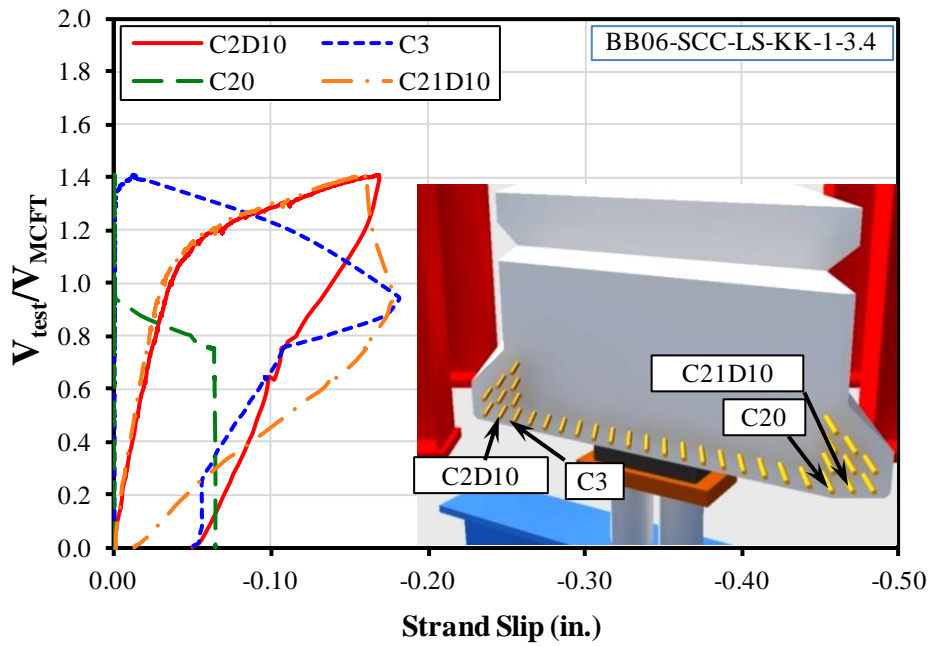
Figure C-32: Strand slip plot for test BB06-SCC-LS-KK-1-3.4

268
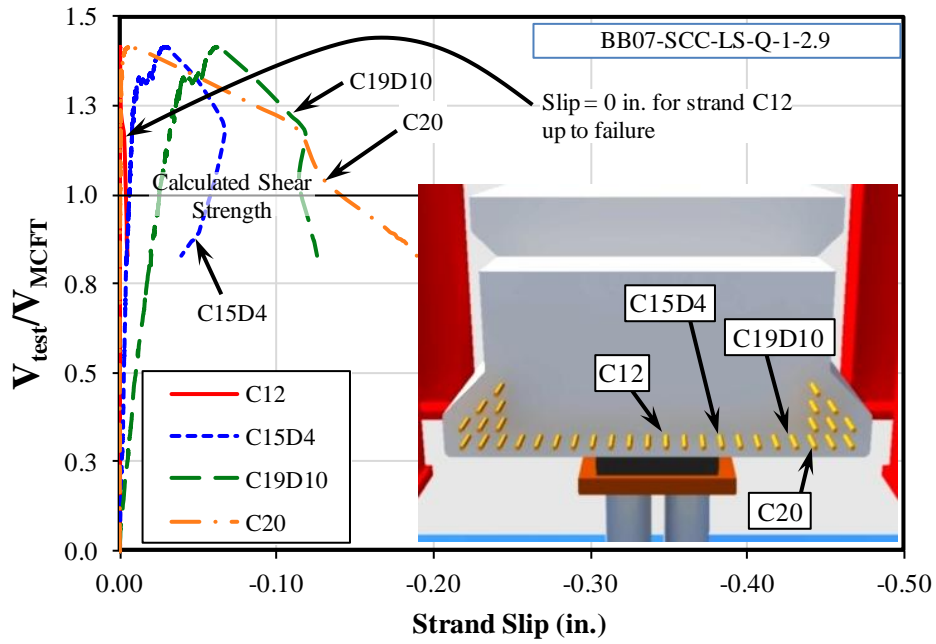
Figure C-33: Strand slip plot for test BB07-SCC-LS-Q-1-2.9
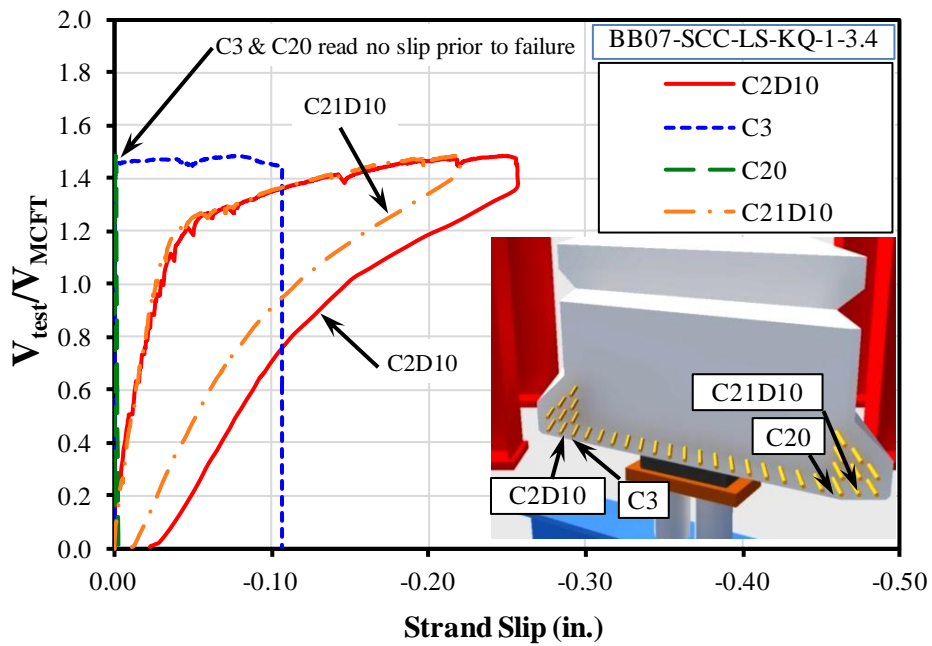
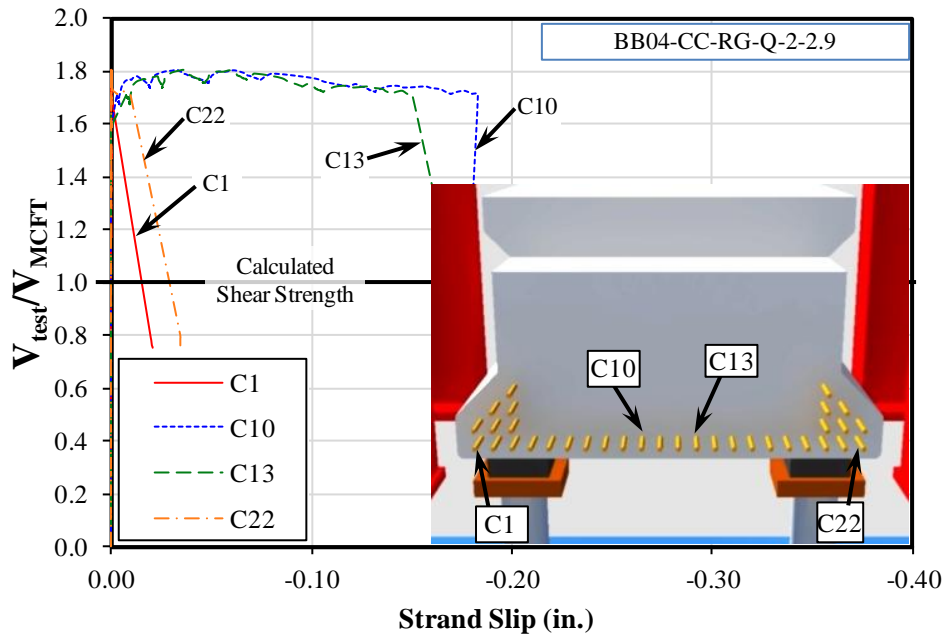**Figure C-34: Strand slip plot for test BB07-SCC-LS-KQ-1-3.4**

269
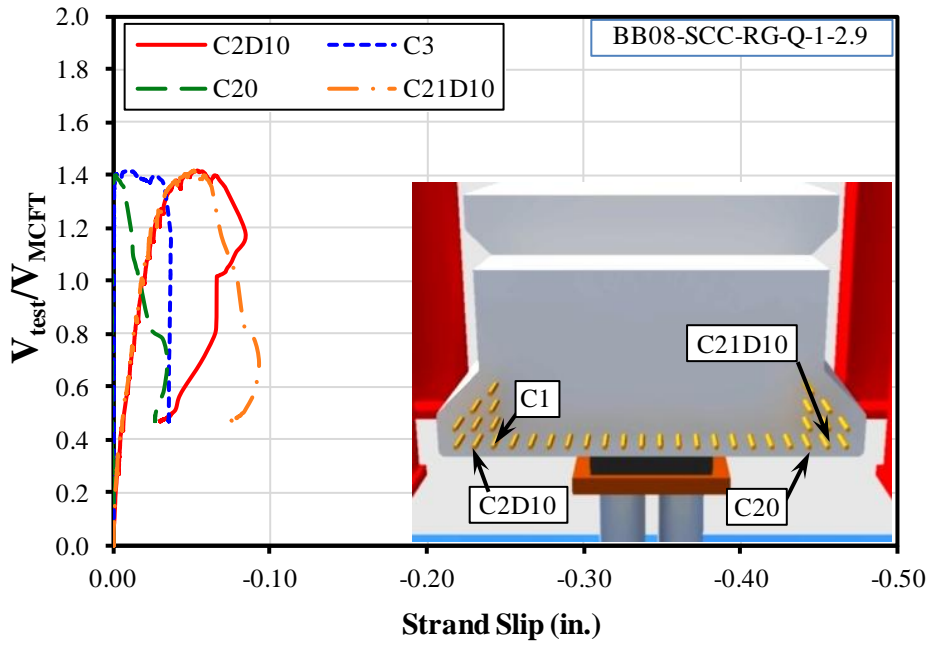
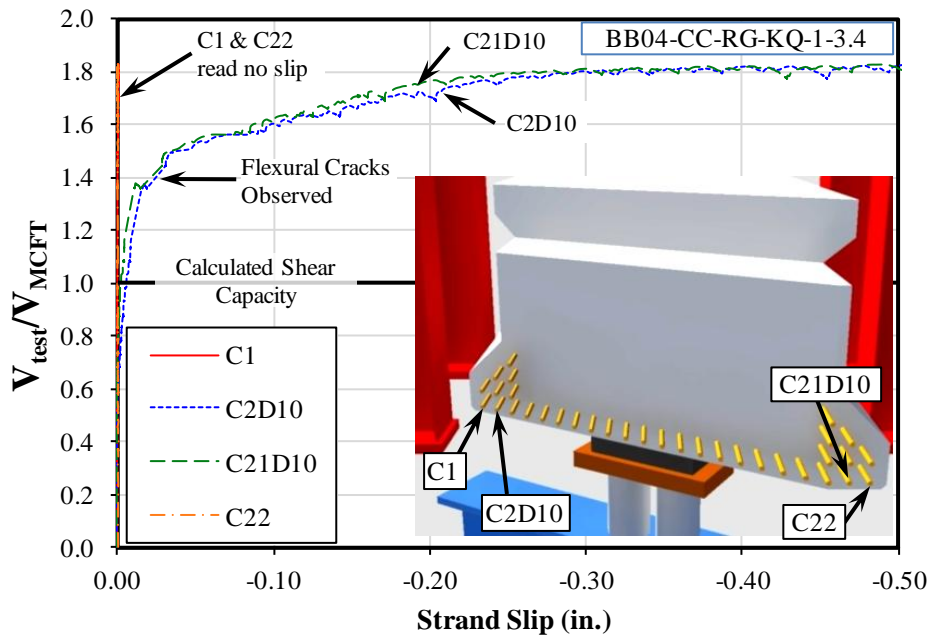**Figure C-35: Strand slip plot for test BB08-SCC-RG-Q-1-2.9**
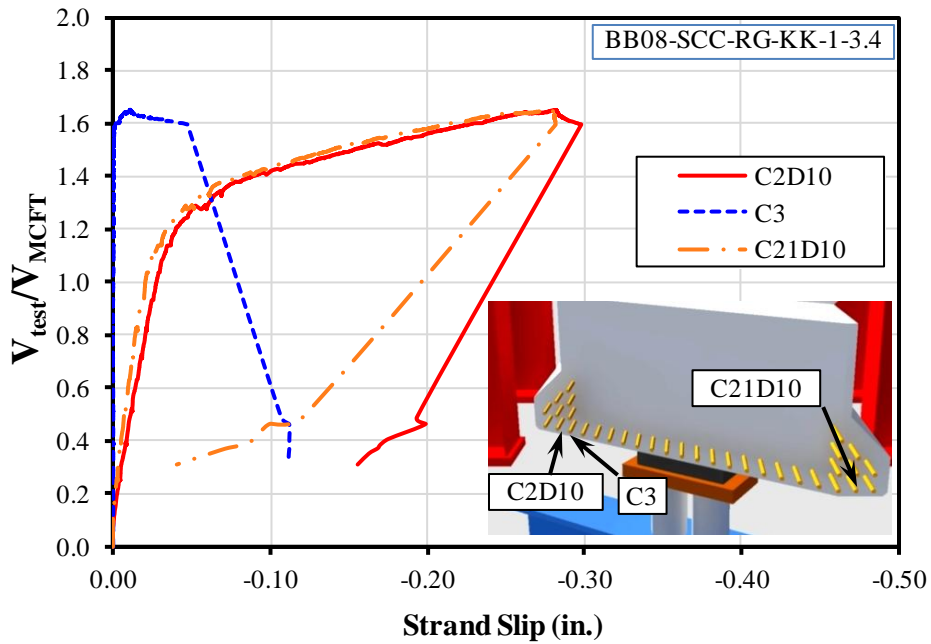
Figure C-36: Strand slip plot for test BB08-SCC-RG-KK-1-3.4
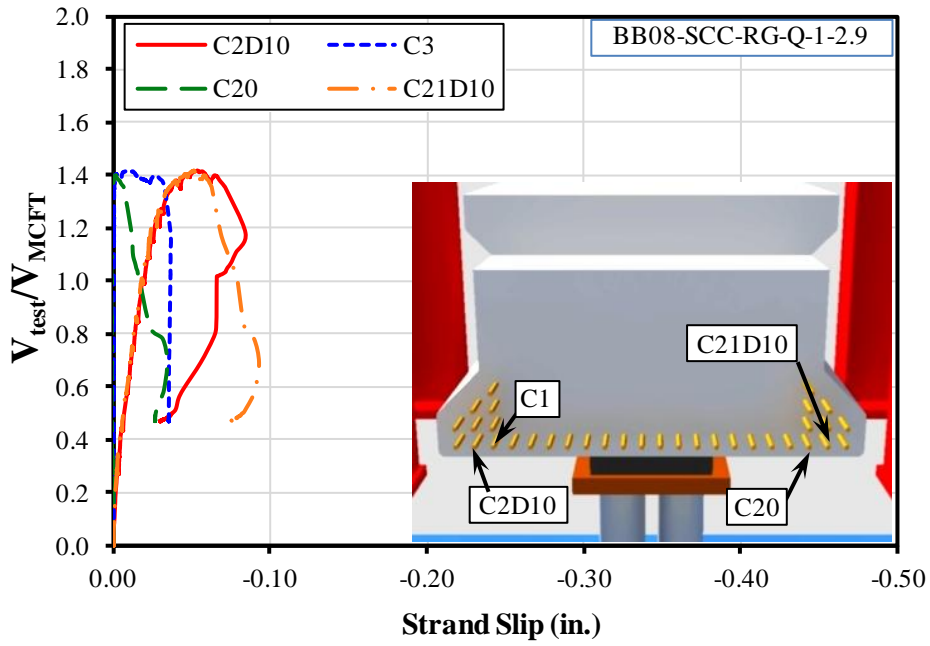
Figure C-37: Strand slip plot for test BB09-SCC-RG-Q-2-2.9
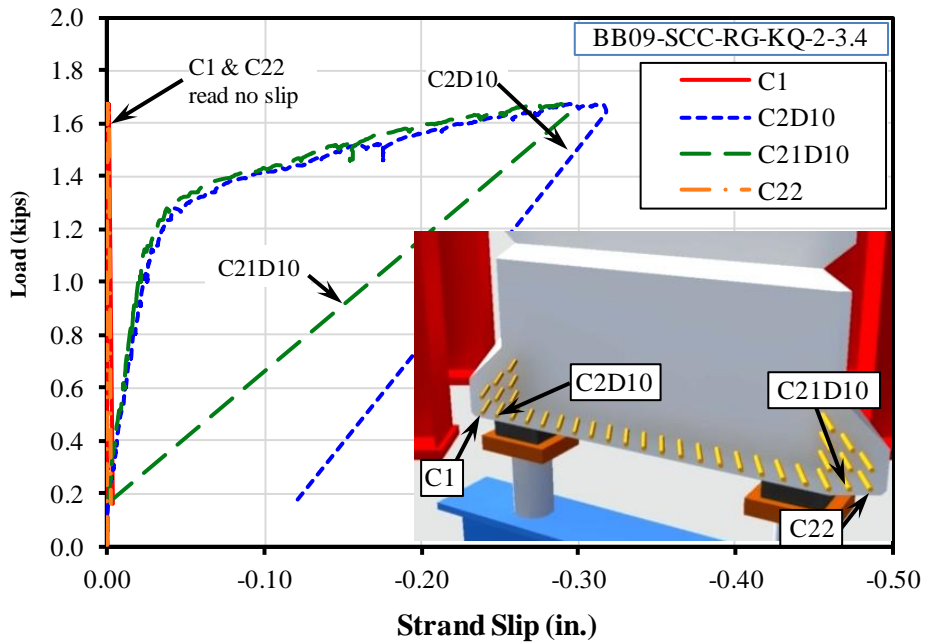
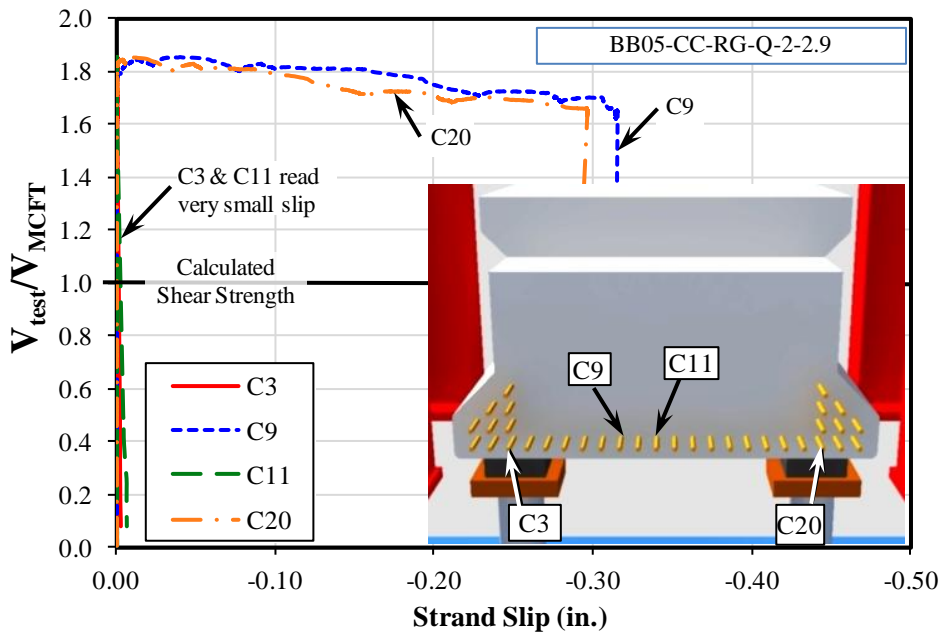**Figure C-38: Strand slip plot for test BB09-SCC-RG-KQ-2-3.4**

271
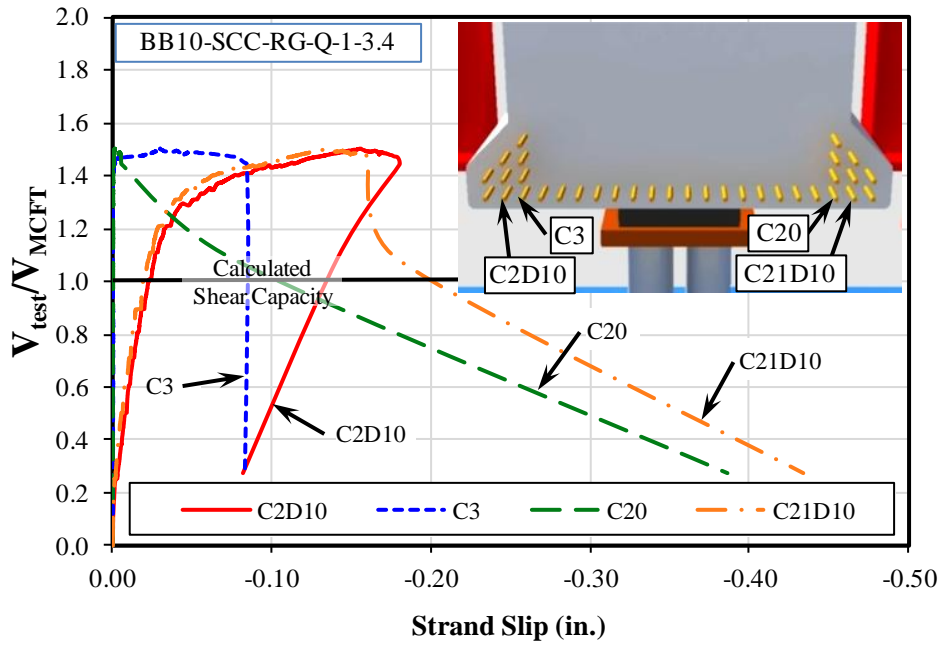
Figure C-39: Strand slip plot for test BB10-SCC-RG-Q-1-3.4
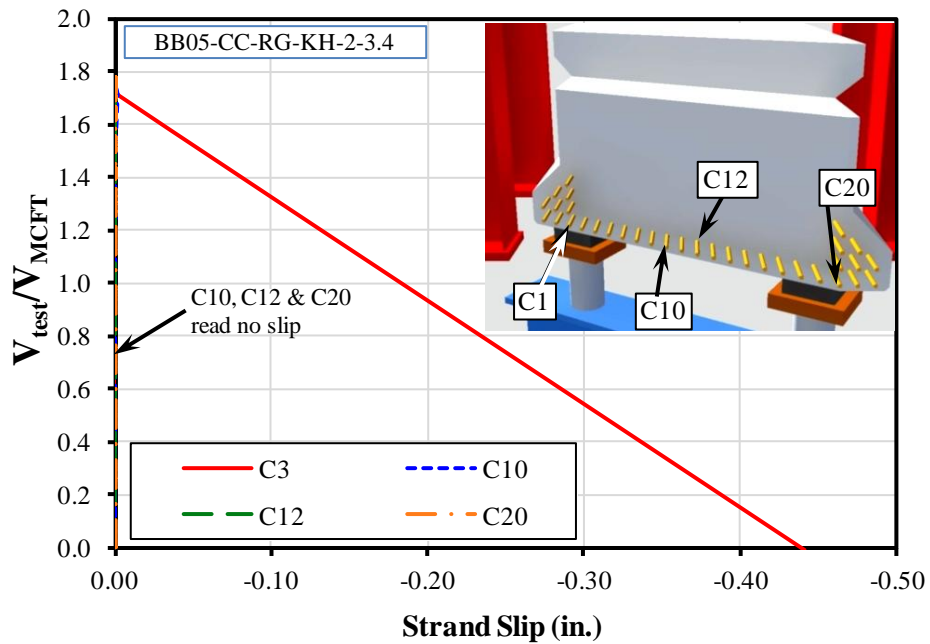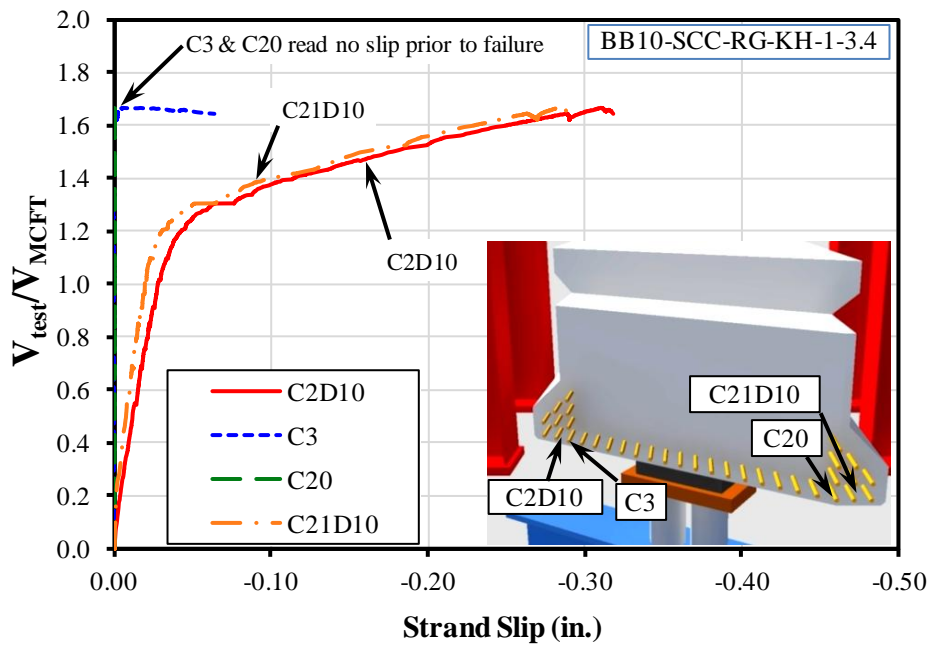

Figure C-40: Strand slip plot for test BB10-SCC-RG-KH-1-3.4

272

APPENDIX D

Temperature Measurements
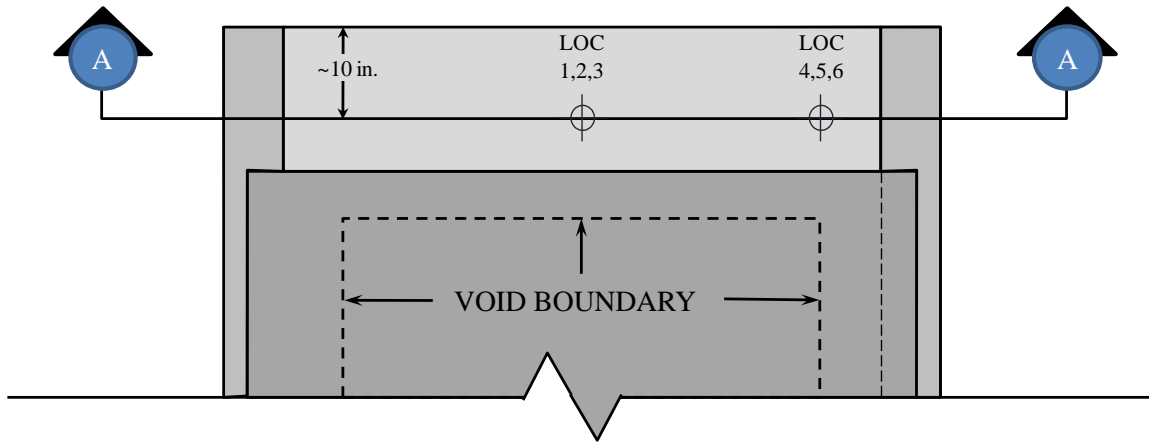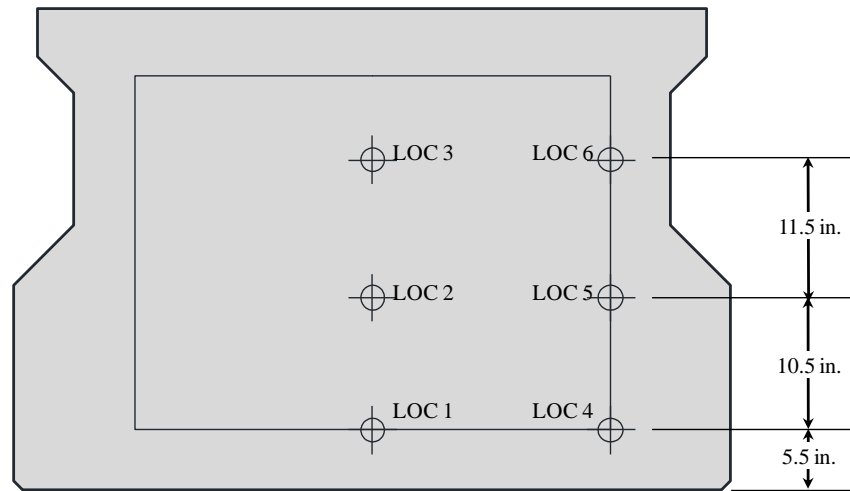
SECTION A

PLAN VIEW

Figure D-1: Thermocouple Locations for Square Ends of Beams 5B40-1 through 5B40-4

SECTION B

PLAN VIEW

Figure D-2: Thermocouple Locations for Skewed Ends of Beams 5B40-1 through 5B40-4

SECTION A

LOC 3   LOC 6

LOC 2   LOC 5

LOC 1   LOC 4

12.5 in.

12.5 in.

7.5 in.

A

~10 in.

LOC
1,2,3

LOC
4,5,6

VOID
BOUNDARY

A

PLAN VIEW

Figure D-3: Thermocouple Locations for Square End beam 5XB40

	5B40-1	
	Square End	**Skewed End**
Maximum Temperature	Max Temp = 151.4 °F Min Temp = 136 °F Differential = 15.4 °F Date = 05/20/2010 11:30 PM Time after pour = 13.5 hours	Max Temp = 155.5 °F Min Temp = 129.8 °F Differential = 25.7 °F Date = 05/21/2010 2:10 AM Time after pour = 16.17 hours
Maximum Differential	Max Temp = 126.7 °F (LOC 2) Min Temp = 100.5 °F (LOC 5) Differential = 26.2 °F Date = 05/20/2010 4:00 PM Time after pour = 6 hours	Max Temp = 147.7 °F (LOC 2) Min Temp = 113.6 °F (LOC 4) Differential = 34.1 °F Date = 05/21/2010 11:00 AM Time after pour = 25 hours
At time of Prestress Transfer	Max Temp = 148.9 °F Min Temp = 129.4 °F Differential = 19.5 °F Date = 05/21/2010 3:30 AM Time after pour = 17.5 hours	Max Temp = 155.3 °F Min Temp = 127.8 °F Differential = 27.5 °F Date = 05/21/2010 3:30 AM Time after pour = 17.5 hours

80   100   120   140   160

Temperature (°F)

Figure D-4: Temperature Profiles for beam 5B40-1

	5B40-2	
	Square End	**Skewed End**
Maximum Temperature	 Max Temp = 149.1 °F Min Temp = 134.6 °F Differential = 14.5 °F Date = 07/23/2010 03:54 AM Time after pour = 17.9 hours	 Max Temp = 138.5 °F Min Temp = 125.9 °F Differential = 12.6 °F Date = 07/23/2010 12:50 AM Time after pour = 14.83 hours
Maximum Differential	 Max Temp = 144.8 ° F (LOC 2) Min Temp = 124.7 °F (LOC 4) Differential = 20.1 °F Date = 07/23/2010 09:06 AM Time after pour = 23.1 hours	 Max Temp = 129.8 ° F (LOC 1) Min Temp = 107.5 °F (LOC 6) Differential = 22.2 °F Date = 07/23/2010 10:20 AM Time after pour = 24.33 hours
At time of Prestress Transfer	 Max Temp = 148.8 °F Min Temp = 132.0 °F Differential = 16.8 °F Date = 07/23/2010 05:00 AM Time after pour = 19 hours	 Max Temp = 135.3 °F Min Temp = 114.4 °F Differential = 20.9 °F Date = 07/23/2010 05:00 AM Time after pour = 19 hours

Temperature (°F)

Figure D-5: Temperature Profiles for beam 5B40-2

	5B40-3	
	Square End	**Skewed End**
Maximum Temperature	Max Temp = 151.6 °F Min Temp = 128.8 °F Differential = 22.8 °F Date = 09/08/2010 01:00 AM Time after pour = 15 hours	Max Temp = 154.8 °F Min Temp = 130.4 °F Differential = 24.4 °F Date = 09/08/2010 01:20 AM Time after pour = 15.33 hours
Maximum Differential	Max Temp = 146.9 °F (LOC 2) Min Temp = 119 °F (LOC 6) Differential = 27.9 °F Date = 09/08/2010 06:24 AM Time after pour = 20.4 hours	Max Temp = 151.7 °F (LOC 2) Min Temp = 123.3 °F (LOC 7) Differential = 28.4 °F Date = 09/08/2010 06:30 AM Time after pour = 20.5 hours
At time of Prestress Transfer	Max Temp = 150.7 °F Min Temp = 125.5 °F Differential = 25.2 °F Date = 09/08/2010 02:42 AM Time after pour = 16.7 hours	Max Temp = 154.6 °F Min Temp = 129.2 °F Differential = 25.4 °F Date = 09/08/2010 02:40 AM Time after pour = 16.67 hours

Temperature (°F)

Figure D-6: Temperature Profiles for beam 5B40-3

	5B40-4	
	Square End	**Skewed End**
Maximum Temperature	 Max Temp = 119.3 °F Min Temp = 113.4 °F Differential = 5.9 °F Date = 01/19/2011 02:42 AM Time after pour = 14.7 hours	 Max Temp = 124 °F Min Temp = 103.4 °F Differential = 20.7 °F Date = 01/19/2011 04:30 AM Time after pour = 16.5 hours
Maximum Differential	 Max Temp = 75 °F (LOC 2) Min Temp = 65.5 °F (LOC 4) Differential = 9.5 °F Date = 01/18/2011 01:24 AM Time after pour = 1.4 hours	 Max Temp = 121.1 °F (LOC 2) Min Temp = 98.8 °F (LOC 6) Differential = 22.3 °F Date = 01/19/2011 10:18 AM Time after pour = 22.3 hours
At time of Prestress Transfer	 Max Temp = 91.9 °F Min Temp = 87.4 °F Differential = 4.5 °F Date = 01/21/2011 02:48 AM Time after pour = 62.8 hours	 Max Temp = 87.9 °F Min Temp = 79.8 °F Differential = 8.0 °F Date = 01/21/2011 02:48 AM Time after pour = 62.8 hours

Temperature (°F)

Figure D-7: Temperature Profiles for beam 5B40-4

280

	5XB40
Maximum Temperature	Max Temp = 147.4 °F Min Temp = 124.6 °F Differential = 22.8 °F Date = 05/03/2011 02:42 AM Time after pour = 16.7 hours
Maximum Differential	Max Temp = 140.5 °F (LOC 2) Min Temp = 114.2 °F (LOC 4) Differential = 26.3 °F Date = 05/03/2011 12:06 PM Time after pour = 26.1 hours
At time of Prestress Transfer	Max Temp = 90.5 °F Min Temp = 88.9 °F Differential = 1.6 °F Date = 05/09/2011 3:06 PM Time after pour = 173.1 hours

Temperature (°F)

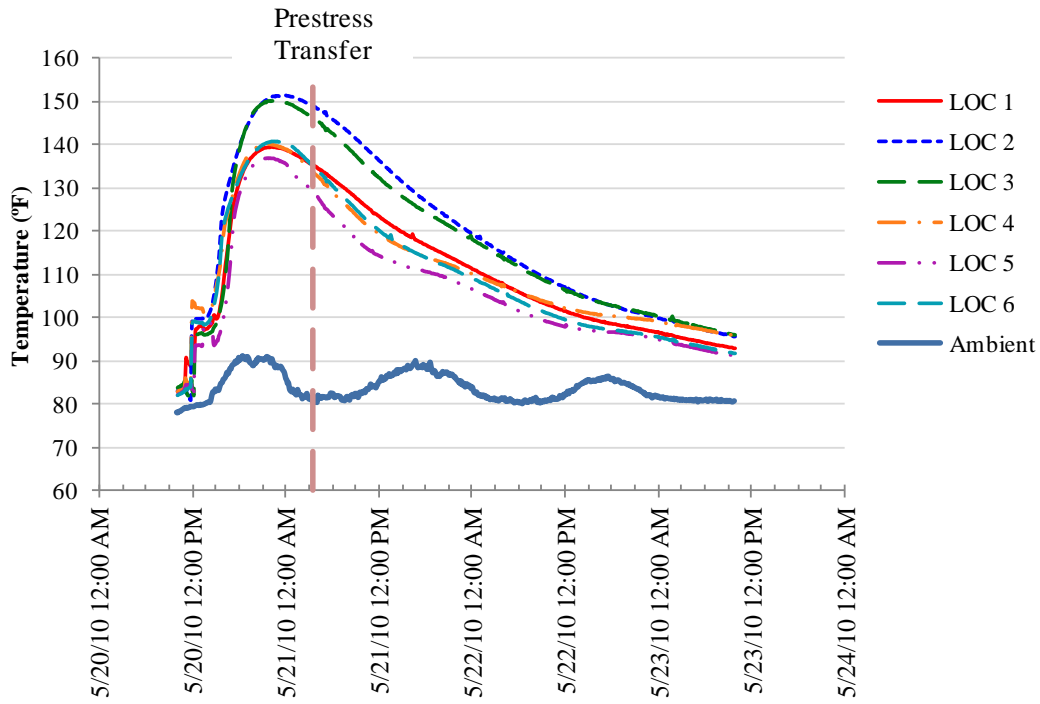**Figure D-8: Temperature Profiles for beam 5XB40**

281

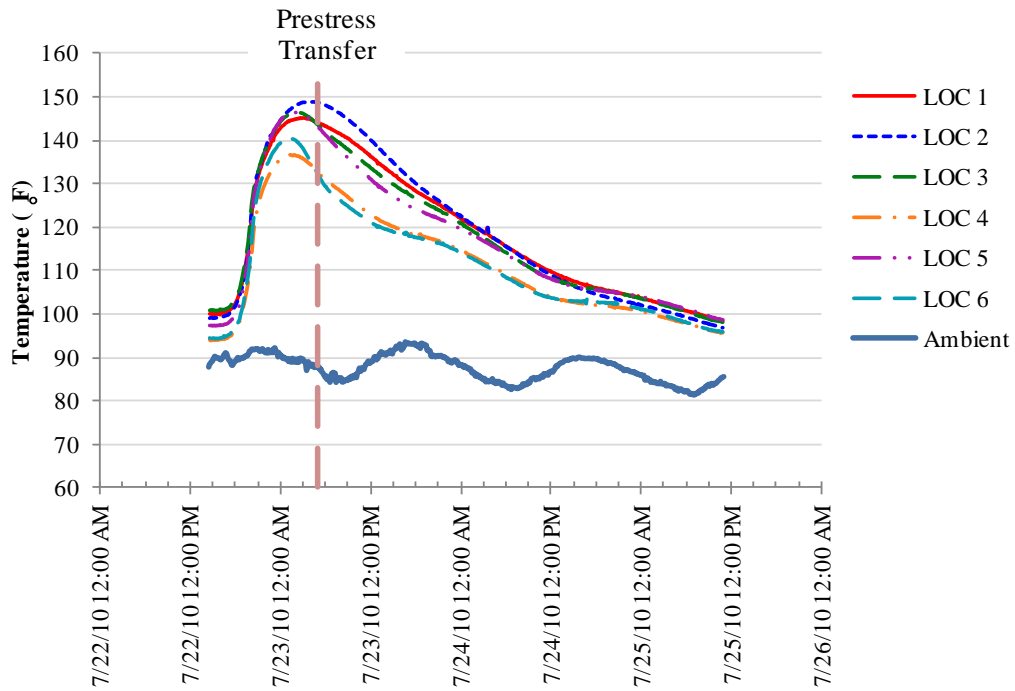**Figure D-9: Temperature History for square end of beam 5B40-1**

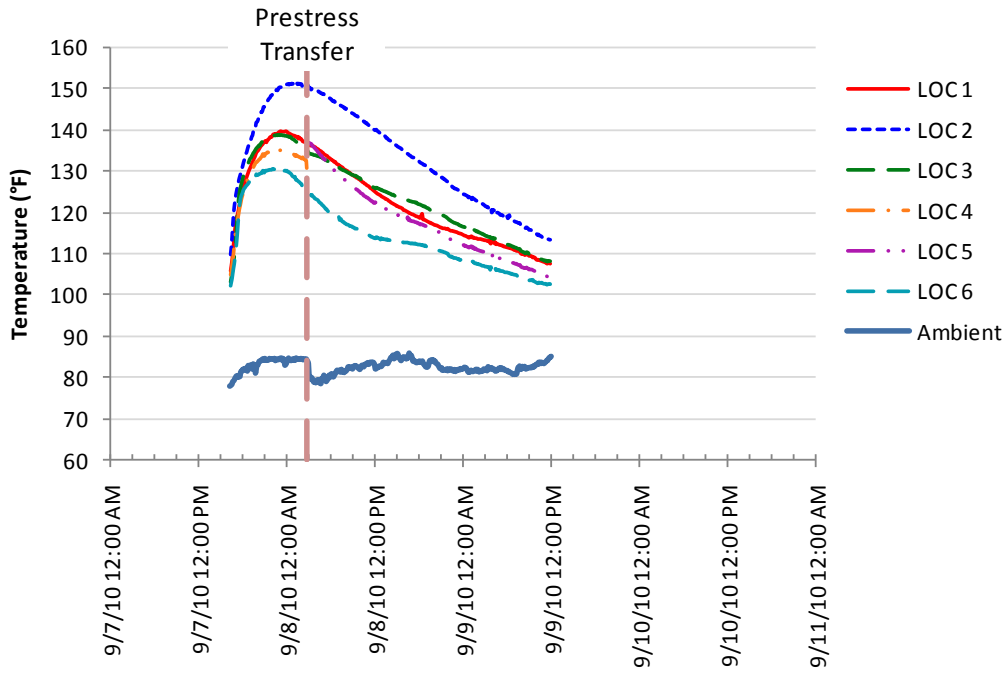**Figure D-10: Temperature History for square end of beam 5B40-2**

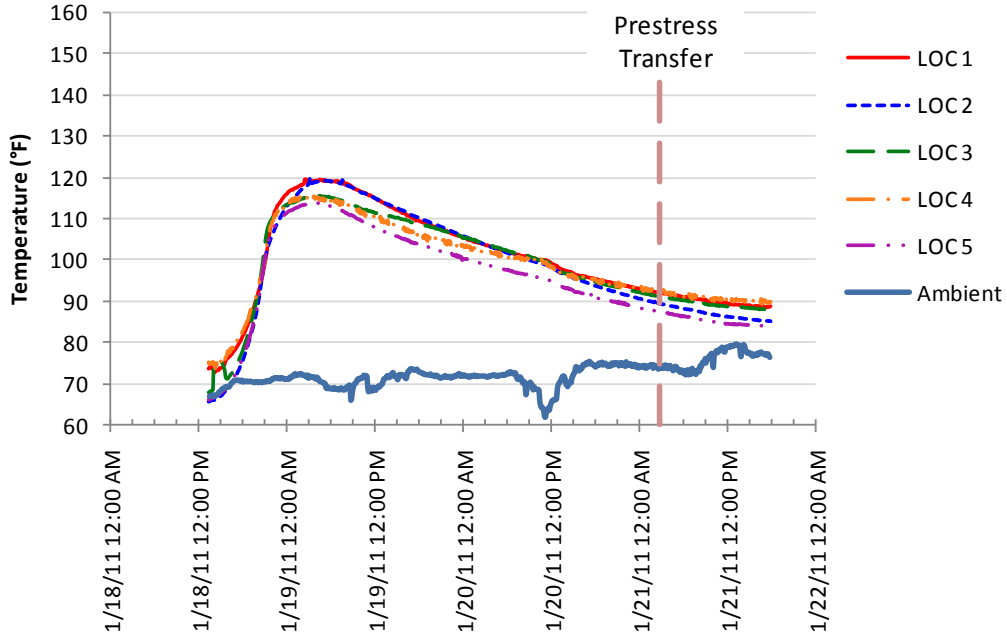**Figure D-11: Temperature History for square end of 5B40-3**

Figure D-12: Temperature History for square end of 5B40-4
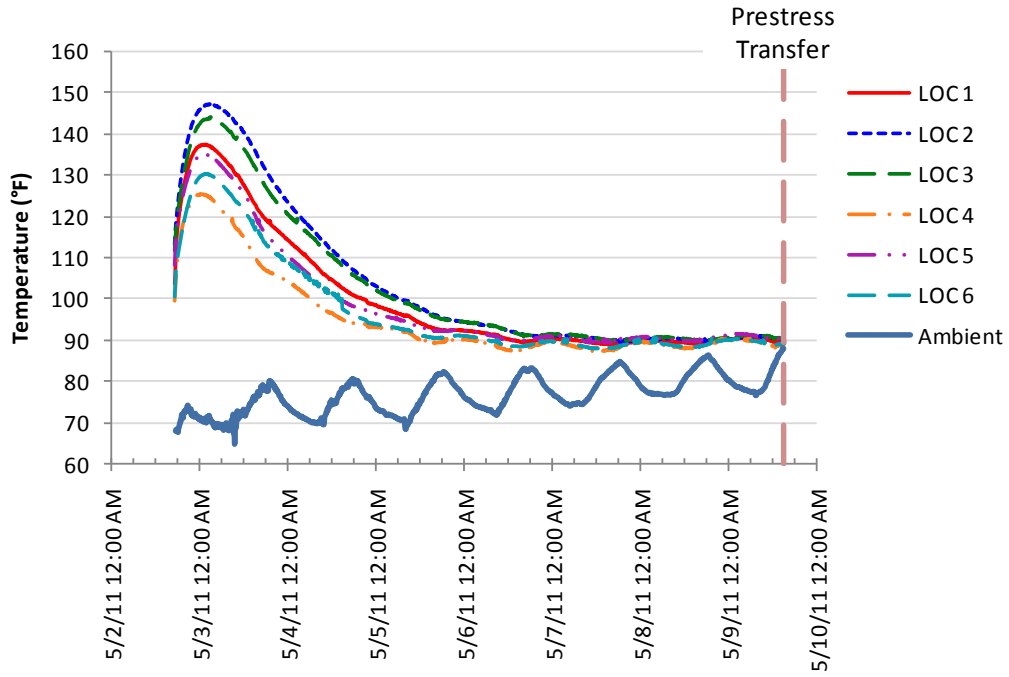
283

Figure D-13: Temperature History for north end of beam 5XB40

References

1. AASHTO. *LRFD Bridge Design Specifications.* 4th Edition. Washington, D.C.: American Association of State Highway and Transportation Officials, 2007.

2. ACI Committee 318. *Building Code Requirements for Structural Concrete (ACI 318-08).* Farmington Hills, MI: American Concrete Institute, 2008.

3. Avendaño, Alejandro, and Oguzhan Bayrak. "Shear Strength and Behavior of Prestressed Concrete Beams." Technical Report: IAC-88-5DD1A003-3, Center for Transportation Research, The University of Texas at Austin, 2008.

4. Base, G.D. "An Investigation of Transmission Length in Pre-Tensioned Concrete." Research Report No. 5, Cement and Concrete Association, 1958, 29 pp.

5. Bender, Brice F., and William G. Kriesel. "Precast, Prestressed Box Beams - A state-of-the-art report." *Journal of the Prestressed Concrete Institute* Vol. 14, no. 1 (1969): 72-95.

6. Burgueño, Rigoberto, and David A. Bendert. "Experimental Evaluation and Field Monitoring of Prestressed Box Beams for SCC Demonstration Bridge." Research Report No. CEE-RR-2007/01, Department of Civil and Environmental Engineering, Michigan State University, 2007.

7. CEB-FIP. *CEB-FIP Model Code 1990: Design Code*. London: T Telford, 1993.

8. Chamberlain, C. "Evaluation of Longitudinal Cracking in End Regions of Pretensioned Box Beams." Masters Thesis, The University of Texas at Austin, 1997, 107 pp.

9. Crispino, E.D. "Anchorage Zone Design for Pretensioned Bulb-Tee Bridge Girders in Virginia." Virginia Polythechnic Institute and State University, Blacksburg, VA, 2007, 155 pp.

10. Day, R.L., Civil Engineering Report CE92-2, Department of Engineering, University of Calgary, PCA Project 92-05, May 1992.

11. Dunkman, David A. "Bursting and Spalling in Pretensioned U-Beams." Masters Thesis, The University of Texas at Austin, 2009, 242 pp.

12. Euro EC2 Code, Design of Concrete Structures, Paris. 1997.

13. Gergely, P., M.A. Sozen, and C.P. Siess. "The Effect of Reinforcement on Anchorage Zone Cracks in Prestressed Concrete Members." Structural Research Series No. 271, University of Illinois, 1963, 170 pp.

14. Halvorsen, G. T., "Code Requirements for Crack Control," *ACI Special Publication* 104 (1987): 275-322.

15. Hanson, John M., and C. L. Hulsbos. "Ultimate Shear Tests of Large Prestressed Concrete Birdge Beams." *ACI Special Publication* 26 (1971): 523-551.

16. Hovell, Catherine G. "Structural Performance of Texas U-Beams at Prestress Transfer and Under Shear-Critical Loads." PhD Dissertation, The University of Texas at Austin, 2011, 388 pp.

17. Lawrence C.D., Materials Science of Concrete, American Ceramic Society, Edited by J Skalny and S Mindess, E (1994).

18. Marshall, W.T. and A.H. Mattock. "Control of Horizontal Cracking in the Ends of Pretensioned Prestressed Concrete Girders." *PCI Journal* Vol. 7, no. 10 (1962): pp. 56-75.

19. Nakamura, Eisuke. "Shear Database for Prestressed Concrete Members." MS Thesis, The University of Texas at Austin, Austin, TX, 2011, 208 pp.

20. O'Callaghan, Matthew R., and Oguzhan Bayrak. "Tensile Stresses in the End Regions of Pretensioned I-Beams at Release." Technical Report: IAC-88-5DD1A003-1, The University of Texas at Austin, Austin, TX, 2008, 251 pp.

21. Saiidi, M. Saiid, and Anita Bush. "Ultimate and Fatigue Response of Shear Dominated Full-Scale Pretensioned Box Girders." *Structural Engineering and Mechanics* Vol. 23, no. 4 (2006): 353-367.

22. Schnittker, Brian, and Oguzhan Bayrak. *Allowable Compressive Stress at Prestress Transfer.* Technical Report 0-5197-4, The University of Texas at Austin, Austin, TX, 2008, 206.

23. Tang, Man-Chung. "Shear Design of Large Concrete Box Girders." *ACI Special Publication* 42 (1974): 305-319.

24. Tuan, C.Y. "End Zone Reinforcement for Pretensioned Concrete Girders." *PCI Journal* Vol. 49, no. 3 (2004): pp.68-82.

25. Uijl, J.A. den, *Tensile Stresses in the Transmission Zones of Hollow-Core Slabs Prestressed with Pretensioned Strands*, TU Delft, Stevinlaboratory, Report No. 5-83-10, Sept. 1983.

26. Yettram, A.L., and K. Robbins. "Anchorage Zone Stresses in Axially Post-Tensioned Concrete Members of Uniform Rectangular Section." *Magazine of Concrete Research* Vol 21, no. 67 (1969): pp.103-112.

27. Yettram, A.L., and K. Robbins. "Anchorage Zone Stresses in Axially Post-Tensioned I-Section Members with End Blocks." *Magazine of Concrete Research* Vol. 23, no. 74 (1971): pp.37-42.